INTRACELLULAR SODIUM AND CONTRACTILE DYSFUNCTION IN LEFT VENTRICULAR HYPERTROPHY

A thesis

presented to University College London

in fulfilment of the regulations

for the degree of

Doctor of Philosophy

by

Dr Rosaire Gray MD, MRCP.

Institute of Urology and Nephrology,

University College London

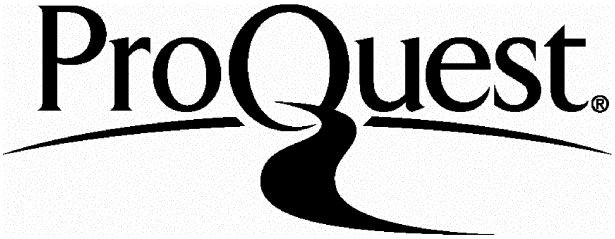

Abstract

Left ventricular hypertrophy (LVH) is associated with the development of heart failure and arrhythmias. The mechanisms underlying this decompensation are unclear. The hypothesis that LVH is associated with a raised intracellular sodium, $[Na^+]_i$ which by upsetting the regulation of other intracellular ions impairs the positive staircase was tested.

LVH was induced in guinea-pigs by ascending aortic constriction and the extent of hypertrophy quantified by measuring heart-to-body weight ratio. The control group consisted of sham-operated and unoperated animals. The tension generated in response to increasing stimulation frequency and $[Na^+]_i$ were measured. The force-frequency response was depressed and $[Na^+]_i$ increased from 7.4 ± 1.4 to 12.1 ± 1.4 mM with LVH. There was a close relationship between the decline of the force-frequency response and the increase of $[Na^+]_i$ which was also observed when the $[Na^+]_i$ was increased with strophanthidin in normal myocardium.

Possible mechanisms to account for the raised $[Na^+]_i$ are explored. The recovery of a raised $[Na^+]_i$ after an acute acidosis was slowed in hypertrophied myocardium and stabilised at a higher level, suggesting that the membrane mechanisms that regulate $[Na^+]_i$ are reset.

Intracellular pH, pH_i, and $[Ca^{2+}]$, $[Ca^{2+}]_i$, were measured in isolated myocytes using epifluoresence microscopy. pH_i decreased progressively with increasing severity of hypertrophy and the sarcoplasmic buffering capacity increased with increasing acidosis. The recovery of pH_i from an intracellular acidosis was slowed in myocytes from aortic constricted (AC) hearts but the total H^+ efflux rate was not different indicating no effect on Na^+-H^+-exchange activity.

Resting $[Ca^{2+}]_i$ was not significantly different in myocytes from AC hearts but the caffeine induced release of $[Ca^{2+}]$ from the sarcoplasmic reticulum (SR) was reduced. The time course of the decay phase of the caffeine was prolonged in myocytes from AC hearts indicating reduced activity of the Na^+-Ca^{2+}-exchanger.

Quantitative immunoblotting of the Na^+-K^+-ATPase pump isoforms was performed in a small number of samples. No significant differences were observed between the two groups.

Acknowledgement

This thesis would not have been completed without the help and support of colleagues and friends to whom I would now like to express my sincere thanks.

In particular I would like to thank the following:

Professor Chris Fry, my supervisor for guiding me, with infinite patience in my study of the cellular pathology of myocardial hypertrophy. I am indebted to him for his enthusiasm and advice, his friendship and support, leading to the completion of this thesis.

Professor James Malone-Lee, my clinical supervisor, who provided endless support and encouragement to enable me to complete this thesis.

Mark Turner for his technical expertise, advice and help.

Phil Eaton for his technical expertise, endless advice and support with the Western blots

My colleagues in the laboratory, especially Dr Richard Wu, Dr Gui-Ping Sui, Valerie Proctor, Dr Peter Carey and Dr Alf Botchway who gave freely of their time, help and advice and made research a rich and enjoyable experience.

A special thanks to Dr Vidya Mohamed-Ali for her support and encouragement.

For the financial support from the Wellcome Trust and the British Heart Foundation that allowed this work to proceed.

CONTENTS

Title 1

Abstract 2

Acknowledgement 3

Contents 4

List of Figures 12

List of Plates 19

List of Tables 20

List of abbreviations 24

Chapter 1. Introduction 28

1. Clinical pathology of left ventricular hypertrophy 28

1.1. Electrophysiological changes in hypertrophy 31

1.2. Gap junctions 33

1.2.1. Connexin proteins in hypertrophy 33

1.3. Contractile function in myocardial hypertrophy 34

1.3.1. Force-frequency relationships in hypertrophy 36

1.4. Excitation-contraction coupling 37

1.4.1. 'Ca overload' 42

1.5. Mechanisms underlying rate-dependant changes in contractile force 43
1.5.1. Intracellular ions and contractile function 43
1.5.1.1. Role of intracellular Ca^{2+} 43
1.5.1.2. Role of intracellular Na^{+} 43
1.5.2. Mechanical restitution 45
1.5.2.1. Mechanical restitution in hypertrophy 46
1.5.3. Post-rest potentiation 46
1.5.4. Effect of strophanthidin 47

1.6. Intracellular ions in myocardial hypertrophy 47
1.6.1. Intracellular Na^{+} in hypertrophy 48
1.6.1.1. Functional implications of the rise in $[Na^{+}]_i$ 48
1.6.2. Intracellular Ca^{2+} in hypertrophy 49
1.6.3. Sarcoplasmic reticulum function in hypertrophy 50
1.6.4. Intracellular pH, pH_i, in hypertrophy 52

1.7. Regulation of intracellular pH, pH_i 52
1.7.1. Cellular mechanisms for control of pH_i in mammalian myocardium 53
1.7.2. Membrane transport systems controlling pH_i 53
1.7.3. Physico-chemical buffering, β 54

1.8. Membrane proteins and channels in hypertrophy 55
1.8.1. The Na^{+}-K^{+}-ATPase pump 55
1.8.1.1. Na^{+}-K^{+}-ATPase pump function in hypertrophy 56
1.8.1.2. Na^{+}-K^{+}-ATPase pump isoform expression in hypertrophy 58
1.8.1.3. Physiological relevance of changes in isoform expression 58
1.8.1.4. Sarcoplasmic reticulum Ca^{2+}-ATPase (SERCA2) expression in hypertrophy 60
1.8.3. The sarcoplasmic reticulum release channel, the ryanodine receptor, in hypertrophy 61
1.8.4. Na^{+}-Ca^{2+}-exchanger expression in hypertrophy 63
1.8.5. Calcium channels in hypertrophy 65
1.8.5.1. The L-type Ca^{2+} channel in hypertrophy 65
1.8.5.2. The T-type Ca^{2+} channel in hypertrophy 65

1.8.6. The Na^+-H^+-exchanger 67

1.8.6.1. The Na^+-H^+-exchanger in hypertrophy 68

1.9. Summary 69

1.10. Hypotheses 71

Chapter 2. Methods 72

2.0. General protocol 72

2.1. The experimental model of left ventricular hypertrophy 72

2.1.1. Details of the animals used 72

2.1.2. Anaesthesia, intubation and ventilation 72

2.1.3. Incision and operation 73

2.1.4. Recovery 74

2.1.5. Regression of left ventricular hypertrophy 74

2.2. Solutions and chemicals 75

2.3. Isolated preparations 75

2.3.1. Tension recordings 76

2.3.2. Experimental procedures 79

2.4. Preparation of ion-selective microelectrodes 80

2.4.1. Manufacture of Ag/AgCl electrodes 81

2.4.2. Preparation of microelectrodes 83

2.4.3. Preparation of reference electrodes 83

2.4.4. Preparation of Na^+-selective microelectrodes 83

2.4.5. Connections to recording devices 84

2.4.6. Description of headstage 84

2.4.7. Measurement of input bias current of headstage 85

2.4.8. Recording of intracellular potentials 87

2.4.9. Calibration of Na^+-selective microelectrodes 89

2.5. Cell isolation 90

2.5.1. Langendorff perfusion method 90

2.6. Measurement of intracellular pH (pH_i) by epifluorescence microscopy 92

2.6.1. Intracellular pH fluorescent indicator 92

2.6.2. Intracellular loading of BCECF 93

2.6.3. The experimental set-up 93

2.6.4. Experimental procedure 96

2.6.5. Calibration of the BCECF fluorescence signal 96

2.6.6. Data storage and analysis 97

2.7. Intracellular buffering capacity 97

2.7.1. Calculation of extracellular $[NH_4^+]$, $[NH_4^+]_o$ 98

2.7.2. Calculation of intracellular $[NH_4^+]$, $[NH_4^+]_i$ 99

2.7.3. Estimation of intracellular buffering capacity 100

2.8. Na^+-H^+ exchange turnover 101

2.8.1. Rate of pH_i recovery from acid load 101

2.8.2. Calculation of acid-equivalent efflux 101

2.9. Measurement of intracellular Ca^{2+} by epifluorescence microscopy 102

2.9.1. Intracellular Ca^{2+} fluorescent indicator 102

2.9.2. Intracellular loading of Fura-2 103

2.9.3. Calibration of the Fura-2 fluorescence signal 103

2.9.3.1 In vitro determination of the Fura-2 dissociation constant 103

2.9.4. Estimation of sarcoplasmic reticulum Ca^{2+} content 104

2.10. SDS-PAGE Western blots 105

2.10.1. Sample preparation 106

2.10.2. SDS-PAGE (sodium dodecyl sulphate-polyacrylamide gel electrophoresis) / Western blotting 106

2.10.3. Antibodies 107

2.11. Statistical analysis 109

Chapter 3. Results 110

3.1. Assessment of magnitude of hypertrophy produced by aortic-constriction 110

3.1.1. Measurement of heart-to-body weight ratio 110

3.1.2. Regression of left ventricular hypertrophy 112

3.2. Mechanical properties of the isolated myocardial preparation 113

3.2.1. The force-frequency relationship 113

3.2.1.1. The force-frequency relationship and heart-to-body weight ratio 117

3.2.2. Post-rest potentiation 119

3.2.3. Effect of regression of LVH on contractile function 120

3.2.4. Summary 120

3.3. Contractility and strophanthidin 121

3.3.1. The inotropic response to strophanthidin 121

3.3.2. The effect of strophanthidin on the force-frequency relationship 122

3.3.3. The effect of strophanthidin on post-rest potentiation 123

3.3.4. Summary 126

3.4. The effect of reduced external [Na] on contractile function 127

3.5. The effect of increased extracellular [Ca] on contractile function 128

3.6. Summary 129

3.7. Intracellular Na^+ concentration, $[Na^+]_i$ and hypertrophy 129

3.7.1. Intracellular Na^+ concentration, $[Na^+]_i$, measurements 129

3.7.2. Calibration of Na^+-selective microelectrodes 131

3.7.3. Intracellular $[Na^+]$, $[Na^+]_i$, measurements and hypertrophy 131

3.7.4. Intracellular $[Na^+]_i$ and contractile function 134

3.7.5. Recovery of $[Na^+]_i$ after intracellular acidosis 134

3.8. Summary 137

3.9. Measurement of intracellular pH, pH_i 138

3.9.1. Measurement of pH_i in isolated cells 138

3.9.2. Effect of hypertrophy on $[pH]_i$ 139

3.9.3. pH_i as a function of heart-to-body weight ratio 139

3.10. Determination of intracellular H^+ buffering capacity 140

3.10.1. Theory of measurement of β 140

3.10.2. Determination of non-bicarbonate intracellular H^+ buffering capacity, β_I 141

3.10.3. β_i in cells from control and aortic-constricted hearts 141

3.10.4. Correlation of β_i with pH_i 143

3.10.5. Determination of bicarbonate and non-bicarbonate intracellular H^+ buffering capacity, β_{tot} 143

3.10.6. β_{tot} in cells from control hearts 146

3.10.7. Bicarbonate dependent buffering, β_{CO2} 146

3.10.8. Correlation of β_{tot} with pH_I 146

3.11. pH_i recovery from intracellular acidosis 147

3.11.1. Calculation of the non-bicarbonate dependent pH_i recovery rate 147

3.11.2. Calculation of the bicarbonate and non-bicarbonate dependent pH_i recovery rate 149

3.12. Calculation of sarcolemmal acid flux (J_H) 150

3.12.1. Non-bicarbonate acid-equivalent flux in myocytes from control and aortic-constricted hearts 150

3.12.2. Non-bicarbonate acid-equivalent flux in myocytes from control hearts 151

3.13. Summary 155

3.14. Measurement of intracellular $[Ca^{2+}]$, $[Ca^{2+}]_i$ 156

3.14.1. Measurement of $[Ca^{2+}]_i$ in isolated cells 156

3.14.2. Effect of hypertrophy on resting $[Ca^{2+}]_i$ 156
3.14.3. Effect of hypertrophy on SR Ca^{2+} content 156
3.14.4. Effect of reduced external Na on SR Ca^{2+} content 161
3.14.5. Estimation of the rate of Ca^{2+} efflux 165
3.14.6. Effect of reduced external [Na] on the rate of Ca^{2+} efflux 168
3.14.7. Refilling of the SR 169
3.14.8. Summary 171

3.15. Na^+-K^+-ATPase pump isoforms 172
3.15.1. Quantitative immunoblotting 172
3.15.2. Calsequestrin in hypertrophy 172
3.15.3. α-isoform expression in hypertrophy 172

3.16. The sarcoplasmic reticulum Ca^{2+}-ATPase pump (SERCA2) 175

3.17. Summary 176

Chapter 4. Discussion 177

4.1. Methods 177
4.1.1. The model of hypertrophy 177
4.1.2. Measurement of intracellular $[Na^+]$ using ion-selective microelectrodes 179
4.1.3. Epifluorescence microscopy and determination of intracellular pH 184
4.1.3. Limitations of epifluorescence microscopy for determination of pH_i and H^+ buffering capacity 185
4.1.5. Use of Fura-2 to measure $[Ca^{2+}]_i$ 188
4.1.6. Use of isolated myocytes 189
4.1.7. SDS-PAGE Western blots and the Na^+-K^+-pump isoforms 191

4.2. Results 191
4.2.1. Mechanical function in hypertrophy 191
4.2.2. The rise of $[Na^+]_i$ and the force-frequency relationship in hypertrophy 192

4.2.3. Effects of reduced $[Na]_o$ on the force-frequency relationship 197
4.2.4. Mechanisms underlying the rise of $[Na^+]_i$ in hypertrophy 198
4.2.4.1. Role of the Na^+-K^+-ATPase pump in the rise of $[Na^+]_i$ in hypertrophy 198
4.2.5. pH_i in hypertrophy 203
4.2.6. Mechanisms underlying intracellular acidosis in hypertrophy 205
4.2.7. Functional implications of the fall in pH_i in hypertrophy 206
4.2.8. Intracellular buffering capacity in hypertrophy 207
4.2.9. Characterisation of recovery from acid-load in normal guinea-pig myocytes 208
4.2.10. $[Ca^{2+}]_i$ in hypertrophy 208
4.2.11. Caffeine and SR calcium content 209
4.2.12. The SR Ca^{2+}-ATPase (SERCA2) pump in hypertrophy 212

4.3. Conclusions 213

5.0. References 214

6.0. Appendix: Publications from thesis 261

List of Figures

Figure 1.1. Schematic diagram showing the events during excitation-contraction coupling 41

Figure 1.2. Schematic representation of the ion pumps and channels involved in the regulation of $[Ca^{2+}]_i$ and $[Na^+]_i$ 42

Figure 1.3. Schematic representation of the sodium dependence of twitch tension 44

Figure 1.4. Model of pH_i control in the ventricular myocyte 54

Figure 2.1. Diagram of the superfusion apparatus 77

Figure 2.2. Calibration of tension transducer at a fixed recording gain 78

Figure 2.3. Schematic representation of a microelectrode selective for Na^+ is shown in (A) and the experimental arrangement is shown in (B) 81

Figure 2.4 Manufacture of Ag/AgCl electrodes. In the upper panel (A), the procedure for cleaning Ag wire is shown and in the lower panel (B), the procedure for coating the Ag wire with AgCl is shown 82

Figure 2.5. Headstage for ion-selective microelectrodes comprising isolation amplifier AD 204 and clock driver AD 246 85

Figure 2.6. The arrangement for measuring the input bias currents at the non-inverting and inverting inputs of an op amp 86

Figure 2.7. Schematic representation of the experimental arrangement for measurement of intracellular $[Na^+]$ using ion-selective microelectrodes 87

Figure 2.8. Calibration of a Na^+-selective microelectrode using calibrating solutions with known [Na] concentrations 89

Figure 2.9. Calibration of Na^+-selective microelectrode. The potential difference recorded is plotted against log [Na] 90

Figure 2.10. A schematic representation of the experimental set-up for epifluoresence microscopy 95

Figure 3.1. Relationship between heart-to-body weight ratio and duration of ascending aortic clip placement (n=60 animals) 111

Figure 3.2. Steady-state isometric tension expressed as a function of stimulation frequency in preparations from control (open circles) and aortic-constricted (filled circles) guinea-pigs 114

Figure 3.3. Steady-state isometric tension as a function of stimulation frequency in aortic-constricted hearts 116

Figure 3.4. The force-frequency relationship ($T_{(1.6/0.8)}$) as a function of heart-to-body weight ratio in isolated preparations from control and aortic-constricted hearts 118

Figure 3.5. (A) Heart-to-body weight ratios (HBR) and (B) force-frequency relationships ($T_{(1.6/0.8)}$) from unoperated LV, sham-operated LV, moderate (HBR 4.0 to 5.5 $g.kg^{-1}$, n=21) and severe hypertrophy (HBR>5.5 $g.kg^{-1}$, n=19) 118

Figure 3.6. Post-rest tension and heart-body weight ratio in left ventricular papillary muscles from control (open circles) and aortic-constricted hearts (filled circles) 119

Figure 3.7. The inotropic response to strophanthidin in isolated preparations from control (open circles) (n=18) and aortic-constricted (filled circles) (n=9) guinea pig hearts 122

Figure 3.8. The force-frequency relationship ($T_{(1.6/0.8)}$) in the presence of strophanthidin in papillary muscles from control (open circles) and aortic-

constricted (filled circles) hearts 123

Figure 3.9. Comparison of the force-frequency response in control and aortic constricted guinea-pigs 124

Figure 3.10. Post-rest tension in the presence of strophanthidin in isolated preparations from control (open circles) and aortic-constricted (filled circles) hearts 125

Figure 3.11. The inotropic response to reduced extracellular [Na] in isolated preparations from control guinea-pig hearts 127

Figure 3.12. The effect of reduced extracellular [Na] on the force-frequency relationship ($T_{(1.6/0.8)}$) in isolated preparations from control hearts 128

Figure 3.13. ΔE_m recorded by a KCl-filled microelectrode and a Na^+-sensitive microelectrode on superfusing the preparation with 40 mM KCl Tyrode's solution 130

Figure 3.14. Calibration of Na^+-selective microelectrodes in mixed NaCl and KCl solutions 131

Figure 3.15. Relationship between intracellular [Na^+] and heart-to-body weight ratio 133

Figure 3.16. Intracellular [Na^+] measured using ion-selective microelectrodes in isolated papillary muscles from unoperated and sham-operated left ventricle, moderate hypertrophy (HBR 4.0-5.5 $g.kg^{-1}$) and severe hypertrophy (HBR >5.5 $g.kg^{-1}$) 134

Figure 3.17. The relationship between the force-frequency response ($T_{(1.6/0.8)}$) and $[Na^+]_i$ 135

Figure 3.18 Recordings of $[Na^+]_i$ and membrane potential, E_m, from A: a sham-operated animal and B: an aortic-constricted animal 136

Figure 3.19. Measurement and intracellular calibration of pH_i in an isolated myocyte 138

Figure 3.20. The relationship between pH_i and heart-to-body weight ratio 140

Figure 3.21. Derived plot of pH_i in a myocyte isolated from an aortic-constricted heart following application of 10mM NH_4Cl and its subsequent removal in the absence and presence of 1mM amiloride 142

Figure 3.22. Relationship between β_i and heart-to-body weight ratio 144

Figure 3.23. Relationship between β_i and steady–state pH_i 145

Figure 3.24. Relationship between β_{tot} and steady–state pH_i of individual cells isolated from control hearts 147

Figure 3.25. Relationship of β_{tot} (filled triangles) and β_i (open circles) and steady-state pH_i in myocytes isolated from control hearts 148

Figure 3.26. The rate of recovery of pH_i on NH_4Cl removal in the absence of amiloride in a myocyte from a control heart (A) and from an aortic-constricted heart (B) 148

Figure 3.27. Non-bicarbonate dependent H^+ efflux rate as a function of intracellular pH at the commencement of acid extrusion in 68 myocytes isolated from control hearts (open circles) and 21 myocytes from aortic-constricted hearts (filled circles) 151

Figure 3.28. Effect of 1 mM amiloride and reduced external Na^+ on recovery from NH_4Cl induced acidosis in a myocyte from a control heart 152

Figure 3.29. Effect of 1 mM amiloride and reduced external Na^+ on recovery from NH_4Cl induced acidosis in a myocyte from a control heart 153

Figure 3.30. Bicarbonate and non-bicarbonate dependent H^+ efflux rate as a function of intracellular pH at the commencement of acid extrusion in 68 myocytes isolated from control hearts 154

Figure 3.31. H^+ efflux rate as a function of intracellular pH in myocytes isolated from control hearts 154

Figure 3.32. Resting $[Ca^{2+}]_i$ in isolated myocytes from control and aortic constricted hearts measured using the fluorescent indicator Fura-2 157

Figure 3.33. Derived plot of a caffeine transient from a control (continuous line) and an aortic-constricted (broken line) heart 158

Figure 3.34. Relationship between SR calcium content, measured in isolated myocytes as the increase in $[Ca^{2+}]_i$ produced on application of 10 mM caffeine, and heart-to-body weight ratio 161

Figure 3.35. Derived plot of the effect of reduced external Na concentration (29 mM NaCl Tyrode's) on $[Ca^{2+}]_i$ measured using the fluorescent indicator, Fura-2 and plotted as the ratio of fluorescence emitted at 340:380 nm in a myocyte from an aortic-constricted heart 164

Figure 3.36. Derived plot of the effect of altering external Na concentration on $[Ca^{2+}]_i$ measured using the fluorescent indicator, Fura-2 and plotted as the ratio of the fluorescence output at 340/380 nm in a myocyte isolated from a sham-operated heart 164

Figure 3.37. Time constant of the decay of the caffeine transient in a myocyte from a control heart (A) and a myocyte from an aortic-constricted heart (B) 166

Figure 3.38. Relationship between the time constant of the recovery phase of the caffeine transient (τ_i) and heart-to-body weight ratio 167

Figure 3.39. Time constant (τ_i) of the recovery phase of the caffeine transient after KCl-induced-depolarisation and reducing external Na in myocytes from control (open circles) and aortic-constricted (closed circles) hearts 169

Figure 3.40. Relationship between the time constant of the recovery phase of the undershoot of the caffeine transient (τ_2) and heart-to-body weight ratio 170

Figure 3.41. Densitometric quantification of western blot analysis of calsequestrin in right (RV) and left ventricular (LV) samples from sham-operated, aortic constricted (AC) and debanded (deb) guinea-pig hearts 173

Figure 3.42. Immunological detection of the α_1-isoform of the Na^+-K^+-ATPase pump 174

Figure 3.43. Densitometric quantification of western blot analysis of the α_1-isoform of the Na^+-K^+-ATPase pump in right (RV) and left ventricular (LV) samples from sham-operated, aortic constricted (AC) and debanded (deb) guinea-pig hearts 174

Figure 3.44. Densitometric quantification of western blot analysis of the α_3-isoform of the Na^+-K^+-ATPase pump in right (RV) and left ventricular (LV) samples from sham operated, aortic constricted (AC) and debanded (deb) guinea-pig hearts 175

Figure 3.45. Densitometric quantification of western blot analysis of SERCA2 pump in right (RV) and left ventricular (LV) samples from sham operated, aortic constricted (AC) and debanded (deb) guinea-pig hearts 176

Figure 4.1. Changes to the force-frequency relationship (A), myocardial $[Na^+]_i$ (B) and pH_i (C) in normal LV myocardium from unoperated (unop) and

sham-operated hearts, moderate LVH (HBR 4.0-5.5 $g.kg^{-1}$) and severe LVH (HBR >5.5 $g.kg^{-1}$) 193

Figure 4.2. Membrane potential (E_m) and equilibrium potential for Na^+-Ca^{2+}exchange (E_{Na-Ca}) 196

Figure 4.3. Values of $[Na^+]_i$ (filled circles) and pH_i (open circles) in unoperated and sham operated hearts, moderate LVH (HBR 4.0-5.5 $g.kg^{-1}$) and severe LVH (HBR >5.5 $g.kg^{-1}$) 199

List of plates

Plate 1. Tension generated in response to increasing stimulation frequency from 0.8 to 1.6 Hz in a papillary muscle from a sham-operated heart in A and an aortic constricted heart in B 115

Plate 2. The effect of addition and removal of NH_4Cl on pH_i in a myocyte from a sham-operated animal 142

Plate 3. In A the increase in $[Ca^{2+}]_i$ in response to 10 mM caffeine in a myocyte from a sham-operated heart is illustrated. In B the increase in $[Ca^{2+}]_i$ in response to 40mM KCl is illustrated followed by a caffeine response in another cell from a sham-operated heart 159

Plate 4. Change in $[Ca^{2+}]_i$ in response to superfusion with reduced external Na solution and 10 mM caffeine in a myocyte from a control heart 163

Plate 5. Change in $[Ca^{2+}]_i$ in response to 10 mM caffeine before and during superfusion with reduced external [Na] solution plotted as 340:380 fluorescence ratio 168

List of Tables

Table 1.1. Studies of Na^+-K^+-ATPase pump function in hypertrophy 57

Table1.2. Summary of studies of Na^+-K^+-ATPase pump isoform expression in hypertrophy 59

Table 1.3. Summary of studies of the SR Ca^{2+}-ATPase (SERCA2) expression in hypertrophy 61

Table 1.4. Summary of studies of Na^+-Ca^{2+}-exchanger expression in hypertrophy 64

Table 2.1. Composition of normal Tyrode's solution 76

Table 2.2. Composition of low-Na Tyrode's solution 79

Table 2.3. Combination of normal and low-Na Tyrode's solutions 80

Table 2.4. Calibrating solutions for Na^+-selective microelectrodes 89

Table 2.5. Nominal calcium free Tyrode's solution 91

Table 2.6. Composition of Kraftbrühe (KB) solution 92

Table 2.7. Composition of solutions used for calibration of BCECF signal 97

Table 2.8. Composition of 10 mM HEPES-buffered Tyrode's solution 100

Table 2.9. Composition of HEPES and bicarbonate-buffered Tyrode's solutions with reduced [Na^+] 102

Table 2.10. Composition of solution used to mimic the intracellular environment 104

Table 2.11. Composition of two-times SDS sample buffer 105

Table 2.12. Details of the specific antibodies used to detect the α-isoforms of the Na^+-K^+-ATPase pump, SERCA2 and calsequestrin 108

Table 3.1. Effect of ascending aortic constriction on heart weight and heart-to-body weight ratio in all animal groups 112

Table 3.2. Effect of removal of the ascending aortic constriction on heart weight and heart-to-body weight ratio 112

Table 3.3. Force-frequency relationships ($T_{(1.6/0.8)}$) and heart-to-body weight ratios in isolated papillary muscles from control and aortic-constricted guinea-pig hearts 117

Table 3.4. Force-frequency relationships ($T_{(1.6/0.8)}$), post-rest tension and heart-to-body weight ratios in LV papillary muscles from debanded and sham-sham operated guinea-pig hearts 120

Table 3.5. Effect of strophanthidin on post-rest tension in control and aortic-constricted guinea-pig myocardium 125

Table 3.6. The effect of increased extracellular [Ca] on contractile function and the force-frequency relationship ($T_{(1.6/0.8)}$) in isolated myocardium from control hearts 129

Table 3.7. Heart-to-body weight ratios and intracellular [Na^+] measured using ion-selective microelectrodes in isolated papillary muscles from control and aortic-constricted hearts 132

Table 3.8. Changes in pH_i and the rate of recovery of pH_i on NH_4Cl removal in the absence of amiloride in bicarbonate- and HEPES-buffered Tyrode's solution 149

Table 3.9. Summary of H^+ efflux rates in HEPES- and bicarbonate-buffered Tyrode's solution in cells from control and aortic constricted hearts 152

Table 3.10. Change of $[Ca^{2+}]_i$ during exposure to 40 mM KCl in isolated myocytes measured using the fluorescent indicator, Fura-2 161

Table 3.11. Change of $[Ca^{2+}]_i$ on application of 10 mM caffeine (after a brief exposure to 40 mM KCl) in isolated myocytes measured using the fluorescent indicator, Fura-2 161

Table 3.12. Change of $[Ca^{2+}]_i$ during superfusion with reduced external Na solution (29 mM NaCl Tyrode's) in isolated myocytes measured using the fluorescent indicator, Fura-2 163

Table 3.13. Change of $[Ca^{2+}]_i$ on application of 10 mM caffeine (after superfusion with reduced external Na solution (29 mM NaCl Tyrode's)) in isolated myocytes measured using the fluorescent indicator, Fura-2 166

Table 3.14. Peak and nadir of $[Ca^{2+}]_i$ and the time constant of the decay of the caffeine response (after a brief exposure to 40 mM KCl) in isolated myocytes. $[Ca^{2+}]_i$ measured using the fluorescent indicator, Fura-2 168

Table 4.1. Summary of published values for $[Na^+]_i$ in muscle strips, isolated myocytes and intact heart 181

Table 4.2. Effect of temperature, species and the method of measurement on $[Na^+]_i$ 183

Table 4.3. Summary of values for pH_i in muscle strips, isolated myocytes and intact heart 186

Table 4.4. Summary of values for resting $[Ca^{2+}]_i$ in muscle strips, isolated myocytes and intact heart 190

Table 4.5. Studies of $[Na^+]_i$ in myocardial hypertrophy 195

Table 4.6. Summary of studies of the α-isoforms of the Na^+-K^+-ATPase pump 201

Table 4.7. Summary of values of pH_i in hypertrophied myocardium 204

Table 4.7. Summary of values of $[Ca^{2+}]_i$ in hypertrophied myocardium 209

List of Abbreviations

β	cellular H^+ buffering capacity (mequiv.l^{-1}.pH $unit^{-1}$)
β_i	intrinsic cellular H^+ buffering capacity (mequiv.l^{-1}.pH $unit^{-1}$)
β_{tot}	combined bicarbonate and intrinsic cellular H^+ buffering capacity (mequiv.l^{-1}.pH $unit^{-1}$)
AII	angiotensin II
AC	aortic constricted
AE	anion exchanger
AL	aldosterone
AM	acetoxymethylester
ANP	atrial natriuretic peptide
AP	action potential
APD	action potential duration
ATP	adenosine triphosphate
BCECF	2',7'-bis(carboxyethyl)-5(6)-carboxyfluorescein
°C	centigrade
$[Ca^{2+}]_i$	intracellular calcium concentration
CAPSO	3-[cyclohexylamino]-2-hydroxyl-1-propanesulphonic acid
CICR	calcium induced calcium release
Cx	connexin
Dahl	deoxycorticosterone-acetate salt sensitive hypertension
Deb	debanded
$\Delta[Ca^{2+}]_i$	change of intracellular Ca^{2+} concentration
DIDS	4,4'-diisothiocyanoto-stilbene-2,2'-disulphonic acid
DOCA	deoxycorticosterone-acetate
DTT	dithiothreitol
ECG	electrocardiogram
ECL	enhanced chemiluminescence
EDTA	ethylene diamine tetra-acetic acid
EGTA	ethylene glycol-bis-(β-aminoethyl ether) N,N,N',N'-tetra acetic acid
E_{Ca}	electrochemical gradient for Ca^{2+}
E_{ISE}	total potential recorded by ion-selective microelectrode
E_m	resting membrane potential

E_{Na}	Na^+ equilibrium potential
$E_{Na.Ca}$	equilibrium potential for the Na^+-Ca^{2+}-exchanger
fA	femptoamps
FET	Field effect transistor
g	gram
HBR	heart-to-body weight ratio
HCM	hypertrophic cardiomyopathy
HEPES	N-[2-hydroxyethyl] piperazine-N'-[2-ethanesulphonic acid]
HOCM	hypertrophic obstructive cardiomyopathy
HRP	horseradish peroxidase
Hz	hertz
I_{Ca}	L-type Ca^{2+} channel current
$I_{Ca(TTX)}$	Tetrodotoxin-inhibitable voltage-gated Ca^{2+} conducting Na^+ channel
ISE	ion-selective microelectrode
J_H	acid-equivalent efflux
KB	Kraftbrühe
K_d	dissociation constant
kg	kilogram
l	litre
LV	left ventricle
LVH	left ventricular hypertrophy
MES	2-[N-morpholino] ethane-sulphonic acid
mm	millimetre
nm	nanometre
M	molar
min	minutes
ml	millilitre
µl	microlitre
mM	millimolar
µM	micromlar
ms	millisecond
mV	millivolt
LV dP/dt_{max}	maximum first derivative of left ventricular pressure
n	number

$[Na^+]_i$	intracellular Na^+ concentration
$[Na^+]_o$	extracellular Na^+ concentration
NHE	Na^+-H^+-exchanger
ns	not significant
Ω	Ohm
3-OMFPase	K-dependent 3-0-methylfluorescein phosphatase
op amp	operational amplifier
PBS	phosphate buffered saline
PCR	polymerase chain reaction
pd	potential difference
pH_I	intracellular pH
pH_o	extracellular pH
pNPPase	K-dependent paranitrophenyl phosphatase activity
PVDF	polyvinyl difluoridine membrane
r	correlation coefficient
R	ratio of fluorescent outputs
RT-PCR	reverse transcription polymerase chain reaction
RV	right ventricle
RVH	right ventricular hypertrophy
SA	sino-atrial
S.D	standard deviation
SDS	sodium dodecyl sulphate
SDS-PAGE	sodium dodecyl sulphate-polyacrylamide gel electrophoresis
secs	seconds
S.E.M	standard error of the mean
SERCA	sarcoplasmic reticulum Ca^{2+}-ATPase
SHR	spontaneously hypertensive rat
SNARF	carboxyseminaphthorhodafluor
SR	sarcoplasmic reticulum
τ_1	time constant of the recovery phase of the caffeine transient
τ_2	time constant of recovery of the undershoot of the caffeine transient
T	tension
TTX	tetrodotoxin
V	volt

vs	versus
wt	weight
w/v	weight/volume
^{31}P-NMR	proton-decoupled phosphorus-31 magnetic resonance spectroscopy
$[i]_i$	intracellular concentration of an ion, i
$[i]_o$	extracellular concentration of an ion, i

Chapter 1: Introduction

Left ventricular hypertrophy (LVH) is an adaptive process that enables the heart to compensate for an increased mechanical load such as aortic stenosis or systemic hypertension. However, in population studies the presence of electrocardiographic or echocardiographic LVH is associated with increased mortality due to ventricular arrhythmias (Levy *et al.*, 1987) and heart failure (Levy *et al.*, 1990). Studies in animal models suggest that there is a gradual transition from compensated hypertrophy to decompensation and heart failure (Siri *et al.*, 1989; Capasso *et al.*, 1990). A similar transition is seen in patients with systemic hypertension and aortic stenosis in whom gradual chronic pressure overload of the left ventricle results in myocardial hypertrophy with subsequent dilatation and heart failure.

The mechanisms underlying this decompensation remain unclear but preliminary evidence suggests that the changes are gradual, originating in the compensated phase of hypertrophy and represent alterations to cell physiology that underlie electrical and mechanical dysfunction. Regression of LVH after removal of the abnormal load is well documented (Ikonomidis *et al.*, 2001; Sleight *et al.*, 2001). It is therefore, of clinical importance to ascertain the properties of hypertrophied myocardium that develop and which if left untreated result in a decline in cardiac function. A better understanding of the primary mechanisms involved in the response of the heart to chronic pressure overload may facilitate the development of new therapeutic modalities, as well as the development of better guidelines for the prevention of cardiac hypertrophy.

1. Clinical pathology of left ventricular hypertrophy

The myocardium has a remarkable ability to alter its structure in response to sustained changes in haemodynamic load. Physiological or pathological circulatory changes that result in a sustained increase in load, eventually result in an increase in heart weight. Growth occurs to normalise wall stress where wall stress is described by Laplace's Law as

$$\text{Wall stress} = \frac{\text{pressure} \times \text{radius}}{2 \times \text{wall thickness}}$$

Under physiological conditions such as growth or aerobic training, cardiac output is maintained by an increase in stroke work. Chamber radius increases and wall stress rises. However, with time myocardial growth occurs and wall thickness increases until wall stress is normalised. The hypertrophy produced is proportional to the increase in chamber size demanded by the increase in stroke work. The hypertrophy is mild and left ventricular function is preserved.

Pathological conditions such as aortic valve stenosis and systemic hypertension also produce a sustained increase in afterload. Left ventricular pressure increases to overcome the resistance to ejection and wall stress increases. Myocardial growth occurs to normalise wall stress by becoming thicker without an increase in radius. As a result there is symmetrical thickening of the ventricular walls at the expense of cavity size. This process is referred to as concentric left ventricular hypertrophy.

It is now recognised that even during the compensated phase of hypertrophy there are changes to the normal physiology of the myocardium. Impaired diastolic relaxation is the earliest evidence of dysfunction in LVH (Topol *et al.*, 1985). As the hypertrophied ventricle becomes stiffer, ventricular filling is impaired (Cuocolo *et al.*, 1990). However, as hypertrophy progresses systolic function also becomes impaired, the ventricle begins to dilate and stroke volume falls. This decompensation is associated with increased sympathetic tone and activation of the renin-angiotensin system in an attempt to compensate for the reduced cardiac output. This decompensated phase is recognised clinically as congestive cardiac failure. It represents the end-stage of the disease process when irreversible structural changes have already occurred. Heart failure is associated with considerable mortality and morbidity, with a median survival of 1.7 years in men and 3.2 years in women (Lloyd-Jones, 2001).

The mechanism underlying mechanical dysfunction in LVH is incompletely understood. LVH increases myocardial oxygen consumption and reduces coronary blood-flow reserve (Houghton *et al.*, 1990) due to raised minimal coronary vascular resistance and greater systolic flow impediment (O'Gorman *et al.*, 1992). This mismatch between supply and demand may predispose the patient to ischaemia and myocardial infarction. Factors associated with hypertension are atherogenic (Levy *et al.*, 1988) so coronary blood flow may be further compromised by atherosclerosis. These effects result in

greater metabolic disadvantage and hypoxia following brief periods of ischaemia especially during increased cardiac work in hypertrophied myocardium (McAinsh *et al.*, 1995).

In addition to mechanical dysfunction, other changes occur to muscle physiology during the process of hypertrophy which affect the electrophysiology of the myocardium and present clinically as sudden death. The Framingham study showed that both electrocardiographically (Kannel *et al.*, 1975) and echocardiographically (Haider *et al.*, 1998) detected LVH are associated with an increased risk of sudden death that was in excess of the risk attributable to hypertension or other associated cardiovascular risk factors (Kannel & Sorlie, 1981). Sudden death is a recognised consequence of ventricular fibrillation or ventricular tachycardia in almost all monitored cases. Electrocardiographic (McLenachan *et al.*, 1987) and echocardiographic (Levy *et al.*, 1987) evidence of LVH are associated with an increased risk of simple and complex ventricular arrhythmias. Mortality is increased in subjects with asymptomatic ventricular arrhythmias and echocardiographically determined LVH (Bikkina *et al.*, 1993).

The susceptibility of the hypertrophied myocardium to ventricular arrhythmias appears to be independent of myocardial ischaemia (Szlachcic *et al.*, 1992), however, in the presence of ischaemia, hypertrophy further increases the risk of arrhythmias (Aronow *et al.*, 1988). Regression of LVH is associated with a reduced risk of arrhythmias (Messerli *et al.*, 1989) but studies to date are too small to determine the effect of regression on sudden cardiac death. These observations suggest that there is a primary abnormality in hypertrophy that predisposes to arrhythmias.

Population screening studies using electrocardiographic and echocardiographic techniques demonstrate that the prevalence of LVH is high in the general population and increases with age. In men and women under the age of 30, echocardiographic evidence of LVH is 8% and 5% respectively, increasing to 33% and 49% respectively in those over the age of 70 (Kannel *et al.*, 1992). Hypertension is the chief precursor of LVH. Sudden cardiac death accounts for between 50,000 and 100,000 deaths per year in the UK (Pye & Cobbe, 1992). LVH is associated with an increased risk of sudden cardiac death and heart failure indicating that LVH is a major public health problem.

Mechanisms of ventricular arrhythmias include automaticity, triggered activity and re-entry. Both automaticity and triggered activity give rise to aberrant pacemaker activity via early and late afterdepolarisations, which are thought to be produced by electrophysiological mechanisms operating at the level of the single cell. Re-entry is a function of multicellular tissue which occurs when propagation of the action potential from cell to cell is impaired. Re-entry is thought to be the most important mechanism in ventricular tachycardia. The requirements for producing re-entry in cardiac muscle include unidirectional block and decremental conduction. Several factors have been proposed to exacerbate re-entrant excitation, including anisotopic conduction and small scale discontinuities (about 100 μm) in the conduction pathway (Spach *et al.*, 1981; Spach & Heidlage, 1995).

1.1. Electrophysiological changes in hypertrophy

The most widely reported electrophysiological change associated with hypertrophy is prolongation of the action potential duration (APD). Prolonged APD has been reported in rats (Gulch *et al.*, 1979; Aranson, 1980; Thollon *et al.*, 1989; Stilli *et al.*, 2001), guinea-pigs (Nordin *et al.*, 1989), cats (Kleiman & Houser, 1988) and rabbits (Bril *et al.*, 1991) using isolated superfused papillary muscles (Gulch *et al.,* 1979; Aronson 1980) and isolated myocytes (Kleiman & Houser, 1988; Nordin *et al.*, 1989; Ahmmed *et al.*, 2000; Milnes & MacLeod, 2001; Stilli *et al.*, 2001). If this occurs *in-vivo* it could result in an increased propensity to arrhythmias. However, no change in APD was observed in isolated superfused tissue from humans with LVH (McIntyre & Fry, 1997). Moreover, the changes in APD observed in isolated superfused tissues have not been consistently observed *in-vivo*. Monophasic action potentials recorded from hypertrophied feline hearts *in-vivo* showed no change in APD compared to control (Kowey *et al.*, 1991) and effective refractory periods were unchanged in dogs with left ventricular hypertrophy (Martins *et al.*, 1989). No change in epicardial action potentials recorded from perfused beating hypertrophied hearts was observed (Winterton *et al.*, 1994), although isolated myocytes from hypertrophied hearts with congestive cardiac failure showed prolongation of early repolarisation (Ryder *et al.*, 1991). An *in-vivo* study in dogs with LVH, showed prolongation of APD and an increased propensity to develop early afterdepolarisations during the plateau phase of the action potential that could trigger ventricular tachycardia (Ben-David *et al.*, 1992). One reason for the discrepancy between *in-vitro* and *in-vivo*

findings is that isolated myocardial tissue is frequently studied at very low stimulation frequencies and since stimulation frequency has a marked influence on action potential duration the changes observed may be related to the stimulation conditions. This explanation is supported by the absence of action potential prolongation in hypertrophied myocytes paced at higher stimulation frequencies (Nordin *et al.*, 1989; Davey *et al.*, 2001).

Non-uniform prolongation of action potential may also be proarrhythmic by increasing dispersion of repolarisation or refractoriness and favouring re-entry. LVH has also been reported to produce regional differences in electrophysiological effects with prolongation of APD in epicardial but not endocardial cells seen both in isolated cells (Hicks *et al.*, 1995; Bryant *et al.*, 1997) and whole hearts (Wolk *et al.*, 2000). Increased dispersion of ventricular repolarisation as measured by the difference between the maximum and minimum monophasic APD on the epicardial surface has also been demonstrated in hypertrophy (Gómez *et al.*, 1997a; Gillis *et al.*, 1998) and this effect is more marked in ischaemia (Wolk *et al.*, 2000). Acute myocardial ischaemia increases APD dispersion between the normal and ischaemic zones in rat hearts and regression of LVH reduces this electrical inhomogenity (Kohya *et al.*, 1995).

Delayed ventricular activation, indicated by prolongation of the QRS duration on the electrocardiogram (ECG) is a recognised feature of LVH in man (Winterton *et al.*, 1994). In patients with echocardiographically documented LVH, programmed electrical stimulation shows significant prolongation of infra-nodal conduction and an increased incidence of non-sustained ventricular tachycardia (Coste *et al.*, 1988). Delayed conduction time has been demonstrated in isolated preparations from guinea-pigs (Winterton *et al.*, 1994) and humans (McIntyre & Fry, 1997) with LVH. Accentuation of the conduction delay was also observed during ischaemia (Winterton *et al.*, 1994; Cooklin *et al.*, 1998). This is likely to increase the arrhythmogenic potential in hypertrophied myocardium as slowed conduction is important in creating conditions necessary to sustain re-entrant arrhythmias.

In the guinea-pig delayed conduction has been attributed to reduced electrical coupling between cells (Cooklin *et al.*, 1997) and is associated with a 3 fold increase in gap-junction resistance under normal conditions and a 5 fold increase during hypoxic

conditions (Cooklin *et al.*, 1998). If the increase in gap junction resistance is sufficient (above 1000 Ω cm) it will delay propagation at the gap junctions and increase the likelihood of unidirectional block and re-entrant arrhythmias by discontinuous propagation (Quan & Ruddy, 1990). Even, if hypertrophy alone were not sufficient to generate discontinuous propagation, the increased susceptibility of the hypertrophied heart to ischaemia would further increase gap junction resistance so that the combination of hypertrophy and ischaemia would be effective in increasing the incidence of such abnormal electrical activity.

The normal pattern of anisotropic conduction in ventricular myocardium, by which conduction parallel to the longitudinal axis of the myocyte is up to 4 times faster than that along the transverse axis is altered in LVH; the anisotropic ratio was reduced largely due to a reduction in longitudinal conduction velocity (Carey *et al.*, 2001). More recently using a three dimensional map of intracellular resistance we have shown that local discontinuities of current flow on a millimetre scale which would be sufficient to increase susceptibility to re-entrant mechanisms are more prevalent in hypertrophied myocardium (Fry *et al.*, 2001).

1.2. Gap junctions

The changes in conduction velocity observed in hypertrophy may result from remodelling and / or redistribution of gap junctions. The normal pattern of anisotropic conduction in ventricular myocardium described above is dependent on the low-resistivity of the gap-junction membranes, their distribution, and their abundance. Gap junctions include a hexagonal array of proteins called connexins, which provide electrical coupling between cells. Three connexins, 43, 40 and 45 are expressed in mammalian heart and the predominant one is connexin 43 (Cx43). In normal myocardium, gap junctions are predominantly located at the axial ends of ventricular myocytes and form end-to-end connections.

1.2.1. Connexin proteins in hypertrophy

Reduced expression of Cx43 has been demonstrated in hypertrophied human myocardium (Peters *et al.*, 1993b). On the other hand there was no alteration in Cx43 in

hypertrophied rat hearts made hypertensive by renal artery clipping or deoxycorticosterone / salt administration (Haefliger *et al.*, 1997) and moreover increased Cx43 protein has been reported in the early phase of hypertrophy due to renovascular hypertension in guinea-pigs (Peters *et al.*, 1993a). Rather than a change in the number of connexins, an altered pattern of distribution may occur. Disturbed Cx43 gap junction distribution has been shown to correlate with the location of re-entrant circuits in the epicardial border zone of healing canine infarcts (Peters *et al.*, 1997). In the hypertrophied left ventricle of aortic-banded rats, redistribution of Cx43 from the longitudinal to the transverse axis has been demonstrated (Emdad *et al.*, 2001). Similar redistribution was observed in pressure overload-induced right ventricular hypertrophy in rats in association with alteration of anisotropic conduction properties (Uzzaman *et al.*, 2000) similar to those reported by Carey *et al* (2001). Gap junction conductance is also influenced by the state of phosphorylation (Moreno *et al.*, 1994) with phosphorylation of Cx43 reducing conductance and changes in cytoplasmic metabolism such as intracellular acidosis (Firek & Weingart, 1995) and an increase in intracellular Ca^{2+}, $[Ca^{2+}]_i$, (Maurer & Weingart, 1987) also reducing conductance. As discussed later changes to intracellular pH and Ca^{2+} have been described in hypertrophy.

1.3. Contractile function in myocardial hypertrophy

Studies of contractile function in animal models of hypertrophy are conflicting. These conflicting findings may be due to the particular model studied, the age of the animal at the time of the insult, differences in the response of the right and left ventricle to pressure-overload, the duration of pressure-overload, the degree of hypertrophy produced or the way in which contractile function was measured.

In isolated myocardial preparations studies of right ventricular myocardium exposed to mechanical overload show either no change to (Yoneda *et al.*, 2001) or decreased (Kaufmann *et al.*, 1971; Gwathmey & Morgan, 1985) peak tension generation at constant stimulation frequency. Comparing juvenile and weanling ferrets subjected to pressure overload, Gwathmey *et al* (1995) showed that peak tension declined in the former but increased in the latter as external calcium was increased, and suggested that this was due to differences in myocyte remodeling in the two groups. In most studies irrespective of

the effect on peak tension, the isometric tension profile and in particular the relaxation phase is prolonged (Gwathmey & Morgan, 1985; Yoneda *et al.*, 2001).

In LVH studies are also conflicting. In isolated myocytes from the spontaneously hypertensive rat (SHR) (Delbridge *et al.*, 1996), and in rats with abdominal aortic-constriction contractile function was depressed (McCall *et al.*, 1997). In left ventricular myocytes from severe hypertrophy in the cat, reduced contraction amplitude, longer duration of contraction and reduced velocity of both contraction and relaxation were observed (Bailey & Houser, 1992). In severe but not mild hypertrophy secondary to aortic banding in the guinea-pig, a decrease in peak tension was associated with slowed tension development (Lecarpentier *et al.*, 1987). Other studies, however (Capasso *et al.*, 1982; Flesch *et al.*, 1997; Milnes & MacLeod, 2001) show no effect on peak isometric tension generation, but prolonged time to peak tension and reduced shortening velocity. In isolated myocytes from guinea-pigs with mild LVH induced by infra-renal aortic banding, contraction size was increased and time-to-peak contraction and half-relaxation time were both prolonged (Davey *et al.*, 2001). In intact ventricles from pigs subjected to pressure-overload indices of contractile function were normal (Wisenbaugh *et al.*, 1983), whereas in ferrets with LVH both systolic and diastolic function were impaired (Bentivegna *et al.*, 1991) and in rats with abdominal aortic-constriction increased systolic function was observed from early to late stages of hypertrophy (Ohkusa *et al.*, 1997). In one study, SHR's showed normal systolic function until the later stages of hypertrophy when it was depressed (Mirsky *et al.*, 1983), whereas in other studies both enhanced (Shorofsky *et al.*, 1999; Mill *et al.*, 1998) and reduced (Wise *et al.*, 1998) contractility were observed in this model. It is important to point out that like the electrophysiological investigations, many of these studies were carried out at low pacing rates and there is little information on cardiac function in hypertrophy at more physiological heart rates.

Changes to the interstitial environment are known to occur at least in some models of hypertrophy, including increases in connective tissue content, in diffusion distance from the capillary to the centre of the muscle cell and in myocardial stiffness, and these could influence contractile function. However, evidence suggests that the abnormalities of contractile function seen in hypertrophy are an intrinsic property of the cardiac muscle

cell rather than a mechanically normal cell contracting in an abnormal interstitial environment (Mann *et al.*, 1991).

1n 1871, Bowditch *et al* noted that in contracting myocardium the interval between beats was one of the most important factors that determined the strength of contraction. This allows quantification of contractile function independent of preload and afterload (Anderson *et al.*, 1973) and can be studied by investigating the strength of contraction (i) in relation to the preceding stimulus interval, mechanical restitution and (ii) in response to sequential increase in the frequency of stimulation, the force-frequency relationship.

To describe the various force-interval relationships in myocardium, Koch-Weser and Blinks (1963) introduced the abstract terms of positive and negative inotropic effects of activation. Increasing stimulation frequency can cause a positive effect on contractility by increasing sarcoplasmic reticulum (SR) Ca^{2+} load or a negative effect due to refractoriness of excitation-contraction coupling. The balance between these factors will determine whether the force-frequency response is positive, negative or biphasic, *i.e.* a combination of both. Normal ventricular myocardium from humans and most animal species demonstrates a positive force-frequency relationship *i.e.* increasing stimulus frequency increases contractility, whereas in failing myocardium a negative relationship is found (Mulieri *et al.*, 1992; Davies *et al.*, 1995; Pieske *et al.*, 1999). Negative force-frequency relationships are also seen in rat and ferret ventricle and in atrial myocardium (Koch-Weser & Blinks, 1963; Wang *et al.*, 1993). The negative force-frequency relationship has been attributed to the short action potential duration typical of rat ventricular muscle and atrial tissue, however, in human myocardium a negative force-frequency response has been observed despite the presence of long action potentials (Mubagwa *et al.*, 1994).

1.3.1. Force-frequency relationships in hypertrophy

We have previously shown a progressive decline from a positive to a negative force-frequency relationship in human myocardium from patients with aortic and mitral valve disease that correlated with the degree of hypertrophy (Gray *et al.*, 2001). In isolated left ventricular myocytes from dogs with chronic atrio-ventricular block induced

hypertrophy, cell shortening was greater at frequencies less than 120 beats per minute and tended to decrease with increasing frequencies (Sipido *et al.*, 2000).

1.4. Excitation-contraction coupling

Excitation-contraction coupling qualifies a process by which voltage changes induce Ca^{2+} movement that originates both from the external milieu and from internal stores. During depolarisation Ca^{2+} influx is mediated by the dihydropyridine sensitive, voltage-activated L-type Ca^{2+} channels and Na^{+}-Ca^{2+}-exchange. During repolarisation Ca^{2+} efflux occurs through Na^{+}-Ca^{2+}-exchange that couples the efflux of 1 Ca^{2+} to the influx of 3 Na^{+}. This efflux of Ca^{2+} is electrogenic without direct energy expenditure and tends to depolarise the cell. This Na^{+} influx together with the Na^{+} influx through the Na^{+} channel increases intracellular $[Na^{+}]$, $[Na^{+}]_i$, which is in turn controlled by the Na^{+}-K^{+}-ATPase which causes Na^{+} efflux in exchange for K^{+} and is closely linked to the Na^{+}-Ca^{2+}-exchanger. The amount of Na^{+} necessary to account for the rapid depolarisation phase of the action potential in cardiac cells is small, approximately 1 $nmol.l^{-1}$ cell water (Pike *et al.*, 1993).

The internal stores of Ca^{2+} are located in the SR where the concentration of Ca^{2+} is much higher than in the rest of the intracellular space. Ca^{2+} needs energy to enter the SR and utilises Ca^{2+} ATPase. The release of Ca^{2+} from the SR is under the control of a Ca^{2+} channel, called the ryanodine receptor. The external Ca^{2+} entering the cell activates the Ca^{2+} release channel, giving rise to the phenomenon of Ca^{2+}-induced Ca^{2+}-release (CICR). The two principal sources of Ca^{2+} that may provide the activating calcium for CICR are the sarcolemmal dihydropyridine sensitive, voltage-activated L-type Ca^{2+} channels and the Na^{+}-Ca^{2+}-exchanger. Under normal circumstances the major source of Ca^{2+} to trigger CICR is Ca^{2+} entry via the L-type Ca^{2+} channels. The resulting rise in intracellular $[Ca^{2+}]$, $[Ca^{2+}]_i$ is too small to activate the myofilaments but can trigger a larger release of Ca^{2+} from the SR. The potential role of Ca^{2+} entry via other mechanisms such as reverse mode Na^{+}-Ca^{2+}-exchange is discussed below.

Myocardial cells contain at least two types of voltage-activated Ca^{2+} channels. The L-type Ca^{2+} channels are responsible for a slow inward current, activate at potentials > -40mV, generate peak inward currents at about 0mV and inactivate relatively slowly. The

L-type Ca^{2+} channels are responsible for the majority of Ca^{2+} that enters the cardiac cell during the plateau phase of the action potential. The T-type Ca^{2+} channels activate at more negative potentials and have faster kinetics. T-type Ca^{2+} channels are present in all types of cardiac cells but are more prevalent in atrial cells, sino-atrial (SA) node cells and Purkinje cells and are thought to play a role in pacemaker activity. Evidence in normal ventricular myocardium suggests that Ca^{2+} influx through T-type Ca^{2+} channels cannot trigger normal phasic contractions (Bouchard *et al.*, 1993).

The threshold level of intracellular Ca^{2+} that causes Ca^{2+}-induced Ca^{2+}-release is approximately 0.5 μM (Fabiato & Fabiato, 1978). However, the amount of Ca^{2+} released from the SR is not simply determined by the amount of Ca^{2+} that enters the cytoplasm but also by the rate of increase (Fabiato & Fabiato, 1978). The local control hypothesis of excitation-contraction coupling proposes that Ca^{2+} influx causes a local increase in $[Ca^{2+}]_i$, in diffusion-limited subsarcolemmal spaces (called the 'restricted space') where the T-tubules and junctional SR are in close proximity. This promotes Ca^{2+} binding to and opening of the Ca^{2+} release channel (the ryanodine receptor) in the junctional SR and the resulting SR Ca^{2+} release causes the cytosolic Ca^{2+} transient. In keeping with this hypothesis detailed ultrastructural studies have demonstrated a close physical relationship between the sarcolemmal L-type Ca^{2+} channel, the Na^{+}-Ca^{2+}-exchanger, and the ryanodine receptor in the junctional SR (Carl *et al.*, 1995; Sun *et al.*, 1995).

Application of laser scanning confocal microscopy and Ca^{2+}-sensitive fluorescent indicators to myocardial cells has made it possible to measure local non-propagating elevations of $[Ca^{2+}]_i$, called Ca^{2+} sparks, at the level of individual sarcomeres (Cheng *et al.*, 1993). These Ca^{2+} sparks represent the release of Ca^{2+} from one or a cluster of SR Ca^{2+} release channels (ryanodine receptors) triggered by the opening of a single L-type Ca^{2+} channel. (Shachlock *et al.*, 1995; Santana *et al.*, 1996). Recent evidence confirms that Ca^{2+} sparks sum independently to produce the whole-cell Ca^{2+} transient (Cleemann *et al.*, 1998; Tanaka *et al.*, 1998). These studies provide direct experimental evidence for local control hypothesis of excitation-contraction coupling in cardiac muscle in which macroscopic L-type Ca^{2+} currents and whole-cell Ca^{2+} transients are explained in terms of spatial and temporal summation of single L-type Ca^{2+} channel currents and Ca^{2+} sparks respectively.

The L-type Ca^{2+} current is the major trigger for Ca^{2+} release, however other triggers have been suggested. It has been proposed that Na^+ entry into the 'restricted space' during the action potential, rapidly increases the local intracellular Na^+ concentration, which activates the Na^+-Ca^{2+}-exchanger in the reverse direction generating an inward Ca^{2+} flux that then triggers the release of Ca^{2+} from the SR. The direction of the Ca^{2+} fluxes produced by Na^+-Ca^{2+}-exchange depends on the electrochemical gradients for Na^+ (E_{Na}), and Ca^{2+} (E_{Ca}) and the membrane potential (E_m). For an electrogenic 3 Na^+ for 1 Ca^{2+} exchange: $E_{NaCa} = 3E_{Na} - 2E_{Ca}$. In cardiac muscle cells the reversal potential is readily encountered under physiological conditions and can be changed by small changes in $[Na^+]_i$. Accordingly when the membrane potential is depolarised strongly or when intracellular Na^+ is elevated, reverse-mode Na^+-Ca^{2+} exchange activity can increase myoplasmic Ca^{2+}.

Reverse-mode Na^+-Ca^{2+} exchange has been demonstrated in feline (Nuss & Houser, 1992) and guinea-pig (Kohmoto *et al.*, 1994; Levi *et al.*, 1994b) ventricular myocytes. However, studies in the rat suggest that the release of SR Ca^{2+}, thought to be due to reverse-mode Na^+-Ca^{2+}-exchange is more likely due to loss of voltage control either throughout the cell or in the T-tubules (Bouchard *et al.*, 1993). Furthermore, Ca^{2+} entry via reverse-mode Na^+-Ca^{2+}-exchange does not trigger Ca^{2+} sparks but rather a slow increase in intracellular Ca^{2+} (López-López *et al.*, 1995) and the contractions initiated are slow (Nuss & Houser, 1992) with a delayed onset of the Ca^{2+} transient (LeBlanc & Hume, 1990). It is possible that there are species differences in the role of the reverse mode of the Na^+-Ca^{2+}-exchanger in the initiation of contraction in the normal heart and the exchange may become important in pathological conditions or if intracellular Na^+ is elevated. Recently, increased Ca^{2+} influx via the exchanger, contributing to SR Ca^{2+} loading has been described in dogs with LVH (Sipido *et al.*, 2000) and in rabbit heart after myocardial infarction (Litwin & Bridge, 1997).

A TTX-inhibitable, voltage-gated Ca^{2+} conducting Na^+ channel ($I_{Ca(TTX)}$) has been identified in human atrial (Lemaire *et al.*, 1995), rat ventricular (Aggarwal *et al.*, 1997) and guinea-pig (LeBlanc *et al.*, 1996) ventricular cells. This channel activates over a more negative voltage range than the classic cardiac Na^+ channels and is highly permeable to Ca^{2+}. Under non-physiological experimental conditions (Na free external and internal solutions), Ca^{2+} entry via this channel can trigger SR Ca^{2+} release (Thomas

et al., 1995) but whether it plays a role in excitation-contraction coupling under physiological conditions is unclear.

Recently, it has been postulated that a component of SR Ca^{2+} release in mammalian cardiac muscle is activated by changes in membrane voltage. However, on present evidence it seems unlikely that this voltage-sensitive Ca^{2+} release mechanism has an important role to play in excitation-contraction coupling (Wier & Balke, 1999).

The target for the released Ca^{2+} is the contractile apparatus composed of thin filament proteins including the troponin complex. The transient rise in $[Ca^{2+}]_i$, initiates a series of chemical events with cross-bridge formation, which result in cell shortening and or the generation of force. A schematic representation of the events during excitation-contraction coupling is shown in figure 1.1. The magnitude of the force developed by cardiac muscle is largely a function of the sarcoplasmic $[Ca^{2+}]$, and changes to the sensitivity of the contractile proteins to Ca^{2+} are of little importance (Lecarpentier *et al.*, 1987). A reduction in myosin ATPase activity has been shown in rats with LVH (Capasso *et al.*, 1982), and in rabbits (Maughan *et al.*, 1979) and cats (Carey *et al.*, 1978) with right ventricular hypertrophy but not in guinea-pigs (Waldenstöm *et al.*, 1985), pigs (Wisenbaugh *et al.*, 1983) or humans (Mercadier *et al.*, 1983).

Ca^{2+} released into the sarcoplasm from the intracellular stores in the SR or from the extracellular pool via the voltage-gated Ca^{2+} channel is then recovered by the intracellular stores by SR Ca^{2+}-ATPase (SERCA2) or removed from the cell via the Na^+-Ca^{2+}-exhanger to initiate relaxation. Ca^{2+} may also be taken up into mitochondria and removed by the sarcolemmal Ca^{2+}-ATPase but under physiological conditions these amounts are small. Under normal conditions, Ca^{2+} enters the myocyte from the extracellular space down a large, inwardly directed electrochemical gradient. At the normal resting potential of -80 mV and with normal levels of $[Na^+]_i$ there is sufficient energy in the Na^+ electrochemical gradient to remove Ca^{2+} from the cell via Na^+-Ca^{2+}-exchange (termed forward mode Na^+-Ca^{2+}-exchange). This is the principal mechanism for Ca^{2+} extrusion in cardiac myocytes. When the membrane potential is depolarised or $[Na^+]_i$ increases, the energy in the Ca^{2+} electrochemical gradient is sufficient to produce Ca^{2+} entry via reverse-mode Na^+-Ca^{2+}-exchange (Eisner *et al.*, 1984; Bers *et al.*, 1988; Nuss & Houser, 1992). The relative importance of the intracellular stores and the cell

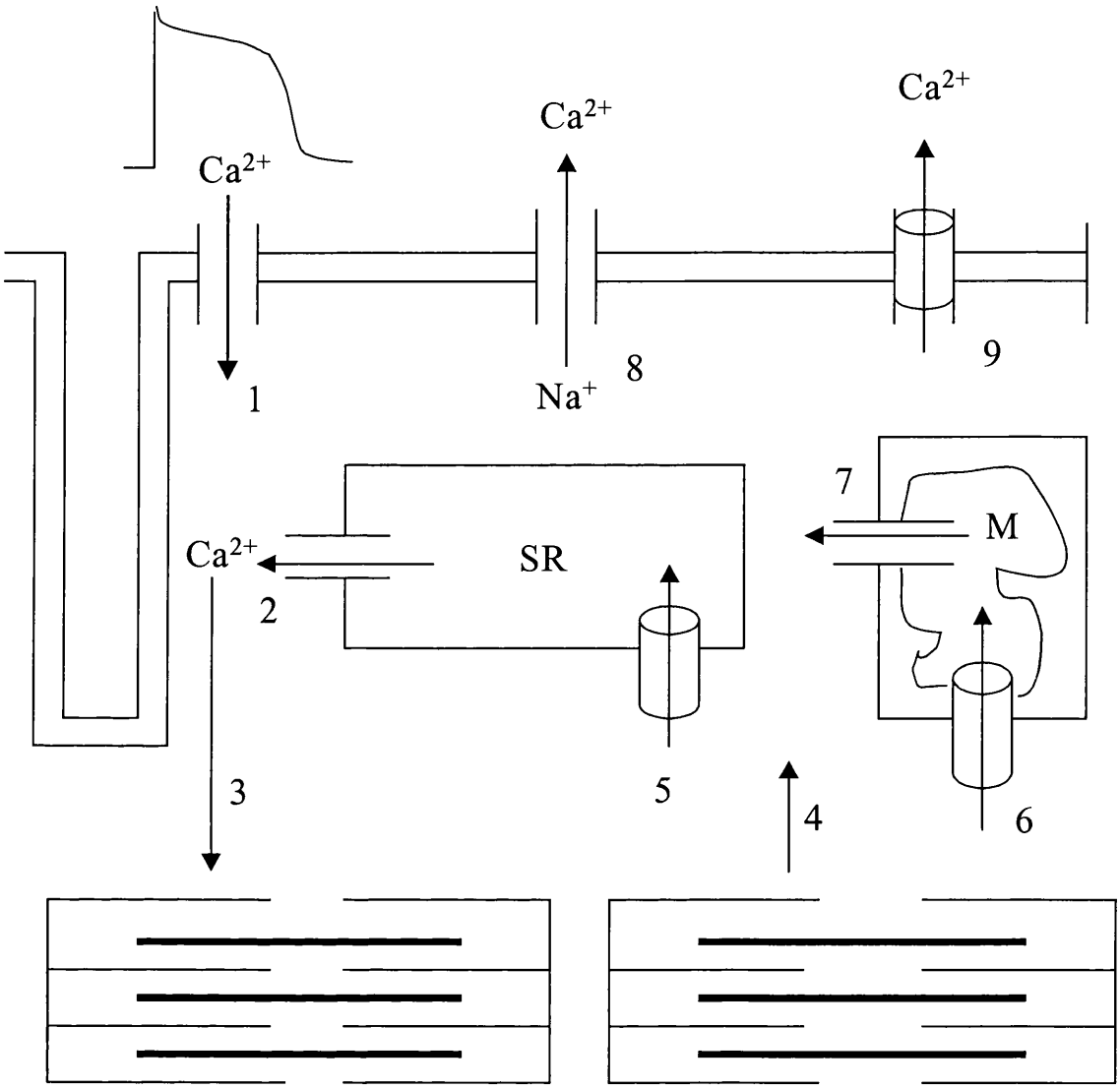

1. Influx of Ca^{2+} via membrane channels during the action potential both directly contributes to the rise in $[Ca^{2+}]_i$ and via;
2. Ca^{2+} induced Ca^{2+} release from the SR
3. Ca^{2+} binds to the myofibrils initiating contraction
4. Relaxation occurs by Ca^{2+} release from the myofibrils consequent upon reduction of $[Ca^{2+}]_i$ due to;
5. Ca^{2+} uptake by the SR Ca^{2+}-ATPase
6. Ca^{2+} uptake by the mitochondria (M) and
7. Transfer to the SR
8. Ca^{2+} efflux via Na^{+}-Ca^{2+} exchange. The net level of $[Ca^{2+}]_i$ is maintained by this exchange and by
9. Ca^{2+} extrusion via the sarcolemmal Ca^{2+}-ATPase

Figure 1.1. Schematic diagram showing the events during excitation-contraction coupling

membrane in regulating sarcoplasmic [Ca^{2+}] varies with species and tissue type (Fabiato & Fabiato, 1979; Cooper & Fry, 1990). In comparison with humans and large mammals, rodents have a higher dependence on SERCA2 relative to Na^+-Ca^{2+}-exchange (Bassani *et al.*, 1994a; Bers *et al.*, 1996). A schematic representation of the ion channels and pumps involved in the regulation of $[Ca^{2+}]_i$ and $[Na^+]_i$ is shown in figure 1.2.

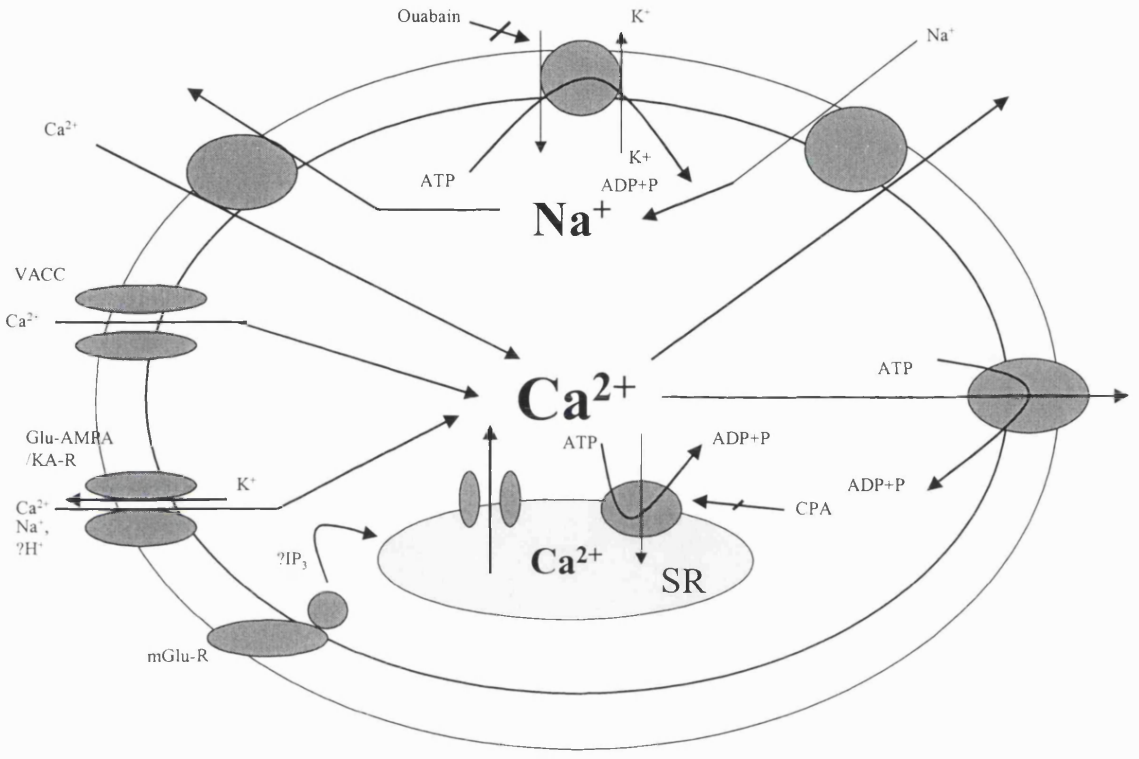

Figure 1.2. Schematic representation of the ion pumps and channels involved in the regulation of $[Ca^{2+}]_i$ and $[Na^+]_i$

1.4.1. 'Ca overload'

Increasing $[Ca^{2+}]_i$ generally results in an increase in tension development. However, under some conditions, developed tension decreases and this fall in tension is described as 'Ca overload'. When calcium levels are progressively elevated, the SR begins to release calcium in oscillatory pulses during diastole and there is a progressive fall in developed tension (Allen *et al.*, 1985a). The fall in tension is presumably due to less Ca^{2+} available for release in systole rather than reduced sensitivity of the contractile proteins to Ca^{2+} in 'Ca overload'. Furthermore, if sufficient amounts of calcium are released during oscillations, the Na^+-Ca^{2+}-exchanger will be activated and since this

exchange is electrogenic it generates an inward current that causes after depolarisations that in turn may contribute to arrhythmias.

1.5. Mechanisms underlying rate-dependant changes in contractile force

1.5.1. Intracellular ions and contractile function

1.5.1.1. Role of intracellular Ca^{2+}

The positive inotropic effect of increasing stimulus frequency is mediated by changes in $[Ca^{2+}]_i$. As stimulation frequency increases the intracellular calcium transient during twitch contraction also increases (Allen & Blinks, 1978). Ca^{2+} entry through the Ca^{2+} channels may increase progressively with increase of stimulation frequency and more Ca^{2+} may accumulate in the SR and be available for release during twitch contraction. The time available for efflux from the cell during diastole is reduced at higher stimulation frequencies resulting in a net gain of $[Ca^{2+}]_i$.

Further support for the hypothesis that the contractile response during changes in stimulation frequency is dependent on the state of calcium loading of the cell comes from the study of Frampton *et al* (1991b). In rat cardiac myocytes demonstrating a positive force-frequency response an increase in systolic Ca^{2+}, diastolic Ca^{2+} and the amount of Ca^{2+} available for release from the SR was observed with increase in stimulation frequency. However, in cells showing a negative force-frequency response, systolic Ca^{2+} decreased or remained unchanged and the amount of Ca^{2+} that could be released from the SR was unchanged.

1.5.1.2. Role of intracellular Na^+

During the action potential $[Ca^{2+}]_i$ rises from ~150 nM to 1μM (Shattock & Bers, 1989) but the influx of Na^+ by I_{Na} is small (1 $nmol.l^{-1}$ cell water). Intracellular Na^+ is typically 6-8 mM but may rise by several mM and result in an increase in contractility as for example after inhibition of the Na^+-K^+-ATPase pump. An increase in stimulation frequency has also been shown to increase $[Na^+]_i$ (Cohen *et al.*, 1982; Harrison *et al.*, 1992b) and appears to be involved in the positive staircase (Boyett *et al.*, 1987; Wang *et*

al., 1988). The rise of $[Na^+]_i$ is believed to result in an elevation of $[Ca^{2+}]_i$ via Na^+-Ca^{2+}-exchange.

The Na^+-Ca^{2+}-exchanger can move Ca^{2+} either inward or outward depending on the magnitude of the electrochemical gradient for Na^+. An increase of $[Na^+]_i$ will decrease the Na^+ gradient across the sarcolemma and thereby attenuate the Ca^{2+} efflux through Na^+-Ca^{2+}-exchange in diastole and increase Ca^{2+} influx during systole. This augments the cellular calcium load, and more Ca^{2+} is available for release during each contraction leading to a larger $[Ca^{2+}]_i$ transient, thus contributing to the positive force-frequency response seen in most species. This is also the mechanism of the positive inotropic action of cardiac glycosides. A schematic representation of this is shown in figure 1.3. Therefore, a rise in $[Na^+]_i$ might contribute to the preservation of myocardial contractility in compensated hypertrophy as the increased $[Na^+]_i$ would enhance Na^+-Ca^{2+} exchange, thereby increasing $[Ca^{2+}]_i$ and contractility.

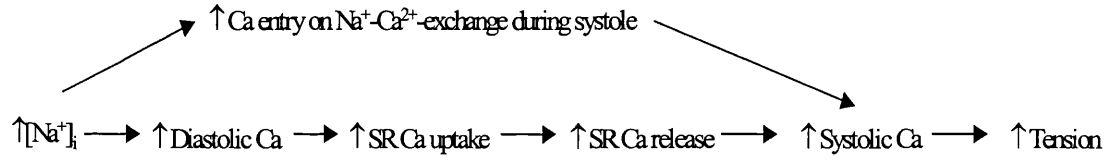

Figure 1.3. Schematic representation of the sodium dependence of twitch tension

As discussed above there is evidence that $[Na^+]_i$ is involved in the positive staircase. However, in species where the $[Na^+]_i$ is elevated at rest such as rat and ferret myocardium, the staircase becomes negative. In isolated sheep Purkinje fibres, a non-linear relationship between the increase of $[Na^+]_i$ and twitch tension was observed and as $[Na^+]_i$ increased sufficiently twitch tension eventually declined (Eisner *et al.*, 1984). Reduction of the force-frequency relationship when $[Na^+]_i$ is raised is probably due to excessive Ca^{2+} influx through Na^+-Ca^{2+}-exchange and overload of intracellular stores. High concentrations of cardiac glycosides reduce twitch force and the intracellular Ca^{2+} transient as the SR is unable to retain Ca^{2+} as the resting SR concentration rises above normal levels (Allen *et al.*, 1985). In the rat, where $[Na^+]_i$ is high, systolic Ca^{2+} transients are diminished at higher frequencies due to enhanced trans-sarcolemmal egress of Ca^{2+} via Na^+-Ca^{2+} exchange (Shattock & Bers, 1989).

The equilibrium potential for the Na^+-Ca^{2+}-exchanger, $E_{Na.Ca}$, is given by the difference between the equilibrium potential for each ion ($E_{Na.Ca} = 3E_{Na}-2E_{Ca}$). In normal myocardium, during diastole $E_{Na.Ca}$ ~-50mV and as the membrane potential, E_m, is ~-80mV, Ca^{2+} extrusion by the exchanger operating in 'forward' mode will be thermodynamically favoured. In contrast when E_m is more positive than $E_{Na.Ca}$, as for example during depolarisation when the rise in membrane potential during the action potential exceeds the rise in $E_{Na.Ca}$ secondary to sarcolemma Ca^{2+} influx, the exchange reverses and Ca^{2+} influx is thermodynamically favoured. When $[Na^+]_i$ is elevated, the $E_{Na.Ca}$ falls, reducing the driving force for Ca^{2+} extrusion thereby elevating Ca^{2+} and consequently tension. This mechanism provides a theoretical basis for the observed species differences in response to alteration in stimulation frequency. The point at which the exchange reverses will be dictated by the duration of the action potential relative to that of the Ca^{2+} transient. This provides a possible explanation for the negative force-frequency relationship in those animals where $[Na^+]_i$ is elevated as Ca^{2+} gain at rest and loss during repetitive activity will be favoured (Shattock & Bers, 1989).

1.5.2. Mechanical restitution

As well as the state of calcium loading of the cell, the recovery of the processes that lead to contraction may play a role in the response of cardiac muscle to changes in stimulation frequency. Mechanical restitution describes the recovery of myocardial contractility during the interval between beats. The processes responsible for the initiation of muscle contraction take a finite time to recover and if a stimulus occurs before this process is complete, contractile force will be reduced.

The processes underlying mechanical restitution remain uncertain but it seems to be largely dependent on the circulation of intracellular Ca^{2+}; an altered sensitivity of the myofilaments to Ca^{2+} does not appear to play a role in intact myocardium (McIvor *et al.*, 1988). In support of the former the variation in isometric force as a function of stimulus interval is mirrored by similar changes in the magnitude of the sarcoplasmic Ca^{2+} transient (Wier & Yue, 1986). The sarcoplasmic Ca^{2+} transient is determined by the Ca^{2+} entering the cell via Ca^{2+} channels and the availability of the calcium sequestered by the SR during relaxation for re-release to activate the myofilaments and initiate contraction. Possible explanations include (i) refractoriness of the inward Ca^{2+} current which acts as a

trigger for release but this is unlikely to be the case in human or guinea-pig myocardium (Cooper & Fry, 1990). (ii) a delay in the transfer of calcium within the SR from the uptake sites in the longitudinal cisternae to the release sites in the terminal cristae (Wier & Yue, 1986; Seed & Walker, 1988) (iii) refractoriness of the SR release channels (Wier & Yue, 1986) and (iv) transiently enhanced uptake by the SR after the Ca^{2+} transient (Schouten, 1990), so that in a subsequent release of Ca^{2+} from the SR, more is taken back immediately into the SR and less enters the cytoplasm to activate the myofilaments.

1.5.2.1. Mechanical restitution in hypertrophy

In hypertrophied human myocardium from patients with aortic stenosis, peak isometric tension and rates of development and relaxation of tension were not significantly different from non-hypertrophied human myocardium (Cooper *et al.*, 1992). However, mechanical recovery of the myocardium between beats was slower in the hypertrophied myocardium and correlated with the degree of hypertrophy measured echocardiographically (Cooper *et al.*, 1992). A similar finding has been reported in cats with right ventricular hypertrophy (Anderson *et al.*, 1977), however, mechanical restitution was faster in guinea-pigs with LVH secondary to infra-renal aortic banding (Davey *et al.*, 2001).

1.5.3. Post-rest potentiation

As well as a negative force-frequency relationship, adult rat ventricle also demonstrates post-rest potentiation, whereas most other mammalian tissues such as rabbit and guinea-pig show rest decay, *i.e.* a decline in the size of the first contraction after rest. Rest decay in normal guinea-pig (Bers *et al.*, 1989) and rabbit (Bers *et al.*, 1993) myocardium is associated with gradual loss of SR Ca^{2+} content. In the guinea-pig this loss of Ca^{2+} is largely due to Ca^{2+} extrusion via Na^{+}-Ca^{2+}-exchange (Bers *et al.*, 1989). Comparison of trans-sarcolemmal Ca^{2+} movements using extracellular double-barreled Ca^{2+}-selective microelectrodes revealed a net loss of cellular Ca^{2+} at rest and a net gain during stimulation in the rabbit, whereas in the rat there was a net gain of Ca^{2+} during rest and a loss during stimulation (Shattock & Bers, 1989). The higher $[Na^{+}]_i$ in the rat would favour Ca^{2+} entry via the Na^{+}-Ca^{2+}-exchanger at resting membrane potential, whereas the lower $[Na^{+}]_i$ in the rabbit would favour Ca^{2+} extrusion at rest. Thus the higher $[Na^{+}]_i$ in

the rat could explain some of the functional differences in contractile function observed in the rat. In another study, post-rest potentiation was observed in the rat despite a constant SR Ca^{2+} content and it was proposed that increased fractional release of SR Ca^{2+} was responsible (Bers *et al.*, 1993). This variation in rat ventricle preparations may be due to the fact the rat ventricle operates very close to the reversal potential for Na^{+}-Ca^{2+}-exchange.

1.5.4. Effect of strophanthidin

Cardiac glycosides bind with high affinity and specificity to an inhibitory site on the α-subunit of the Na^{+}-K^{+}-ATPase pump, resulting in complete inhibition of Na^{+} and K^{+} transport as long as the cardiac glycoside molecule remains attached to the site. This inhibition increases intracellular $[Na^{+}]$ and reduces the driving force for Na^{+} entry and coupled Ca^{2+} extrusion via the Na^{+}-Ca^{2+}-exchanger leading to increased intracellular stores of Ca^{2+} and increased contractile force.

It is convenient to use cardiac glycoside-induced inotropy as an index of the inotropic effects of changes in $[Na^{+}]_i$. Inotropy has been shown to correlate closely with sodium pump inhibition in normal myocardium in a number of studies (Eisner *et al.*, 1981; Cohen *et al.*, 1982). The increase in $[Na^{+}]_i$ observed in these studies would be sufficient to reduce the electrochemical gradient for calcium extrusion on the Na^{+}-Ca^{2+} exchanger, resulting in a rise in $[Ca^{2+}]_i$ and a positive inotropic effect.

1.6. Intracellular ions in myocardial hypertrophy

Changes to the resting cytoplasmic concentration of intracellular ions have been reported in hypertrophy. Because $[Ca^{2+}]_i$ is of central importance in contractile activation many studies have concentrated on measuring the transient increase of $[Ca^{2+}]_i$, the $[Ca^{2+}]$ transient. However, $[Na^{+}]_i$ is involved in the regulation of $[Ca^{2+}]_i$, via Na^{+}-Ca^{2+} exchange and intracellular pH, $[pH]_i$, via Na^{+}-H^{+} exchange, and is therefore also important in the regulation of myocardial contractility.

1.6.1. Intracellular Na^+ in hypertrophy

There is little information at present concerning the $[Na^+]_i$ in hypertrophied myocardium. Using ^{23}Na NMR spectroscopy an increase of $[Na^+]_i$ was observed in compensated LVH secondary to aortic banding in the guinea-pig which then decreased in decompensated hypertrophy (Jelicks & Siri, 1995). An increase of $[Na^+]_i$ was also demonstrated in the spontaneously hypertensive rat (Jelicks & Gupta, 1994) and another study showed that ischaemia generated a 3.5-fold increase of $[Na^+]_i$ in hypertrophied rat hearts compared to a 1.6-fold increase in control hearts (Clarke *et al.*, 1990). In a model of right ventricular hypertrophy (RVH) no increase of $[Na^+]_i$ was observed (Baudet *et al.*, 1991); however, these experiments were performed at $\approx 20^oC$ when the Na-pump would be partially inhibited and the $[Na^+]_i$ already raised (Shattock, 1984).

1.6.1.1. Functional implications of the rise in $[Na^+]_i$

The functional implications of an increase of $[Na^+]_i$ need to be viewed in context of changes to other intracellular ions and the underlying mechanisms, and cannot be viewed in isolation. Abnormal intracellular Ca^{2+} and H^+ regulation have also been observed in LVH and may contribute to the progressive decline in function. Because $[Na^+]_i$ is involved in the regulation of $[Ca^{2+}]_i$, via Na^+-Ca^{2+} exchange and pH_i, via Na^+-H^+ exchange, it is important in the regulation of myocardial contractility as discussed above.

There are several possible explanations for the rise of $[Na^+]_i$ in hypertrophy; *i.e.* a result of increased Na^+-H^+-exchange activity or Na^+-Ca^{2+}-exchange activity or indicative of reduced Na^+-K^+-ATPase pump activity. The effect of hypertrophy on these membrane pumps and exchangers is discussed below.

The mechanism of the rise in $[Na^+]_i$ may also have functional implications. A rise secondary to an increased number or activity of Na^+-Ca^{2+}-exchange sites may promote increased Ca^{2+} extrusion and negative inotropic effects whereas an increased net Na^+ influx resulting from changes in total Na^+ channel conductance or the Na^+-K^+-ATPase pump might have opposite effects on $[Ca^{2+}]_i$ and contractility. By reducing the driving force for Ca^{2+} extrusion via Na^+-Ca^{2+}-exchange, a high $[Na^+]_i$ could contribute to higher Ca^{2+} loading of the hypertrophied myocardium. Despa *et al* (2002) demonstrated that the

higher resting $[Na^+]_i$ in the rat was associated with higher Na^+ efflux via the Na^+-K^+-ATPase pump and concluded that the higher $[Na^+]_i$ was due to greater Na^+ influx. All three pathways appeared to contribute to this influx, namely the Na^+ channel, Na^+-Ca^{2+}-exchange and Na^+-H^+-exchange, however, these results need to be interpreted with caution as the experiments were performed at room temperature which will affect the activity of the Na^+-K^+-ATPase pump and the $[Na^+]_i$ itself.

1.6.2. Intracellular Ca^{2+} in hypertrophy

$[Ca^{2+}]_i$ has been measured in a number of models of hypertrophy. The results are variable and appear to be experiment- and model- dependent. Gwathmey *et al* (1985; 1995) reported no change in diastolic $[Ca^{2+}]$ or the amplitude of the Ca^{2+} transient in RVH in spite of changes in peak tension generation, and similar findings have been reported in rats with abdominal aortic constriction (McCall *et al.*, 1998). Other studies in aortic-banded rats (Siri *et al.*, 1991), aortic banded cats (Bailey & Houser, 1992) and rats with renovascular hypertension (Moore *et al.*, 1991) show a decrease in the peak amplitude of the Ca^{2+} transient. In SHR's with LVH and increased systolic function peak Ca^{2+} transient magnitude was increased in a voltage-dependent manner, whilst resting $[Ca^{2+}]_i$ was unchanged (Shorofsky *et al.*, 1999). In dogs with LVH, Ca^{2+} transients were increased especially at low frequencies of stimulation (Sipido *et al.*, 2000). Some of these differences may reflect differences in experimental conditions and in conditions that increase cellular Ca^{2+} loading, such as faster pacing rates, high external $[Ca^{2+}]$ and catecholamine exposure when the peak systolic Ca^{2+} transient is depressed (Brooks *et al.*, 1994). Furthermore, as discussed above the Ca^{2+} transient is a relatively insensitive measure of the elemental events involved in excitation-contraction coupling and alterations in the local release and re-uptake of Ca^{2+} by the SR may play a role in excitation-contraction dysfunction in hypertrophy. Indeed, in spontaneously hypertensive rats (SHR) with LVH Shorofsky *et al* (1999) demonstrated a shift in Ca^{2+} sparks behaviour to a population of larger amplitude but no associated change in Ca^{2+} current kinetics or ryanodine receptor density. This suggests that there is an alteration in the coupling between the triggering and release of Ca^{2+} in this model of hypertrophy. However, Gómez *et al* (1997b) found no difference in Ca^{2+} sparks between Dahl salt-sensitive hypertensive rats and controls (administration of salt (1% NaCl) and

deoxycorticosterone acetate can be used to increase blood pressure and induce LVH in uninephrectomised guinea-pigs (Tiritilli & Ruff, 1994)).

Intracellular Ca^{2+} handling is abnormal in RVH with prolongation of the Ca^{2+} transient (Gwathmey *et al.,* 1985; 1995) associated with prolongation of the isometric twitch (Gwathmey *et al.*, 1985). Prolongation of the Ca^{2+} transient has also been reported in LVH (Bentivegna *et al.*, 1991; Moore *et al.*, 1991; Bailey & Houser, 1992; Naqvi & MacLeod, 1994). In aortic-banded rats, relaxation of twitch force and $[Ca^{2+}]_i$ decline were impaired at higher frequencies in combination with higher diastolic $[Ca^{2+}]_i$ (Maier *et al.*, 1998). However, in another study in SHR's with LVH, no change in the time course of the Ca^{2+} transient was observed in spite of prolongation of the relaxation phase of unloaded contractions (Shorofsky *et al.*, 1999). These studies used chemiluminescent or fluorescent dyes to measure whole cell or averaged Ca^{2+} transients, therefore the cellular mechanisms responsible for the prolongation of the Ca^{2+} transients are unclear. The most likely explanation is that Ca^{2+} re-uptake into the intracellular stores is impaired in compensated hypertrophy. No change in the Ca^{2+}-sensitivity of the contractile proteins had been observed in hypertrophy (Scamps *et al.*, 1990) which could have explained the prolongation of relaxation.

1.6.3. Sarcoplasmic reticulum function in hypertrophy

In end-stage heart failure SR dysfunction has been proposed to contribute to the impaired contractile performance. Changes in the size of the Ca^{2+} transient could result from a change in the SR Ca^{2+} content or a change in the fractional release of Ca^{2+} from the SR. The Ca^{2+} content of the SR is a major determinant of the amount of Ca^{2+} released from the SR and the amplitude of the Ca^{2+} transient. The amplitude of the Ca^{2+} transient, in turn, controls Ca^{2+} fluxes across the sarcolemma and thence SR Ca^{2+} content.

The effect of hypertrophy on SR Ca^{2+} content appears to depend on the experimental conditions, the model and the stage of hypertrophy. In spontaneously hypertensive rats with compensated hypertrophy, enhanced SR Ca^{2+} release without any change in L-type Ca^{2+} current (I_{Ca}) density, SR function or expression of Ca^{2+} cycling proteins was reported (Shorofsky *et al.*, 1999). In dogs with LVH, SR Ca^{2+} release and SR Ca^{2+} content were increased at low frequencies of stimulation but the differences were no

longer significant at a frequency of 1 Hz (Sipido *et al.*, 2000). Delbridge *et al* (1997) showed no change in SR Ca^{2+} load or amount of Ca^{2+} released per twitch in rats with LVH secondary to abdominal aortic banding. However, in the same model, SR Ca^{2+} content estimated by rapid cooling contractures was depressed at high pacing frequencies and long rest intervals (Maier *et al.*, 1998). In another study in the same model, McCall *et al* (1998) also showed no changes in SR Ca^{2+} load or fractional SR Ca^{2+} release under basal conditions. However, the latter was reduced in low external Ca^{2+} suggesting that there may be a subtle defect in excitation-contraction coupling during compensated hypertrophy.

It has recently been shown that the flattened force-frequency relationship of failing human ventricular myocytes is due to the fact that SR calcium loading does not increase normally with increased stimulation rates (Bassani *et al.*, 1995; Pieske *et al.*, 1999). SR Ca^{2+} uptake relative to Na^{+}-Ca^{2+}-exchange increased as stimulation frequency increased in normal but not in failing myocardium. These findings suggest that SR Ca^{2+} ATPase activity is reduced in heart failure or that the SR is already fully loaded with Ca^{2+} and cannot take up any more. Similarly, in mice with decompensated hypertrophy, secondary to ascending aortic-constriction, contractile function in response to rapid pacing was reduced, peak systolic $[Ca^{2+}]_i$ was reduced and SR calcium loading was impaired (Ito *et al.*, 2000) but these changes were not seen in compensated hypertrophy in this model.

Ca^{2+} transport activity measured in isolated SR preparations from hypertrophied hearts and has been shown to be either decreased (Ito *et al.*, 1974; Heilmann *et al.*, 1980) or increased (Limas *et al.*, 1980; Nakanishi *et al.*, 1989; Ohkusa *et al.*, 1997). However, most of these studies used microsomal preparations and the yield of proteins in the studies varied and furthermore, it has also been shown that a major fraction of the Ca^{2+} pump system remains in the pellet after low-speed centrifugation (Levitsky *et al.*, 1981). In the model of LVH secondary to abdominal aortic-constriction, Ohkusa *et al* (1997) found that SR Ca^{2+} transport activity decreased to normal later in hypertrophy in spite of the persistence in this model of augmentation of contractile function. In another study using the same model of hypertrophy, SR Ca^{2+} transport capacity measured as oxalate-supported Ca^{2+} uptake per unit mass was reduced but the total capacity was unchanged (la Bastie *et al.*, 1990). This decrease, as well as that observed in rabbits with RVH was

accompanied by a parallel reduction in the number of functionally active Ca^{2+}-ATPase molecules (Matsui *et al.*, 1995).

1.6.4. Intracellular pH, pH_i, in hypertrophy

Previous studies have shown the pH_i of myocardial tissue to be increased (Saborowski *et al.*, 1973; Oldershaw & Cameron, 1988; Astaire *et al.*, 1992; Peréz *et al.*, 1995), deceased (Aufferman *et al.*, 1990; de Roos *et al.*, 1992; Wallis *et al.*, 1997) or unchanged (Lortet *et al.*, 1993; Do *et al.*, 1996) in hypertrophy. Some of the difference may be due to the differences in the models or in the methods used to measure pH_i.

1.7. Regulation of intracellular pH, pH_i

Maintenance of a stable pH_i is important for the equilibria of the many sarcoplasmic processes to remain within the physiological range. Changes of pH_i have important effects on enzyme activity and contractile function. In mammalian skinned muscle fibres and intact preparations, tension falls with decreasing pH_i roughly according to the equation (Fabiato & Fabiato, 1978; Vanheel *et al.*, 1985)

$$T \propto [H^+]^{-2}$$

Conversely, intracellular alkalosis produces a positive inotropic effect (Fry & Poole-Wilson, 1981). H^+ may act at several sites to reduce contractility. Intracellular acidosis has been shown to attenuate I_{Ca} (Kaibara & Kameyama, 1988) and to affect Ca^{2+} handling by the SR (Fabiato & Fabiato, 1978; Vaughan-Jones *et al.*, 1987) and to reduce the sensitivity of the contractile proteins to $[Ca^{2+}]_i$ (Orchard & Kentish, 1990). The partial recovery of twitch force observed during acidosis is due to the decrease in pH activating Na^+-H^+-exchange leading to an increase in $[Na^+]_i$ and $[Ca^{2+}]_i$ presumably via Na^+-Ca^{2+}-exchange (Vaughan-Jones *et al.*, 1989; Harrison *et al.*, 1992a). This in turn may lead to increased Ca^{2+} loading of, and hence release from the SR, allowing partial recovery of contraction during acidosis. In sheep cardiac Purkinje fibres, pH_i falls reversibly as stimulation frequency increases and therefore may contribute to a decline in twitch force (Bountra *et al.*, 1988).

The pH_i of all mammalian cells is more alkaline than that predicted from the passive distribution of H^+ and HCO_3^- ions expected from the resting membrane potential. In active tissues such as ventricular myocardium an additional lactic acid load is present.

This tendency for cells to become acidified by passive fluxes of H^+ must be counteracted by membrane systems that actively extrude them from the cell.

1.7.1. Cellular mechanisms for control of pH_i in mammalian myocardium

There are two separate processes involved in the regulation of pH_i in myocardial tissue. The first consists of a number of membrane transport systems that are capable of extruding an acid or alkali load from the cell. These operate slowly and require metabolic energy in the form of ion gradients to operate. The second is physicochemical buffering, β, that is involved with the relatively instantaneous control of pH_i within the sarcoplasm.

1.7.2. Membrane transport systems controlling pH_i

In mammalian myocardium four symmetrically arranged membrane counter-transport protein systems are involved in the control of pH_i. One pair, coupled to Na^+, extrudes acid loads from the cell and the other pair coupled to Cl^-, extrudes alkali loads from the cell as shown in figure 1.4.

The two electroneutral transport proteins responsible for acid extrusion are the amiloride sensitive Na^+-H^+-antiporter and a Na^+-HCO_3^- symport. In guinea-pig myocardium acid-equivalent extrusion is known to rely roughly equally between these two mechanisms and the same probably holds true for other mammalian species (Buckler *et al.*, 1990; Dart & Vaughan-Jones, 1992). Both these systems are passive and rely on the sarcolemmal Na^+ gradient for their activity.

Intracellular alkalosis can activate HCO_3^- efflux and Cl^- influx via a coupled Cl^--HCO_3^--exchange mechanism. This electroneutral transporter is inhibited by the stilbene anion exchange inhibitor DIDS (4,4-disothiocyanoto-stilbene-2,2'-disulphonic acid). More recently it has been demonstrated that following reduction of extracellular pH, acid-loading of the sarcoplasm continues even in the absence of extracellular HCO_3^-, suggesting the existence of a Cl^--OH^--exchanger working in parallel with the Cl^--HCO_3^--exchanger (Sun *et al.*, 1996). Acid-loading whatever its mechanism is highly non-linear.

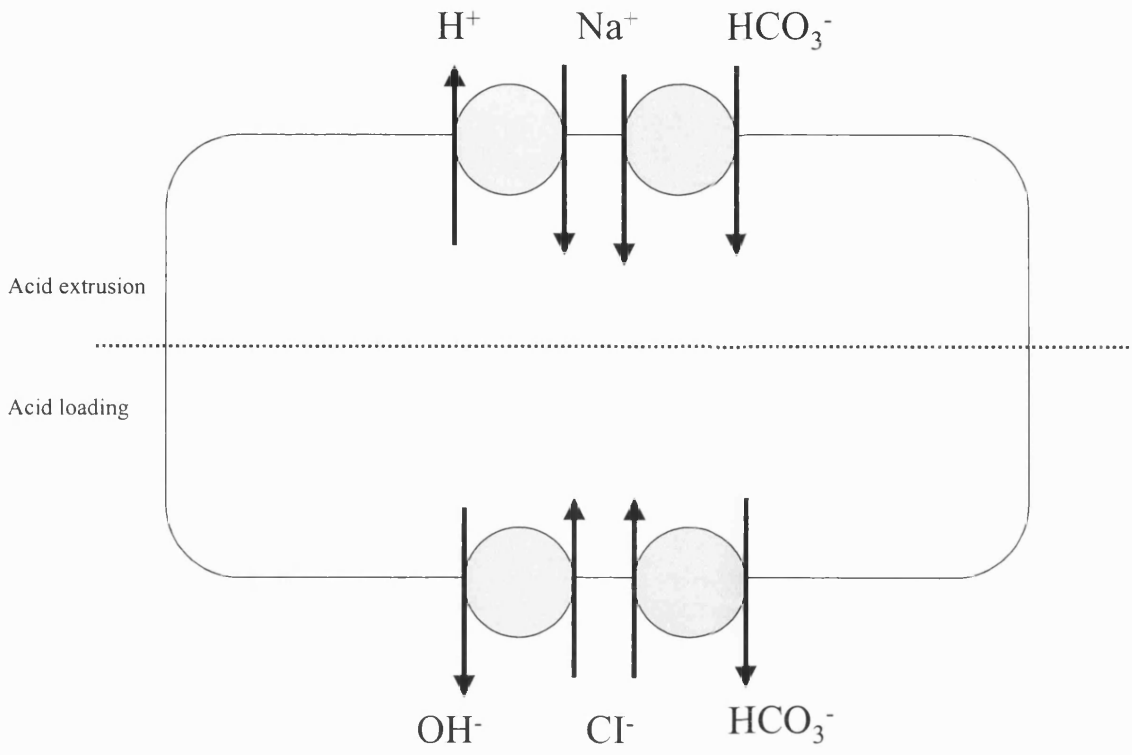

Figure 1.4. Model of pH_i control in the ventricular myocyte

It is not activated over the pH range 6.7-7.2 and is therefore not involved in the recovery of pH_i from intracellular acid loads (Vaughan-Jones, 1982; Vanheel *et al.*, 1985). pH_i is set by the balance between the activity of the acid extruders and the acid loaders in the sarcolemma. Perturbations of pH_i will be resisted by increased activity of either depending on the direction of the pH change induced and any imbalance in the activity of these transporters will produce a new set point.

1.7.3. Physico-chemical buffering, β

Intracellular buffering minimises pH_i changes in the short-term and may also be involved in helping to control the mobility of intracellular H^+, hence influencing the uniformity of distribution of pH in the cell. There are two forms of physico-chemical buffering in the cell sarcoplasm. The first is provided by the intrinsic buffering of the cellular proteins themselves and in myocardial tissue this accounts for the majority of the cells' buffering capacity, β_i. The remainder of the buffering capacity of the cell can be attributed to the presence of a high $[HCO_3^-]_i$. The cell membrane is highly permeable to CO_2, which is always present in the extracellular environment *in vivo*, thus intracellular CO_2 levels will

also be elevated and in the presence of carbonic anhydrase the HCO_3^- produced is available to act as a powerful addition to overall cell buffering capacity.

1.8. Membrane proteins and channels in hypertrophy

Regulation of $[Na^+]_i$, $[Ca^{2+}]_i$ and pH_i ultimately involves the function of primary active transporters such as the sarcolemmal Na^+-K^+-ATPase pump (Na-pump) and the SR Ca^{2+}-ATPase pump (SERCA2), and the secondary active transporters such as Na^+-H^+- and Na^+-Ca^{2+}-exchange. There are conflicting reports regarding the density and function of these various processes in hypertrophy and there has been no systematic study to correlate their activity with functional changes to the electro-mechanical properties of myocardium.

1.8.1. The Na^+-K^+-ATPase pump

Na^+-K^+-ATPase is the primary active transport mechanism that determines the level of $[Na^+]_i$ in the cardiac myocyte. It plays an important role in excitation-contraction coupling by maintaining electrochemical membrane gradients for Na^+ and by indirectly regulating intracellular $[Ca^{2+}]$ by its functional coupling to the Na^+-Ca^{2+} exchanger. By generating the Na^+ gradient across the sarcolemma, the Na^+-K^+-ATPase creates a driving force for secondary active Ca^{2+} extrusion via the Na^+-Ca^{2+}-exchanger.

Na^+-K^+-ATPase is a heterodimer composed of a catalytic α-subunit and a smaller glycoprotein β-subunit. There are 3 isoforms of the α-subunit (α_1-α_3) and 2 isoforms of the β-subunit (β_1-β_2). A fourth α-subunit isoform (α_4) has been identified at the transcriptional level in mammalian testes (Shamaj & Lingrel, 1994). The α-subunit has the binding sites for Na^+, K^+ and cardiac glycosides and the different subunits differ in their affinities for Na^+, K^+ and cardiac glycosides. The β-subunit is required for normal insertion of the α-subunit into the cell membrane and has some regulatory activity over the α-subunit. The isoforms have been cloned and sequenced and their expression is tissue and species specific and varies during ontogenic development. Comparison of the amino-acid sequences for the α_1, α_2 and α_3-isoforms in the rat show approximately 85-86% similarity (Shull *et al.*, 1986).

The α_1-isoform is ubiquitous in mammalian heart. It has a low affinity for ouabain / cardiac glycosides in rat (Sweadner, 1989), guinea-pig (Berrebi-Bertrand *et al.*, 1991), ferret (Ng & Akera, 1987) and dog (Maixent *et al.*, 1987) heart and a high affinity in human (Shamraj *et al.*, 1993) and sheep (Price & Lingrel, 1988) heart. The α_2-isoform has been reported in adult rat (Charlemagne *et al.*, 1987; Sweadner, 1989), human (Shamraj *et al.*, 1993; Wang *et al.*, 1996) and guinea-pig myocardium (Ramírez-Gil *et al.*, 1998) and has a high affinity for ouabain in the rat (Sweadner, 1989) and guinea-pig (Berrebi-Bertrand *et al.*, 1991). It has recently been identified in mice with genetically reduced levels of α_2-isoform expression as the specific isoform involved in the regulation of cardiac Ca^{2+} handling (James *et al.*, 1999). The α_3-isoform is expressed in human (Ramírez-Gil *et al.*, 1998), neonatal rat (Orlowski & Lingrel, 1988) ferret (Ng & Book, 1992) and dog heart (Berrebi-Bertrand & Maixent, 1994; Zahler *et al.*, 1996). The β_1-isoform is the predominant β-subunit in the heart.

The sub-cellular distribution of sodium pump isoforms also differs in different species. In rat heart the α_1-isoform is mainly localised to T-tubules and intercalated discs whereas α_2-isoforms are uniformly distributed in T-tubules, sarcolemma and intercalated discs. In the guinea-pig heart only the α_1-isoform was detected and was distributed evenly in sarcolemma, T-tubules and intercalated discs (McDonough *et al.*, 1996). The α_3-isoforms in neonatal rat heart are localised to excitable tissues (Zahler *et al.*, 1996). The co-distribution of the Na-pump and the Na^+-Ca^{2+}-exchanger in the T-tubules may have functional significance.

1.8.1.1. Na^+-K^+-ATPase pump function in hypertrophy

A change in Na^+-K^+-ATPase pump number has also been assessed by quantitative ouabain binding. Ouabain binds only to sodium pump units that are correctly inserted into the cell membrane and are physiologically active. Several studies have shown a reduction of Na^+-K^+-ATPase activity in hypertrophied myocardium, accompanied by a reduction in the number of high-affinity binding sites for ^{3}[H] ouabain (Khatter & Hoeschen, 1984; Silver & Houser, 1985; Whitmer *et al.*, 1986; Nirasawa & Akera, 1987; Ellingsen *et al.*, 1994). The results of these studies are summarised in table 1.1 and a consensus is that the reduction in pump function could be due to a reduction in the membrane density of pump sites in hypertrophy.

Table 1.1. Studies of Na^+-K^+-ATPase pump function in hypertrophy. Values are mean ± SE, * denotes $p<0.05$, ↑ increased, ↓ decreased, ↔ unchanged, SHR = spontaneously hypertensive rat, pNPP = K-dependent paranitrophenyl phospatase activity

Species	Model	Heart-body weight ratio (control vs hypertrophy)	Methods	Changes reported	Reference
Cat	Pulmonary artery banding	4.8±0.3 vs 6.2±0.4 ($g.kg^{-1}$)*	Ouabain sensitive 42-K uptake	23.5% ↓ in active K influx	Silver & Houser, 1985
Cat	Pulmonary artery banding	0.514±0.031 vs 0.924±0.059 ($g.kg^{-1}$)*	^{3}[H] ouabain binding	↓ in binding sites Affinity for ouabain ↔	Nirasawa & Akera, 1987
Rats	One-kidney, one-clip hypertension	2.97±0.09 vs 4.37±0.13 ($g.kg^{-1}$)*	Enzyme-linked spectrophotometry Na^+ dependant phosphorylation ^{3}[H] ouabain binding	20% ↓ in activity 40% ↓ in activity 45% ↓ in ouabain binding	Whitmer *et al.*, 1986
Rats	Abdominal aortic constriction	2.14±0.05 vs 3.14±0.06 ($g.kg^{-1}$)*	Na^+ dependent phosphorylation	Activity ↔	Nakanishi *et al.*, 1989
Rats	SHR	1.7±0.08 vs 2.4±0.08 ($g.kg^{-1}$)*	Na^+ dependent phosphorylation	Activity ↓	Nakanishi *et al.*, 1989
Pigs	Thoracic aortic-banding	Not available	^{3}[H] ouabain binding	26% ↓ in binding sites Affinity for ouabain ↔	Khatter & Hoeschen 1984
Ferret	Abdominal aortic Constriction	2.45±0.12 vs 3.73±0.40 ($g.kg^{-1}$)*	K^+ stimulated PNPPase activity	Activity ↔	Book *et al.*, 1994b
Human	Autopsy	LV weight >225g in LVH vs < 190g in control	^{3}[H] ouabain binding	19% ↓ in binding sites	Ellingsen *et al.*, 1994

However, no change in pump density was observed in a rat model of hypertrophy (Charlemagne *et al.*, 1994) and it has also been suggested, therefore, that the changes are

due to differential expression of the α-subunit isoforms that have different affinities for ouabain and Na^+ in different models of hypertrophy leading to an alteration in the ratio of isoenzymes. However, ouabain sensitivity alone is not a sufficient criterion for detecting Na^+K^+-ATPase isoenzymes as a number of reports suggest that ouabain sensitivity can be modulated by intracellular factors or cytoskeletal interactions (Sweadner, 1989). No change in Na^+-K^+-ATPase activity estimated by K^+ dependent nitrophenyl phosphatase activity was observed in hypertrophied ferret hearts in spite of the increase in α_1-subunit protein levels (Book *et al.*, 1994b).

1.8.1.2. Na^+-K^+-ATPase pump isoform expression in hypertrophy

Changes in α-isoform expression have been reported in hypertrophy. Initial studies mainly examined mRNA expression. However, mRNA levels may not be proportional to amounts of pump isoform protein nor to the number of functional pump units. Subsequent studies have examined both mRNA and protein levels and indicated that changes may be pre-translational, translational and/or post-translational. These studies are summarised in table 1.2. Most studies show that α_1-isoform expression is unchanged but α_2 and α_3-isoform expression is altered. The changes vary in different species and models, as well as with the degree of hypertrophy. These apparent differences may reflect model-dependant phenomena, differences in the severity and stage of hypertrophy or species differences in the regulation of the Na^+-K^+-ATPase isoform genes. No change in expression of the β_1 subunit has been observed in hypertrophy (Book *et al.*, 1994a, Book *et al.*, 1994b; Charlemagne *et al.*, 1994).

1.8.1.3. Physiological relevance of changes in isoform expression

Species, developmental and pathological differences in isoform expression suggest that the Na^+-K^+-ATPase isoforms are functionally tailored to meet the sodium pump requirements of hearts with different electrophysiological and contractile properties. Changes in mRNA and protein levels of the isoforms may alter the functional activity of the Na^+K^+-ATPase, as the isoforms differ in their affinities for Na^+ (Jewell & Lingrel, 1991). The α_1-subunit has the lowest K_m value of about 12mM, while the α_2 and α_3 sub-units have higher K_m values of 22 to 33mM respectively (Zahler *et al.*, 1997b). Thus if the total number of pump sites remains constant but the isoform expression changes

Table 1.2. Summary of studies of Na^+-K^+-ATPase pump isoform expression in hypertrophy. Values are mean ± SE, * denotes $p<0.05$, ↑ increased, ↓ decreased, ↔ unchanged, nd = not detected. RV = right ventricle

Species	Model	Heart-body weight ratio (control vs hypertrophy)	Changes in isoform expression	Methods	Reference
Rat	Aldosterone-salt induced hypertension	1.7±1.9 vs 3.0±2.7 ($g.kg^{-1}$)*	α_1 mRNA ↔ α_2 mRNA ↓ α_3 mRNA ↓	Northern blots	Herrera *et al.*, 1988
Rat	Partial constriction of left renal artery	20.3±0.6 vs 27.5±1.0 ($g.mm^{-1}$)* (LV vs tibia bone length)	α_1 mRNA and protein ↔ α_2 mRNA and protein ↓	Northern blots and Immunoblots	Book *et al.*, 1994 (a)
Rat	Abdominal aortic constriction	1.78±0.28 vs 2.4±0.07(mild) and 3.15±0.45 (severe) ($g.kg^{-1}$)	α_1 ↔ α_2 mRNA and protein ↓ α_3 mRNA and protein ↑	Northern blots and Immunoblots	Charlemagne *et al.*, 1994
Rat	Aldosterone-salt induced hypertension	2.07±0.1 vs 3.02±0.16 ($g.kg^{-1}$)	α_1 protein ↔ α_2 protein ↓	Immunoblots	Charlemagne *et al.*, 1994
Guinea-pig	Abdominal aortic constriction	1.62±0.05 vs 2.27±0.14 (12 months)* 2.39±0.22 (20 months)* ($g.kg^{-1}$)	α_1 mRNA and protein ↔ α_2 mRNA and protein ↑ α_3 mRNA ↑ α_3 protein nd	Northern blots and Immunoblots	Trouve *et al.*, 2000
Guinea-pig	Aldosterone-salt induced Hypertension	2.05±0.1 vs 3.3±0.1 ($g.kg^{-1}$)*	α_1 mRNA and protein ↔ α_2 mRNA and protein ↑ α_3 mRNA ↑ α_3 protein nd	Northern blots and Immunoblots	Ramírez-Gil *et al.*, 1998
Dog	Aortic banding	Not available	α_1 mRNA ↑ α_1 protein ↔ α_3 mRNA and protein ↓	Northern blots and Immunoblots	Zahler *et al.*, 1997a
Rabbit	Aortic constriction	2.4±0.1 vs 3.8±0.2 ($g.kg^{-1}$)*	α_1 protein ↓	Western blot	Naqvi *et al.*, 2001
Ferret	Abdominal aortic constriction	2.45±0.12 vs 3.73±0.40 $g.kg^{-1}$*	α_1 mRNA ↔ α_1 protein ↑ α_3 mRNA and protein ↔	Northern blots and Immunoblot	Book *et al.*, 1994b
Human	Hypertension	Not available	α_1 mRNA ↔ α_2 mRNA ↑ α_3 mRNA ↑	Northern blots	Jager *et al.*, 2001
Human	Pressure overloaded RV (autopsy)		α_1 mRNA ↓ α_2 mRNA ↓ α_3 mRNA ↓	Northern blots	Zahler *et al.*, 1993

from a predominantly α_1-subunit to a more mixed pattern with an increase in α_2 or α_3, this could influence intracellular Na^+ handling leading to an increase of $[Na^+]_i$.

1.8.2. Sarcoplasmic reticulum Ca^{2+}-ATPase (SERCA2) expression in hypertrophy

In human and animal models of heart failure, SERCA2 activity is decreased, resulting in abnormal Ca^{2+} handling. This disturbance in Ca^{2+} metabolism is though to contribute to the contractile dysfunction observed in heart failure. Adenoviral transfer of SERCA2 has been shown to improve left ventricular function in aortic banded rats in transition to heart failure (Miyamoto *et al.*, 2000). The results of studies of SERCA2 expression in hypertrophy are summarised in table 1.3. There is considerable variation depending on the model studied and the degree of hypertrophy. In rats with LVH secondary to abdominal aortic constriction the reduction in SERCA2 mRNA is associated with a similar reduction in thapsigargin-sensitive Ca-stimulated ATPase activity in ventricular homogenates (McCall *et al.*, 1998).

1.8.3. The sarcoplasmic reticulum release channel, the ryanodine receptor, in hypertrophy

Changes to mRNA levels for the ryanodine receptor have been reported in myocardial hypertrophy. It is increased in hypertrophy secondary to overproduction of thyroid hormone (Arai *et al.*, 1991) and in rats with mild LVH secondary to suprarenal abdominal aortic banding (Arai *et al.*, 1996), reduced in rabbits with RVH (Matsui *et al.*, 1995) and LVH (Milnes & MacLeod, 2001) and in rats with severe LVH secondary to suprarenal abdominal aortic banding (Arai *et al.*, 1996), and unchanged in rats with LVH secondary to abdominal aortic constriction (McCall *et al.*, 1998), Dahl salt-sensitive rats (Okayama *et al.*, 1997) or humans with hypertrophic cardiomyopathy (Somura *et al.*, 2001). However, the amount of Ca^{2+} released from the SR is not simply determined by the number of ryanodine receptors but rather by that of the activated form, which is largely depended on Ca^{2+} influx through dihydropyridine receptors. In the early stage of hypertrophy in rats ryanodine receptor binding is increased by approximately 30% but declines again in moderate hypertrophy in spite of a persistent increase of contractile function (Ohkusa *et al.*, 1997).

Table 1.3. Summary of studies of the SR Ca^{2+}-ATPase (SERCA2) expression in hypertrophy. Values are mean ± SE, * denotes $p<0.05$, ↑ increased, ↓ decreased, ↔ unchanged, PCR = polymerise chain reaction, SHR = spontaneously hypertensive rat, HOCM = hypertrophic obstructive cardiomyopathy, HCM = hypertrophic cardiomyopathy, RT-PCR = reverse transcription-polymerase chain reaction

Species	Model	Heart-body weight ratio (control vs hypertrophy)	Changes reported	Methods	Reference
Guinea-pig	Abdominal aortic constriction	1.62±0.05 vs 2.27±0.14 * (compensated) vs 2.39±0.22 (decompensated) ($g.kg^{-1}$)*	mRNA ↔ in compensated mRNA ↓ in decompensated	Northern blots	Trouve *et al.*, 2000
Rat	Thoracic aortic constriction	2.67±0.05 vs 3.49±0.23* (compensated) 2.32±0.05 vs 4.22±0.15 (decompensated) ($g.kg^{-1}$)	mRNA ↔ in compensated mRNA ↓ in decompensated	Quantitative PCR and Northern blots	Feldman *et al.*, 1993
Rat	SHR	2.37±0.04 vs 2.77±0.06 ($g.kg^{-1}$)*	mRNA ↔	Northern Blots	Ohta *et al.*, 1995
Rat	SHR	3.8±0.5 vs 5.1±0.8 ($g.kg^{-1}$)	Protein ↔	Quantitative immunoblots	Shorofsky *et al.*, 1999
Rat	Aldosterone-salt induced Hypertension	2.27±0.04 vs 3.34±0.03* (compensated) 4.08±0.14* (decompensated) ($g.kg^{-1}$)	mRNA ↔ in compensated mRNA ↓ in decompensated	Northern blots	Okayama *et al.*, 1997
Rat	Abdominal aortic constrictio n	1.76±0.07 2.1±0.08 (mild)* 2.7±0.14 (severe)* ($g.kg^{-1}$)	mRNA and protein ↔ in mild and ↓ in severe	Dot blot analysis	De la Bastie *et al.*, 1990
Rat	Abdominal aortic constriction	↑ by 33±4%*	mRNA ↓ (31±2%)	Northern blots	Calderone *et al.*, 1995
Rat	Abdominal aortic constriction	2.4±0.1 vs 3.0±0.1($g.kg^{-1}$)*	Protein ↓	Western Blots	Tsutsui *et al.*, 1997
Rat	Abdominal aortic constriction	25% ↑	mRNA ↓	Northern blots	McCall *et al.*, 1998
Rat	Abdominal aortic constriction	0.30±0.01 vs 0.37±0.01 ($g.cm^{-1}$)**	Protein ↓	Western Blots	Boateng *et al.*, 1998

Rat	Suprarenal aortic constriction	2.3±0.13 vs 3.01±0.03 ($g.kg^{-1}$)* (severe)	mRNA ↑ in mild LVH mRNA ↓ in severe LVH	Northern Blots	Arai *et al.*, 1996
Rat	Isoproteronol infusion	33+2% ↑	Protein ↓ by 40%	Western blots	Stein *et al.*, 1996
Rat	Transgenic with the Renin-2d gene	1.42±0.03 vs 1.82±0.03g** Heart weight	mRNA and protein ↓	Northern blots and Western blots	Flesch *et al.*, 1997
Mouse	Thoracic aortic constriction	3.1±0.1 vs 5.4±0.2 ($g.kg^{-1}$)*	mRNA ↑ and protein ↔ in compensated mRNA and protein ↓ in decompensated	Northern blots and Western blots	Ito *et al.*, 2000
Rabbit	Pulmonary artery constriction	3.6±0.7 vs 7.3±0.07 ($g.kg^{-1}$)*	mRNA and protein ↓	Northern blots and Western blots	Matsui *et al.*, 1995
Rabbit	Pulmonary artery constriction	3.4±0.2 vs 7.7±0.7 ($g.kg^{-1}$)*	mRNA ↓ to 56% of control	RNAase protection assay and slot blot assay	Nagai *et al.*, 1989
Rabbit	Thoracic aortic constriction	2.4±0.1 vs 3.8±0.2 ($g.kg^{-1}$)*	Protein ↔	Western blot	Naqvi *et al.*, 2001
Human	HOCM or aortic stenosis	Not available	Protein ↓ by 30%	Western blots	Schotten *et al.*, 1999
Human	HCM	Biphasic force frequency relationship	mRNA ↓	Quantitative RT-PCR	Somura *et al.*, 2001
Human	Hypertension	Not available	mRNA ↑	Northern blots	Jager *et al.*, 2001

In rabbits with LVH secondary to ascending aortic constriction, ryanodine receptor density decreased while dihydropyridine receptor density was unchanged and this may result in a degree of functional uncoupling causing defective release of Ca^{2+} from the SR (Milnes & MacLeod, 2001). No change in ryanodine receptor binding was observed in SHR's with LVH and increased systolic function (Shorofsky *et al.*, 1999) or in humans with hypertrophic obstructive cardiomyopathy or aortic stenosis (Schotten *et al.*, 1999). A recent study in failing hearts suggested that an increase in diastolic Ca^{2+} release as a result of hyperphosphorylation of the ryanodine receptor increasing sensitivity to

activating Ca^{2+}, could account for the decrease of the Ca^{2+} transient in heart failure (Marx *et al.*, 2000).

1.8.4. Na^+-Ca^{2+}-exchanger expression in hypertrophy

Isoforms of the Na^+-Ca^{2+}-exchanger also occur and isoform shifts in hypertrophy have been reported. In the newborn rat heart shortly after birth (6 hours), two forms of the exchanger are detected, that have a high or low affinity to Ca^{2+} and respond differently to Ca^{2+} chelators. At day 12 both forms are no longer expressed and are replaced by the adult form, with an intermediate sensitivity to Ca^{2+}. These changes occur in parallel with a fully functioning SR. The neonatal form with low affinity for Ca^{2+} is found in adult hypertrophied and spontaneously hypertensive rat hearts (Hanf *et al.*, 1988).

Studies of expression of the Na^+-Ca^{2+}-exchanger in hypertrophy are summarised in table 1.4. Again considerable variation between models and the degree of hypertrophy is observed. Despite a depression in Na^+-Ca^{2+}-exchange mRNA in rats with abdominal aortic constriction, no difference in sarcolemmal Na-dependent ^{45}Ca uptake activity was observed in ventricular homogenates from this model (McCall *et al.*, 1998). In patch-clamp studies in myocytes from the same model, no changes in Na^+-Ca^{2+}-exchange current characteristics were observed (Delbridge *et al.*, 1997) whereas a prolonged time course of the Na^+-Ca^{2+} exchange current was observed in isolated myocytes from guinea -pigs with mild LVH (Ryder *et al.*, 1993). In guinea-pigs with thoracic aortic constriction, both Na^+ current and Na^+-Ca^{2+}-exchange current densities were increased in association with raised protein levels of the exchanger (Ahmmed *et al.*, 2000). However, the physiological function of the Na^+-Ca^{2+}-exchanger during normal twitch contraction may be altered by factors such as changes of $[Na^+]_i$, $[Ca^{2+}]_i$, membrane potential, or SR Ca^{2+}ATPase activity. When measured directly, Ca^{2+} influx via the exchanger and outward Na^+-Ca^{2+}-exchange were increased in dogs with LVH (Sipido *et al.*, 2000), that could be explained by up-regulation of the exchanger and / or a change in reversal potential.

Table 1.4. Summary of studies of Na^+-Ca^{2+}-exchanger expression in hypertrophy. Values are mean ± SE, * denotes $p<0.05$, ** $P<0.01$, ↑ increased, ↓ decreased, ↔ unchanged SHR = spontaneously hypertensive rat, HOCM = hypertrophic obstructive cardiomyopathy, HCM = hypertrophic cardiomyopathy

Species	Model	Heart-body weight ratio (control vs hypertrophy)	Changes reported	Methods	Reference
Guinea-pig	Abdominal aortic constriction	1.62±0.05 vs 2.27±0.14* (compensated) vs 2.39±0.22 (decompensated) ($g.kg^{-1}$)*	mRNA ↔ in compensated mRNA ↑ in decompensated	Northern blots	Trouve *et al.*, 2000
Guinea-pig	Thoracic aortic constriction	5.0±0.08 vs 5.1±0.1 (compensated) vs 5.2±0.1 (decompensated)	Protein ↑ in compensated and decompensated	Western blots	Ahmmed *et al.*, 2000
Guinea-pig	Aldosterone-salt induced hypertension	2.05±0.1 vs 3.3±0.1 ($g.kg^{-1}$)*	mRNA ↓	Northern blots	Ramírez-Gil *et al.*, 1998
Rabbit	Thoracic aortic constriction	2.4±0.1 vs 3.8±0.2 ($g.kg^{-1}$)*	Protein ↔	Western blot	Naqvi *et al.*, 2001
Rat	Abdominal aortic constriction	25% ↑	mRNA ↓	Northern blots	McCall *et al.*, 1998
Rat	Abdominal aortic constriction	36% ↑	mRNA and protein ↑	RNase protection Western blot	Boateng *et al.*, 2001
Rat	SHR	1.88±0.26 vs 3.84±0.44 ($g.kg^{-1}$)**	mRNA ↑	Northern blots	Brooks *et al.*, 2000
Mouse	Thoracic aortic constriction	3.1±0.1 vs 5.4±0.2 ($g.kg^{-1}$)*	Protein ↑ in compensated & decompensated	Western blots	Ito *et al.*, 2000
Human	HOCM or aortic stenosis	Not available	Protein ↔	Western blots	Schotten *et al.*, 1999
Human	HCM	Not available	mRNA ↔	Northern blots	Somura *et al.*, 2001
Human	Hypertension	Not available	mRNA ↑	Northern blots	Jager *et al.*, 2001

Na^+ dependent Ca^{2+} uptake in purified sarcolemmal vesicles from hypertrophied rat heart was reduced by 60% in association with a reduced sensitivity to Ca^{2+} (Hanf *et al.*, 1988). However, in the SHR and rats with LVH secondary to abdominal aortic constriction increased uptake was observed (Nakanishi *et al.*, 1989). Thus qualitative or quantitative defects may occur but are not consistent between models.

Abnormal intracellular Ca^{2+} handling appears to play an important role in the progressive deterioration from compensated to decompensated hypertrophy and heart failure, however, the mechanisms underlying this remain incompletely understood. As discussed above alterations in Ca^{2+} regulatory proteins have been described in hypertrophy, but it is unlikely that a change in the abundance of one specific Ca^{2+} regulatory protein is responsible. However changes in the interaction of the Ca^{2+} regulatory proteins that work together to modulate the size and shape of the Ca^{2+} transient could be responsible. Alterations in Ca^{2+} regulatory proteins described in one model of hypertrophy cannot be extrapolated to other models or to humans as there are fundamental differences in Ca^{2+} regulation in different species (Bassani *et al.*, 1994a). Furthermore, *in-vivo* function of a Ca^{2+} regulatory protein may not be directly related to its abundance as measured in a Western blot and activity of regulatory protein could be altered because of changes in their regulation rather than a simple change in protein abundance.

1.8.5. Calcium channels in hypertrophy

1.8.5.1. The L-type Ca^{2+} channel in hypertrophy

The role of the L-type Ca^{2+} channel in the pathogenesis of cardiac hypertrophy remains controversial. In most models the total number of functional channels increases proportionately with the degree of hypertrophy but as myocyte surface area also increases, the density of the Ca^{2+} channels remains constant. This has been demonstrated electrophysiologically in ventricular cells from SHR's (Brooksby *et al.*, 1993), rats with aortic banding (Scamps *et al.,* 1990; Delbridge *et al.*, 1997; McCall *et al.*, 1998), DOCA-salt-hypertrophied rats (Momtaz *et al.*, 1996; Gómez *et al.*, 1997b), cats with pulmonary artery banding (Kleiman & Houser, 1988), guinea-pigs with thoracic aortic banding (Ahmmed *et al.*, 2000) and cardiomyopathic hamsters (Sen & Smith, 1994). This finding is not universal and appears to be model dependent. Decreased I_{Ca} density has

been reported in cats with aortic banding (Nuss & Houser, 1993), rats with abdominal aortic banding (Nakanishi *et al.*, 1989) and ferrets with pulmonary artery banding (Bouron *et al.*, 1992). Increased I_{Ca} has been reported in guinea-pigs with aortic banding (Ryder *et al.*, 1993), rats with renal artery banding (Goldblatt) (Keung, 1989) and in SHR's (Nakanishi *et al.*, 1989; Xiao & McArdle, 1994). Since, in hypertrophy the Ca^{2+} current density has been shown to be increased, decreased and unchanged in different models, the changes may be explained either due to the stimulus used to produce hypertrophy or the degree of hypertrophy produced rather than simply the presence of hypertrophy itself. It is also important to point out that many of these studies include small numbers of cells with wide confidence intervals in the data so the possibility of a type II error cannot be excluded.

The kinetic variables of the Ca^{2+} current have been studied using whole-cell patch-clamp techniques in hypertrophied myocytes. The voltage dependence of the steady state activation variable is unchanged in most models of hypertrophy (Kleiman & Houser, 1988; Scamps *et al.*, 1990; Nuss & Houser, 1991; Ryder *et al.*, 1993; Delbridge *et al.*, 1997). The steady-state inactivation properties of the L-type current were unchanged in most studies (Scamps *et al.*, 1990; Nuss & Houser, 1991; Delbridge *et al.*, 1997; Sipido *et al.*, 2000) but two studies show a significant upward shift in the voltage dependence of inactivation (Kleiman & Houser, 1988; Ryder *et al.*, 1993). The time course of Ca^{2+} current inactivation is usually described by the sum of two exponential functions. Both components were unchanged in most studies (Scamps *et al.*, 1990; Nuss & Houser, 1991; Shorofsky *et al.*, 1999), however, prolongation of both components (Ryder *et al.*, 1993) and of the slow component only (Kleiman & Houser, 1988; Keung, 1989) have been described. These results must be interpreted with caution as the time course may reflect changes intrinsic to the Ca^{2+} current, and / or overlapping currents. The time course of Ca^{2+} current recovery from inactivation is also unchanged in most studies (Kleiman & Houser, 1988; Scamps *et al.*, 1990; Delbridge *et al.*, 1997) but in the guinea-pig was increased in mild hypertrophy (Ryder *et al.*, 1993) and decreased in severe hypertrophy (Ryder *et al.*, 1991). In rats with LVH secondary to abdominal aortic banding (Scamps *et al.*, 1990) and in guinea-pigs with LVH secondary to thoracic aortic constriction (Wallis *et al.*, 2001), β-adrenergic stimulation was less effective in increasing I_{Ca} in hypertrophied than in control hearts. However, this effect was not observed in another study in the SHR (Delbridge *et al.*, 1997). Some of these disparities may result from

variation in the experimental conditions, e.g. Ca^{2+} currents are frequently measured using high concentrations of Ca^{2+} chelators that may mask changes in the kinetics of the Ca^{2+} current.

These electrophysiological studies on the Ca^{2+} current density would suggest that changes to the L-type Ca^{2+} current are unlikely to explain the alterations in excitation-contraction coupling in hypertrophy. However, the release of Ca^{2+} from the SR is not determined simply by the amount of Ca^{2+} entering the cell through the L-type Ca^{2+} channel but may rather depend on single channel properties of the channel that is not reflected in the magnitude of the current. To date there are few data available on the single channel properties of the L-type Ca^{2+} current in hypertrophy. The principal regulator of the L-type Ca^{2+} current in cardiac cells is β-adrenergic stimulation, which activates the intracellular cAMP cascade resulting in an increased opening probability of the channel (McDonald *et al.,* 1994). Using confocal microscopy and patch-clamp methods in hypertension-induced hypertrophy and heart failure in rats, Ca^{2+} current density and SR Ca^{2+}-release channels were normal but the ability of the Ca^{2+} channels to activate SR Ca^{2+} release was impaired (Gómez *et al.*, 1997b). This defect could be corrected by β-adrenergic stimulation in the hypertrophied but not the failing myocytes.

1.8.5.2. The T-type Ca^{2+} channel in hypertrophy

In addition to a putative contribution to automaticity, T-type Ca^{2+} channels are associated with hypertrophy. However, a pathophysiological role for them in the development of hypertrophy remains to be determined. T-type Ca^{2+} channel expression is promoted by long-standing pressure induced hypertrophy in cats and is absent in normal adult feline myocardium (Nuss & Houser, 1993). An increase in the density of the T-type Ca^{2+} current has also been demonstrated in cardiomyopathic hamsters (Sen & Smith, 1994). In voltage-clamp studies T-type Ca^{2+} currents have been demonstrated in rats with pressure-overload hypertrophy (Martinez *et al.*, 1999). However, T-type Ca^{2+} currents have not been demonstrated in humans with hypertrophy secondary to aortic valve disease (Bénitah *et al.*, 1992) or cardiomyopathy (Beuckelmann *et al.*, 1991) or in guinea-pigs with thoracic aortic constriction (Ahmmed *et al.*, 2000).

1.8.6. The Na^+-H^+-exchanger

Five isoforms of the Na^+-H^+-exchanger (NHE) have been cloned (NHE-1 through to NHE-5). The NHE-1 isoform is expressed in virtually all tissues and species and is the primary NHE subtype found in mammalian cardiac cells. NHE is the major regulator of intracellular pH by extruding H^+ in exchange for Na^+ influx in a 1:1 stoichiometric relationship rendering the process electroneutral. The NHE-1 is localised primarily in the intercalated disc region of atrial and ventricular myocytes and the transverse tubular system (Petrecca *et al.*, 1999) and thus may be important in cell-to-cell communication and regulation of $[Ca^{2+}]_i$. The major stimulus for NHE-1 activation is intracellular acidosis and approximately 60% of the H^+ removal capability of the cardiac cell is mediated via NHE (Lagadic-Gossman *et al.*, 1992). Na^+ can affect NHE-1, but is unlikely to be a major regulator within the physiological range (7-16 mM) of $[Na^+]_i$ (Wu & Vaughan-Jones, 1997).

There is increasing evidence from a variety of tissues that cell growth and proliferation may be regulated by NHE. Stretch-induced protein synthesis in neonatal cardiac myocytes (Yarmazaki *et al.*, 1998) and noradrenaline induced protein synthesis in cultured rat cardiac myocytes (Hori *et al.*, 1990) can be blocked by NHE inhibitors. Interestingly, in rats with LVH secondary to aortic banding, the ability of endothelin-1 and angiotensin II to activate NHE is impaired (Ito *et al.*, 1997a). This may represent a potential protective compensatory response to attenuate potential deleterious effects of NHE activation.

1.8.6.1. The Na^+-H^+-exchanger in hypertrophy

Hyperactivity of the Na^+-H^+-exchanger could result in an increase of $[Na^+]_i$. There is evidence that the Na^+-H^+-exchanger plays an important role in the increase in $[Na^+]_i$ seen in ischaemia (Pike *et al.*, 1993) but its role in hypertrophy is unclear. Enhanced activity of the Na^+-H^+-exchanger has been demonstrated in the SHR (Peréz *et al.*, 1995; Schussheim & Radda, 1995). The increased activity in this model is mediated by a protein kinase C dependent mechanism and inhibited by the ACE-inhibitor, enalapril (Ennis *et al.*, 1998). However, in rats with thoracic aortic banding resting pH_i and its rate of recovery from maximal intracellular acidification were similar in control and

hypertrophied cells (Ito *et al.*, 1997a) and similar findings were reported in ferrets with right ventricular hypertrophy (Do *et al.*, 1996).

Increased NHE-1 mRNA has been demonstrated in rabbits with LVH secondary to ascending aortic constriction (Takeawaki *et al.*, 1995). Altered mRNA isoform expression of the Na^+ independent Cl^--HCO_3^- anion exchanger (AE) has been demonstrated in the SHR with a decrease in the AE1 isoform and an increase in the AE3 isoform, in association with increased activity of the AE (Chiappe de Cingolani *et al.*, 2001).

1.9. Summary

There is conflicting data concerning the effects of cardiac hypertrophy on contractile function, intracellular ion concentrations and the membrane pumps and ion channels involved in their regulation. These discrepancies are probably due to multiple factors, including species differences, the age of the animal at the time of the insult and the severity of hypertrophy produced. The effects are also model-dependent and even within the same species the mechanism by which cardiac hypertrophy is generated, pressure overload, volume overload, genetic alteration, rapid rate pacing, catecholamine administration etc, will influence the results obtained.

Many of the experimental studies on cardiac hypertrophy and heart failure have concentrated on the transition period from hypertrophy to heart failure and there is less information on the mechanisms that underlie the initial development of myocardial hypertrophy and the earlier stages of compensated hypertrophy. Furthermore, in many animal models and in diseased human hearts, hypertrophy may be concentric or eccentric and the disease process may not be uniformly distributed throughout the myocardium. Thus it is difficult to compare results from different models of hypertrophy at different stages of disease. More consistent data are likely to be obtained using a single animal model of disease, which can be studied longitudinally during the progression of the disease process.

LVH secondary to hypertension and aortic stenosis are often considered together to be "pressure overload" hypertrophy, however, there are few studies directly comparing

hearts hypertrophied secondary to these two causes. Because hypertension and aortic stenosis place different mechanical loads on the heart, present the heart with different neuroendocrine environments, and result in different coronary artery perfusion pressures, it is hardly surprising that differences exist in the behaviour of the myocardium hypertrophied by hypertension and aortic stenosis. A recent study suggested that there are differences in the tolerance to ischaemia in these two models with a protective effect seen in Dahl salt-sensitive hypertensive rats but not in rats with LVH secondary to aortic banding (Saupe *et al.*, 2000). The aim of this thesis was to study contractile function and changes to intracellular ions in a guinea-pig model of LVH, induced by ascending aortic constriction. This model closely mimics aortic stenosis in humans.

1.10. Hypotheses

The following hypotheses will be tested.

1. Left ventricular hypertrophy is associated with an alteration to the resting intracellular concentrations of Na^+ and H^+ and consequent changes of contractile performance.
2. The changes to the intracellular ion concentrations are mediated by altered activities of the primary and secondary active transport processes.
3. Intracellular Ca^{2+} regulation is downregulated.

Chapter 2: Methods

2.0. General protocol

In vitro experiments were performed to investigate the mechanical properties of left ventricular hypertrophy in a model of surgically-induced pressure-overload in guinea-pigs and to determine the effect of hypertrophy on intracellular ion concentrations and their regulation.

2.I. The experimental model of left ventricular hypertrophy

Left ventricular hypertrophy was induced in adult guinea-pigs by partial constriction of the ascending thoracic aorta.

2.1.1. Details of the animals used

Male Dunkin-Hartley barrier maintained guinea-pigs (Bantin & Kingsman Universal Ltd, UK) weighing 600-900g were used. They were housed for 7-14 days prior to surgery in solid floor pens 52 x 85 x 25 cm (Modular Systems & Development Company Ltd, UK) and in single pens 54 x 37 x 25 cm (North Kent Plastics, Ltd, UK) post-operatively. Neither food nor water were restricted pre- or post-operatively. LVH was induced by aortic banding using a modification of the method described by Ling & De Bold (1976).

2.1.2. Anaesthesia, intubation and ventilation

Animals were anaesthetised with a 1:1 mixture of O_2 and N_2O with 2% halothane ((Fluothane, Zeneca Ltd, UK) and at a rate of 1 l. min^{-1} via an open face mask with the aid of a standard anaesthetic apparatus (Model 3000, Gardner Medical Engineering, Ltd, UK). Under deepening anaesthesia, an intra-peritoneal dose of (30 $mg.kg^{-1}$) methohexitone sodium (Brietal®, Eli Lilly, UK) was administered. Animals were intubated by direct visualisation with a curved 12 gauge intravenous cannula (Sherwood Medical Ltd, Ireland) using a purpose-designed laryngoscope (Turner *et al.*, 1992). Throughout the process of intubation, mucous and ingestia were removed from the pharynx using a sterile 10 FG suction catheter (Portex, Ltd, UK) connected to a suction pump, to prevent death by tracheal occlusion. The animal was placed in the dorsal

recumbent position and the cannula connected to a small animal ventilator (Model 501916, Harvard Apparatus Ltd, UK). The pressure 'pre-set control' of the ventilator was adjusted to the minimum position, allowing the inflation pressure to be controlled using oxygen from the anaesthetic apparatus. The animal was ventilated with 0.4 $l.min^{-1}$ O_2 at a rate of 100 $breaths.min^{-1}$ throughout the procedure, and supplementary anaesthesia using 0.5% halothane by inhalation was administered if required. Requirement for additional anaesthesia was assessed visually and 0.5% halothane was introduced from a calibrated vaporiser when it was considered necessary to deepen the anaesthetic plane of the animal.

The animal was covered with sterile surgical drapes leaving the left side of the chest exposed. This area was shaved with Oster A5 animal clippers and swabbed with a proprietary iodine/alcohol preparation (Betadine®, Seton Healthcare, UK).

2.1.3. Incision and operation

The eventual line of incision and the pectoral muscles were injected with 1 ml 0.5% lignocaine with adrenaline 1:200,000 (Xylocaine®, Astra Pharmaceuticals, Ltd, UK). On attaining a suitable level of anaesthesia (assessed by loss of pedal reflex), a left thoracotomy was performed by making an incision in the second intercostal space using a size 10 surgical blade and cutting through the pectoral and intercostal muscles with 6" McIndoe scissors. At this stage ventilation was reduced to 0.3 $l.min^{-1}$ to reduce lung inflation around the surgical site. The ribs were held apart using modified 2.5" Alm skin retractors. Excess fat was cleared from the aorta by blunt dissection and the careful use of Pott's Iris scissors (45^{o} angled on side) to avoid damage to the pulmonary artery or the aorta. The pulmonary artery was separated from the aorta by blunt dissection and a piece of suture was gently pulled around the aorta using haemostatic forceps to facilitate further clearing of excess fat from around the aorta and to guide placement of the aortic clip.

A small high-density plastic clip (1.5 mm thick, Goodfellow, UK) with an internal diameter of 1.99 mm smeared with 0.4% sodium hyaluronate (Sepracot, Genzyme, UK) was placed around the ascending aorta. Sepracote was used in order to reduce collagen and connective tissue adhesion. The clip was positioned as high as possible on the aorta

to enable subsequent Langendorff perfusion of the isolated whole heart for single cell isolation. In the sham animals, the same operative procedure, including manipulation of the aorta, was performed but no clip was placed round the aorta.

At the end of the procedure the retractors were removed and the ventilation increased to 0.4 $l.min^{-1}$. The ribs were apposed and sutured with a non-absorbable polypropylene monofilament suture (3/0 Prolene® W8522, Ethicon, UK) interrupted in a 'figure 8' while pulmonary inflation was maintained. The intercostal and pectoral muscle layers were closed using continuous sutures with braided absorbable suture (3/0 Vicryl® W9114, Ethicon, UK). The skin was closed using braided non-absorbable suture (3/0 Mersilk®, W328, Ethicon, UK).

2.1.4. Recovery

The guinea-pig was left to recover from the operation while still intubated and receiving oxygen. When the animal showed signs of breathing spontaneously it was disconnected from the ventilator, placed in the prone position and oxygenated via a face mask at a rate of 1 to 1.5 $l.min^{-1}$. Subcutaneous injections of 0.6 $\mu g.kg^{-1}$ buprenorphine (Temgesic®, Reckitt & Coleman, UK) were given for analgesia. Mucous and ingestia were removed from the pharynx by suction and the animal was extubated. The animal was placed into an open-topped rodent cage where the body temperature was maintained using an overhead heating lamp. Each animal was observed for at least one hour before being introduced into a single cage to continue recovery. Animals were housed at 20 ± 2 °C with a relative humidity of 50 ± 5% and a 13 hour light, 11 hour dark cycle. Animals received Biosure RGP diet (Biosure Ltd, UK) and fresh water *ad libitum*.

All procedures were performed in accordance with the "Guidance on the operation of the Animals (Scientific Procedures) Act 1986" HMSO, London.

2.1.5. Regression of left ventricular hypertrophy

42 ± 3 and 100 ± 3 days after induction of LVH animals were anaesthetised, intubated and ventilated as described above. A thoracotomy was performed in the third right intercostal space, the constricted portion of the ascending aorta was cleared of connective

tissue and the clip was cut and removed. The thoracotomy was then closed and the animals were allowed to recover as before.

To provide age-matched controls, animals underwent a second sham operation, 42 ± 3 or 100 ± 3 days after the initial sham operation. The operative procedure was as described above; a right-sided thoracotomy was performed, the ascending aorta was visualised but there was no constricting clip to remove and the thoracotomy was closed. Animals were allowed to recover and housed as described above.

2.2. Solutions and chemicals

Experimental solutions were freshly prepared each day. AnalaR® grade reagents in solid form (BDH Laboratory Supplies, Poole, UK) were weighed and added to 'ultra-pure' reverse osmosis water from a Milli-Q system (Millipore, UK).

Strophanthidin-G (ouabain), (Merck Ltd, UK) was dissolved in AnalaR® grade water to make a 1 mM stock solution. Aliquots of this were added to Tyrode's solution to provide a final concentration of 10 nM to 3 μM.

Amiloride hydrochloride (Sigma Chemical Company, USA) at a concentration of 1 mM, ammonium chloride (NH_4Cl) (Sigma Chemical Compamy, USA) at a concentration of 10 mM and caffeine (Sigma Chemical Compamy, USA) at a concentration of 10 mM were added to experimental solutions prior to their application.

Solid KCl (112.8 g) was dissolved in 500 ml 'ultra-pure' water to provide an electrolyte solution with a concentration of 3 M and used as a micropipette filling solution.

2.3. Isolated preparations

Between 50 and 250 days post-operatively animals were weighed immediately prior to study and then sacrificed by cervical dislocation. No animals showed clinical evidence of heart failure. All procedures were performed according to Guidance on the Operation of the Animals (Scientific Procedures) Act 1986, Her Majesty's Stationery Office, London, UK. The hearts were removed immediately, weighed, (OHAUS® LS 200, OHAUS

Scale Corporation, New Jersey, USA) and placed in a dissection tray containing pre-gassed Tyrode's solution at 37 ^{0}C. The right or left ventricle was opened along the interventricular septum and a papillary muscle was identified. A 7/0 silk tie (D1550, Dixey Instruments, Ltd, UK) was secured around each end of the muscle and the tissue excised. The preparations were <1mm in diameter and between 3 and 5 mm in length.

2.3.1.Tension recordings

The isolated papillary muscle was transferred to a horizontal Perspex tissue superfusion trough (figure 2.1). The preparation was tied to a hook, fixed to the proximal end of the trough, using the suture already attached to the muscle. The other end was secured to a hook on an isometric tension transducer (Statham UC2, USA) that was mounted on a micromanipulator (Prior Instruments, UK) to facilitate adjustment of the resting length of the muscle.

The preparations were superfused with Tyrode's solution (table 2.1). The solutions were warmed in a water bath maintained at 37 ± 0.5 °C supported on a shelf three feet higher than the experimental table, and equilibrated with 95% O_2/5% CO_2. The solution was fed to the tissue preparation by gravity, in tubing enclosed within circulating water at 37 ± 0.5 °C, at a flow rate of 5 ml.min^{-1}. The superfusate then drained directly to waste.

Table 2.1. Composition of normal Tyrode's solution

Compound	Concentration (mM)
NaCl	118
$NaHCO_3$	24
KCl	4.0
$MgCl_2.6H_20$	1.0
$NaH_2PO_4.H_20$	0.4
$CaCl_2.6H_20$	1.8
Glucose	6.1
Na pyruvate	5.0

Gassed with 95% O_2, 5% CO_2, pH 7.35

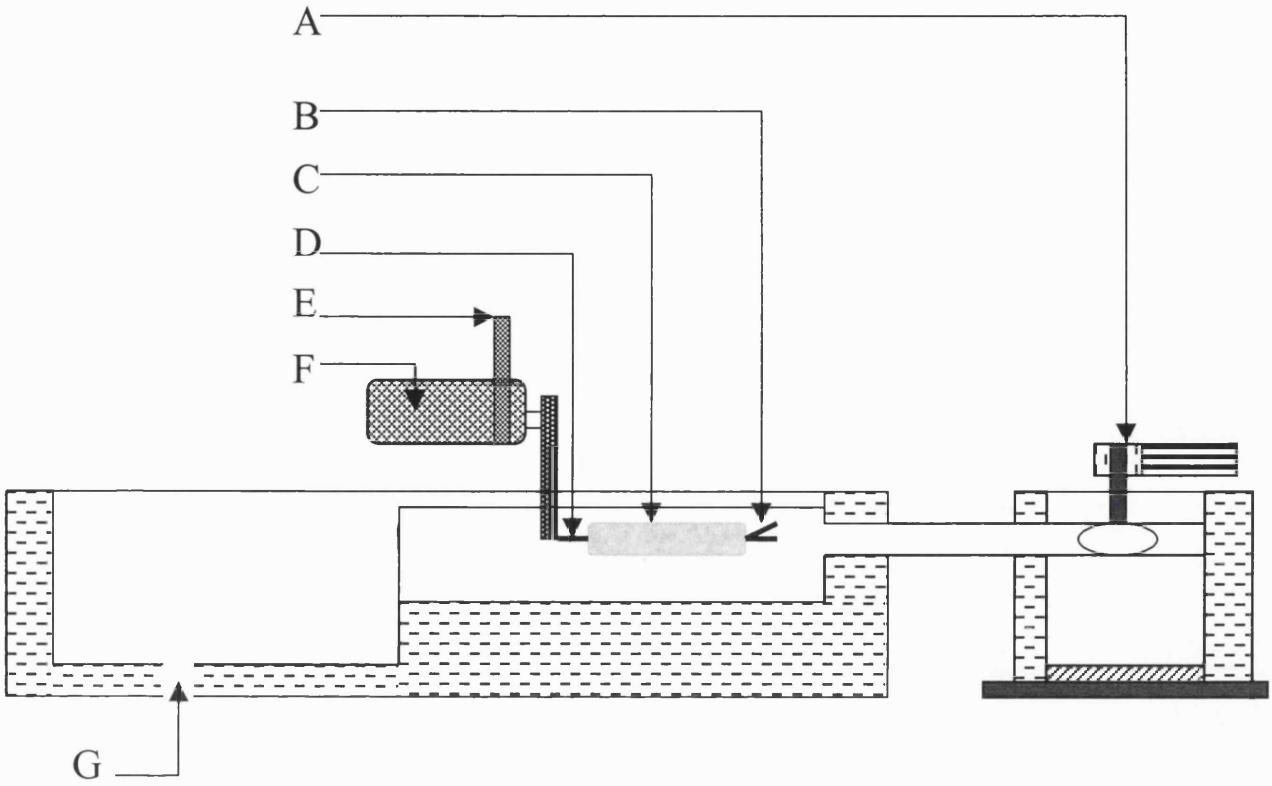

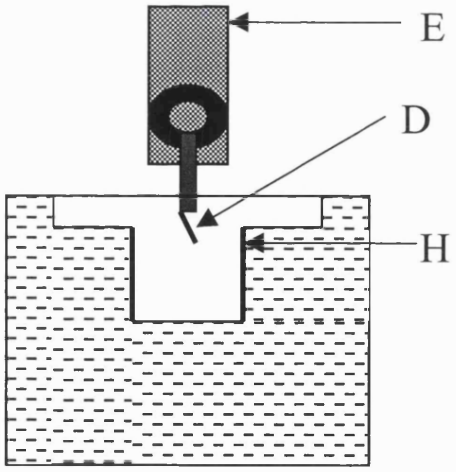

Figure 2.1. Diagram of superperfusion apparatus

A. Two-way tap
B. Fixed hook
C. Muscle preparation
D. Hook attached to tension transducer
E. Plate securing tension transducer to micromanipulator
F. Tension transducer
G. Waste outlet
H. Platinum plate electrode

Isometric tension was measured via the tension transducer that formed the variable arm of a Wheatstone bridge. Output from the transducer was amplified, and low pass filtered at 15 Hz. The signal was displayed on a digital oscilloscope (Hameg HM205- 3, GMBH, Frankfurt, Germany) and via a pen recorder (Gould BS-273, Gould Instruments Ltd, Ilford, Essex, UK).

The signal from the tension recorder was calibrated by suspending solder blocks of known weights from the hook of the force transducer. The voltage deflection for each applied weight was then recorded and a calibration curve plotted (figure 2.2). Force, F, was expressed in Newtons from the relationship F = mg where g = 9.81 $m.s^{-2}$. The relationship between force in mg (or mN), and recorded output voltage for the tension recording system was linear over the range studied.

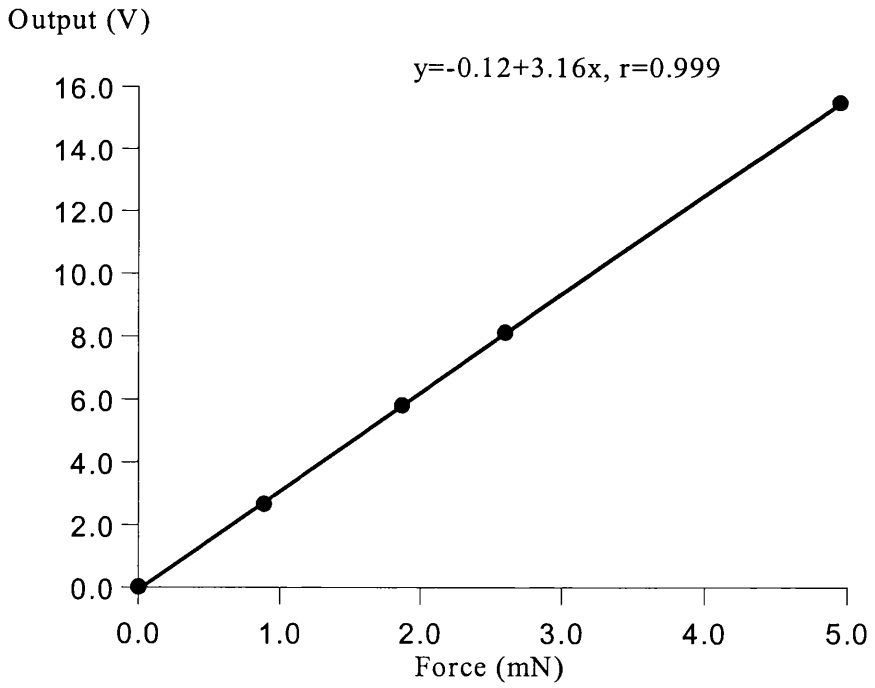

Figure 2.2. Calibration of tension transducer at a fixed recording gain

Mechanical stability of the preparation was ensured by performing experiments on a steel table top which was isolated from its base by neoprene and teflon anti-vibration padding (Neoprine-Teflon Composite, SK Bearings, Cambridge, UK). The base was further protected from vibration by immersing the legs in sand. The perfusion bath was screwed into aluminium slots bolted to the steel top table.

2.3.2. Experimental procedures

Once the preparation was mounted, suprathreshold stimulation was initiated to elicit contraction. The preparation was stretched gently at intervals using the micromanipulator until maximum tension was recorded. The stimulation threshold was then reduced until just supramaximal and the preparation allowed to equilibrate for one hour.

Interventions and experiments included:

(i) Force-frequency response. The stimulation frequency was increased between 0.4 and 2.0 Hz. At each frequency tension was recorded when steady state was achieved.

(ii) Effect of strophanthidin. The force-frequency response in (i) was repeated in the presence of increasing concentrations of strophanthidin (10 nM to 3 μM)

(iii) Effect of reduced external Na concentration. The force–frequency response in (i) was performed in the presence of low Na^+ Tyrode's. NaCl was substituted with Tris-Cl as shown in table 2.2 to give Tyrode's with a [Na] concentration of 29 mM. This solution was then mixed with 147 mM Tyrode's to produce Tyrode's with [Na] concentrations of 29, 50, 70, 90, 110, 130 and 147 mM as shown in table 2.3.

(iv) Measurement of $[Na^+]_i$ using ion-selective microelectrodes.

Table 2.2. Composition of low-Na Tyrode's solution

Compound	Concentration (mM)
Tris-Cl	118
$NaHCO_3$	24
KCl	4.0
$MgCl_2.6H_20$	1.0
$NaH_2PO_4.H_20$	0.4
$CaCl_2.6H_20$	1.8
Glucose	6.1
Na pyruvate	5.0

Adjust to pH 7.8 with HCl. Gassed with 95% O_2, 5% CO_2.

Table 2.3. Combination of normal and low-Na Tyrode's solutions

$[Na^+]_e$	147 mM NaCl Tyrode's	118 mM Tris-Cl Tyrode's
29mM	0 %	100 %
50mM	17.8 %	82.2 %
70mM	34.75 %	65.25 %
90mM	51.7 %	48.3 %
110mM	68.65 %	31.35 %
130mM	85.6 %	14.4 %
147mM	100 %	0 %

2.4. Preparation of ion-selective microelectrodes

An ion-selective microelectrode can be considered as a layer separating two electrolyte solutions, a test solution and a filling solution of known composition. A typical arrangement of an ion-selective electrode is shown in figure 2.3. A potential will be generated at the interface between the test solution and the ion-selective electrode (V_4), the magnitude of which will depend upon the electrolyte composition of the test solution.

The potential, however, cannot be measured in isolation but only with respect to another stable potential as a potential difference (pd). The second stable potential is generated at a reference electrode (V_1-V_3) also placed in the test-solution to complete the circuit. The reference electrode was an Ag/AgCl electrode placed in a solution of 3 M KCl. The pd was measured by a voltmeter and the ion-selective electrode connected to the voltmeter via an Ag/AgCl electrode. At each interface in the system a potential, V_i, develops and the pd recorded by the voltmeter is the sum of these potentials. The recorded pd is $\sum_{i=1\text{-}7} V_i$;

Ag /AgCl /3M KCl /test solution /ion-selective membrane /filling solution /AgCl / Ag
V_1 V_2 V_3 V_4 V_5 V_6 V_7

Each slash (/) represents a junction where a potential develops. The potential at the ion-selective membrane / test solution interface, V_4, is the one of interest. V_1 and V_7 are potentials between the Ag wire and the AgCl coating, V_2 and V_6 are potentials between

the AgCl coating and the filling solutions of the reference and ion-selective electrodes, V_3 is a liquid junction potential between the reference electrode and the test solution. All of these potentials must remain constant, otherwise changes may be interpreted as an alteration of V_4. The 3 M KCl bridge was placed between the reference Ag/AgCl electrode and the test solution to prevent a variable potential being developed when the test solution [Cl^-] was altered.

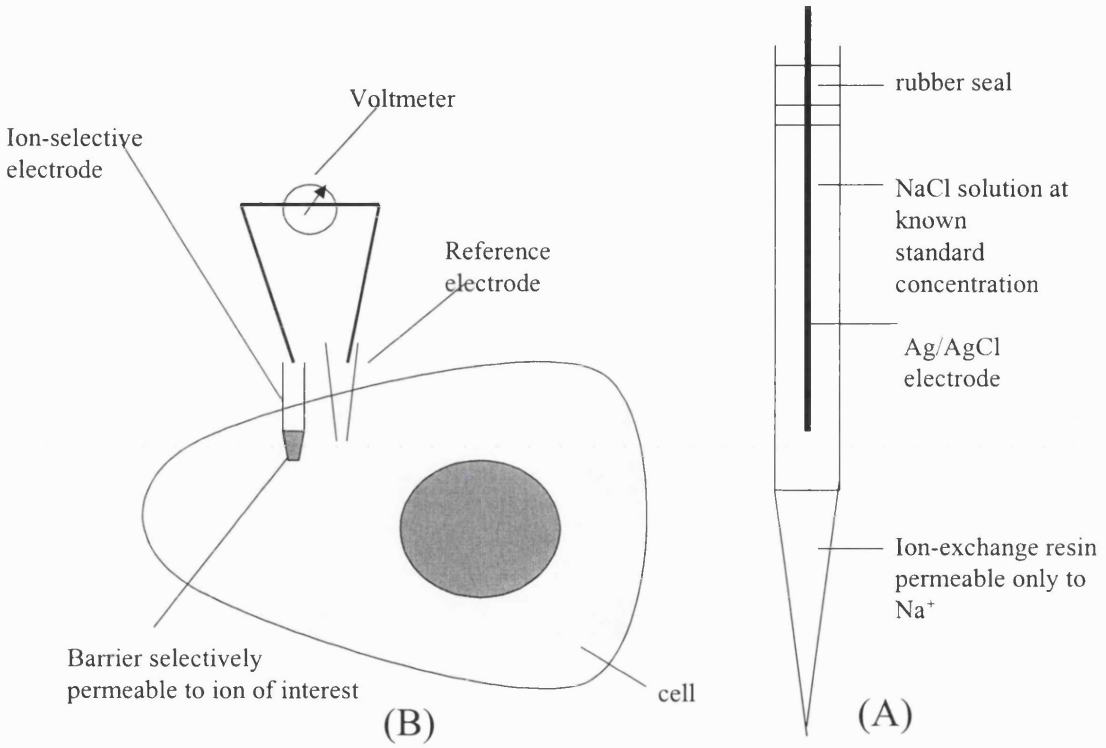

Figure 2.3. Schematic representation of a microelectrode selective for Na^+ is shown in (A) and the experimental arrangement is shown in (B).

2.4.1. Manufacture of Ag/AgCl electrodes

Connection between the ion-selective electrode, filling solution, reference salt bridge and the recording apparatus was made with Ag/AgCl electrodes. These were made by slowly depositing a layer of AgCl onto a segment of clean silver wire by electrolysis. Using a blunt scalpel blade, 1-2 cm of coating was scraped off thin Teflon® coated silver wire (Advent Research Materials, Ltd, UK) lengths to reveal bare metal and leaving the remainder of the wire length covered by insulating material. A second thicker piece of silver rod was prepared for the electrolysis process. To clean the silver wires before coating, the prepared silver wires and the rod were placed into a solution of 100 mM KCl

and connected to a 9 V battery as in figure 2.4(A). A vigorous stream of bubbles emanated from the silver wires and a whitish deposit of AgCl formed on the thick silver rod connected to the positive pole of the battery. The silver rod was cleaned with tissue paper and the silver wires and rod were placed into a fresh solution of 100 mM KCl. The polarity of the connections to the battery were reversed and a large resistor (50 kΩ) was placed in series to limit current through the circuit as shown in figure 2.4(B). Over a period of several minutes a blackish deposit of AgCl was deposited on the silver wires. The wires were removed and stored in air for later use. To maintain a stable reference junction, all electrode solutions in which the Ag/AgCl electrodes were placed were saturated with AgCl to prevent solubilisation of the coating.

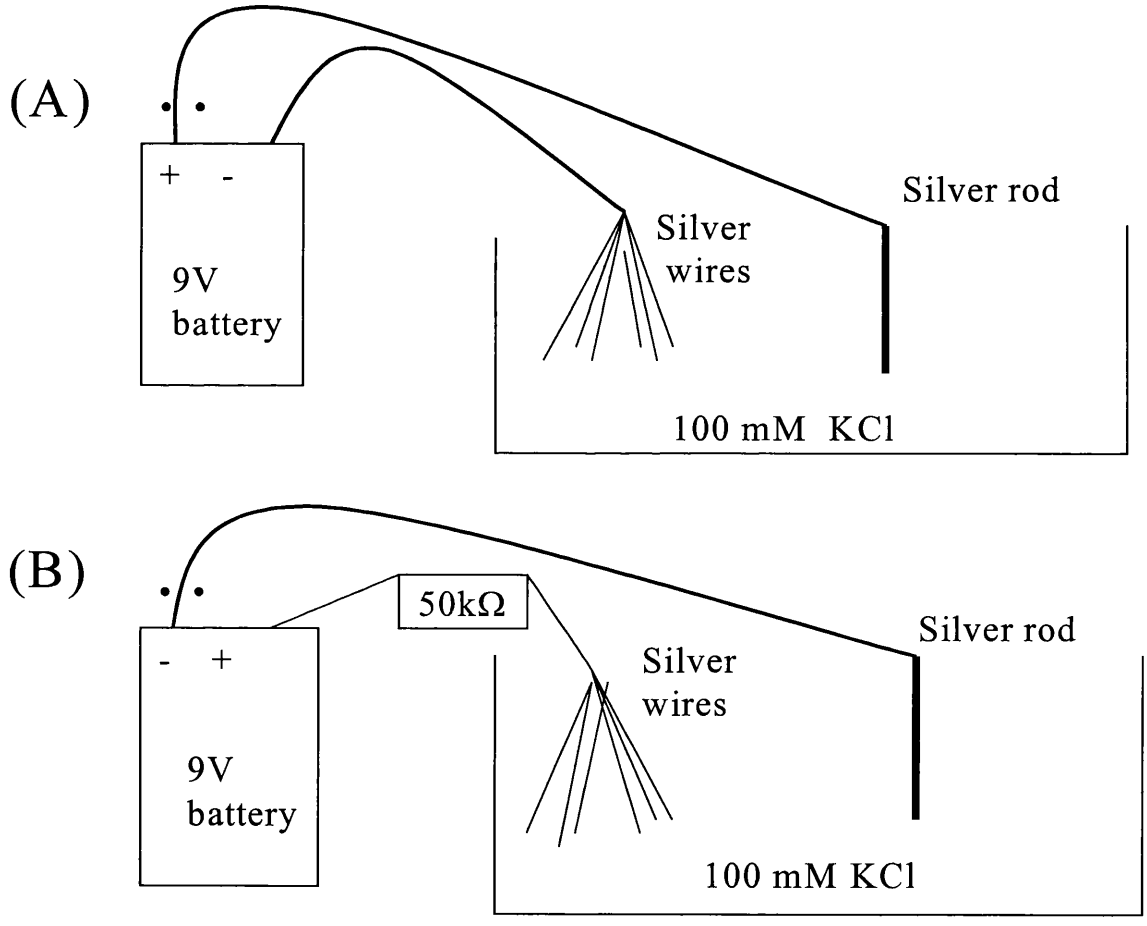

Figure 2.4. Manufacture of Ag/AgCl electrodes. In the upper panel (A), the procedure for cleaning Ag wire is shown and in the lower panel (B), the procedure for coating the Ag wire with AgCl is shown.

2.4.2. Preparation of microelectrodes

Conventional glass microelectrodes made from borosilicate glass capillaries, (GC 150F-15, Clark Electromedical Instruments, UK) with tip impedance of 10-18 MΩ when filled with 3 M KCl, were pulled using a horizontal micropipette puller (Flaming/Brown P-87, Sutter Instruments Co, California, USA).

2.4.3. Preparation of reference electrodes

Polyvinyl chloride tubing (5 cm) with a ceramic plug in one end was filled with 3 M KCl solution to allow insertion and immersion of a coated Ag/AgCl electrode to form the reference electrode. The reference electrode was placed downstream from the preparation, to prevent possible contamination of the superfusate with KCl.

2.4.4. Preparation of Na^+-selective microelectrodes

Glass microelectrodes were silanised to render the inside of the pipette hyprophobic to allow oily ion-selective ligand solution to fill the tip and prevent electrolyte shunt via an aqueous layer on the inner wall of the pipette. Microelectrode blanks were pulled from borosicilicate glass capillaries, 1.5 mm outer diameter, 0.8 mm inner diameter (GC 150 F-15, Clark Electromedical Instruments, Pangbourne Reading, UK) using a Flaming/Brown microelectrode puller, model P-87 (Sutter Instrument Co. USA). The tip-size and taper was varied by alteration in the heat, velocity or strength of the pull. These pipettes have a resistance of 10-18 MΩ when filled with 3 M KCl, and these were used for intracellular potential recording. To prepare the Na^+-selective microelectrodes the blanks were heated at 200 °C for 10 minutes to drive off any water from within the barrel and transferred in a dessicator to a fume cupboard for silanisation. About 2 ml of a silane (dimethylchlorosilane) (Fluka Chemie, Sigma-Aldric Corporation, UK) was placed in a 20 ml beaker and the top covered with parafilm. 4 to 5 microelectrodes were poked through holes in the parafilm and the stems exposed to vapour for 3 minutes. The pipettes were then baked at 200 °C for 40 minutes and stored in a dessicator until ready for filling. The microelectrodes were filled by introducing a small amount of Na^+ selective material, *N,N',N''*-triheptyl-*N,N',N''*-trimethyl-4,4',4''-propylidyne-tris(3-oxabutyramide), with sodium tetraphenylborate (ETH227, Fluka Chemicals, Glossop,

Derbyshire, UK) into the tip using a drawn out piece of polythene tubing. The remainder of the micropipette was filled with a reference solution containing 10 mM NaCl and 140 mM KCl. Filling was achieved by injecting the solution through another piece of polythene tubing taking care to avoid any air bubbles between the ligand and the reference columns.

2.4.5. Connections to recording devices

Ion-selective microelectrodes have a high direct current impedance (between 10^{10} and 10^{12} Ω) and special care must be taken over the recording system used and arrangement of the experimental system. The microelectrodes and recording devices were shielded from extraneous fields by a Faraday cage.

2.4.6. Description of the headstage

Due to the high impedance of the ion-selective microelectrodes, a commercial isolation amplifier from Analog Devices (AD 204) was used instead of a conventional electrometer amplifier. In this system, electrical isolation between between input and output is achieved by transformer coupling between these stages. Power for the device was supplied by a clock driver (AD 246). The manufactures specification quotes an input impedance of 10^{12} Ω, however, in practice it was found to have a much higher value, especially when a Field effect transistor (FET) operational amplifier (op amp) is placed in series with the input stage as a voltage follower. The arrangement is shown in figure 2.5.

The input impedance was checked by imposing a 50 s square wave to the input and recording the amplitude of the signal. A similar procedure was followed with accurate resistors of values 10^{11}, 10^{12}, 10^{13} Ω and no degradation of the steady-state signal amplitude was observed. The source impedance of the ion-selective electrode was about 10^{11} Ω as gauged by carrying out a similar procedure but using a Junction-FET input stage pre-amplifier (input resistance 10^{12} Ω) and with known resistances in parallel with the ion-selective electrode.

The input bias current of the head-stage was about 10 fA measured as described below (Fry & Langley, 2001).

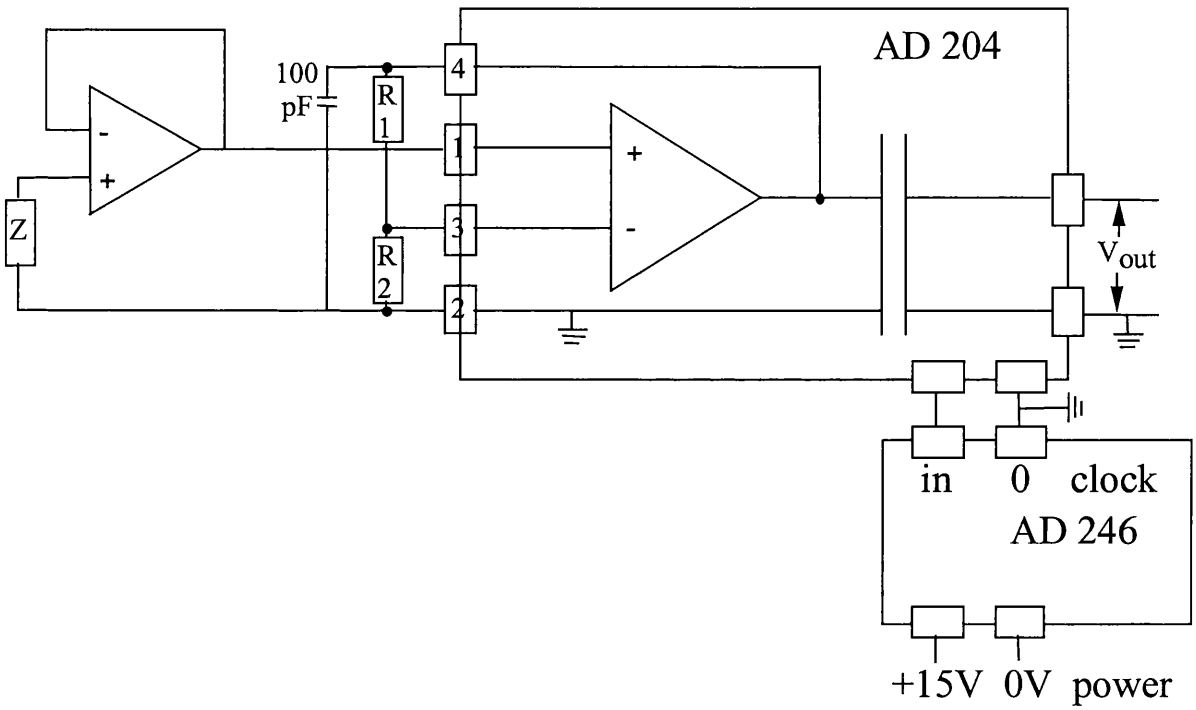

Figure 2.5. Headstage for ion-selective microelectrodes comprising isolation amplifier AD 204 and clock driver AD 246. The clock is driven from a +15V power source. The gain of the amplifier is (1+ (R1/R2)), Z is the ion-selective microelectrode impedance.

2.4.7. Measurement of input bias current of the headstage

With an ideal op amp the resistance between the two inputs should be infinite when they are unconnected (open circuit) and the voltage between them zero. In the real case the internal circuitry generates a small current at each input. If i_{b+} and i_{b-} are these small currents at the non-inverting and inverting inputs respectively, the input bias current, i_b, is the average of i_{b+} and i_{b-}. If an impedance, Z, (*i.e.* an electrode) is placed on the non-inverting input a voltage i_{b+} .Z will be generated. If either of these two variables does not vary much there would be no problem because the output is referenced to another (arbitrary) voltage at the reference electrode. If however, Z changed then this would alter this voltage and manifest as a drift if the change was slow. Therefore it is important that i_b is low enough not to generate a significant error.

FET op amps have an input bias current of ~ 1 pA (10^{-12} A) or a bit higher. If the electrode resistance is 1 MΩ a voltage of 1 μV will develop. If the electrode resistance is 1 GΩ (10^9 Ω) this voltage would be 1 mV. An increase in the electrode resistance to 5 GΩ, because of gradual deterioration, would increase the input offset voltage to 5 mV. This drift of 4 mV must not be of a significant magnitude compared to the true potential change at the ion-selective electrode.

The input bias current can be measured using the circuit shown in figure 2.6. Resistors R_1 and R_2 can be shorted using the switches S_1 and S_2. The capacitors are used to reduce transient effects. When S_1 and S_2 are closed the circuit is a voltage follower. Any output voltage, V_{out}, will be due to internal imbalances in the two inputs and is termed the input offset voltage, V_{io}. When S_1 is open and S_2 is closed V_{out} is now $V_{io} + R_1 . i_{b+}$. When S_1 is closed and S_2 is open V_{out} is now $V_{io} + R_1 . i_{b-}$. The values of i_{b+} and i_{b-} can be calculated from these measurements. Values of R_1 and R_2 have to be chosen appropriate to the likely values of i_b. If i_b is 1 pA, values of R_1 and R_2 should be 10^9 Ω and larger values for smaller i_b.

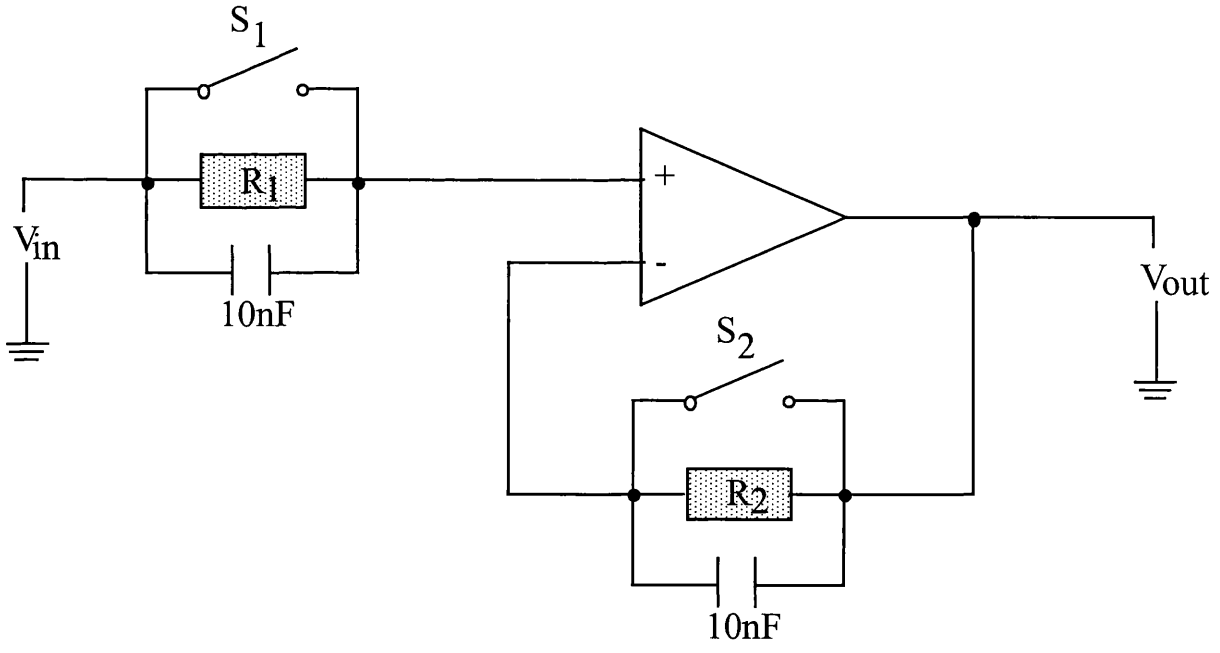

Figure 2.6. The arrangement for measuring the input bias currents at the non-inverting and inverting inputs of an op amp.

2.4.8. Recording of intracellular potentials

The Na^+-selective and KCl microelectrodes were mounted on separate micromanipulators (World Precision Instruments Ltd, Stevenage, UK) and immersed in the superfusate. The experimental arrangement is shown in figure 2.7. A streaming KCl electrode was used as a reference electrode. Junction field-effect transistors (7621, RadioSpares, Corby, UK) were used as input stages in the pre-amplifiers for the KCl microelectrode and reference electrode pair, arranged in an instrumentation mode and with a gain of 10. The pre-amplifier outputs were flat to 5 KHz with a 20 MΩ load on the input.

The KCl electrode was first advanced into the muscle until a stable impalement was achieved, manifest as a constant resting potential of -75 to -95 mV. The Na^+-selective microelectrode was then advanced into the muscle until a stable impalement was achieved.

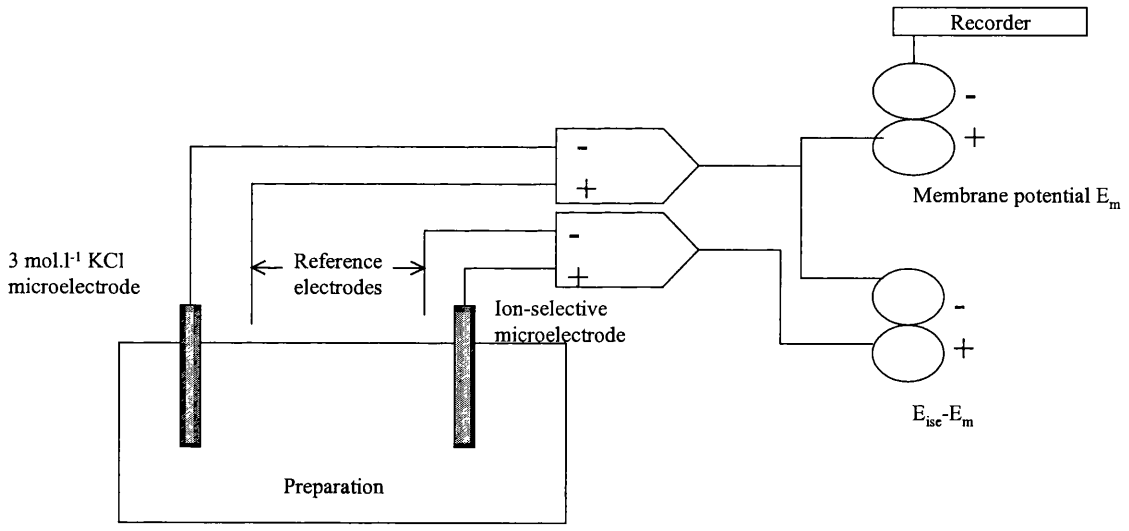

Figure 2.7. Schematic representation of the experimental arrangement for measurement of intracellular $[Na^+]$ using ion-selective microelectrodes

Outputs were displayed on a digital storage oscilloscope (Hameg HM205-3, GMBH, Frankfurt, Germany) and downloaded to a pen recorder (Gould BS-273, Gould Instruments Ltd, Illford, Essex, UK)

When the Na^+-selective electrode penetrates the cell, the total recorded potential difference, E_{ise}, has two components, one is the membrane potential, E_m and the second, E_{Na} results from the difference of Na^+ activity between the inside and outside of the cell. The membrane potential measured by a separate 3 M KCl filled microelectrode was subtracted from the total potential. Different cells were penetrated with ion-selective and conventional KCl microelectrodes but it is assumed that the membrane potential of all cells is similar due to electrotonic coupling. This was verified by depolarising the preparation with 40 mM KCl. When the two intracellular electrodes recorded identical depolarisations (within 1mV) the above assumption was regarded as viable and then E_{Na} was recorded as E_{ise}-E_m.

2.4.9. Calibration of Na^+-selective microelectrodes

Ion-selective microelectrodes measure the chemical activity, *a*, of an ion in solution which is related to concentration, *c*, by an activity coefficient, ∂. Calibrating solutions were made up as standards with known concentrations of Na and the calibration curve used these concentrations to relate to a given voltage. Thus the potential differences recorded by the ion-selective/reference electrode pair will be a function of the concentration of the $[Na^+]$, C_{Na}, provided the relationship between activity and concentration does not alter. In practice this was achieved by working over a limited range of concentrations and ensuring that the ionic strength remained constant and was similar to the test solution.

The [Na] calibrating solutions contained NaCl and KCl so that the sum of the NaCl and KCl concentration was 147 mM. The solution also contained 3mM $MgCl_2$, 10 mM HEPES to buffer the pH to 7.2 and low $[Ca^{2+}]$, 0.4 μM, maintained by the Ca^{2+} buffer, EGTA, to mimic the intracellular space (table 2.4). The $[Na^+]$ was varied between 0 and 147 mM (0 mM, 5 mM, 7 mM, 10 mM, 15 mM, 20 mM, 50 mM and 147 mM with $[Na^+]+[K^+]=147$ mM.

Table 2.4. Calibrating solutions for Na^+-selective microelectrodes

	147 mM KCl	147 mM NaCl
$MgCl_2$	3.0 mM	3.0 mM
EGTA	4.0 mM	4.0 mM
$CaCl_2$	2.1 mM	2.1 mM
HEPES	5.0 mM	5.0 mM
KCl	147 mM	
NaCl		147 mM

Adjust to pH 7.1 with 1M KOH

A typical calibration curve is shown in figure 2.8. Note the potential difference recorded in Tyrode's solution is not the same as that in 147 mM [Na] calibrating solution, even though the [Na] is the same in both solutions; this is largely due to the difference in $[Ca^{2+}]$ between the two solutions and reflects the Ca^{2+} interference on the ion-selective electrode. As shown in figure 2.9 the relationship between potential difference and log [Na] is linear over the higher range of concentrations but deviates when [Na] concentration < 10 mM. The reason for the deviation at low $[Na^+]$ is because of the increasing interference by ions such as K^+.

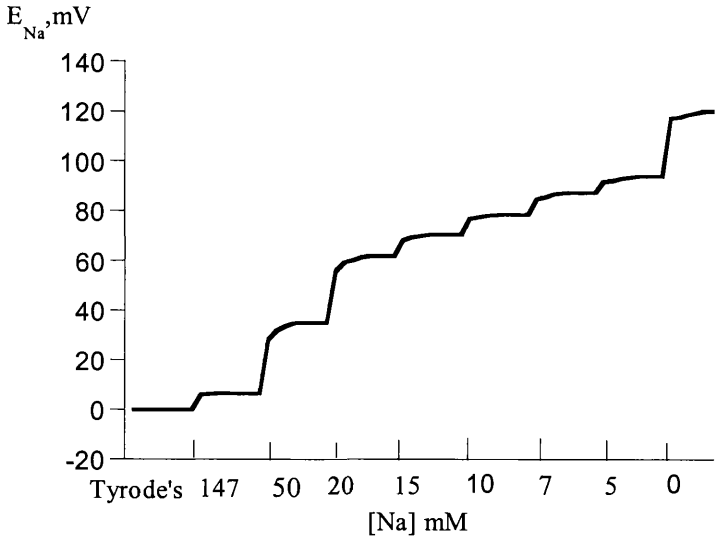

Figure 2.8. Calibration of a Na^+-selective microelectrode using calibrating solutions with known [Na] concentrations

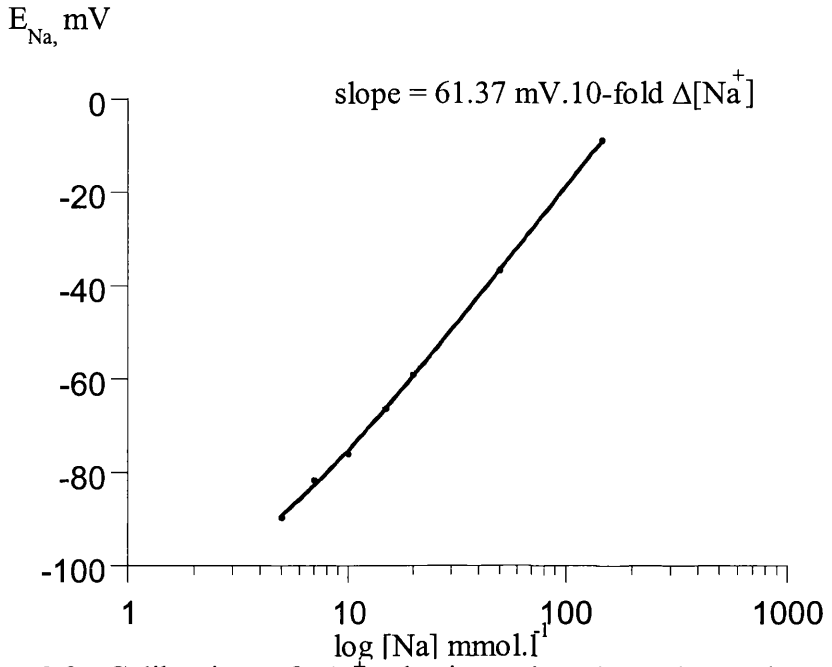

Figure 2.9. Calibration of Na^+-selective microelectrode. The potential difference recorded is plotted against log [Na]

2.5. Cell isolation

Ventricular myocytes were prepared by enzymatic disruption of the isolated heart using a Langendorff perfusion system (Hall & Fry, 1992). All solutions used in the cell isolation procedure were made using laboratory grade II distilled water (BDH AnalaR®, Poole, UK).

2.5.1. Langendorff perfusion method

The animals were weighed and then sacrificed by cervical dislocation. The thorax was opened and the heart removed as rapidly as possible. The heart was placed in a beaker of ice-cold, nominally calcium-free Tyrode's solution (see table 2.5) and weighed (OHAUS® LS 200, OHAUS Scale Corporation, New Jersey, USA). It was then transferred to a second beaker of the same solution and the left ventricle gently massaged to expel all blood from ventricular cavities. The heart was then tied to a Langendorff perfusion apparatus using 2/0 silk. The heart was then secured to the perfusion cannula via the transected aorta, care being taken to avoid damage to the aortic valve. Successful cannulation was indicated by prompt perfusion of the coronary arteries and a physiological perfusion pressure.

Table 2.5. Nominal calcium-free Tyrode's solution

Compound	Concentration (mM)
NaCl	120
KCl	5.4
$MgSO_4$	5.0
HEPES	10
Na pyruvate	5.0
Glucose	20
Taurine	20

Adjusted to pH 6.98 with 1 M NaOH

Perfusion was commenced with nominal calcium-free Tyrode's solution for approximately 5 minutes, followed by the same solution containing 200 μM $CaCl_2$ and protease 0.30 $mg.ml^{-1}$ (Protease Type XXIV, Sigma Chemical Company, USA) for 2 to 3 minutes. The perfusate was then changed to one without protease but containing 0.25 – 0.30 $mg.ml^{-1}$ collagenase (Type II, Worthington Biochemical Company, New Jersey, USA) and 0.60 $mg.ml^{-1}$ hyaluronidase (Sigma Type I-S, Sigma Chemical Company, USA) for 5-8 minutes. All perfusion solutions were heated to 37 °C ± 0.5 and gassed with 99.9% oxygen giving a pH of 6.98.

Subjective assessment that digestion was complete was made by inspection and palpation of the heart. When digestion was complete, the heart would acquire a more pear-shaped morphology, become more translucent and feel softer to touch. The left ventricle was identified and its free wall cut away from the rest of the heart. The tissue was placed immediately in oxygenated Kraftbrühe (KB) solution (see table 2.6) and the rest of the heart was discarded. The ventricular muscle was gently macerated using scissors and watchmaker's forceps. The solution was then filtered through surgical gauze and left to stand to allow the cells to separate out. The supernatant was removed carefully with a pipette and the remaining cell pellet gently resuspended in KB solution. This procedure was repeated once more before the cell suspension was ready for use.

Table 2.6. Composition of Kraftbrühe (KB) solution

Compound	Concentration (mM)
KCl	30
KH_2PO_4	30
KOH	85
$MgSO_4$	3.0
HEPES	10
EGTA	0.5
l-glutamic acid	50
Glucose	10
Taurine	20

Adjusted to pH 7.4 with 1M KOH

This isolation method typically yielded between 50-80% rod-shaped cells. The same protocol was used for isolation of cells from control and aortic banded animals and no subjective difference in cell yield or quality was observed between experimental groups. Cells were used immediately and for the next 12 hours and were stored in KB solution at 4 °C when not in use.

2.6. Measurement of intracellular pH (pH_i) by epifluorescence microscopy

2.6.1. Intracellular pH fluorescent indicator

The analogue of 6-carboxyfluorescein, 2'7'-bis(carboxyethyl)-5,6-carboxyfluorescene, BCECF, (Calbiochem®, Calbiochem-Novabiochem Corporation, La Jolla, CA, USA) (pK_a 6.97) was used as a fluorescent indicator of intracellular [H^+] (Rink *et al.*, 1982). The pH dependence of BCECF fluorescence is a function of the wavelength of the excitation light to which it is exposed. The cell with trapped intracellular indicator is alternately excited by light at 430 and 490 nm. The emission intensity measured between 530 and 580 nm shows a decrease with raised pH when excited at 430 nm and an increase when excited at 510 nm. The ratio of emision signals when excited at 490 and 430 (R) is an index of the intracellular pH, pH_i.

The ratiometric method corrects for signal degradation caused by bleaching or leakage of dye from the cell. It produced a stable signal for the period of the experiments described below.

2.6.2. Intracellular loading of BCECF

The acetoxymethylester of BCECF (BCECF-AM) was dissolved in the organic solvent dimethyl sulphoxide (DMSO, Sigma Chemical Co. USA) to a concentration of 1 mM and stored frozen at –20°C in 100 µl aliquots. This compound is readily permeable across the cell membrane and is subsequently hydrolysed in the cell sarcoplasm to the membrane impermeable parent compound, effectively trapping the dye within the cell. Isolated cardiac myocytes were loaded at room temperature by adding 5 µl of the AM ester solution to 1 ml of KB solution containing a suspension of isolated myocytes. Cells were incubated with the ester for at least 30 minutes at room temperature prior to superfusion with Tyrode's to allow equilibration with the sarcoplasm. No adverse effect of the ester on cell morphology was observed even after prolonged exposure.

2.6.3. The experimental set-up

i) Perfusion chamber and microscope

The superfusion chamber was in a water-jacketed Perspex perfusion chamber attached to the microscope stage. The base of the chamber was formed by a thin glass microscope cover slip, the bath being illuminated from above, and observed using an inverted stage light microscope (Olympus IX50). Bath temperature was maintained at 37 ± 0.5 °C during the experiments. The apparatus was placed on a nitrogen pressurised air table and surrounded by a Faraday cage that was covered with a light-proof cloth. Experiments were performed in a darkened room.

ii) Light source, transmission, and collection

A 75 watt xenon arc light source was used to provide a high intensity, focused and broadband white light source which was filtered prior to transmission to the microscope stage via a quartz fibre optic cable (Cairn Spectrophotometer System, Cairn Research

Ltd, Kent, UK). The light was filtered using a rotating wheel containing up to eight radially distributed filters of different wavelengths. The filters used for BCECF were 430 and 490 nm and those for Fura-2 were 340 ± 10 and 380 ± 10 nm. The wheel rotated at 32 revolutions per second. A dichroic mirror directed the filtered beams through the objective of the microscope (x40) to be focused on the cell under observation. The emitted light passed back through the objective, straight through the dichroic mirror and was reflected by the microscope mirror to be focused in the light tube prior to a variable rectangular diaphragm. The diaphragm could be adjusted to eliminate light from around the cell under observation. A red light produced by filtering the microscope's own light source (>580 nm) was used to position the cell and adjust the diaphragm. This light source was extinguished during data acquisition.

The partially screened emitted light and red light beam were differently reflected by a second dichroic mirror acting as a beam splitter. Higher wavelengths were directed to a CCD viewing camera and the image displayed on a monitor to facilitate adjustment of the diaphragm. Lower wavelengths were transmitted to the photomultiplier tube, PMT, for signal detection (figure 2.10). A high-pass gelatin filter was placed in the path of the emitted light beam prior to its entry into the PMT. This was to prevent overlap of the excitation and emission light sources.

iii) Signal detection and recording

The intensity of the emitted light produced by both excitation frequencies was recorded by two sample and hold amplifiers (see figure 2.10). Amplifier switching was coupled to the rotating wheel using a high frequency internal clock permitting synchronised channel recording. An analogue division circuit was incorporated into the spectrophotometer system to allow measurement of the signal ratio. The ratio produced and the two individual signals were recorded on a pen recorder (Gould TA 240S, Ilford, Essex, UK) and simultaneously displayed on a digital storage oscilloscope (Gould DSO 420, Ilford, Essex, UK). Hard-copy of a captured oscilloscope screen trace could also be made for quantification of the absolute signal strengths.

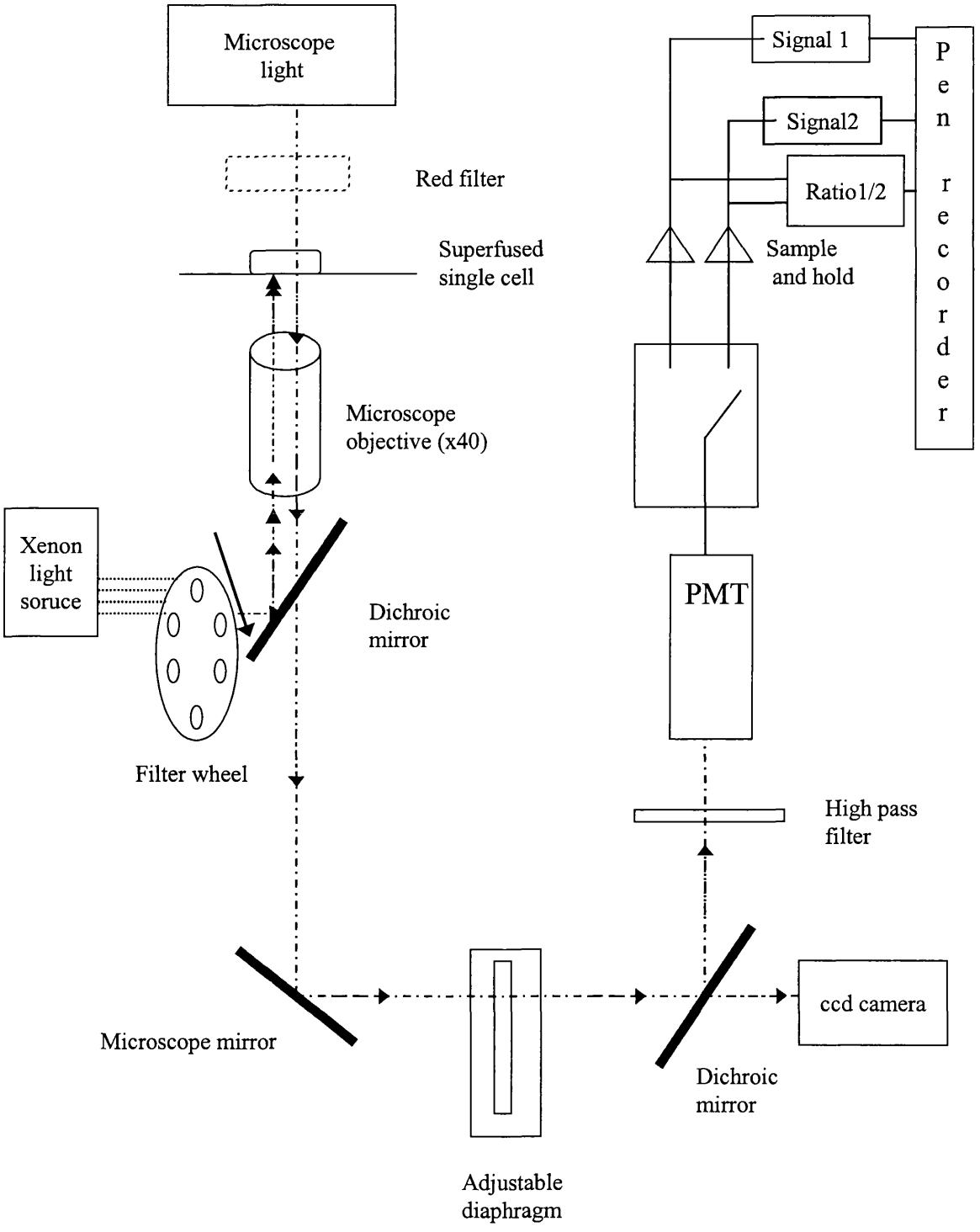

Figure 2.10. A schematic representation of the experimental set-up for epifluoresence microscopy

2.6.4. Experimental procedure

A small drop of loaded cell suspension was placed in the superfusion chamber. This drop was left unperfused for 15-20 minutes to allow viable healthy cells to settle to the bottom of the trough and become adherent to the cover-slip which constituted the base of the superfusing chamber. The cells were then superfused with normal Tyrode's solution. Solutions passed to the bath via heated plastic tubing. Solution flow was maintained at a rate of 1 $ml.min^{-1}$ by gravity feed from one of 3 water jacketed glass reservoirs, switching between solutions been accomplished by means of 3-way taps. Solution was removed by suction using a peristaltic pump (Watson Marlow, Cornwall, England) allowing a constant bath level to be maintained.

Some of these cells became dislodged once superfusion had commenced but generally enough remained to allow experimentation. Intact cells were recognisable under light microscopy as elongated striated cells surrounded by a bright halo. Viable cells were selected by their appearance under phase contrast and positioned using the monochrome monitor image, the diaphragm was then adjusted to reduce the background fluorescence. The microscope cage was then blacked out and the room lights extinguished.

2.6.5. Calibration of the BCECF fluorescence signal

Following recording of pH_i at rest and during interventions, cells were exposed to pH calibration solutions containing the ionophore nigericin (10 μM) (Sigma Chemical Company, USA) as described by Eisner *et al* (1989). Calibrating solutions were designed to mimic the sarcoplasm and buffered with HEPES (table 2.7). Three pH values, 4.0, 7.0, and 9.0 were used to calibrate the traces recorded. Cells were exposed sequentially to pH 7.0, 4.0, and finally 9.0 to obtain a complete calibration trace.

The pK of the dye was determined from the relationship shown in equation 2.1

$$pK = 7.0 - \log(R_{7.0}-R_{4.0}/R_{9.0}-R_{7.0}) - \log(F430_{4.0}/F430_{9.0}) \qquad (2.1)$$

where $R_{7.0}$, $R_{4.0}$, and $R_{9.0}$ are the steady state values of the radiometric signal for solutions at pH 7.0, 4.0 and 9.0 respectively, and $F430_{4.0}$ and $F430_{9.0}$ are the steady-state absolute values of fluorescence intensity at pH 4.0 and 9.0 respectively.

This determination allowed calculation of pH_i from the relationship shown here (equation 2.2) (Eisner *et al.*, 1989),

$$pH_i = pK + \log (R_i\text{-}R_{4.0}/R_{9.0}\text{-}R_i) + \log (F430_{4.0}/F430_{9.0}) \qquad (2.2)$$

where R_i is the steady-state value of the ratiometric signal under initial control conditions.

Table 2.7. Composition of solutions used for calibration of BCECF signal

Compound	Concentration (mM)
KCl	140
$MgSO_4$	1.2
KH_2PO_4	1.2
HEPES	10

Titrated to pH 4.0, 7.0 and 9.0 with 1M KOH or HCl

2.6.6. Data storage and analysis

All data were written in paper form and measurements were made directly from the hard copy. Data was entered into a personal computer by hand and further analysis performed using Excel and the Scientific Analysis application; KaleidaGraph™, version 3.5 (Synergy Software, USA)

2.7. Intracellular buffering capacity

Once a steady state value for pH_i had been recorded, buffering capacity, β, was determined in a proportion of cells. Determination of β was made using application of 10 mM NH_4Cl in the presence of 1 mM amiloride to block the membrane H^+ extrusion mechanisms. NH_4Cl exists in solution in equilibrium as

$$NH_4Cl \leftrightarrow NH_4^+ + Cl^- \leftrightarrow NH_3 + H^+ + Cl^- \quad (2.3)$$

Exposure of the cell to a solution containing NH_3 and NH_4^+ results in rapid entry of NH_3 into the cell as the membrane is permeable to the NH_3 molecule but less so to NH_4^+. Once within the cell each NH_3 molecule combines with a single H^+ to form an NH_4^+ ion. This consumption of H^+ results in an intracellular alkalosis. When NH_4Cl is removed from the extracellular medium, NH_3 molecules recross the cell membrane in the opposite direction leaving behind an excess of H^+ and hence producing an intracellular acidosis. β is calculated from the relationship shown (equation 2.4).

$$\beta \text{ (mequiv.l}^{-1}\text{.pH unit}^{-1}) = [H^+]_i / \Delta pH_i \quad (2.4)$$

where ΔpH_i represents the change in intracellular pH at the moment of removal of the extracellular NH_4Cl. $[H^+]_i$ is equivalent to $[NH_4^+]_i$ immediately prior to removal of the extracellular NH_4Cl solution and the latter can be calculated as follows.

It is assumed that NH_3 is in equilibrium inside and outside the cell (equation 2.5):

$$[NH_3]_o = [NH_3]_i \quad (2.5)$$

As the pH_o is fixed in the superfusate $[NH_4^+]_o$ can be calculated starting from the Henderson- Hasselbalch equation. The overall pK of the reaction is 9.0 (Roos & Boron, 1981, Lagadic-Gossmann *et al.,* 1992)

2.7.1. Calculation of extracellular $[NH_4^+]$, $[NH_4^+]_o$

$$NH_4^+ \Leftrightarrow NH_3 + H^+$$

$$K=[H^+][NH_3]/[NH_4^+]$$

$$pK = \log ([NH_4^+]/[H^+]\,[NH_3]) = \log [NH_4^+] - \log [H^+] - \log [NH_3]$$

$$pK = pH_o + \log [NH_4^+]/[\,NH_3]$$

$$pH_o = pK + \log [NH_3]/[NH_4^+]$$

$$pH_o - pK = \log [NH_3]_o/[NH_4^+]_o$$

$$\Rightarrow\Rightarrow 10^{pHo-pK} = [NH_3]_o/[NH_4^+]_o=[NH_4Cl]_o-[NH_4^+]_o / [NH_4^+]_o =([NH_4Cl]_o/[NH_4^+]_o) - 1$$

$$\Rightarrow\Rightarrow [NH_4^+]_o = [NH_4Cl]_o/ (10^{pHo-pK} + 1) \qquad (2.6)$$

Therefore if external pH is 7.35;

$$[NH_4^+]_o = [NH_4Cl_o]/(1 + 10^{-1.65})= [NH_4Cl]_o/1.022$$

$$\text{if } [NH_4Cl_o] = 10 \text{ mM}; [NH_4^+]_o = 9.78 \text{ mM}$$

2.7.2. Calculation of intracellular $[NH_4^+]$, $[NH_4^+]_i$

As $[NH_4^+]_o$ is known and pH_i has been measured, $[NH_4^+]_i$ can now be calculated. Again from the Henderson-Hasselbalch equation

$$pH_i = pK + \log ([NH_3]_i/[NH_4^+]_i)$$

$$pH_i - pK = \log ([NH_3]_i/[NH_4^+]_i)$$

But $$[NH_3]_i = [NH_3]_o$$

$$pH_i - pK =\log ([NH_4Cl]_o - [NH_4^+]_o / [NH_4^+]_i)$$

But $$pH_o - pK = \log ([NH_3]_o/[NH_4^+]_o) = \log ([NH_4Cl]_o - [NH_4^+]_o / [NH_4^+]_o)$$

$$pH_o - pH_i = \log ([NH_4Cl]_o - [NH_4^+]_o / [NH_4^+]_o) - \log ([NH_4Cl]_o - [NH_4^+]_o / [NH_4^+]_i)$$

$$pH_o - pH_i = \log [NH_4^+]_i - \log [NH_4^+]_o$$

$$10^{pHo - pHi} = [NH_4^+]_i/[NH_4^+]_o$$

$$[NH_4^+]_i = [NH_4^+]_o * 10^{pHo - pHi} \quad (2.7)$$

For example if pH_o= 7.35, pH_i = 7.1, $[NH_4^+]_0$ = 9.78 mM ;

$$[NH_4^+]_i = 9.78 * 10(^{7.35-7.1}) = 17.39$$

2.7.3. Estimation of intracellular buffering capacity

The combined non-bicarbonate and bicarbonate buffering power (β_{tot}) was calculated by exposing the cells to CO_2/HCO_3^- -buffered Tyrode's containing 10 mM NH_4Cl and 1 mM amiloride. The non-bicarbonate intracellular H^+ buffering capacity (β_i) was calculated following exposure to HEPES-buffered Tyrode's containing 10 mM NH_4Cl and 1 mM amiloride. The composition of HEPES-buffered Tyrode's solution is shown in table 2.8.

Table 2.8. Composition of 10 mM HEPES buffered Tyrode's solution

Compound	Concentration (mM)
NaCl	132
HEPES	10
KCl	4.0
$MgCl_2.6H_2O$	1.0
$Na_2H_2PO_4.H_2O$	0.4
$CaCl_2.6H_2O$	1.8
Glucose	6.1
Na pyruvate	5.0

Adjust to pH 7.35 with 1 M NaOH

In both cases exposure to NH_4Cl resulted in a prompt slowly declining intracellular alkalosis. Superfusion was then changed to a CO_2/HCO_3^- or HEPES-buffered Tyrode's solution containing 1 mM amiloride alone. This abrupt removal of NH_4Cl resulted in an intracellular acidosis approximately equal in magnitude to the initial alkalosis. The

acidosis was maintained by the sarcoplasm for a brief period before some recovery of pH_i was seen allowing accurate determination of β_{tot} and β_i respectively.

2.8. Na^+-H^+ exchange turnover

2.8.1. Rate of pH_i recovery from acid load

The rate of recovery of pH_i from the intracellular acidosis produced on NH_4Cl removal in the absence of amiloride was measured in individual cells in both bicarbonate-free (HEPES-buffered) and bicarbonate-buffered conditions. The ΔpH_i was plotted against time and a single exponential curve fitted to calculate the time constant, τ, of the recovery phase using the equation

$$pH_i = A(1-\exp(-(t-t_o)/\tau))) \qquad (2.8)$$

where, pH_i is the starting pH and t_o and A are constants.

2.8.2. Calculation of acid-equivalent efflux (J_H)

Acid-equivalent effluxes were estimated from the pH_i recovery rates determined above. Acid efflux was calculated from the recovery rate of pH_i after the intracellular acidosis produced on NH_4Cl removal in the absence of amiloride. Net acid equivalent efflux was calculated (J_H mequiv.l^{-1}.min^{-1}) using the following equation:

$$J_H = \beta^*(\Delta pH_i/dt)$$

where β is the buffering power of the cell and $\Delta pH_i/dt$ is the rate of change of pH_i at any given pH_i. In HEPES-buffered solution, β was taken as the intrinsic intracellular buffering power (β_i) and in CO_2/HCO_3^--buffered solutions, β was taken as the total buffering power of the cell (β_{tot}) where $\beta_{tot} = \beta_i + \beta_{CO2}$ at peak acidosis.

Recovery from intracellular acidosis is dependent on Na^+-H^+ exchange under bicarbonate free conditions and on both Na^+-H^+ exchange and Na^+-$HCO3^-$ exchange in the presence of bicarbonate. Recovery was partly or completely inhibited by 1 mM amiloride or

reducing external Na. The composition of 0 mM and 24 mM NaCl solution is shown in table 2.9.

Table 2.9. Composition of HEPES and bicarbonate-buffered Tyrode's solutions with reduced Na

Compound	0 mM Na HEPES-buffered	24 mM Na HEPES-buffered	24 mM Na Bicarbonate-buffered
	Concentration (mM)	Concentration (mM)	Concentration (mM)
NaCl		24	
Tris-Cl	137	113	123
Hepes	10	10	
$NaHCO_3$			24
KCl	4	4	4
$MgCl_2.6H_2O$	1	1	1
$NaH_2PO_4.H_20$	0.4	0.4	0.4
$CaCl_2.6H_2O$	1.8	1.8	1.8
Glucose	6.1	6.1	6.1
pH	7.35*	7.35*	7.35**

*Adjust to pH 7.35 with 1 M NaOH and **adjust to pH 7.8 with HCl

2.9. Measurement of intracellular Ca^{2+} by epifluorescence microscopy

The experimental set up and procedure is as outlined above for measurement of intracellular pH.

2.9.1. Intracellular Ca^{2+} fluorescent indicator

The fluorescent indicator Fura-2 (Calbiochem®, Calbiochem-Novabiochem Corporation, La Jolla Ca, USA) (Grynkiewicz *et al.*, 1985) was used as an index of the intracellular free Ca^{2+} concentration, ($[Ca^{2+}]_i$). Fura-2 has a high affinity and selectivity for Ca^{2+} and the K_d (224 nm) lies within the physiological range. The fluorescence excitation spectrum of Fura-2 shifts progressively to a shorter wavelength as $[Ca^{2+}]_i$ increases; as a

result the emission intensity at 340 nm excitation is increased and at 380 nm excitation the emission is decreased. The isofluorescence wavelength is about 360 nm. The emission spectrum is unaltered by Ca^{2+} binding and has a maximum at about 510 nm (Grynkiewicz *et al.*, 1985). Fura-2 was excited at 340 and 380 nm and the emitted light was collected at between 520 and 580 nm. Employing a ratio of these two outputs ensures that the signal is independent of fluorochrome concentration which may arise from any uneveness in the thickness of the cell and the eliminated artefacts due to loading or loss of indicator from the cell.

2.9.2. Intracellular loading of Fura-2

The acetoxymethylester of Fura-2 (Fura-2-AM) was dissolved in the organic solvent dimethyl sulphoxide (DMSO, Sigma Chemical Co.Ltd.) to a concentration of 1 mM and stored frozen at –20 °C in 50 µl aliquots. The AM ester is strongly lipophilic and therefore freely penetrates the cell membrane (Thomas & Delaville, 1991). Once inside the cell the ester is cleaved by non-specific intracellular esterases, releasing the hydrophilic free acid, which cannot cross the cell membrane and is thus retained inside the cell. Isolated cardiac myocytes were loaded at room temperature by adding 5 µl of the AM ester solution to 1 ml of KB solution containing a suspension of isolated myocytes. Cells were incubated with the ester for at least 30 minutes at room temperature prior to superfusion with Tyrode's to allow equilibration with the sarcoplasm. No adverse effect of the ester on cell morphology was observed even after prolonged exposure.

2.9.3. Calibration of the Fura-2 fluorescence signal

2.9.3.1 In vitro determination of the Fura-2 dissociation constant

An in vitro calibration was performed. This determined the fluorescence ratio at increasing concentrations of Ca^{2+} in the absence of cells. A solution was made to mimic the intracellular environment using EGTA as a Ca^{2+} buffer (table 2.10).

Various free [Ca^{2+}] were obtained by varying the amount of added $CaCl_2$ and calculated using an apparent EGTA dissociation constant (pK_{Ca}) of 6.44 (Fry *et al.*, 1984) at pH 7.0 according to the equation:

$$pCa = pK_{Ca} + \log([EGTA]/[Ca\ EGTA]) \qquad (2.9)$$

[EGTA] is the total added EGTA and the [Ca EGTA] is equivalent to the concentration of added $CaCl_2$.

Fura-2 fluorescence was measured at room temperature for each concentration of free Ca^{2+}. The determination of the apparent dissociation constant K_d of Fura-2 for Ca^{2+} used the following equation (Grynkiewicz *et al.*, 1985).

$$[Ca^{2+}] = K_d\,[(R-R_{min})/(R_{max}-R)].\beta \qquad (2.10)$$

where R is the ratio of 340/380 nm for a given [Ca^{2+}], R_{min} is the ratio in the absence of Ca^{2+}, R_{max} is the ratio in the presence of saturating Ca^{2+}. $\beta = F380_{min}/F380_{max}$, *i.e.* the ratio of fluorescence intensities in the absence of Ca^{2+} ($F380_{min}$) and in the presence of saturating Ca^{2+} ($F380_{max}$) and K_d is the dissociation constant. Zero Ca^{2+} solution and saturating solution were obtained by using the mock intracellular solution containing 5 mM EGTA with no added $CaCl_2$ and 20 mM added $CaCl_2$ respectively.

A plot of R as a function of [Ca^{2+}] was obtained and the value of K_d obtained using a least squares fit of equation 2.10 to the data was 223 nM.

Table 2.10. Composition of solution used to mimic the intracellular environment

Compound	Concentration (mM)
KCl	120
HEPES	20
NaCl	10
$MgCl_2$	1.0
EGTA	5.0

Titrate to pH 6.9 with 1 M KOH

2.9.4. Estimation of sarcoplasmic reticulum Ca^{2+} content

Contraction of cardiac and smooth muscle cells is activated by Ca^{2+} entry into the sarcoplasm from two sources: the extracellular fluid and the sarcoplasmic reticulum (SR). Ca^{2+} release from the SR was evoked by the addition of 10 mM caffeine to the superfusate. The SR Ca^{2+} content was estimated by measuring the rise of Ca^{2+} when released by caffeine (Varro *et al.*, 1993).

2.10. SDS-PAGE Western blots

To determine levels of the α-isoforms of the Na^{+}-K^{+}-ATPase pump and the SR Ca^{2+}-ATPase pump, SDS-PAGE (sodium dodecyl sulphate-polyacrylamide gel electrophoresis) was carried out according to the method of Laemmli (1970). The proteins were electrophoretically transferred to PVDF (polyvinyl difluoridine) membranes using the method described by Towbin (1979) and the PVDF membrane was probed using characterised antibodies to the proteins of interest (table 2.11).

Table 2.11. Composition of two-times SDS sample buffer. (w/v = weight/volume)

Compound	Concentration
Tris-HCl (pH 6.8)*	100 mM
Dithiothreitol (DTT)	200 mM
Sodium dodecyl sulphate (SDS) (electrophoresis grade)	4% (w/v)
Bromophenol blue	0.02% (w/v)
Glycerol	20% (w/v)

*Tris-HCl buffer was made using Tris base (Trizma) and pH titrated to 6.8 with HCl

The infiltration of new cell types and collagen deposition in hypertrophied hearts could have a diluting effect on the protein of interest. Equal volumes of sample were loaded from sham-operated and aortic constricted hearts. To correct for any differences in the amount of protein loaded from samples from different tissues, the samples were also analysed for calsequestrin, a protein that is not altered by the process of hypertrophy (Arai *et al.*, 1996; Tsutsui *et al.*, 1997; Shorofsky *et al.*, 1999; Schotten *et al.*, 1999;

Somura *et al.*, 2001) and the results were normalised to calsequestrin levels as described by Meyer *et al* (1995).

2.10.1. Sample preparation

Samples of right or left ventricular myocardial tissue from sham-operated, aortic-constricted and debanded hearts were snap-frozen and stored in liquid nitrogen until used. Samples were prepared by adding 10 ml of 50 mM tris(hydroxymethyl)aminomethane(Tris)·HCl buffer (pH 6.8) per gram of tissue; after which the sample was then homogenised on ice using a polytron tissue grinder. This made a 10% homogenate. The samples were divided into aliquots and stored at -70 ^{o}C until use.

A volume of the homogenate was thawed, then mixed with an equal volume of two-times SDS sample buffer (Laemmli *et al.*, 1970). The sample was not boiled as this may complicate the analysis of membrane proteins such as Na^{+}-K^{+}-ATPase. Samples were centrifuged for 5 minutes at 20,000g and the supernatant applied to SDS-PAGE gels.

2.10.2. SDS-PAGE (sodium dodecyl sulphate-polyacrylamide gel electrophoresis) / Western blotting

Electrophoresis of the proteins from the prepared samples was carried out using the mini Protean II system (Bio-Rad Laboratories, Ca, USA) with 10% polyacrylamide gels (0.4 M Tris, 0.1% (w/v) SDS and 10% acrylamide, pH 8.8 with HCl) using a stacking gel (0.1 M Tris, 0.1% (w/v) SDS and 5% acrylamide, pH 6.8 with HCl). Equal volumes of sample (10 µl) were loaded on to the gel at the top of each lane using a pipette. Measurements with normal rat myocardium have shown that this gives about 30 µg of protein per well.

The negatively charged molecules of sodium dodecyl sulphate (SDS) bind to the hydrophobic regions of the protein molecules, causing them to unfold into extended polypeptide chains. A reducing agent, dithiothreitol (DTT) was present in the sample buffer to reduce any disulphide bonds present within proteins. The individual proteins are thus rendered free from their associations with other proteins or lipid molecules and

rendered freely soluble in the detergent solution. The individual polypeptide chains migrate as a negatively charged SDS-protein complex through the porous gel of polyacrylamide. Under these conditions the speed of migration is greater the smaller the peptide, thus allowing separation of the proteins according to molecular weight (Laemmli *et al.*, 1970).

After electrophoresis proteins were electrophoretically transferred to a PVDF membrane (Pharmacia AB, Stockholm, Sweden) with a semi-dry blotter (Pharmacia AB, Stockholm, Sweden) and a current of 100 mA per gel for 2 hours (Towbin *et al.*, 1979). The transfer buffer contained 20% methanol (v/w), 0.5 M glycine, 25 mM Tris and 0.01% SDS (w/v).

To reduce non-specific binding, PVDF membranes were blocked with 5% skimmed milk in phosphate-buffered saline (PBS) for at least 4 hours at room temperature. The membranes were then incubated with primary antibodies specific for the α-1, α-2 and α-3 isoforms of the Na^+-K^+-ATPase pump, sarcoplasmic reticulum Ca^{2+}-ATPase (SERCA2) and calsequestrin (table 2.12).

2.10.3. Antibodies

Monoclonal antibodies and polyclonal antisera directed against the specific isoforms of the Na^+-K^+-ATPase pump and the SR Ca^{2+}-ATPase pump were used (table 2.12). A mouse monoclonal antibody specific for α_1-isoform was purchased from Upstate Biotechnology (USA). A monoclonal antibody specific for α_2 (McB2), raised against purified rat axolemma Na^+-K^+-ATPase, showing broad species cross-reactivity was a generous gift from KJ Sweadner (Massachusetts General Hospital, Boston MA, USA). A monoclonal antibody against mouse α_3-isoform was purchased from Affinity Bioreagents Inc (USA). Polyclonal antisera against rabbit α_2-isoform was purchased from Upstate Biotechnology (USA). A monoclonal antibody directed against mouse SR Ca^{2+}-ATPase (SERCA2A) and polyclonal antisera against rabbit calsequestrin were obtained from Affinity Bioreagents Inc (USA).

Table 2.12. Details of the specific antibodies used to detect the α-isoforms of the Na^+K^+-ATPase pump, SERCA2 and calsequestrin

Antibody	Isoform	Source	Reference
Mouse (Monoclonal)	α1	Upstate Biotechnology (USA)	
Rabbit (Polyclonal)	α2	Upstate Biotechnology (USA)	
McB2 (rat) (Monoclonal)	α2	KJ Sweadner	Urayama *et al.*, 1989
Mouse (Monoclonal)	α3	Affinity Bioreagents Inc (USA)	
Mouse (Monoclonal)	SERCA2A	Affinity Bioreagents Inc (USA)	
Rabbit (Polyclonal)	Calsequestrin	Affinity Bioreagents Inc (USA)	

The α_1, calsequestrin and SERCA 2 antibodies were incubated for 1 hour at room temperature. The α_2 and α_3 antibodies were incubated overnight at 4 °C. Non-specific primary antibody binding was removed by washing the blots in PBS 0.05% Tween-20 with multiple changes of wash buffer over 1 hour. Blots were then incubated with a secondary antibody, conjugated to horseradish peroxidase (HRP) for 1 hour at room temperature (anti-rabbit IgG antibody (dilution 1: 1000) for α_1 and α_3 and calsequestrin and anti-mouse IgG (dilution 1: 1000) for α_2 and SERCA2, Amersham UK). After both the primary and secondary antibodies were applied, the blots were washed again with multiple changes of PBS 0.05% Tween-20 for I hour. The PVDF membrane was then soaked for approximately 1 minute in ECL (enhanced chemiluminescence) detection reagent (ECL system, Amersham, UK). This elicits a peroxidase-catalysed oxidation of luminol, and subsequently enhanced chemiluminescence where the HRP labeled protein is bound to the antigen on the membrane, thus enabling visualisation of the primary antibody binding. The resulting light was detected by exposing the membrane to autoradiograph film (Hyperfilm ECL). The ECL images were digitised using a flatbed scanner (Hewlett Packard, ScanJet 11C), and quantitative analysis performed using the NIH software (Freeware, NIH, Baltimore, USA).

After taking images, blotting integrity was confirmed by staining the PVDF membranes with 0.25% Coomassie brilliant blue (BDH, UK) in 10% acetic acid, 50% methanol for 5 minutes. The membranes were transferred to destaining solution (40% methanol, 7% glacial acetic acid) and agitated, to remove non-specific background staining.

2.11. Statistical analysis

All data analysis was performed on a personal computer. Mathematical functions, graphical presentation of data and curve fitting were all performed using the Scientific Analysis application; KaleidaGraph ™, for Windows, version 3.5, (Synergy Software (PCS Inc)). Values in the text are quoted as the arithmetic mean ± one standard deviation (mean ± SD) unless otherwise stated when the arithmetic mean ± one standard error (mean ± SEM) was used. Two tailed Students's t-tests were used to test for the significance between all normally distributed sets of data. Straight lines were fitted by least square analysis and the slope, intercept, and correlation coefficient derived using KaleidaGraph™, for Windows, version 3.5, (Synergy Software (PCS Inc)). The null hypothesis was rejected when $p \leq 0.05$.

Chapter 3: Results

3.1. Assessment of magnitude of hypertrophy produced by aortic constriction.

It was essential to demonstrate, quantitatively, that left ventricular myocardial mass had increased as a result of the surgical ascending aortic-constriction. It has previously been shown in this model of LVH that the increase in left ventricular mass results from cellular hypertrophy, rather than hyperplasia (Cooklin *et al.*, 1998).

Muscle mass increase was, of necessity, estimated from the whole heart weight assuming that only the left ventricle increased in size as a result of aortic-constriction. This is not an unreasonable assumption as in the absence of prolonged congestive cardiac failure there is no reason to suggest that significant right ventricular hypertrophy should occur as a result of aortic-constriction. Such a chronic pathological state was not observed in the animals used in these studies as assessed by evidence of respiratory distress or fluid retention on observation. In addition, lung-to-body weight ratios were measured in a subset of animals and were not significantly different between the sham-operated and aortic-constricted groups (5.78 ± 0.67 $g.kg^{-1}$ (n=18) vs 6.15 ± 2.03 $g.kg^{-1}$ (n=23), mean ± SD: $p>0.05$). Changes in heart weight attributable to atrial enlargement were assumed to be small and were neglected. The data obtained were normalised for animal weight, as animals varied in size and were expressed as a heart-to-body weight ratio.

Animals were sacrificed between 42 and 250 days post-operatively. As observed in previous studies using this model the degree of hypertrophy did not correlate with the duration of clip placement. There was considerable variation in the degree of hypertrophy induced from animal to animal, due presumably to variations in clip size, surgical placement, and the biological response to the intervention (figure 3.1). This scatter in heart-to-body weight ratio (HBR) allowed interpretation of the data in terms of a continuum of the degree of hypertrophy present.

3.1.1. Measurement of heart-to-body weight ratio

Estimation of the severity of hypertrophy was made by determination of the heart-to-body weight ratio (expressed as $g.kg^{-1}$) at the time of heart removal immediately prior to

removal of a papillary muscle or cell isolation. Whole hearts were weighed in a beaker containing Tyrode's solution. Animals were weighed prior to sacrifice. Typically some small residuum of mediastinal tissue remained with the heart following rapid removal and was included in the estimate of heart mass. The ventricles contained some residual blood, of the order of 100 μl, which may have produced a slight (0.1 g) overestimate of heart weight.

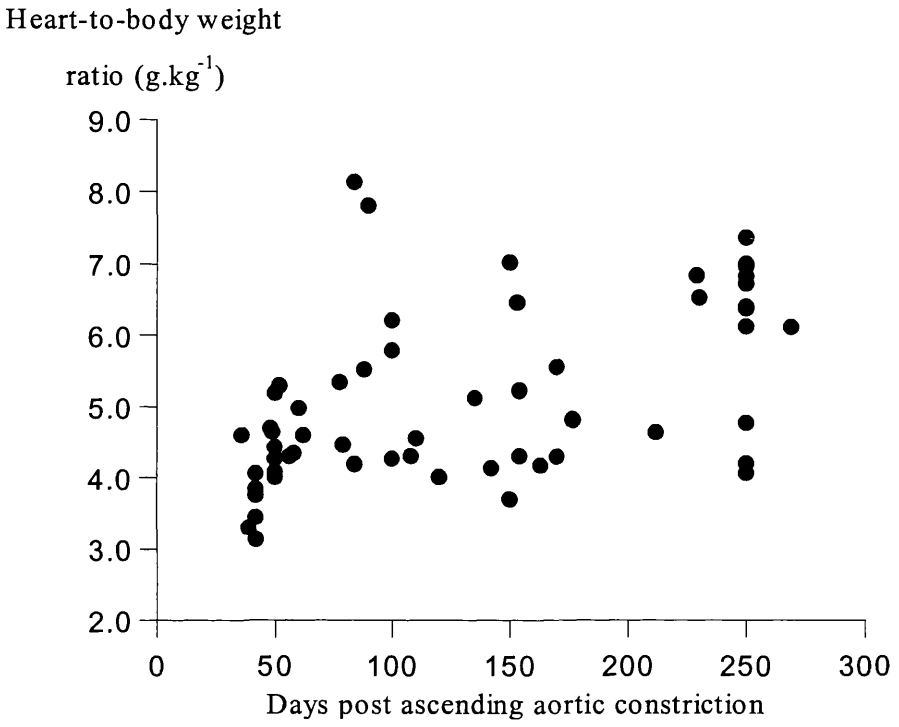

Figure 3.1. Relationship between heart-to-body weight ratio and duration of ascending aortic clip placement (n=60 animals)

Table 3.1 lists the heart-to-body weight ratio for unoperated, sham-operated and aortic constricted groups. As expected the ratio was significantly increased in the aortic constricted animals ($p<0.0001$). Heart weights were lower in the unoperated group than in the sham-operated group ($p<0.0001$) as these animals were younger and therefore their body weights were also lower.

Table 3.1. Effect of ascending aortic-constriction on heart weight and heart-to-body weight ratio in all animal groups. Data shown are mean ± SD. *p<0.0001 for aortic-constricted compared to sham-operated and aortic-constricted compared to unoperated groups, **p<0.0001 for sham-operated compared to unoperated group. HBR = Heart-to-body weight ratio

	Unoperated	Sham-operated	Aortic-constricted
Heart weight (g)	2.27±0.55	4.16±0.57**	5.85±1.55*
HBR ($g.kg^{-1}$)	3.74±0.32	3.57±0.44	5.15±1.21*
N	100	27	61

3.1.2. Regression of left ventricular hypertrophy

The heart-to-body weight ratios for debanded and sham-sham operated guinea pigs are shown in table 3.2. Comparison with results in table 3.1 shows that removal of the previously placed constriction resulted in regression of LVH. There were no significant differences in heart or heart-to-body weight ratios between either the debanded and sham-sham operated groups. Both heart weight and heart-to-body weight ratios were significantly reduced in both debanded groups compared to the aortic-constricted group (table 3.1)

Table 3.2. Effect of removal of the ascending aortic constriction on heart weight and heart-to-body weight ratio. Data shown are mean ± SD. HBR = Heart-to-body weight ratio. * denotes p<0.05 and ** p<0.001 compared to corresponding values in aortic-constricted hearts in table 3.1

	Debanded 42±3 days	Debanded 100±3 days	Sham-Sham 100±3 days
Heart weight (g)	4.22±1.03*	3.19±0.44**	3.7±0.36
HBR ($g.kg^{-1}$)	3.57±0.45**	3.18±0.44**	3.2±0.16
N	6	4	4

3.1. Mechanical properties of the isolated myocardial preparation

Mechanical function of isolated myocardium from control (unoperated and sham-operated) and aortic-constricted guinea-pigs was investigated by measurement of the alteration in twitch tension of the isolated preparation following chronotropic augmentation of contractility. The data from the unoperated and sham-operated groups did not differ and the 2 groups were therefore combined to a single control group.

The effect of regression of LVH on mechanical function was assessed by measuring the force-frequency response and post-rest potentiation in LV preparations from guinea-pigs in whom the ascending aortic clip was removed after 42 or 100 days.

To examine further the contractility of the myocardium certain experiments were repeated in the presence of strophanthidin. The effect of altering external sodium concentration on normal myocardial preparations was also investigated.

In all experiments the preparation was stimulated at 1 Hz, in normal Tyrode's at 37 ^{0}C, pH 7.35, unless otherwise stated.

3.2.1. The force-frequency relationship

Previous investigations of the force-frequency response have often used low basal stimulation frequencies (i.e.~0.01 Hz) which precludes interpretation of the results during physiological changes of heart rate. In this study the frequency at which the preparation was stimulated was over the range 0.4 to 2 Hz. At each new frequency, the steady-state tension was recorded after 5 minutes, prior to further increment.

Figure 3.2 shows steady-state isometric tension as a function of stimulation frequency in left ventricular papillary muscles from 33 control (open circles) and 45 aortic-constricted guinea-pigs (closed circles). Tension is expressed as the percentage generated with respect to tension at a stimulation frequency of 1 Hz. Compared to control, left ventricular papillary muscles from aortic-constricted hearts showed a depressed force-frequency relationship. There was no significant difference in the peak isometric force generated by preparations from control and aortic-constricted hearts at stimulation

frequency of 1 Hz (1.29 ± 0.42 $mN.mm^{-2}$ vs 1.00 ± 0.65 $mN.mm^{-2}$, respectively, mean ± SD, $p>0.05$). Plate 1 shows the effect of increasing stimulation frequency from 0.8 to 1.6 Hz on tension in a papillary muscle from a sham-operated heart in A and an aortic-constricted heart in B.

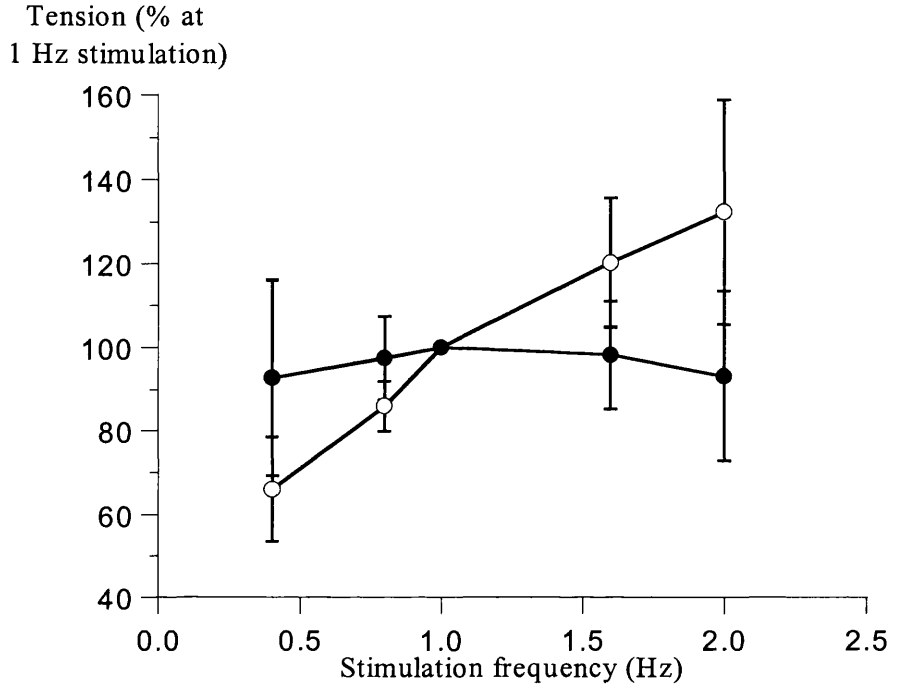

Figure 3.2. Steady-state isometric tension expressed as a function of stimulation frequency in preparations from control (open circles) and aortic-constricted (filled circles) guinea-pigs. Tension is expressed as % control (100% at 1 Hz). Values are mean ± SD.

However, the force-frequency relationship was a variable phenomenon with some preparations showing a positive response and others a pronounced negative response to increasing frequency of stimulation. The range of responses in different preparations is shown in figure 3.3 with the most positive (open circles) and most negative (open squares) relationships illustrated.

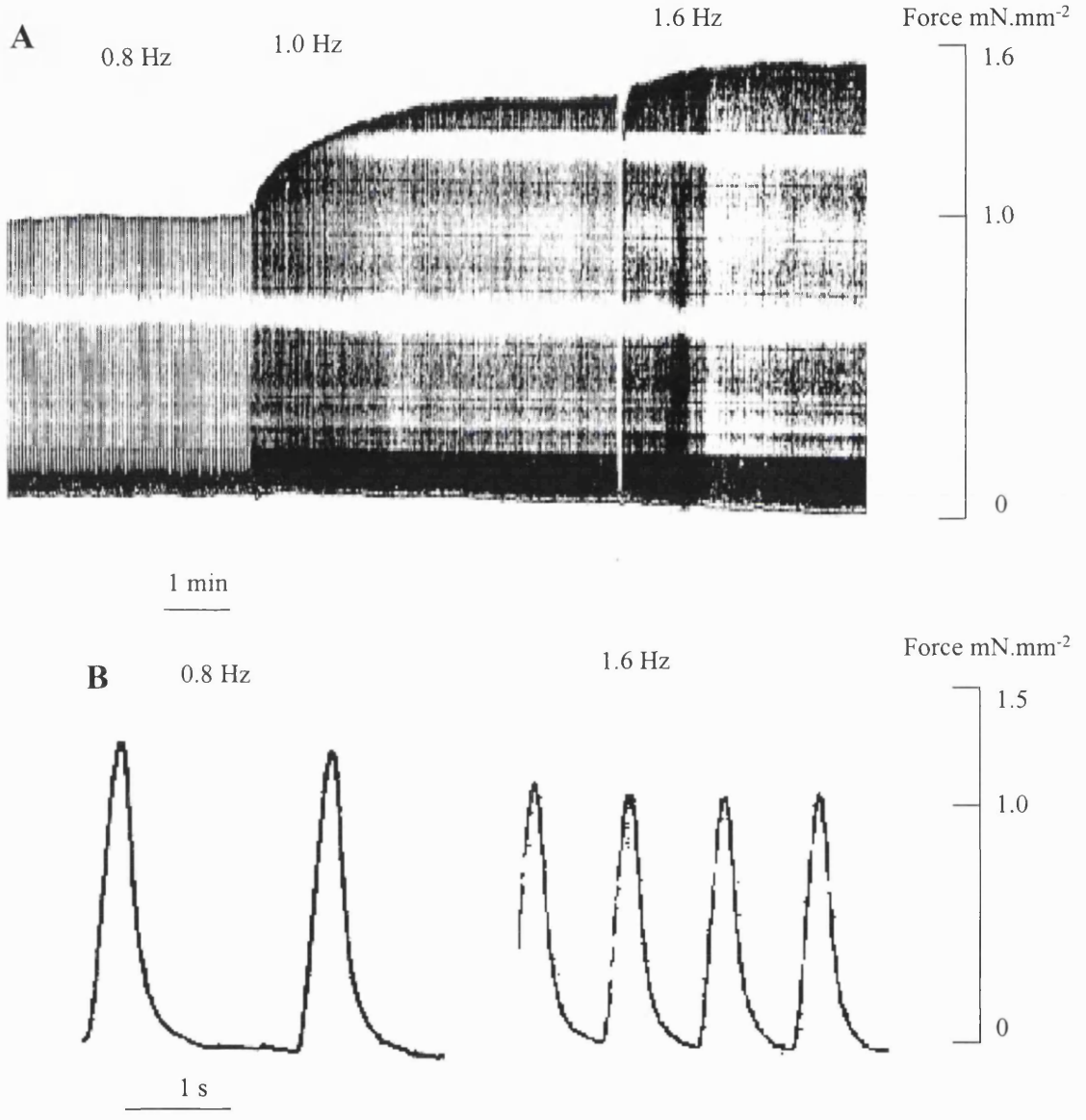

Plate 1: Tension generated in response to increasing stimulation frequency from 0.8 to 1.6 Hz in a papillary muscle from a sham-operated heart in A and an aortic constricted heart in B

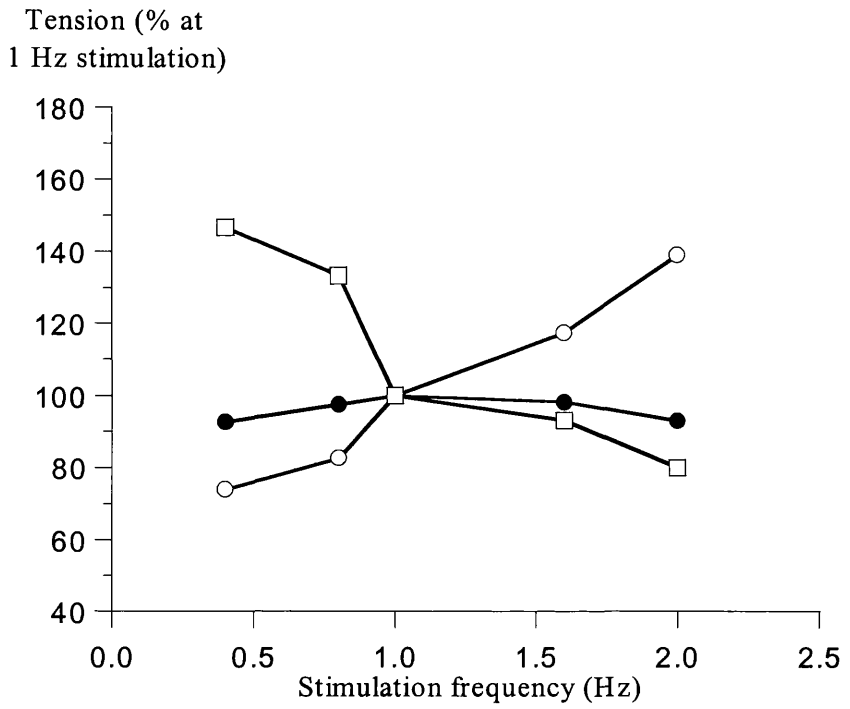

Figure 3.3. Steady-state isometric tension as a function of stimulation frequency in aortic-constricted hearts. Closed circles represent mean values, n=26. Open circles and squares reflect the most pronounced positive and negative staircase response respectively.

In order that the range of responses between preparations may be compared tension is expressed as a ratio of the steady-state tension generated in response to a doubling of the stimulation frequency from 0.8 to 1.6 Hz ($T_{(1.6/0.8)}$). Ratios greater than 1.0 and less than 1.0 equate with positive and negative force-frequency response respectively. Table 3.3 shows $T_{(1.6/0.8)}$ values in right and left ventricular papillary muscles from control and aortic-constricted hearts. Positive force-frequency responses were observed in right (RV) and left ventricular (LV) papillary muscles from unoperated and sham-operated hearts and in RV papillary muscle from aortic-constricted hearts. The responses were greater ($p<0.05$) in RV compared to LV papillary muscles from unoperated animals but there was no significant difference ($p>0.05$) in the response between the LV papillary muscles from the unoperated and sham-operated groups. The force-frequency response from the aortic-constricted hearts was significantly depressed compared to the sham-operated or unoperated groups ($p<0.0001$).

Table 3.3. Force-frequency relationships ($T_{(1.6/0.8)}$) and heart-to-body weight ratios in isolated papillary muscles from control and aortic-constricted guinea-pig hearts. Values are mean ± SD. RV= right ventricle, LV = left ventricle. * denotes $p<0.0001$ compared to sham operated or unoperated groups and ** denotes $p<0.05$ compared to RV unoperated group (unpaired Student's T-test).

	Force-frequency relationship ($T_{(1.6/0.8)}$)	Heart-to-body weight ratio ($g.kg^{-1}$)
RV unoperated (n=9)	1.67±0.19	3.69±0.23
RV aortic constricted (n=3)	1.48±0.13	6.31±0.85*
LV unoperated (n=16)	1.48±0.21**	3.43±0.27
LV sham operated (n=17)	1.35±0.21**	3.52±0.37
LV aortic constricted (n=45)	1.02±0.21*	5.28±1.32*

3.2.1.1. The force-frequency relationship and heart-to-body weight ratio

In order to explain these findings it was proposed that as in human myocardium, the force-frequency response becomes negative as hypertrophy develops. Figure 3.4 shows the relationship between $T_{(1.6/0.8)}$ and heart-to-body weight ratio for LV preparations from control and aortic-constricted hearts ($r=-0.58$, $n=78$, $p<0.01$).

The force-frequency response data can be grouped in an alternative manner according to heart-to-body weight ratio as in figure 3.5. Data from aortic-constricted hearts were divided into two groups with moderate ($4.0 < HBR < 5.5$ $g.kg^{-1}$; mean increase 38%) and severe hypertrophy ($HBR > 5.5$ $g.kg^{-1}$; mean increase 83%). As stated above HBR was significantly larger in the aortic-constricted groups compared to the sham-operated and unoperated groups. The $T_{(1.6/0.8)}$ ratio was significantly reduced in the aortic-constricted groups (1.02 ± 0.20; $4.0 < HBR < 5.5$ $g.kg^{-1}$, $n=21$ and 1.00 ± 0.23; $HBR > 5.5$ $g.kg^{-1}$, $n=19$) compared to the two control groups (1.35 ± 0.21, $n = 17$ - sham-operated; 1.47 ± 0.21, $n = 16$ - unoperated left ventricle, (mean ± SD)).

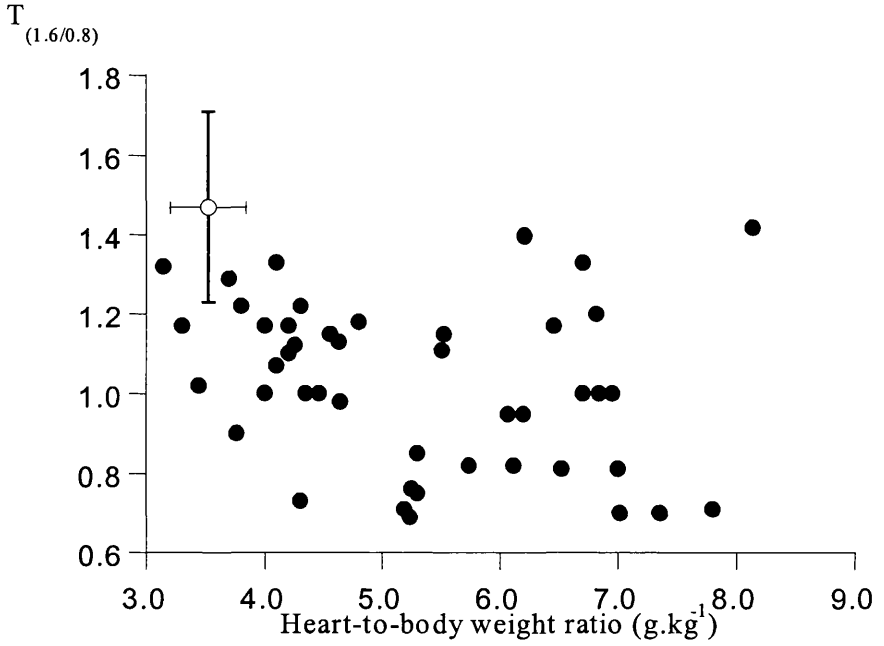

Figure 3.4. The force-frequency relationship ($T_{(1.6/0.8)}$) as a function of heart-to-body weight ratio in isolated preparations from control and aortic-constricted hearts. The open circle represents combined data (mean ± SD) from unoperated and sham-operated left ventricle (n=33) and the filled circles individual left ventricle papillary muscles from aortic-constricted hearts (n=45).

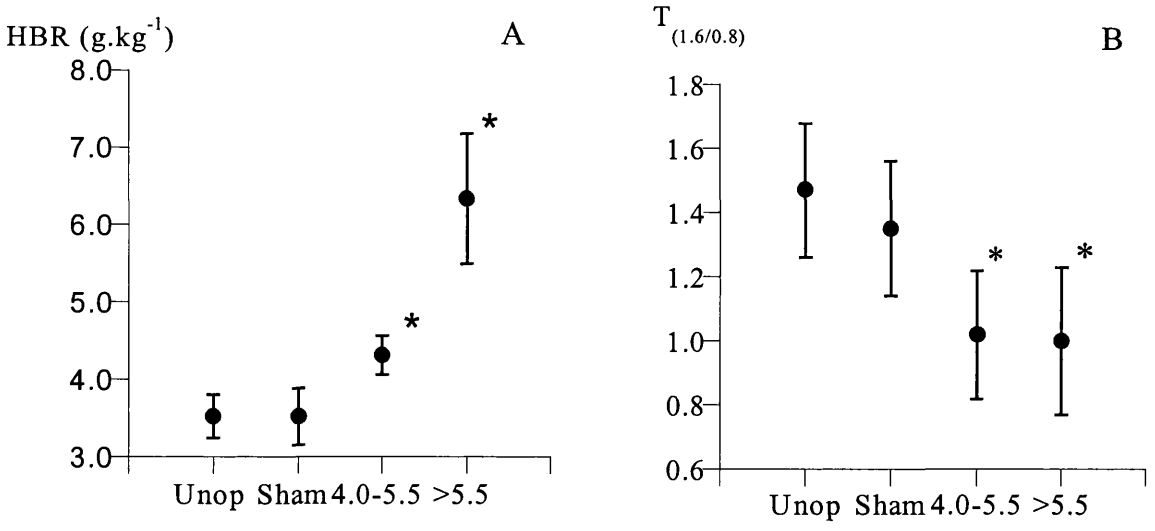

Figure 3.5. (A) Heart-to-body weight ratios (HBR) and (B) force-frequency relationships ($T_{(1.6/0.8)}$) from unoperated LV, sham-operated LV, moderate (4.0 to 5.5 $g.kg^{-1}$, n=21) and severe hypertrophy (>5.5 $g.kg^{-1}$, n=19). Values are mean ± SD. * denotes $p < 0.0001$.

3.2.2. Post-rest potentiation

The phenomenon of post-rest potentiation, whereby restimulation after a period of quiescence is associated with enhancement of the contractile response is not observed in normal myocardium where the force-frequency response is positive. Figure 3.6 illustrates the tension generated during the first beat, on re-stimulation at a frequency of 1Hz, after a 30 second period of quiescence in left ventricular papillary muscles from control and aortic-constricted hearts. Tension is expressed as the percentage post-rest tension compared to steady-state tension at frequency of 1 Hz prior to cessation of stimulation. Mean percentage tension generated post-rest was 69 ± 20 % in control hearts (n=13) compared to 139 ± 30 % in moderate hypertrophy (HBR = 4.0-5.5 $g.kg^{-1}$; n=11) and 130 ± 31 % in severe hypertrophy (HBW > 5.5 $g.kg^{-1}$, n=14); $p<0.0001$ for hypertrophy groups compared to control, (all values mean ± SD).

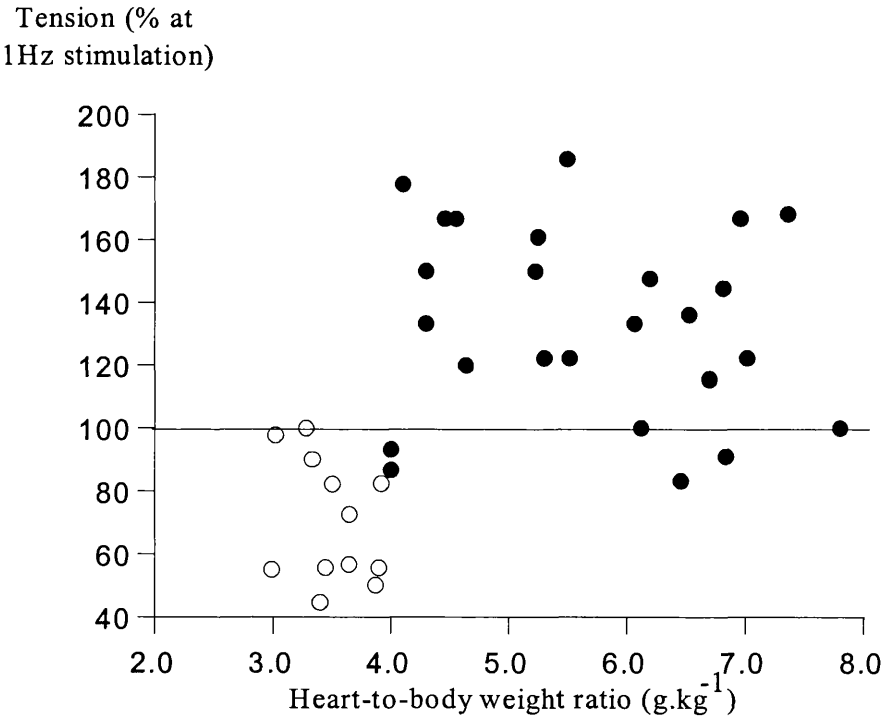

Figure 3.6. Post-rest tension and heart-to-body weight ratio in left ventricular papillary muscles from control (open circles) and aortic-constricted hearts (filled circles). Potentiation occurs when tension is greater than the control level of 100%, illustrated by the horizontal line.

3.2.3. Effect of regression of LVH on contractile function

Table 3.4 summarises the effect of removal of the ascending aortic clip on the force-frequency relationship expressed as a ratio of the steady-state tension generated in response to a doubling of the stimulation frequency from 0.8 to 1.6 Hz ($T_{(1.6/0.8)}$). The number of preparations was small but no significant differences were observed between the debanded and sham-sham operated groups. Compared to the results in table 3.3, the combined debanded group had a significantly more positive force-frequency response than the preparations from the aortic-constricted hearts (P=0.012). The effect on the tension generated on restimulation at 1 Hz after a 30 second period of quiescence (post-rest potentiation) was also measured and the findings were similar.

Table 3.4. Force-frequency relationships, post-rest tension and heart-to-body weight ratios in LV papillary muscles from debanded and sham-sham operated guinea-pig hearts. Values are mean ± SD. * denotes $p<0.05$ compared to aortic-constricted group in table 3.3.

	Force-frequency relationship ($T_{(1.6/0.8)}$)	Post-rest tension (% tension at 1 Hz)	Heart-to-body weight ratio ($g.kg^{-1}$)
Debanded +42 days (n=6)	1.23±0.25*	88.7±34.7*	3.57±0.45
Debanded +100 days (n=4)	1.25±0.18*	68.8±28.1*	3.18±0.44
Sham-sham +100 days (n=4)	1.32±0.09	47.5±18.8	3.2±0.16

3.2.4. Summary

As expected, normal guinea-pig myocardium demonstrated a positive force-frequency response. In contrast, similar to our findings in human myocardium, the progression of hypertrophy altered the ability of guinea-pig myocardium to generate a positive inotropic response to an increase of stimulation frequency. It is likely that the decline in the force-frequency relationship is a consequence of hypertrophy as in three right ventricular

papillary muscles obtained from hearts with LVH but presumably normal right ventricles, the force-frequency response was also positive. Furthermore in a small number of preparations from animals in which the ascending aortic clip was removed resulting in regression of LVH, the force-frequency response was positive and post-rest potentiation was not observed.

Both a negative force-frequency response and post-rest potentiation are known to occur in species where intracellular [Na^+] is elevated. The association of cardiac hypertrophy with a negative force-frequency response and post-rest potentiation leads to the hypothesis that intracellular [Na^+] is elevated in hypertrophy.

This hypothesis was addressed initially by investigating the effect of elevation of intracellular [Na^+], consequent upon addition of strophanthidin to the perfusate, on the contractile response to increasing frequency of stimulation.

3.3. Contractility and strophanthidin

3.3.1. The inotropic response to strophanthidin

Strophanthidin is known to increase contractility secondary to inhibition of the sarcolemmal Na^+-K^+ATPase and elevation of intracellular [Na^+], $[Na^+]_i$. In control guinea-pig myocardium, increasing the concentration of strophanthidin resulted in elevation of tension to a new steady-state. The increase in tension was gradual over 3 to 5 minutes and the tension generated was measured once steady-state had been achieved. However, as can be seen in figure 3.7 the inotropic effect was less consistent in preparations from aortic-constricted hearts and the tension developed decreased at concentrations of 1μM and 3 μM.

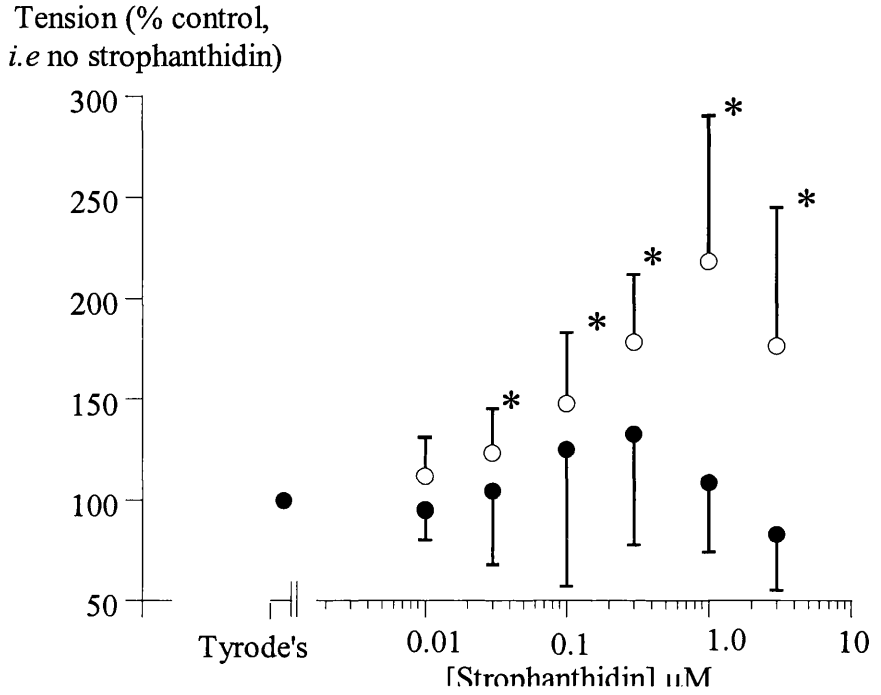

Figure 3.7. The inotropic response to strophanthidin in isolated preparations from control (open circles) (n=18) and aortic-constricted (filled circles) (n=9) guinea-pig hearts. Values are mean ± SD. * denotes $p<0.05$ compared to control. Stimulation frequency is 1 Hz

3.3.2. The effect of strophanthidin on the force-frequency relationship

To determine the effect of strophanthidin on the force-frequency relationship the effect of alteration of stimulus frequency was studied at increasing concentrations of strophanthidin (0.01 to 3μM) in papillary muscle preparations from both control and aortic-constricted hearts. The concentrations of strophanthidin were incrementally increased in a given preparation and the results are shown in figure 3.8. In control myocardium, the force-frequency response became progressively flatter as the concentration of strophanthidin increased and at 3 μM was negative. This effect is unlikely to be due to hypoxia or fatigue in the preparation as on reperfusing the same preparation with normal Tyrode's solution, a positive force-frequency relationship was restored. In aortic-constricted hearts a similar effect of increasing concentrations of strophanthidin was observed with further depression of the response.

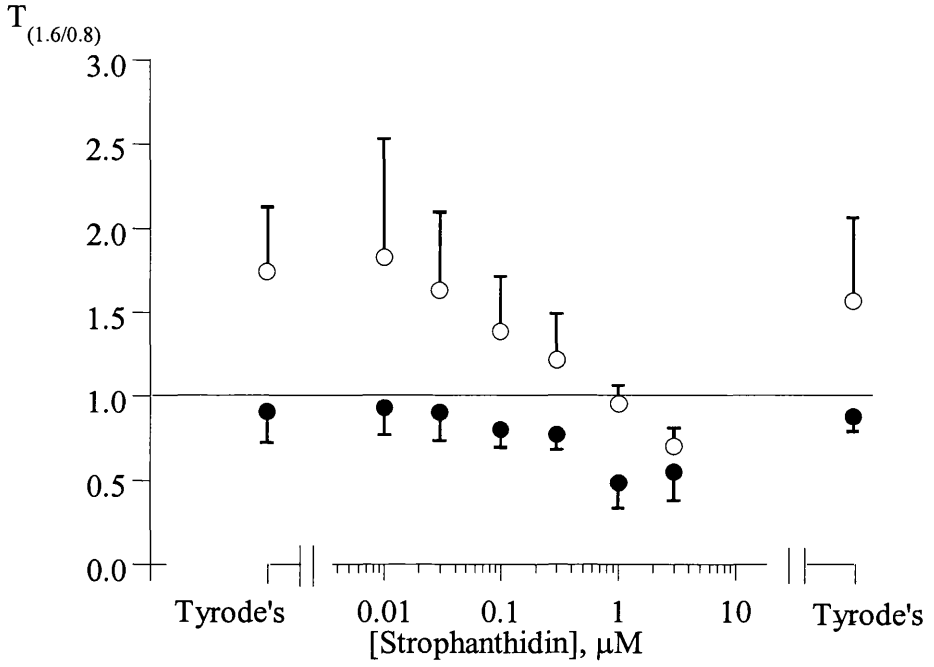

Figure 3.8. The force-frequency relationship ($T_{(1.6/0.8)}$) in the presence of strophanthidin in papillary muscles from control (open circles) and aortic-constricted (filled circles) hearts. Ratio of 1.0 illustrated by the horizontal line. Values are mean ± SD.

Comparison of the force-frequency response in control guinea-pig myocardium in the presence and absence of 1 μM strophanthidin to that in aortic-constricted myocardium is shown in figure 3.9. The response in aortic-constricted guinea-pig myocardium is similar to that in control guinea-pig myocardium exposed 1μM strophanthidin.

3.3.3. The effect of strophanthidin on post-rest potentiation

The effect of strophanthidin on the contractile response in control and aortic-constricted hearts was further investigated by measuring post-rest potentiation.

In preparations from control and aortic-constricted hearts the tension generated after a period of 30 seconds quiescence was expressed as a percentage of control tension at 1Hz. The results are shown in table 3.5. At concentrations of strophanthidin > 0.3 μM the post-rest tension generated was significantly greater than in the absence of strophanthidin in both control and aortic-constricted hearts. Again this effect is unlikely to be due to

hypoxia developing in the preparation as the values returned to baseline in the preparations after replacement of the perfusate with normal Tyrode's solution.

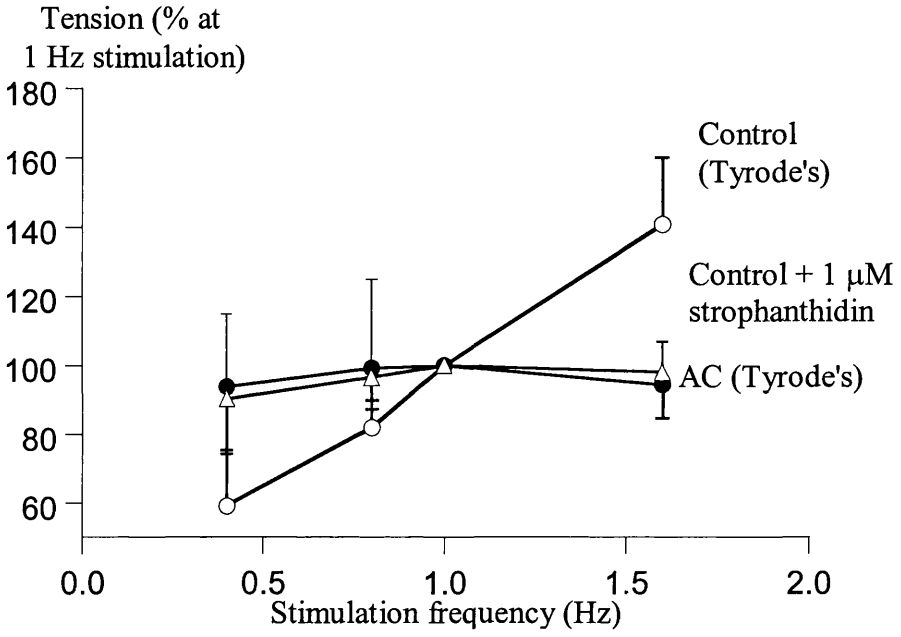

Figure 3.9. Comparison of the force-frequency response in control and aortic-constricted guinea-pigs. The response in control myocardium is shown by open circles in the absence and open triangles in the presence of 1 μM strophanthidin and the response in aortic-constricted (AC) myocardium is shown by filled circles. Values are mean ± SD.

The results are illustrated in figure 3.10. The effect of increased concentration of strophanthidin on post-rest tension in normal guinea-pig myocardium is similar to that in aortic-constricted myocardium in the absence of strophanthidin.

Table 3.5. Effect of strophanthidin on post-rest tension in control and aortic-constricted guinea-pig myocardium. Values are mean ± SD. * denotes $p<0.01$ and ** $p<0.05$ when compared to Tyrode's.

[Strophanthidin] (μM)	Tension (% control) Control (n=8)	Tension (% control) Aortic-constricted (n=5)
0	53±14	112±27
0.01	51±12	106±27
0.03	64±15	112±22
0.1	69±19*	119±16
0.3	82±23*	146±25**
1.0	118±11*	177±24**
3.0	124±20*	
0	56±8	111±29

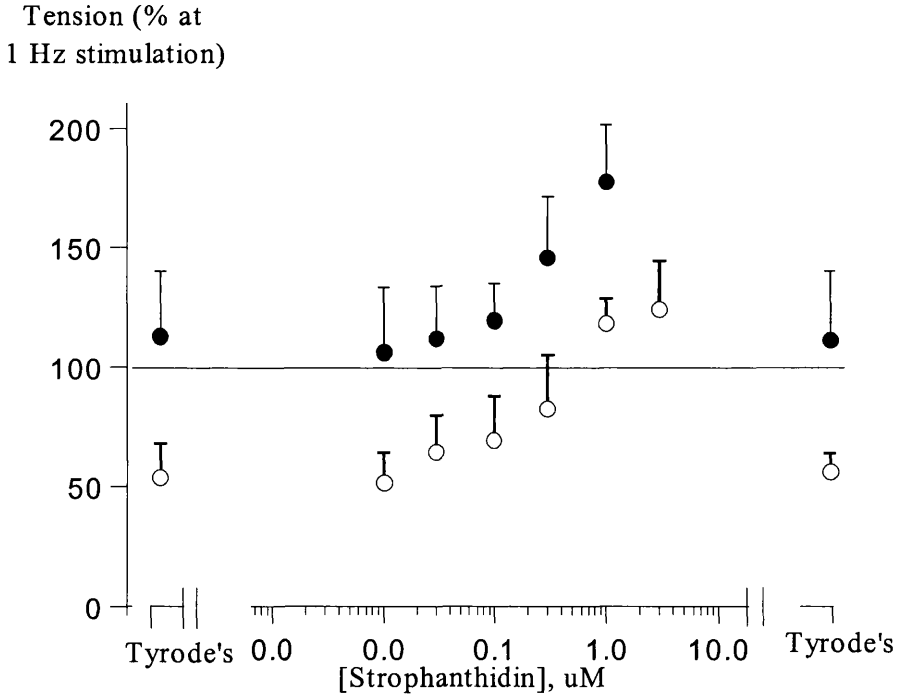

Figure 3.10. Post-rest tension in the presence of strophanthidin in isolated preparations from control (open circles) and aortic-constricted (filled circles) hearts. Values are mean ± SD. Potentiation occurs when tension is greater than the control level of 100%, illustrated by the horizontal line.

3.3.4. Summary

In normal guinea-pig myocardium the addition of strophanthidin to the perfusate resulted in alteration of the contractile response to changes in stimulation frequency. At concentrations of strophanthidin above 0.3μM the response resembled that seen in hypertrophied guinea-pig myocardium. This effect may be related to an increase in intracellular $[Na^+]$ since a negative force-frequency response is seen in species where intracellular $[Na^+]$ is naturally high.

In the rat where $[Na^+]_i$ is high, the systolic intracellular calcium transients were reduced at higher frequencies (Orchard & Lakatta, 1985) and intracellular calcium gain $[Ca^{2+}]_i$ occurred during periods of rest (Shattock & Bers, 1989). The net depletion of $[Ca^{2+}]_i$ at higher frequencies was explained by enhanced trans-sarcolemmal egress of Ca^{2+} via Na^+-Ca^{2+} exchange.

The transmembrane Na gradient needs to be considered as well and an alternative way to alter the transmembrane $[Na^+]$ and $[Ca^{2+}]$ gradients was to perfuse the preparation with low-Na or high-Ca containing solutions. As shown by Sheu & Fozzard (1982), a graded decrease of external [Na], results in a decrease of $[Na^+]_i$ and an increase of $[Ca^{2+}]_i$ whereas an increase of external Ca^{2+} results in an increase of $[Ca^{2+}]_i$ and a decrease of $[Na^+]_i$.

3.4. The effect of reduced external [Na] on contractile function

As outlined in the methods section reduced Na-containing Tyrode's was prepared by substituting NaCl with Tris and adjusting the pH to 7.35±0.5 (mean ± SD) with HCl. The inotropic response at a stimulation frequency of 1 Hz to reduced external Na, $[Na]_o$ solution in normal guinea-pig myocardium is shown in figure 3.11. Reducing the extracellular [Na] resulted in elevation of tension to a new steady state. The increase in tension occurred over 2 to 3 minutes and the measurements were made once steady state tension was reached. It was observed that in a number of preparations the tension generated in 29 mM Na was less than that in 50 mM Na but the difference was not significant ($p>0.05$).

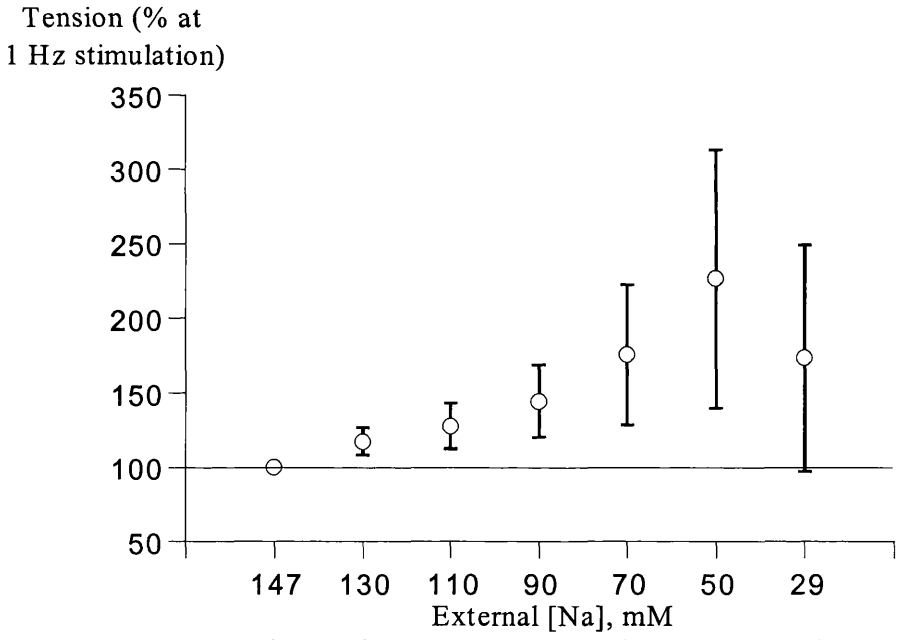

Figure 3.11. The inotropic response to reduced extracellular [Na] in isolated preparations from control guinea-pig hearts (n=12). Values are mean ±SD. Stimulation frequency is 1Hz. Control tension (100%) is illustrated by the horizontal line.

The effect of reduced $[Na]_o$ on the force-frequency relationship in isolated preparations from control guinea-pig myocardium is shown in figure 3.12. The response became progressively flatter as the concentration of $[Na]_o$ was reduced from 147 mM to 29 mM. This effect was unlikely to be due to hypoxia or fatigue in the preparation as on reperfusing the same preparation with normal Tyrode's solution (containing 147 mM Na), a positive force-frequency relationship was restored.

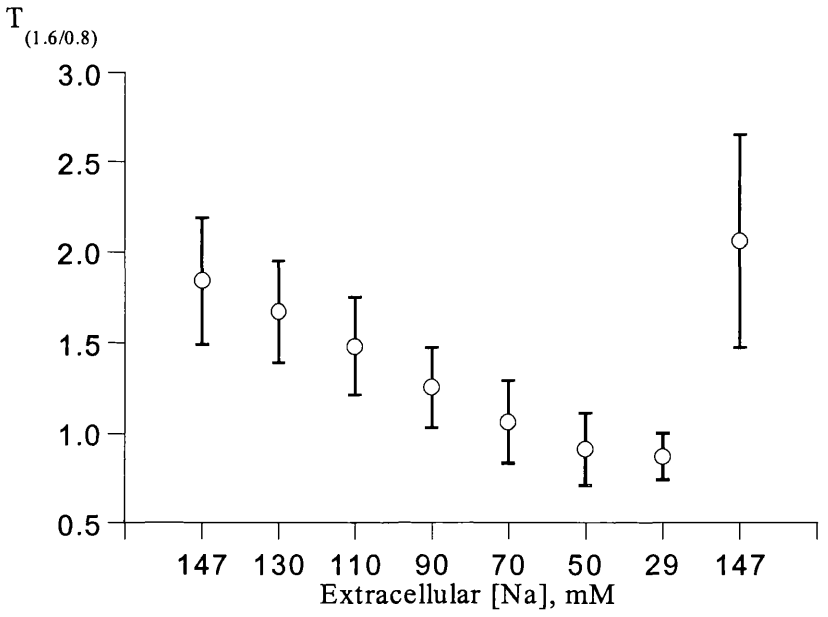

Figure 3.12. The effect of reduced extracellular [Na] on the force-frequency relationship ($T_{(1.6/0.8)}$) in isolated preparations from control hearts (n=12). Values are mean ± SD.

3.5. The effect of increased extracellular [Ca] on contractile function

Extracellular [Ca] was increased by the addition of $CaCl_2$ to standard Tyrode's (1.8 mM Ca) to produce solutions containing 3.6 and 5.4 mM Ca. The effect of increasing calcium, $[Ca]_o$ on contractile function and the response to increased frequency of stimulation in isolated preparations from control hearts is shown in table 3.6.. Increasing $[Ca]_o$ resulted in an increase in tension to a new steady-state at a stimulation frequency of 1Hz, however, the force-frequency relationship became progressively flatter.

Table 3.6. The effect of increased extracellular [Ca] on contractile function and the force-frequency relationship ($T_{(1.6/0.8)}$) in isolated myocardium from control hearts. Values are mean ± SD.

External [Ca]	Inotrophy (% control at 1 Hz)	$T_{(1.6/0.8)}$	Post-rest potentiation (% control)
1.8 mM (n=5)	100	1.56±0.18	68±13
3.6 mM (n=2)	167	1.25	72
5.4 mM (n=3)	209±16	0.92±0.61	86±5

3.6. Summary

The series of experiments described thus far showed that compared to control, left ventricular papillary muscles from aortic-constricted hearts showed a depressed force-frequency relationship indicating impaired contractile function. This was similar to the finding in hypertrophied human myocardium. The positive force-frequency relationship in normal guinea-pig myocardium was changed to a negative response by interventions that alter intracellular $[Na^+]$ and $[Ca^{2+}]$. This lead to the proposal that left ventricular hypertrophy is accompanied by an increase of intracellular $[Na^+]$. Such an increase in $[Na^+]_i$ could be responsible for the inability of hypertrophied myocardium to increase the force of contraction when stimulation frequency is raised.

3.7. Intracellular Na^+ concentration, $[Na^+]_i$ and hypertrophy

3.7.1. Intracellular Na^+ concentration $[Na^+]_i$, measurements

$[Na^+]_i$ was measured in some of the guinea-pig papillary muscle from control and aortic-constricted hearts used for the tension recordings using ion-selective microelectrodes. The ion-selective microelectrodes and KCl-filled microelectrodes were prepared as outlined in the methods (Chapter 2, section 2.4). Stable microelectode impalements were achieved in 28 preparations from control hearts and 12 preparations from aortic-constricted hearts.

The KCl-filled microelectrodes recorded resting membrane potential and the Na^+-selective microelectrodes recorded both the membrane potential and the change in Na^+ activity when penetrating a cell. Different cells were penetrated with Na^+-sensitive microelectrodes and conventional KCl microelectrodes but it was assumed that the membrane potential of all cells is similar due to electrotonic coupling. The equivalence of the membrane potential recorded by the two electrodes after cell impalement was tested by superfusing the preparation with a Tyrode's solution containing 40 mM KCl as shown in figure 3.13. When the two intracellular electrodes recorded identical depolarisations (within 1 mV) the above assumption was regarded as viable. To give the change in Na^+ activity when penetrating a cell, the membrane potential, E_m, measured by the KCl-filled microelectrode was subtracted from the total potential, E_{ISE}, measured by the Na^+-selective electrode as shown in equation 3.1.

$$E_{Na} = E_{ISE} - E_m \qquad (3.1)$$

where E_m is the membrane potential recorded by the KCl-filled microelectrode and E_{ISE} is the potential recorded by the Na^+-sensitive microelectrode.

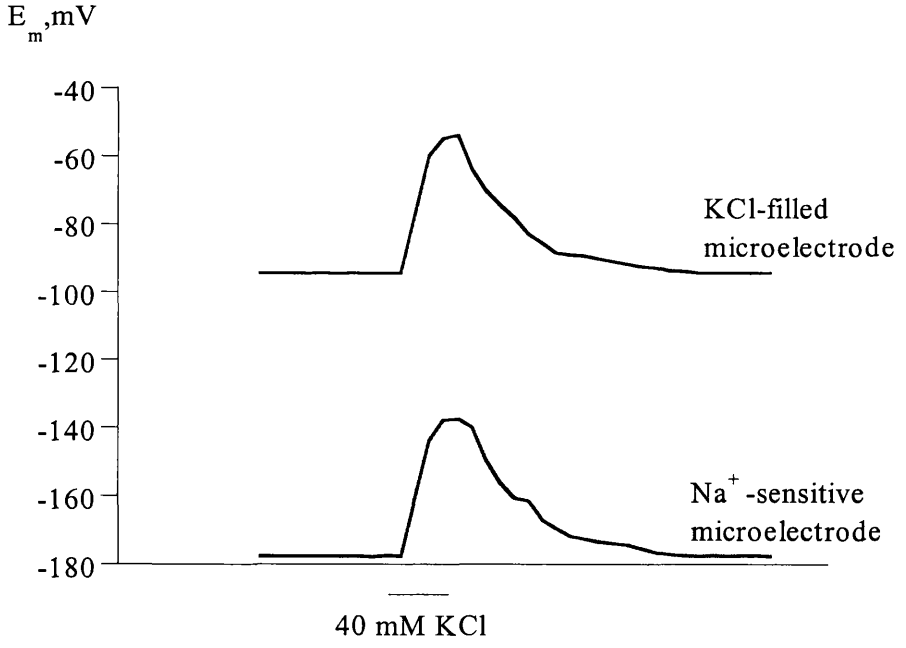

Figure 3.13. ΔE_m recorded by a KCl-filled microelectrode and a Na^+-sensitive microelectrode on superfusing the preparation with 40 mM KCl Tyrode's solution. ΔE_m for KCl-filled electrode = 40.4 mV and ΔE_m for the Na^+-sensitive microelectrode = 40.1 mV.

3.7.2. Calibration of Na^+-selective microelectrodes

The Na^+-selective microelectrodes were calibrated in mixed NaCl and KCl solutions as outlined in methods (Chapter 2, section 2.4.9). Each electrode was calibrated separately. A typical calibration curve is shown in figure 3.14.

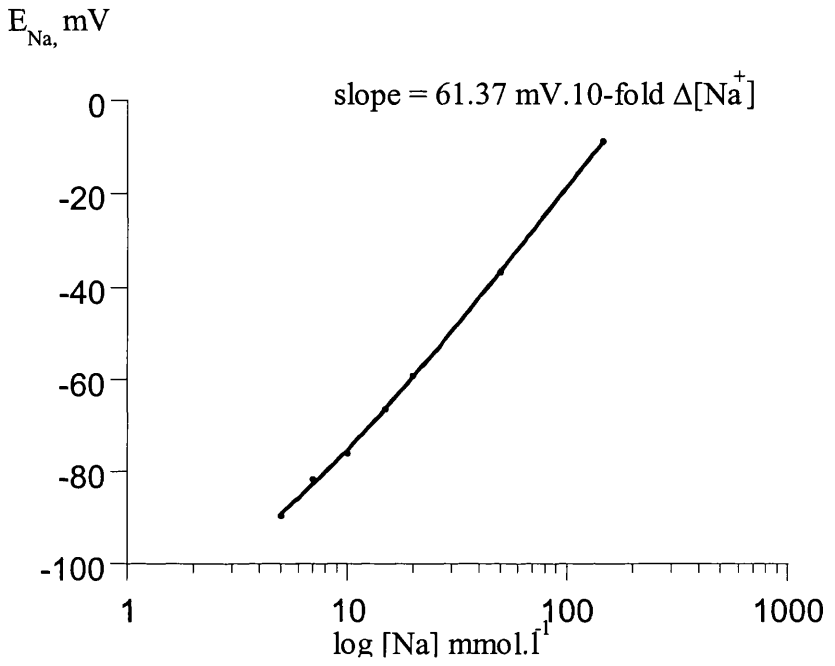

Figure 3.14. Calibration of Na^+-selective microelectrodes in mixed NaCl and KCl solutions.

3.7.3. Intracellular $[Na^+]$, $[Na^+]_i$, measurements and hypertrophy

$[Na^+]_i$ measurements from control and aortic-constricted hearts are shown in table 3.7. Although the ISE's measure ionic activity, the results are expressed in terms of concentration relative to the Na concentration of standard solutions. This ignores any difference between the Na ion activity coefficients in the calibrating solutions and the sarcoplasmic phase. Furthermore, Fry *et al* (1990) have shown that the potential differences recorded with intracellular Na^+-selective electrodes, E_{Na}, are normally distributed and that the estimated ion concentrations are positively skewed. Therefore in addition to calculating the mean $[Na^+]_i$ from E_{Na} values, the mean value and standard deviation of the pNa were also calculated and then an antilogarithmic transformation was

performed on this to give the $[Na^+]_i$. The mean values in the last column of table 3.7 are the antilogarithmic transformed mean pNa values and the values in parentheses are the ranges of $[Na^+]_i$ calculated from one standard deviation above and below the pNa value. The mean $[Na^+]_i$ values calculated using this method were slightly lower compared to the more usual approach using the individually estimated values in column three.

Table 3.7. Heart-to-body weight ratios and intracellular $[Na^+]$ measured using ion-selective microelectrodes in isolated papillary muscles from control and aortic-constricted hearts. Values are mean ± SD. HBR = heart-to-body weight ratio, RV = right ventricle, LV = left ventricle. † denotes $[Na^+]_i$ calculated from the individually estimated values, †† denotes $[Na^+]_i$ calculated from antilogarithmic transformation of the mean pNa with one SD shown in parentheses * denotes $p<0.001$ compared to sham and unoperated groups.

	HBR ($g.kg^{-1}$)	Intracellular $[Na^+]$ mM †	PNa	Intracellular $[Na^+]$ mM ††
RV, unoperated (n=6)	3.7±0.2	6.7±0.4	2.18±0.02	6.6 (5.6 -7.7)
LV, unoperated (n=12)	3.5±0.3	7.2±1.4	2.15±0.08	7.1 (5.9-8.3)
LV, sham-operated (n=9)	3.7±0.3	7.7±1.5	2.12±0.08	7.6 (6.4-8.8)
LV, aortic-constricted (n=12)	5.7±1*	12.1±1.4*	1.92±0.05 *	12.0(10.9-13.3)*
RV, aortic-constricted (n=2)	6.3/6.4	6.2/6.9		

No significant differences were observed between $[Na^+]_i$ in the sham-operated and unoperated control preparations. Statistical analysis was performed on the normally distributed pNa values. $[Na^+]_i$ was significantly higher in left ventricular papillary muscles from aortic-constricted compared to control hearts. $[Na^+]_i$ was also measured in two right ventricular papillary muscles taken from hearts with left ventricular hypertrophy with values of 6.2 and 6.9 mM. These values compare with that of $[Na^+]_i$ of

6.7 ± 0.4 mM (n = 6) (mean ± SD) in similar muscles from unoperated hearts. Thus these limited data suggest that the increase of $[Na^+]_i$ in the aortic-constricted hearts was confined to the left ventricle.

Figure 3.15 shows the relationship between $[Na^+]_i$ and heart-body weight ratio for all data in more detail (r=0.72, n=40, p<0.001). The $[Na^+]_i$ was higher in hypertrophied myocardium but the raised values were already established in moderate hypertrophy.

In figure 3.16 the animals were divided into control and moderate and severe hypertrophy groupings based on heart-to-body weight ratios as described above (section 3.2.1.1), showing that $[Na^+]_i$ had already increased substantially in moderate hypertrophy (n=6) and that there was no further increase in severe hypertrophy (n=6).

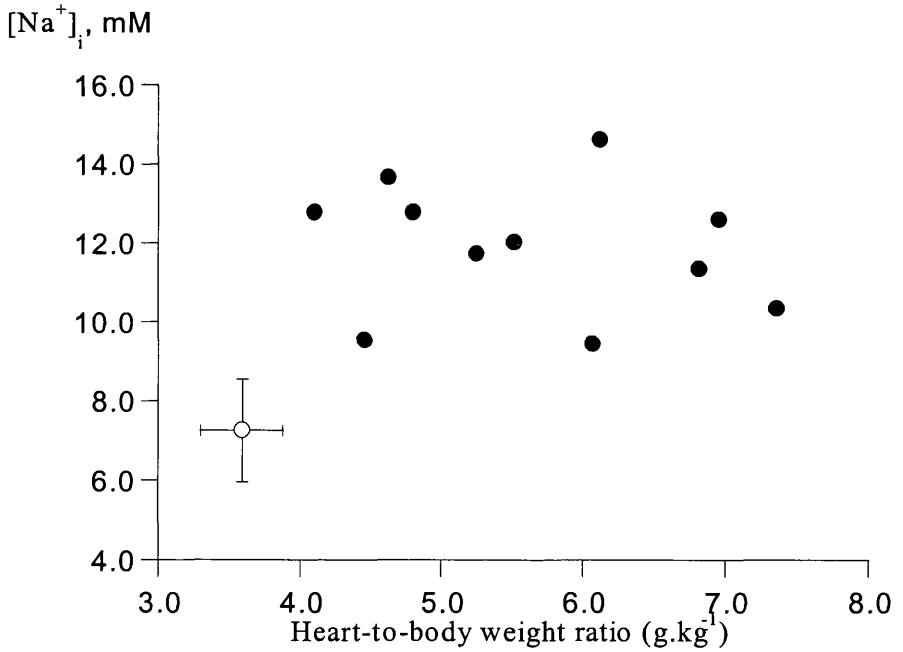

Figure 3.15. Relationship between intracellular $[Na^+]$ and heart-to-body weight ratio. The open circle represents combined data (mean ± SD) from unoperated and sham-operated left ventricle (n=28) and the filled circles individual left ventricle papillary muscles from aortic-constricted hearts (n=12).

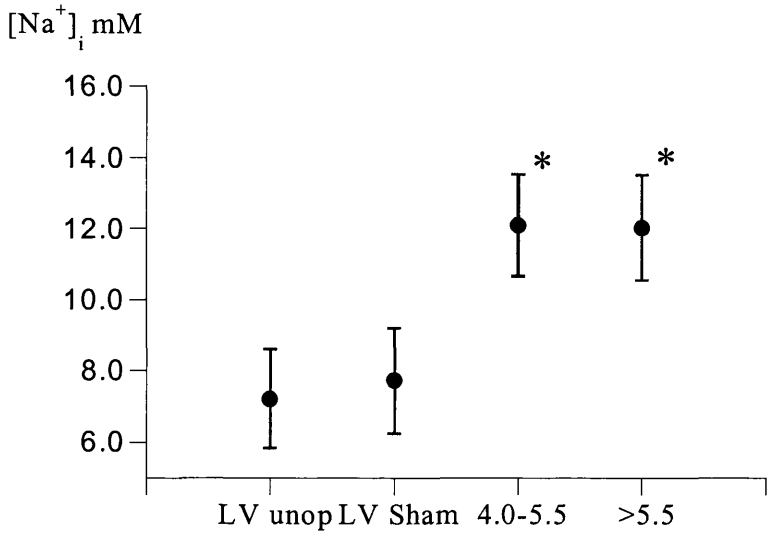

Figure 3.16. Intracellular [Na^+] measured using ion-selective microelectrodes in isolated papillary muscles from unoperated and sham-operated left ventricle, moderate hypertrophy (HBR 4.0-5.5 $g.kg^{-1}$) and severe hypertrophy (HBR >5.5 $g.kg^{-1}$). Values are mean ± SD. * denotes $p<0.001$ compared to sham and unoperated groups respectively.

3.7.4. Intracellular [Na^+] and contractile function

Figure 3.17 shows the dependence of the force-frequency relationship ($T_{(1.6/08)}$) on intracellular [Na^+] in isolated preparations from control and aortic-constricted hearts. The figure shows that as $[Na^+]_i$ increased the force-frequency declined from a positive to a negative relationship and that a continuum of points were seen from control and hypertrophied preparations. The increase in $[Na^+]_i$ correlated significantly with the decline in the force-frequency relationship ($r=-0.76$, $n=40$, $p<0.001$).

3.7.5. Recovery of $[Na^+]_i$ after intracellular acidosis

One cause of the raised $[Na^+]_i$ in hypertrophied myocardium may be a reduced ability of the cell to extrude Na^+. This was investigated by measuring the rate and extent of recovery of $[Na^+]_i$ in response to an intracellular acidosis. In preparations where prolonged stable microelectrode impalements were obtained, intracellular acidosis was generated after termination of a brief exposure to 10 mM NH_4Cl. Figure 3.18 shows examples of recordings from preparations taken from a control (Part A) and an aortic-constricted heart (Part B). During application of NH_4Cl, $[Na^+]_i$ decreased and on

removal, the $[Na^+]_i$ increased above control levels before returning to the resting value over a period of minutes. Application of 1 mM amiloride prevented the increase of $[Na^+]_i$ above the resting level after NH_4Cl removal suggesting it accompanied H^+ extrusion. In control hearts the $[Na^+]_i$ recovered from a peak of 11.4 ± 3.4 mM to a mean value of 6.2 ± 1.3 mM with a time constant of 171 ± 77 s (n=8). Corresponding experiments from aortic-constricted hearts showed a recovery of the $[Na^+]_i$ from 21.1 ± 3.2 mM to 12.6 ± 1.6 mM (n=6) with a time constant of 306 ± 140 s (mean ± SD). Both the recovery time constant ($p<0.05$) and the peak and final values of $[Na^+]_i$ ($p<0.001$) were significantly greater in the preparations from aortic-constricted hearts. The change in $[Na^+]_i$ (ΔNa_i) between the peak value and the recovery value was also greater in the aortic-constricted hearts (8.4±2.1 vs 5.2±2.1 mM, (mean ± SD) $p<0.05$).

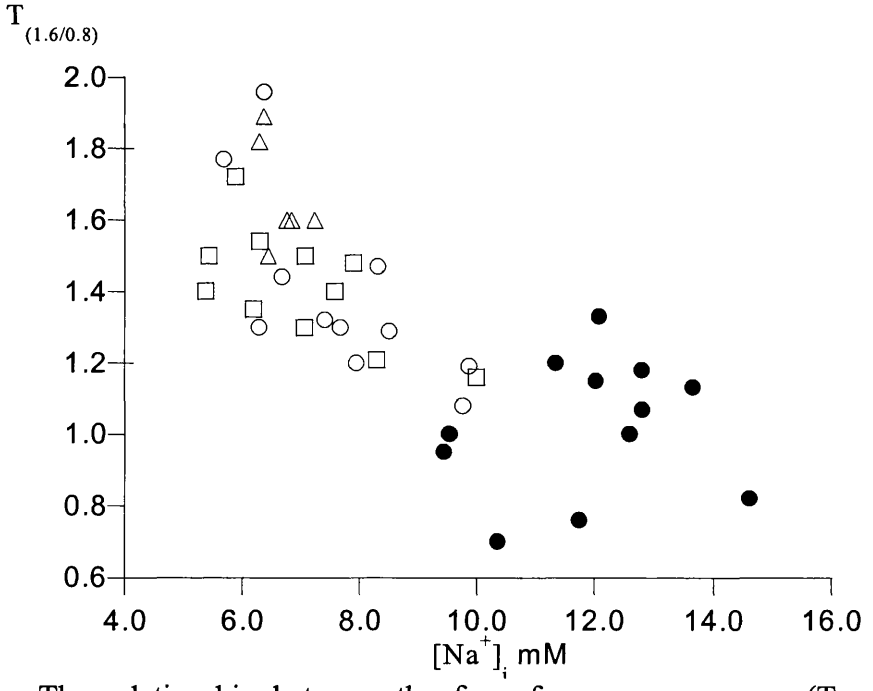

Figure 3.17. The relationship between the force-frequency response ($T_{(1.6/0.8)}$) and $[Na^+]_i$. Open triangles represent data obtained from right ventricular myocardium, open squares data from unoperated controls, open circles data from sham-operated controls and filled circles data from aortic-constricted hearts

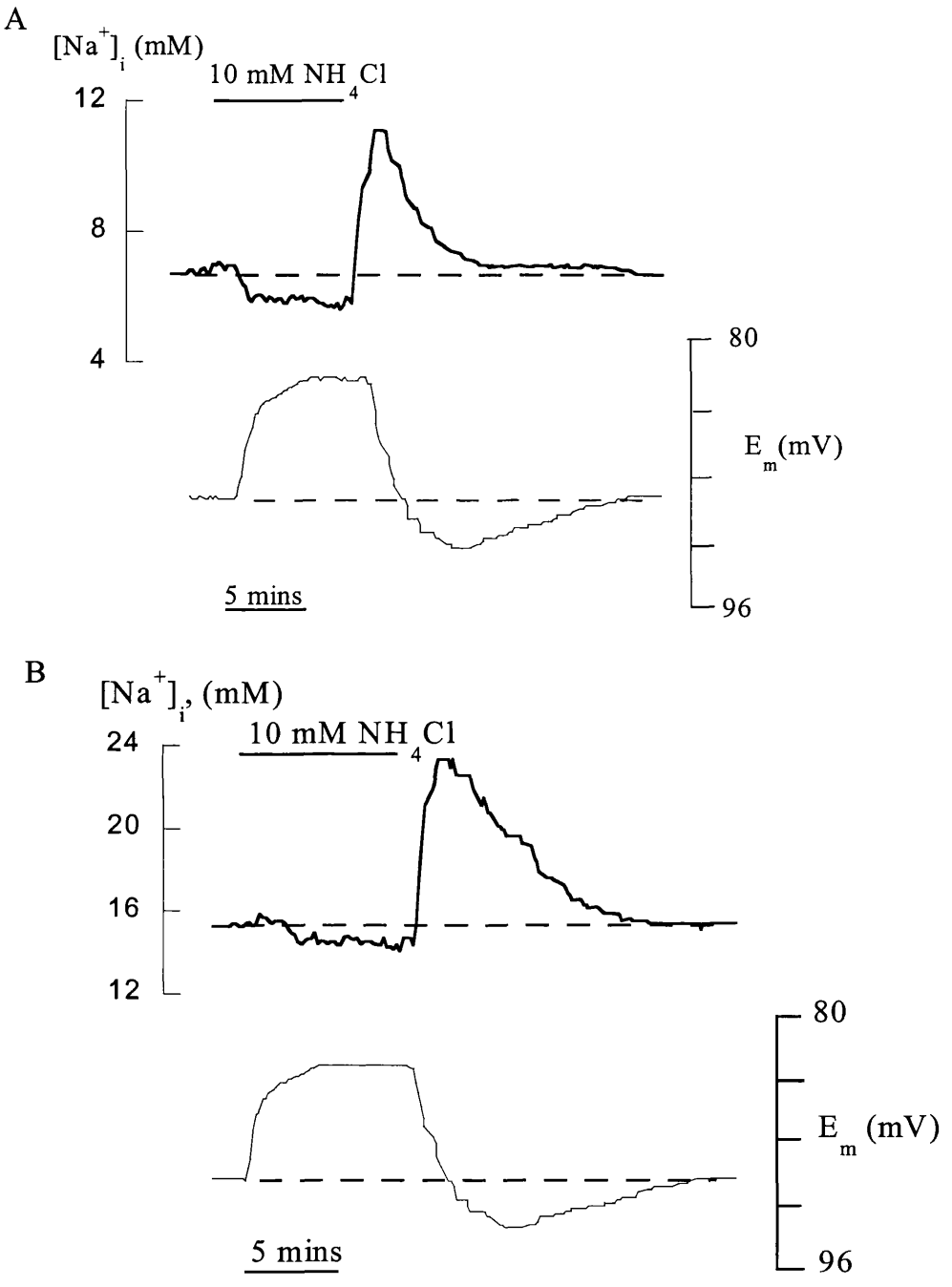

Figure 3.18. Recordings of $[Na^+]_i$ and membrane potential, E_m, in papillary muscles from A: a sham-operated animal and B: an aortic-constricted animal. 10 mM NH_4Cl was added to the superfusate when shown by the horizontal bar. The dotted lines show the pre-intervention control levels of $[Na^+]_i$ and E_m.

3.8. Summary

These experiments confirm the first hypothesis that the $[Na^+]_i$ is increased in hypertrophied guinea-pig myocardium. The rise of $[Na^+]_i$ occurred in moderate hypertrophy with little further increase in severe hypertrophy. This is in contrast to other cellular changes, such as intracellular acidosis or an increase in gap junction resistance, which occur throughout the hypertrophy process, or only in more severe hypertrophy, respectively (Wallis *et al.,* 1997, Cooklin *et al.,* 1997). This preliminary observation raises the important point that an increase of $[Na^+]_i$ represents the primary event in left ventricular hypertrophy and may be causal to other cellular changes. It is possible that as hypertrophy progresses changes occur which halt the rise in $[Na^+]_i$.

These experiments support the hypothesis that a negative force-frequency relationship in hypertrophied guinea-pig myocardium is due to a raised $[Na^+]_i$.

The mechanical function and $[Na^+]_i$ of the left ventricular myocardium from age-matched sham-operated animals, or from the right ventricle of aortic-constricted hearts behaved in an analogous manner to younger, unoperated guinea-pigs. Thus, it is unlikely that these changes are due to progressive ageing of the myocardium.

The finding that the recovery of a raised $[Na^+]_i$ after an acute acidosis was slowed in hypertrophied myocardium and stabilised at a higher level, suggests that the membrane mechanisms that regulate $[Na^+]_i$ are reset.

There are a number of possible explanations for the rise of $[Na^+]_i$ and the decline in contractile function in hypertrophy, namely, altered Na^+/H^+ exchange activity, altered Na^+-K^+ATPase activity and altered sarcoplasmic reticulum Ca^{2+} handling. The next series of experiments were designed to investigate these possibilities.

3.9. Measurement of intracellular pH, pH_i

3.9.1. Measurement of pH_i in isolated cells

Determination of pH_i was made in isolated ventricular myocytes from control and aortic-constricted guinea-pigs. Measurement was made in all cases using epifluoresence microscopy, by observing the ratio of the fluorescence output at 490/430 nm of cells loaded with the pH sensitive fluorochrome, BCECF. Calibration of the ratiometric signal was performed in individual cells allowing calculation of the absolute value of pH_i in each cell. In addition to determination of the baseline pH_i further interventions were made to determine the intracellular H^+ buffering capacity, the rate of H^+ recovery and the acid-equivalent efflux from intracellular acidosis. All recordings were made from cells superfused, at 37 °C with either HEPES or CO_2/HCO_3^- buffered Tyrode's solution as described in Methods (Chapter 2, section 2.6).

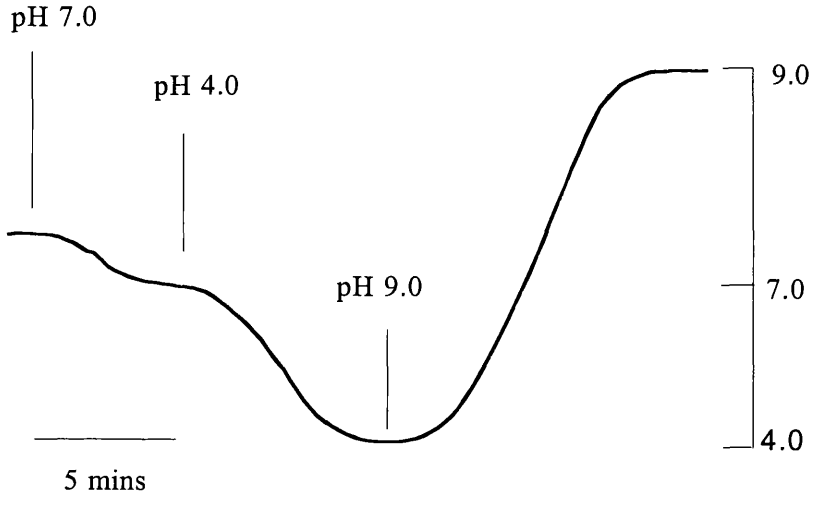

Figure 3.19. Measurement and intracellular calibration of pH_i in an isolated myocyte from a control heart superfused with HEPES buffered Tyrode's solution equilibrated with 100% O_2. Vertical lines indicate where solution changes were made for calibration solutions of pH 7.0, 4.0 and 9.0. pH_i measured prior to calibration was 7.17.

Myocytes were superfused with HEPES buffered Tyrode's solution for 5 to 10 minutes to allow stabilisation before steady-state values of pH_i were measured. A recording of pH_i including calibration readings in a cell isolated from a control animal superfused with HEPES-buffered Tyrode's is shown in figure 3.19.

3.9.2. Effect of hypertrophy on pH_i

The mean pH_i in HEPES-buffered Tyrode's solution was 7.22 ± 0.12 (pH units, mean ± SD, n=89 cells from 37 animals) in cells isolated from unoperated hearts and 7.20 ± 0.12 (pH units, mean ± SD, n=37 cells from 11 animals) in cells from sham-operated hearts. No significant difference in steady state pH_i was observed between cells isolated from unoperated and sham-operated animals. A significant decrease of the mean value of pH_i to 6.95 ± 0.08 (pH units, mean ± SD, n=37 cells from 7 animals) was observed in cells isolated from aortic-constricted hearts, $p<0.001$.

3.9.3. pH_i as a function of heart-to-body weight ratio

All the experiments were pooled to determine pH_i as a continuous function of heart-to-body weight ratio. Values of pH_i of all the cells isolated from any particular heart were grouped and the mean value ± SD was determined. The mean values for aortic-constricted hearts were plotted as a function of the heart-to-body weight ratio of the animal from which they were derived and the data from control hearts are expressed as a single value in Figure 3.20. Between 3 and 11 cells were used for the determination of each mean value of pH_i. There was a significant negative correlation between pH_i and heart-to-body weight ratio ($r=-0.715$, $p<0.001$).

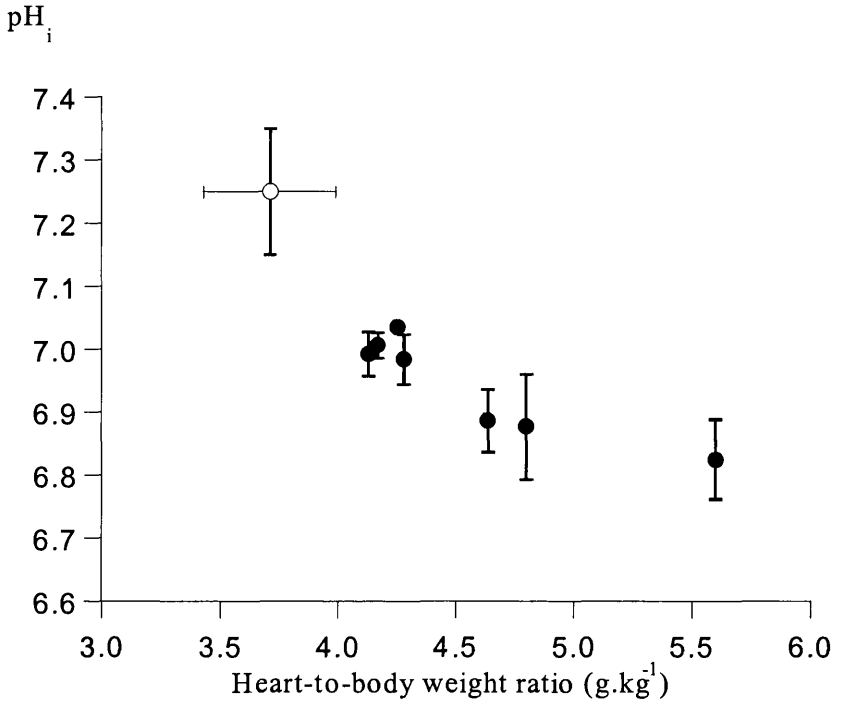

Figure 3.20. The relationship between pH_i and heart-to-body weight ratio. Data derived from 163 cells from 51 animals. Between 3 and 11 cells were used for the determination of each data point. The mean value obtained from control hearts is shown as an open circle (mean ± SD) and values obtained from aortic-constricted hearts are shown as filled circles. ($r=-0.715$, $p<0.001$).

3.10. Determination of intracellular H^+ buffering capacity

3.10.1. Theory of measurement of buffering capacity, β

The addition and subsequent removal of the weak acid NH_4Cl to the superfusing solution of isolated ventricular myocytes has been shown to alter pH_i in a predictable way without altering extracellular pH, pH_o (Baro *et al.*, 1989) as described in Methods (Chapter 2, section 2.7, page 97).

Determination of the H^+ load allows measurement of the intracellular H^+ buffering capacity of the cell assuming there is no significant contribution from a physiological NH_3-NH_4^+ buffering system. If the change in pH_i following removal of NH_4Cl is measured then, as the H^+ load is known, β can be calculated from the relationship given as equation 3.2.

$$\beta \text{ (mequiv.l}^{-1}\text{.pH unit}^{-1}) = (\Delta[NH_4^+]_i/\Delta pH_i) \quad (3.5)$$

In practice the experimental determination of β was made in the presence of 1 mM amiloride to block the effects of H^+ membrane transport systems. Active or passive membrane transport systems would be anticipated to blunt any change in pH_i produced by chemical perturbation leading to an overestimation of β.

3.10.2. Determination of non-bicarbonate intracellular H^+ buffering capacity, β_i

The intrinsic or non-bicarbonate H^+ buffering capacity, β_i, was determined in cells isolated from control (unoperated and sham-operated) and aortic-constricted hearts. As described in the Methods (Chapter 2, section 2.7.3) the extracellular Tyrode's solution was buffered with HEPES and equilibrated with 100% O_2. The absence of HCO_3^- ions allowed calculation of the non-bicarbonate chemical buffering capacity of the sarcoplasm.

3.10.3. β_i in cells from control and aortic-constricted hearts

The intrinsic or non-bicarbonate buffering capacity, β_i was measured in myocytes isolated from hearts of control and aortic-constricted hearts using the method described above. 10 mM NH_4Cl and 1 mM amiloride were used in all experiments and all cells were superfused with HEPES-buffered Tyrode's solution equilibrated with 100% O_2.

Addition of 10 mM NH_4Cl increased pH_i in myocytes from control hearts from baseline of 7.22 ± 0.15 by 0.20 ± 0.06 pH units (mean ± SD) and removal generated a peak intracellular acidosis of -0.50 ± 0.16 units (mean ± SD). An example is illustrated in plate 2. Corresponding values in myocytes from aortic-constricted hearts were an increase in pH_i from a baseline of 6.91 ± 0.11 by 0.26 ± 0.14 pH units (mean ± SD) and a peak intracellular acidosis of -0.21 ± 0.12 units (mean ± SD). The actual pH_i produced on removal of NH_4Cl was similar in both groups of cells (6.73 ± 0.2, n=75 cells from control hearts and 6.71 ± 0.19, n=19 cells from aortic-constricted hearts (mean ± SD)) but the baseline pH_i was significantly lower in the cells from aortic-constricted hearts.

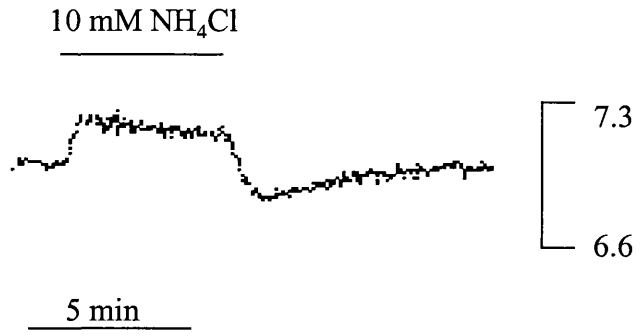

Plate 2. The effect of addition and removal of NH_4Cl on pH_i in a myocyte from a sham-operated animal

A plot of pH_i taken from a myocyte isolated from an aortic-constricted heart is shown in figure 3.21. This recording illustrates the typical effect, in the absence and presence of amiloride of the removal of NH_4Cl on pH_i.

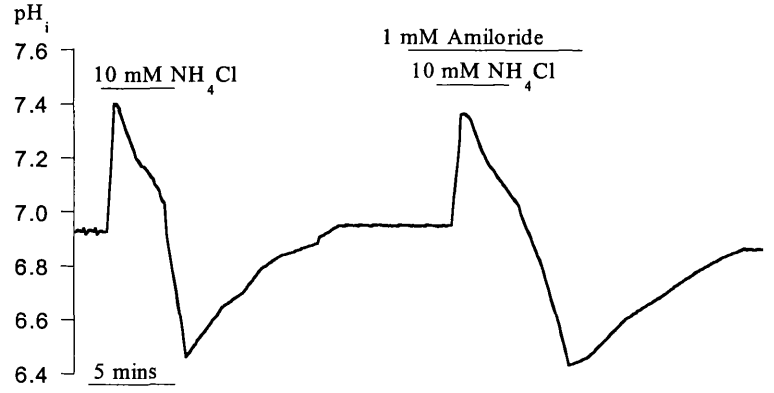

Figure 3.21. Derived plot of pH_i in a myocyte isolated from an aortic-constricted heart following application of 10 mM NH_4Cl and its subsequent removal in the absence and presence of 1 mM amiloride. Myocyte superfused with HEPES-buffered Tyrode's at 37°C. Steady state pH_i was 6.93, and β_i was 102 mequiv.l^{-1}.pH unit^{-1}.

In cells isolated from control hearts β_i was 30.5 ± 15.1 mequiv.l^{-1}.pH unit^{-1} (mean ± SD, n=75 cells from 31 animals). In cells isolated from hearts with aortic constriction β_i was significantly higher, 104.2 ± 25.5 mequiv.l^{-1}.pH unit^{-1} (mean ± SD, n=19 cells from 6 animals), $p<0.0001$. A significant correlation was observed between β_i and heart–to-body weight ratio as shown in individual values in figure 3.22, part A ($r=0.625$, $p<0.001$). In Part B the individual values for myocytes from aortic-constricted hearts are

plotted as a function of heart-to-body weight ratio and the data from control hearts are expressed as a single value.

3.10.4. Correlation of β_i with pH_I

A significant correlation was observed between β_i and the steady-state value of pH_i measured prior to the application of NH_4Cl as shown in individual values in figure 3.23, part A. The more acidic the baseline value of pH_i, the higher the value of β_i calculated for that cell. These data were fitted to a linear relationship ($r=-0.80$, $p<0.001$). In figure 3.23, part B the individual values for myocytes from hypertrophied hearts are plotted as a function of heart-to-body weight ratio and the data from control hearts are expressed as a single value.

3.10.5. Determination of bicarbonate and non-bicarbonate intracellular H^+ buffering capacity, β_{tot}

The total, bicarbonate and non-bicarbonate, H^+ buffering capacity, β_{tot}, was also determined in some cells isolated from control hearts. As described in the Methods (Chapter 2, section 2.7.3) the extracellular Tyrode's solution contained HCO_3^- and was equilibrated with 95% O_2, 5% CO_2 gas mixture. CO_2 is freely diffusable across cell membranes and results in a constant $[CO_2]_i$. In this situation intracellular HCO_3^- ions become a very powerful buffer, even though the pK_a of carbonic acid is 6.1, as intracellular CO_2 levels, effectively clamped by the extracellular solution remain constant. Hence determination of β_{tot} under these conditions includes intracellular buffering attributable to intracellular HCO_3^- ions (β_{CO2}) as well as the non-bicarbonate chemical buffering (β_i) of the sarcoplasm measured above in the absence of HCO_3^- ions.

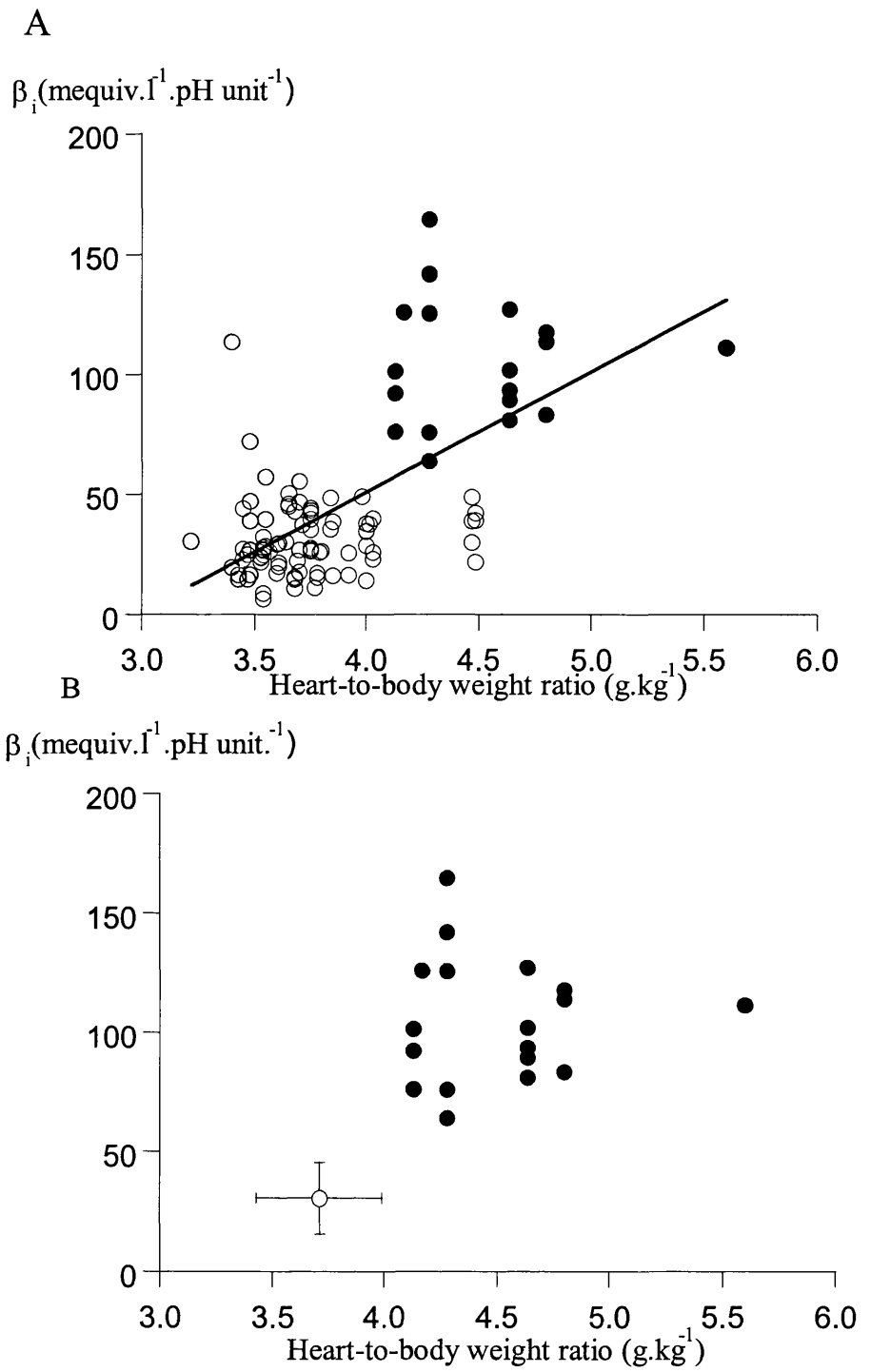

Figure 3.22. Relationship between β_i and heart-to-body weight ratio. In A data from individual cells (n=94) from all experimental groups with values from control hearts represented by open circles and from aortic constricted hearts represented by filled circles. In B the mean value obtained from control hearts is shown as an open circle (mean ± SD) and the values from aortic-constricted hearts are shown as filled circles. Data in A fitted to a linear relationship ($r=0.625$, $p<0.001$).

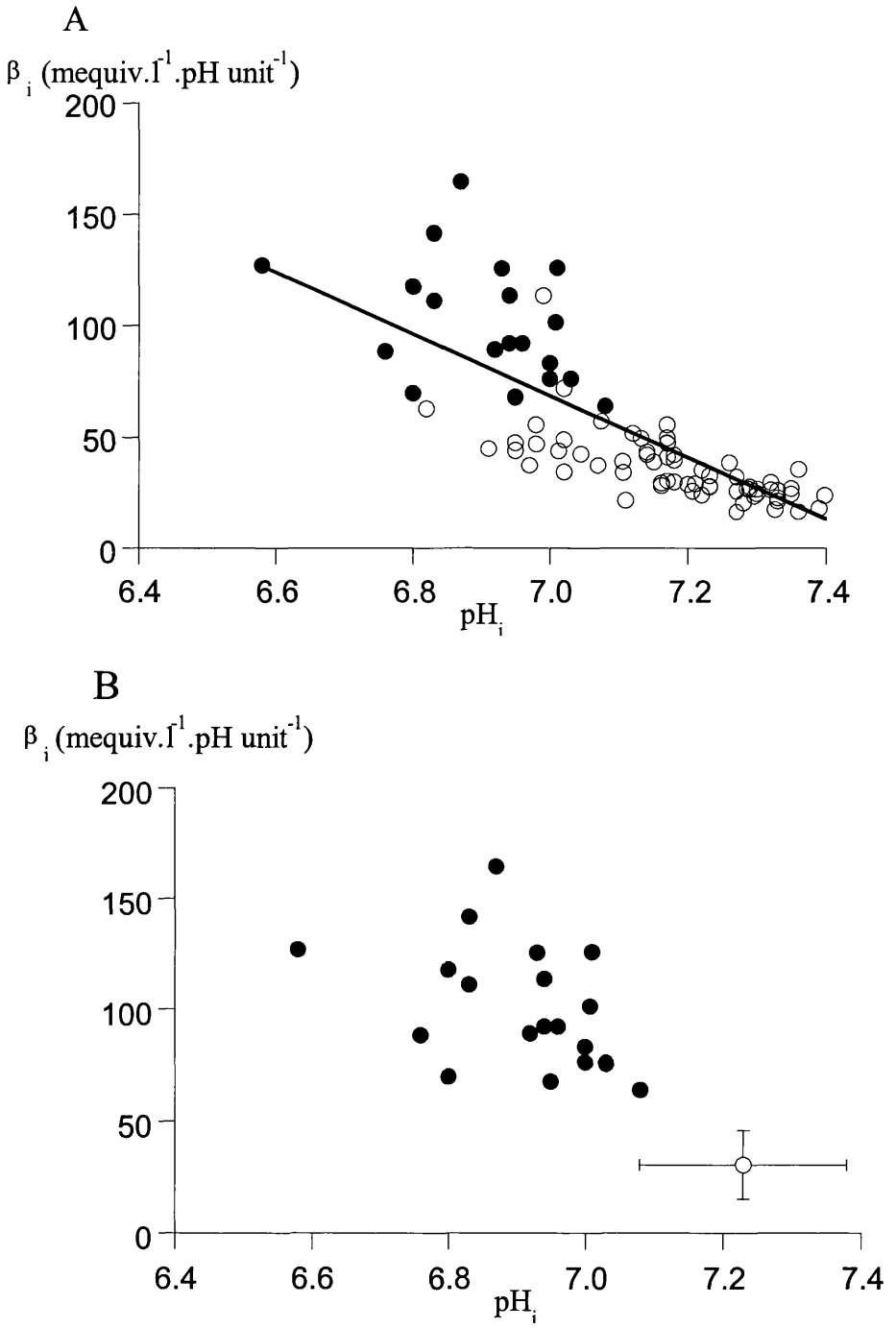

Figure 3.23. Relationship between β_i and steady–state pH_i. Cells superfused with HEPES buffered Tyrode's solution. In A data from individual cells (n=94) from all experimental groups (values from control hearts represented by open circles and from aortic-constricted hearts represented by filled circles) and in B data from the control hearts shown as a single point (open circle). Data in A fitted to a linear relationship ($r=-0.80$, $p<0.001$).

3.10.6. β_{tot} in cells from control hearts

The bicarbonate and non-bicarbonate H^+ buffering capacity, β_{tot}, was also determined in some cells isolated from control hearts. Determination was made using the methods described above. 10 mM NH_4Cl and 1 mM amiloride were used in all the experiments and the cells were superfused with a bicarbonate buffered Tyrode's solution equilibrated with 95% O_2, 5% CO_2 gas mixture. Addition of 10 mM NH_4Cl increased pH_i from baseline of 7.25 ± 0.13 by 0.24 ± 0.11 units (mean ± SD) and removal generated an intracellular acidosis of -0.42 ± 0.10 units (mean ± SD). Steady state pH_i (7.22 ± 0.11, mean ± SD, n=102 vs 7.22 ± 0.12, n=126) and the degree of alkalosis produced did not differ from that in HEPES-buffered Tyrode's solution. The acidosis produced in bicarbonate-buffered solution was significantly less than that produced in HEPES-buffered solution (see above, 0.50 ± 0.16 units, (mean ± SD) $p<0.005$). β_{tot} was determined to be 38.8 ± 12.1 mequiv.l^{-1}.pH $unit^{-1}$ (mean ± SD, 52 cells from 23 hearts) in control hearts and was significantly higher than β_i (30.5 ± 15.1 mequiv.l^{-1}.pH $unit^{-1}$, (mean ± SD) in 75 cells from 31 hearts, p=0.003).

3.10.7. Bicarbonate dependent buffering, β_{CO2}

In 11 individual cells both β_{tot} and β_i were determined. The mean value of β in bicarbonate-buffered Tyrode's was 34.4 ± 12.8 mequiv.l^{-1}.pH $unit^{-1}$ which decreased to 22.0 ± 7.3 mequiv.l^{-1}.pH $unit^{-1}$ in HEPES-buffered Tyrode's (mean ± SD), (p=0.0003, paired t-test). The value of β_{tot} comprises the algebraic sum of β_i and β_{CO2}. Subtracting the buffering power determined in HEPES-buffered solution from that in bicarbonate-buffered solution therefore gives a value for β_{CO2}. Using this method β_{CO2} was calculated to be 12.4 ± 7.8 mequiv.l^{-1}.pH $unit^{-1}$ (mean ± SD). In these cells the proportion of the total buffering power due to bicarbonate was 34 ± 10 % (mean ± SD).

3.10.8. Correlation of β_{tot} with pH_i

A significant correlation was observed between β_{tot} and the steady-state value of pH_i measured prior to the application of NH_4Cl in cells isolated from control hearts as shown in individual values figure 3.24. The more acidic the baseline value of pH_i, the higher

the value of β_{tot} calculated for that cell. These data were fitted to a linear relationship (r=-0.62, p<0.001).

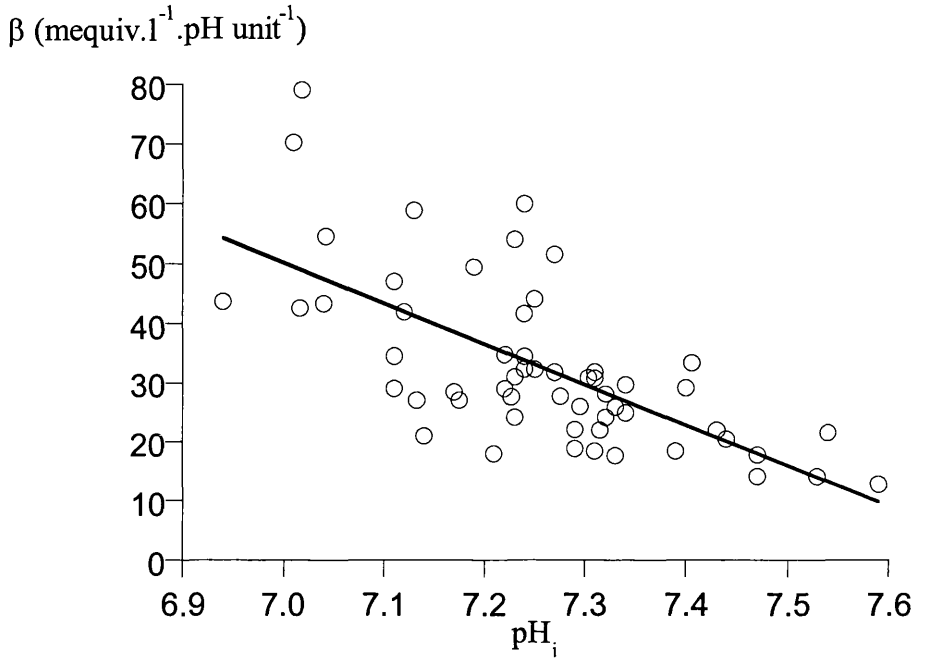

Figure 3.24. Relationship between β_{tot} and steady–state pH_i of individual cells isolated from control hearts (n=52). Cells superfused with bicarbonate-buffered Tyrode's solution and equilibrated with 95%CO_2 and 5%O_2. Data fitted to a linear relationship (r=-0.62, p<0.001).

Figure 3.25 shows the relationship between β_{tot} and β_i and pH_i in cells from control hearts. Both sets of data were fitted to a linear relationship.

3.11 pH_i recovery from intracellular acidosis

3.11.1. Calculation of the non-bicarbonate dependent pH_i recovery rate

The rate of recovery of pH_i, $\Delta pH_i/dt$, on NH_4Cl removal in the absence of amiloride was measured in individual cells. The cells were superfused with HEPES-buffered Tyrode's solution equilibrated with 100% O_2. The pH_i was plotted against time and a single exponential curve fitted to calculate the time constant of the recovery phase. Typical curves in myocytes from a control and aortic constricted heart are shown in figure 3.26. Curve fitting was performed using the Scientific Analysis application; KaleidaGraph ™, for Windows, version 3.5, (Synergy Software (PCS Inc)).

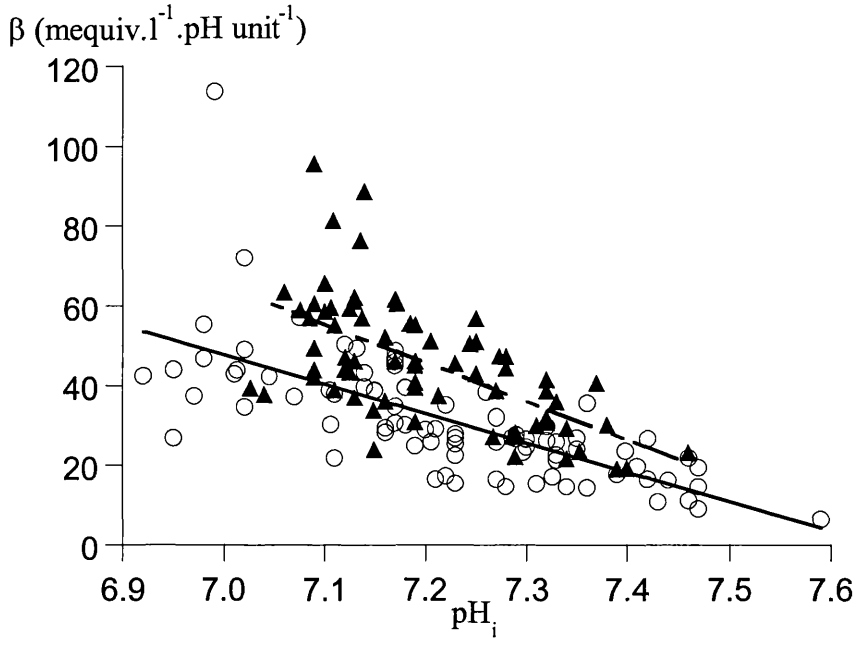

Figure 3.25. Relationship of β_{tot} (filled triangles) and β_i (open circles) and steady-state pH_i in myocytes isolated from control hearts. Data plotted as individual points and fitted to linear relationship (r=-0.62 for β_{tot}, dashed line, and r=-0.70 for β_i, continuous line).

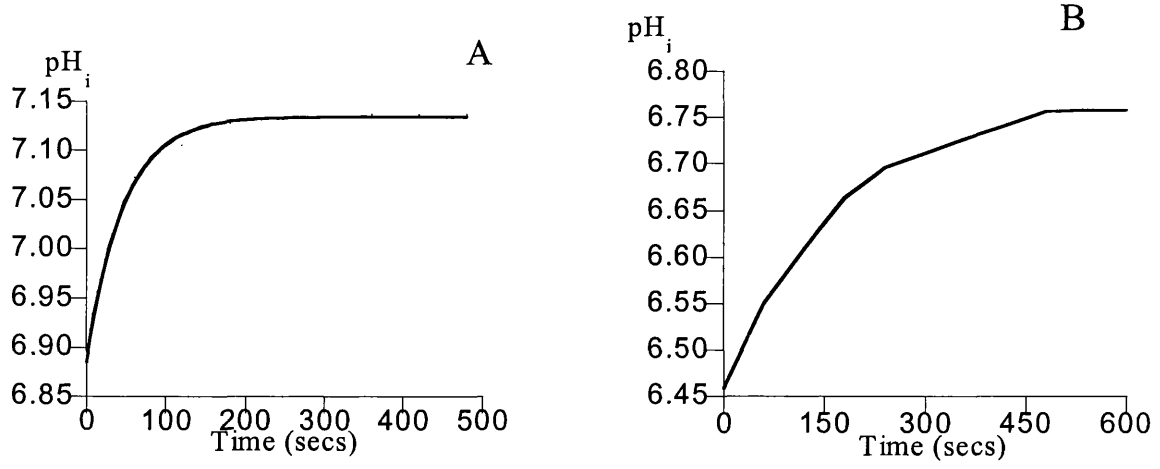

Figure 3.26. The recovery of pH_i on NH_4Cl removal in the absence of amiloride in a myocyte from a control heart (A) and from an aortic-constricted heart (B). In A the resting pH_i was 7.18, and recovered from a nadir of 6.88 to 7.13 on removal of NH_4Cl with a time constant of 63 s. In B the resting pH_i was 6.84 and recovered from a nadir of 6.45 to 6.76 with a time constant of 174 s.

In control hearts pH_i recovered from a nadir of 6.76 ± 0.21 to a mean value of 7.14 ± 0.11 with a time constant of 165 ± 88 s (n=68)(mean ± SD). Corresponding data from aortic-constricted hearts show a recovery of pH_i from 6.71 ± 0.19 to a mean value of 6.93 ± 0.11 with a time constant of 231 ± 82 s (n=26) (mean ± SD). The degree of acidosis produced was similar in cells from control and aortic-constricted hearts but the steady-state recovery pH_i was significantly lower ($p<0.0001$) and the recovery time constant was significantly greater in cells from aortic-constricted hearts ($p=0.001$).

3.11.2. Calculation of the bicarbonate and non-bicarbonate dependent pH_i recovery rate

The recovery of pH_i, on NH_4Cl removal in the absence of amiloride was measured in 10 cells from control hearts initially in bicarbonate-buffered Tyrode's and then in HEPES-buffered Tyrode's. The data are summarised in table 3.8. Baseline pH_i was not significantly different in the two solutions. The acidosis generated was greater in HEPES-buffered solution. In the absence of bicarbonate, pH_i recovery following acid loading was slower and the H^+ efflux rate was also significantly less.

Table 3.8. Changes in pH_i and the rate of recovery of pH_i on NH_4Cl removal in the absence of amiloride in bicarbonate- and HEPES-buffered Tyrode's solution (n=10 cells from control hearts). Values are mean ± SD. * denotes $p<0.01$ and ** $p<0.05$ compared to bicarbonate-buffered solution (paired Students t-tests).

Baseline pH_i	Alkalosis	Acidosis	Recovery pH_i	Time constant (s)	H^+ efflux.min^{-1}
Bicarbonate-buffered solution					
7.28±0.11	7.49±0.16	6.77±0.17	7.27±0.10	128±64	4.6±2.0
HEPES-buffered solution					
7.26±0.11	7.43±0.09	6.58±0.26**	7.15±0.08	173±81*	3.7±1.9**

3.12. Calculation of sarcolemmal acid-equivalent flux (J_H)

Measurement of the cellular H^+ buffering capacity allowed calculation of the rate of acid efflux during the recovery of acidosis after removal of NH_4Cl. The average rate of pH_i recovery was calculated between 30 and 150 seconds after the peak acidosis. The net H^+ efflux rate was calculated as the product of the average rate of pH_i recovery over this time period, $\Delta pH_i/dt$, and the intracellular buffering power as described in the methods (Chapter 2, section 2.8.2). In HEPES-buffered solution, β was taken as the intrinsic intracellular buffering power (β_i) at peak acidosis and in CO_2/HCO_3^--buffered solutions, β was taken as the total buffering power of the cell (β_{tot}) at peak acidosis.

$$J_H = \beta^*(\Delta pH_i/dt)$$

3.12.1. Non-bicarbonate acid-equivalent flux in myocytes from control and aortic constricted hearts

The non-bicarbonate acid efflux rate was calculated as the product of $\Delta pH_i/dt$, and the intrinsic buffering power, β_i (as determined above) measured in myocytes superfused with HEPES-buffered Tyrode's solution. The mean value in 68 cells from control hearts was 3.7 ± 1.9 mequiv.l^{-1}.min^{-1} and was not significantly different from the value in 21 cells from aortic-constricted hearts (4.2 ± 1.9 mequiv.l^{-1}. min^{-1}). Figure 3.27 shows that the efflux-rate was dependent on the value of pH_i at the commencement of acid extrusion. At more acid values of pH_i, the rate of extrusion was greater irrespective of the origin of the cell.

The recovery of pH_i from an acid load in HEPES-buffered Tyrode's is known to be mediated by acid extrusion on Na^+-H^+ exchange (Lagadic-Gossmann *et al.*, 1992). Consistent with this, pH_i recovery was completely inhibited in 17 out of 45 myocytes isolated from control hearts in the presence of 1 mM amiloride and greatly attenuated in the remainder (0.75 ± 0.9 mequiv.l^{-1}.min^{-1}, mean ± SD). Results were similar for myocytes isolated from aortic-constricted hearts with complete inhibition of pH_i recovery in 11 out of 19 cells and a mean value in the remainder of 0.75 ± 1.3

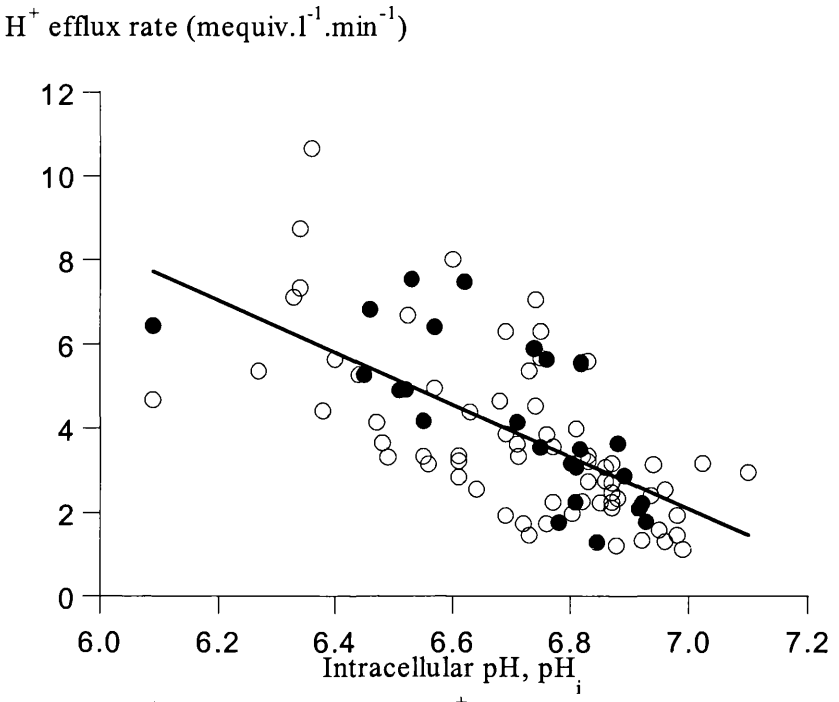

Figure 3.27. Non-bicarbonate dependent H^+ efflux rate as a function of intracellular pH at the commencement of acid extrusion in 68 myocytes isolated from control hearts (open circles) and 21 myocytes from aortic-constricted hearts (filled circles). Cells were superfused with HEPES-buffered Tyrode's. Acid loading was induced after removal of superfusate NH_4Cl. r=-0.65, p<0.001.

mequiv.l^{-1}.min^{-1} (mean ± SD). A similar inhibitory effect on pH_i recovery from intracellular acidosis in myocytes from control hearts was observed by reducing external Na, thereby reducing the gradient for Na^+-H^+ exchange. The cells were superfused with HEPES-buffered Tyrode's containing 24 mM and 0 mM Na^+ (NaCl replaced with Tris-Cl, see Chapter 2, section 2.8.1, table 2.9). Recovery was completely inhibited in 26 out of 35 cells in 24 mM Na and 5 out of 6 cells in 0 mM Na. Figure 3.28 shows the effect of 1 mM amiloride and reducing external Na on recovery from intracellular acidosis in a myocytes from a control heart. The results are summarised in table 3.9.

3.12.2. Non-bicarbonate acid-equivalent flux in myocytes from control hearts

Figure 3.29 illustrates a similar experiment to that shown in figure 3.28 in a myocyte from a control heart, but performed in bicarbonate-buffered Tyrode's equilibrated with 95% O_2 and 5% CO_2. Recovery of pH_i from the acid load is now mediated by a

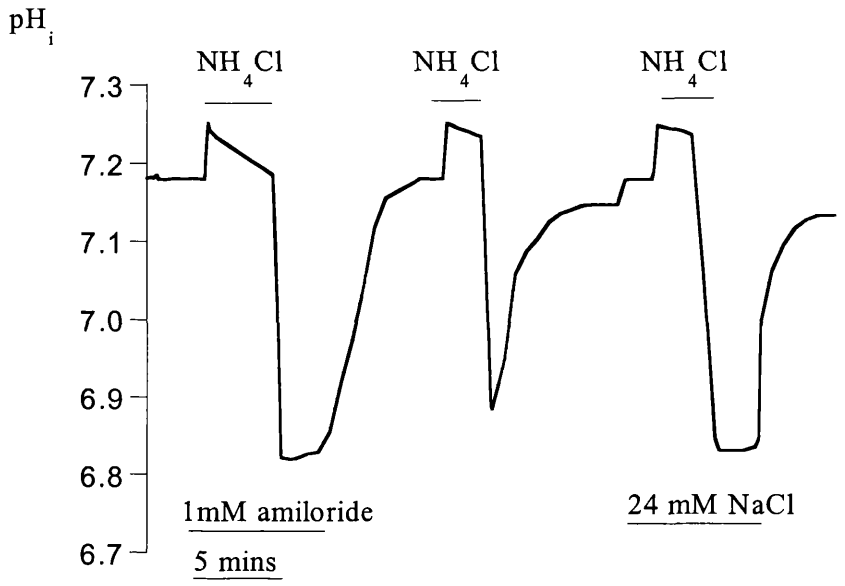

Figure 3.28. Effect of 1 mM amiloride and reduced external Na on recovery from NH_4Cl induced acidosis in a myocyte from a control heart. Cell superfused with HEPES-buffered Tyrode's solution at 37 °C

Table 3.9. Summary of H^+ efflux rates in HEPES- and bicarbonate-buffered Tyrode's solution in cells from control and aortic-constricted hearts. Values are mean ± SD. * denotes $p<0.01$compared to HEPES-buffered and ** denotes $p<0.01$ compared to baseline rate (*i.e* in absence of amiloride or reduced external sodium).

H^+ efflux rate (mequiv.l^{-1}.min^{-1})		
	Control hearts	Aortic-constriction
HEPES-buffered Tyrode's	3.7 ± 2.0 (n=68)	4.2 ± 1.9 (n=19)
1 mM amiloride (HEPES)	0.75 ± 0.9 (n=45)**	0.75 ± 1.3 (n=19)
24 mM NaCl (HEPES)	0.31 ± 0.7 (n=35)**	
Bicarbonate-buffered Tyrode's	4.6 ± 2.0 (n=68)*	
1 mM amiloride (Bicarbonate)	1.6 ± 0.8 (n=29)**	
24 mM NaCl (Bicarbonate)	1.3 ± 1.3 (n=19)**	

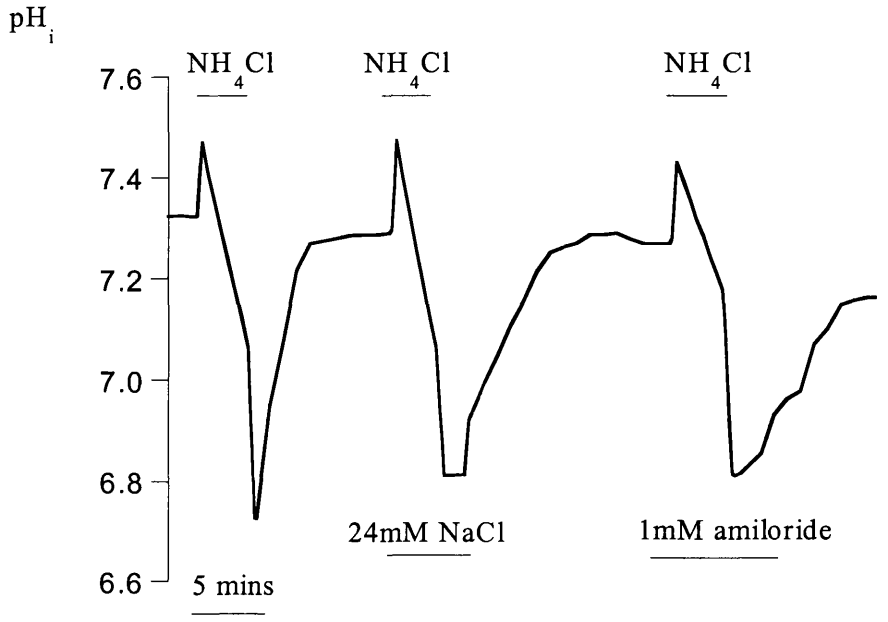

Figure 3.29. Effect of 1mM amiloride and reduced external Na^+ on recovery from NH_4Cl induced acidosis in a myocyte from a control heart. Cell superfused with bicarbonate-buffered Tyrode's solution at 37 °C

combination of Na^+-H^+ exchange and Na^+-HCO_3^- cotransport (Dart & Vaughan-Jones, 1992; Lagadic-Gossmann *et al.*, 1992). The H^+ efflux rate calculated in 68 myocytes from control hearts superfused with bicarbonate-buffered Tyrode's solution was significantly higher than that in HEPES-buffered solution (4.6 ± 2.0 vs 3.7 ± 1.9 mequiv.l^{-1}.min^{-1}, (mean ± SD) $p=0<0.01$). Figure 3.30 shows that the efflux rate was dependent on the value of pH_i at the commencement of acid extrusion. The data from figure 3.27 and 3.30 are combined in figure 3.31 to show the efflux rate in both HEPES- and bicarbonate-buffered Tyrode's solution. Both sets of data fitted to a linear relationship.

1mM amiloride reduced the H^+efflux rate in 29 cells to a mean value of 1.6 ± 0.8 mequiv.l^{-1}.min^{-1} (mean ± SD) ($p<0.001$, paired Student's t-test) but recovery was not completely inhibited in any cell. Reducing the external Na^+ in Tyrodes to 24 mM (NaCl replaced with Tris-Cl, see Chapter 2, section 2.3.2, table 2.2) reduced the H^+efflux rate in 19 cells to a mean value of 1.3 ± 1.3 mequiv.l^{-1}.min^{-1} (mean ± SD) with complete inhibition of recovery in 6 of the cells.

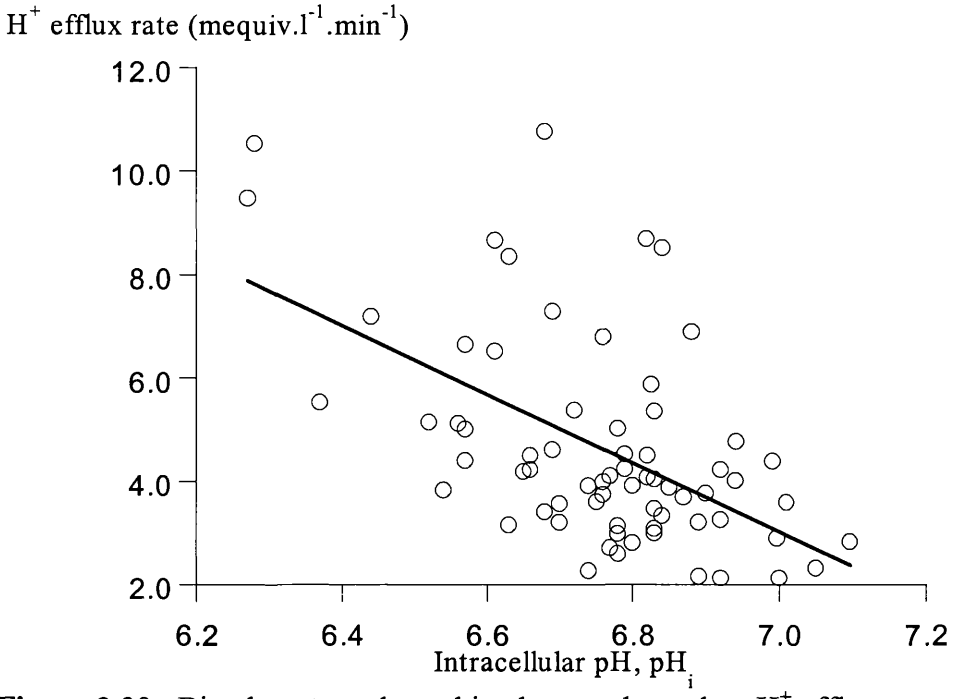

Figure 3.30. Bicarbonate and non-bicarbonate-dependent H^+ efflux rate as a function of intracellular pH at the commencement of acid extrusion in 68 myocytes isolated from control hearts. Myocytes were superfused with bicarbonate-buffered Tyrode's solution. Acid loading was induced after removal of superfusate NH_4Cl. r=-0.55, p<0.001.

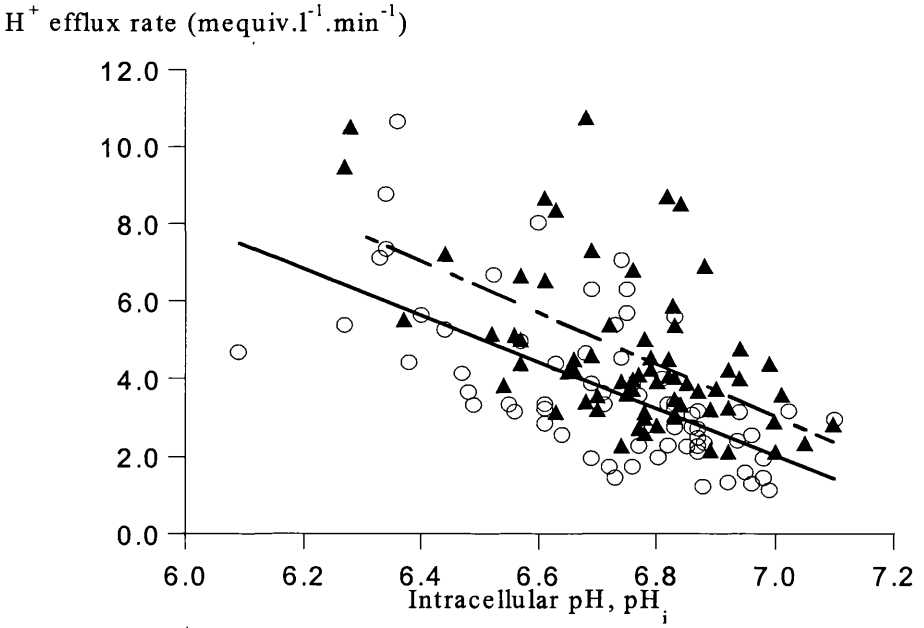

Figure 3.31. H^+ efflux rate as a function of intracellular pH in myocytes isolated from control hearts (HEPES-buffered shown as open circles and bicarbonate-buffered as filled triangles). Data plotted as individual points and fitted to a linear relationship using a least squares fit. (r=-0.64 for HEPES-buffered, continuous line and r=-0.55 for bicarbonate-buffered, dashed line).

3.13. Summary

1. Recovery from intracellular acidosis is dependant on Na^+-H^+ exchange and Na^+-HCO_3^- exchange and could be modulated by 1 mM amiloride and reducing the external Na concentration. In bicarbonate-free conditions recovery from acute intracellular acidosis in myocytes from control hearts was slower and incomplete compared to that in bicarbonate-buffered conditions. The H^+ efflux rate during recovery from acidosis was also reduced in bicarbonate-free conditions.
2. In bicarbonate-buffered conditions, intracellular buffering power, β_{tot} was increased by approximately 35% in myocytes from control hearts.
3. In bicarbonate-free conditions, the recovery rate from acute intracellular acidosis was slowed in isolated myocytes from aortic-constricted hearts. In the papillary muscles preparations the recovery of raised $[Na^+]_i$ was also slowed in aortic-constricted hearts.
4. The H^+ efflux rate during the recovery from acidosis was not significantly different between the myocytes from the control and aortic-constricted hearts in bicarbonate-free conditions.

3.14. Measurement of intracellular $[Ca^{2+}]$, $[Ca^{2+}]_i$

3.14.1. Measurement of $[Ca^{2+}]_i$ in isolated cells

Determination of $[Ca^{2+}]_i$, was made in isolated ventricular myocytes from control and aortic-constricted guinea-pigs. Measurement was made in all cases using epifluoresence microscopy, by measuring the ratio of the fluorescence output at 340/380 nm of cells loaded with the calcium sensitive fluorochrome, Fura-2. An *in-vitro* calibration was performed by determining the fluorescence ratio at increasing concentrations of Ca^{2+} in the absence of cells as described in the Methods (Chapter 2, section 2.9.3). In addition to determination of baseline $[Ca^{2+}]_i$, 10 mM caffeine was applied to allow estimation of sarcoplasmic reticulum (SR) Ca^{2+} content. All recordings were made from cells superfused, at 37°C with CO_2/HCO_3^--buffered Tyrode's solution prepared as described in Methods (Chapter 2, section 2.3, table 2.1).

Myocytes were superfused with CO_2/HCO_3^- buffered Tyrode's solution for 5 to 10 minutes to allow stabilisation before steady-state values of $[Ca^{2+}]_i$ were determined.

3.14.2. Effect of hypertrophy on resting $[Ca^{2+}]_i$

The mean resting $[Ca^{2+}]_i$ of cells from control hearts was 247 ± 68 nM (mean ± SD, n=74 cells from 25 hearts). No significant difference in resting $[Ca^{2+}]_i$ was observed between cells from unoperated and sham-operated hearts. The mean resting $[Ca^{2+}]_i$ of cells from aortic- constricted hearts was 235 ± 75 nM (mean ± SD, n=34 cells from 7 hearts). Figure 3.32 shows the median and interquartile ranges for $[Ca^{2+}]_i$ in the different groups.

3.14.3. Effect of hypertrophy on SR Ca^{2+} content

To estimate the SR Ca^{2+} content, the rise of $[Ca^{2+}]_i$ when released by caffeine was recorded. Application of 10 mM caffeine produced a transient rise of $[Ca^{2+}]_i$ which spontaneously decreased back to resting levels. In 34 cells from control hearts, mean $[Ca^{2+}]_i$ increased from 287 ± 64 nM to 421 ± 91 nM with a mean change 133 ± 70 nM (mean ± SD).

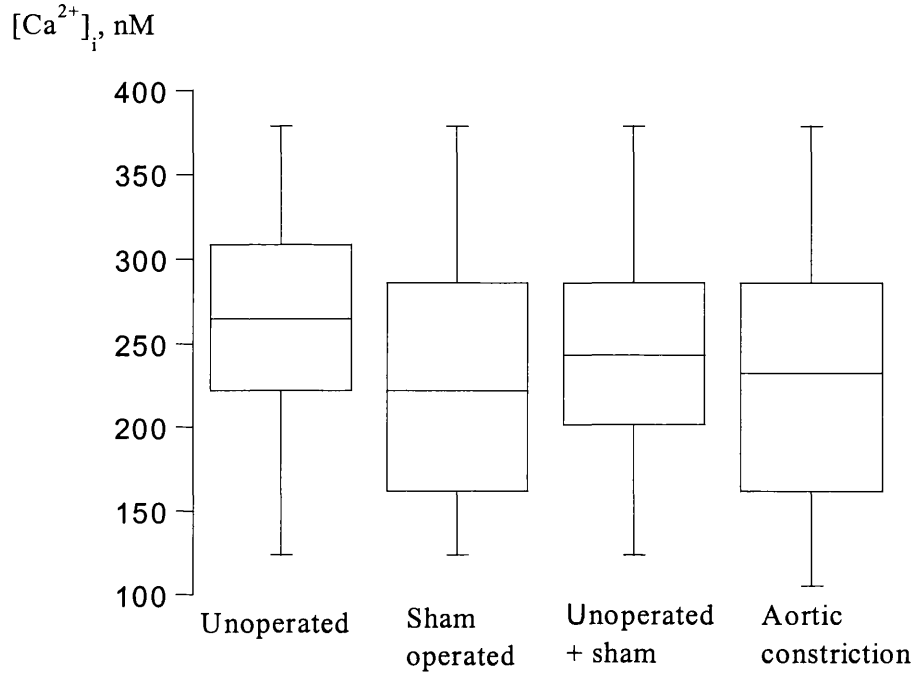

Figure 3.32. Resting $[Ca^{2+}]_i$ in isolated myocytes from control and aortic constricted hearts measured using the fluorescent indicator Fura-2. The boxes enclose 50% of the data points with the median value displayed as the central line and the top and bottom of the box marking the limits of ± 25% of the data. The lines extending from the top and bottom indicate the maximum and minimum values.

However, it was observed that this response was very variable with 52% of cells in the resting state showing no response to caffeine. Following KCl induced depolarisation, most cells showed a transient increase in $[Ca^{2+}]_i$ when caffeine was subsequently applied and this intervention was therefore used in all subsequent experiments and also served to confirm the viability of the cells. A typical caffeine transient in a myocyte from a sham-operated heart is shown in plate 3A. In figure 3.33 derived caffeine transients from a control and an aortic-constricted heart are superimposed. In both cells Ca^{2+} rises to a peak and then falls below baseline levels before recovering back to baseline. The fall is clearly more rapid in the myocyte from the control heart illustrated by the continuous line.

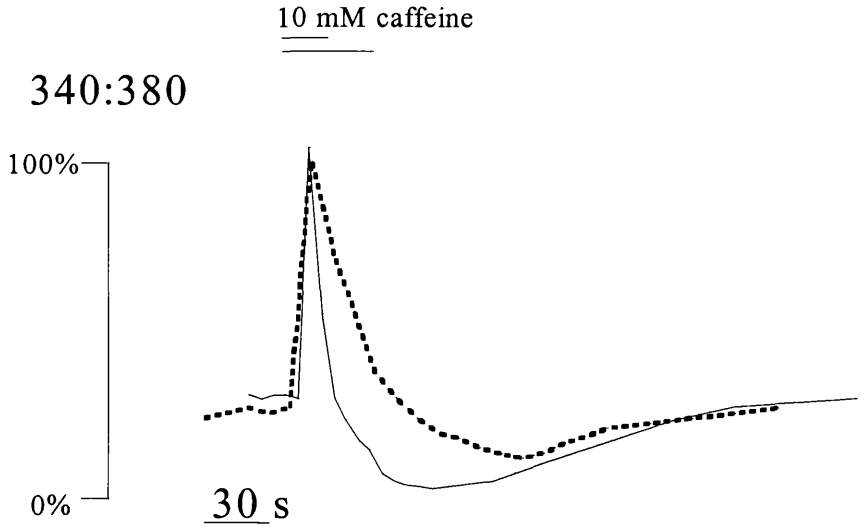

Figure 3.33. Derived plot of a caffeine transient from a control (continuous line) and an aortic-constricted (broken line) heart both scaled to 100% to allow comparison . $[Ca^{2+}]_i$ measured using the fluorescent indicator, Fura-2 and plotted as the ratio of the fluorescence output at 340/380 nm. In the control cell resting $[Ca^{2+}]_i$ was 253 nM and increased to 428 nM and in the aortic-constricted cell resting $[Ca^{2+}]_i$ was 254 nM and increased to 364 nM.

Following exposure to 40 mM KCl for one minute, $[Ca^{2+}]_i$ increased to a plateau and on removal of KCl the $[Ca^{2+}]_i$ declined rapidly to baseline. The results are shown in table 3.10. The typical effect of exposure to 40 mM KCl is illustrated in plate 3B. The magnitude of the increase in $[Ca^{2+}]_i$ during exposure to KCl was significantly higher in the combined control group compared to the aortic constricted hearts ($p=0.017$) but comparing myocytes from sham-operated and aortic-constricted hearts no significant difference was observed ($p=0.54$).

After a KCl-induced depolarisation, subsequent application of 10 mM caffeine produced a transient increase of $[Ca^{2+}]_i$ in most myocytes. The results are shown in table 3.11. The increase of $[Ca^{2+}]_i$ in myocytes isolated from aortic-constricted hearts was significantly lower than in the control hearts (69 ± 51 vs 107 ± 68 nM, (mean $\pm$ SD) $p<0.01$). A significant negative relationship was observed between the increase of

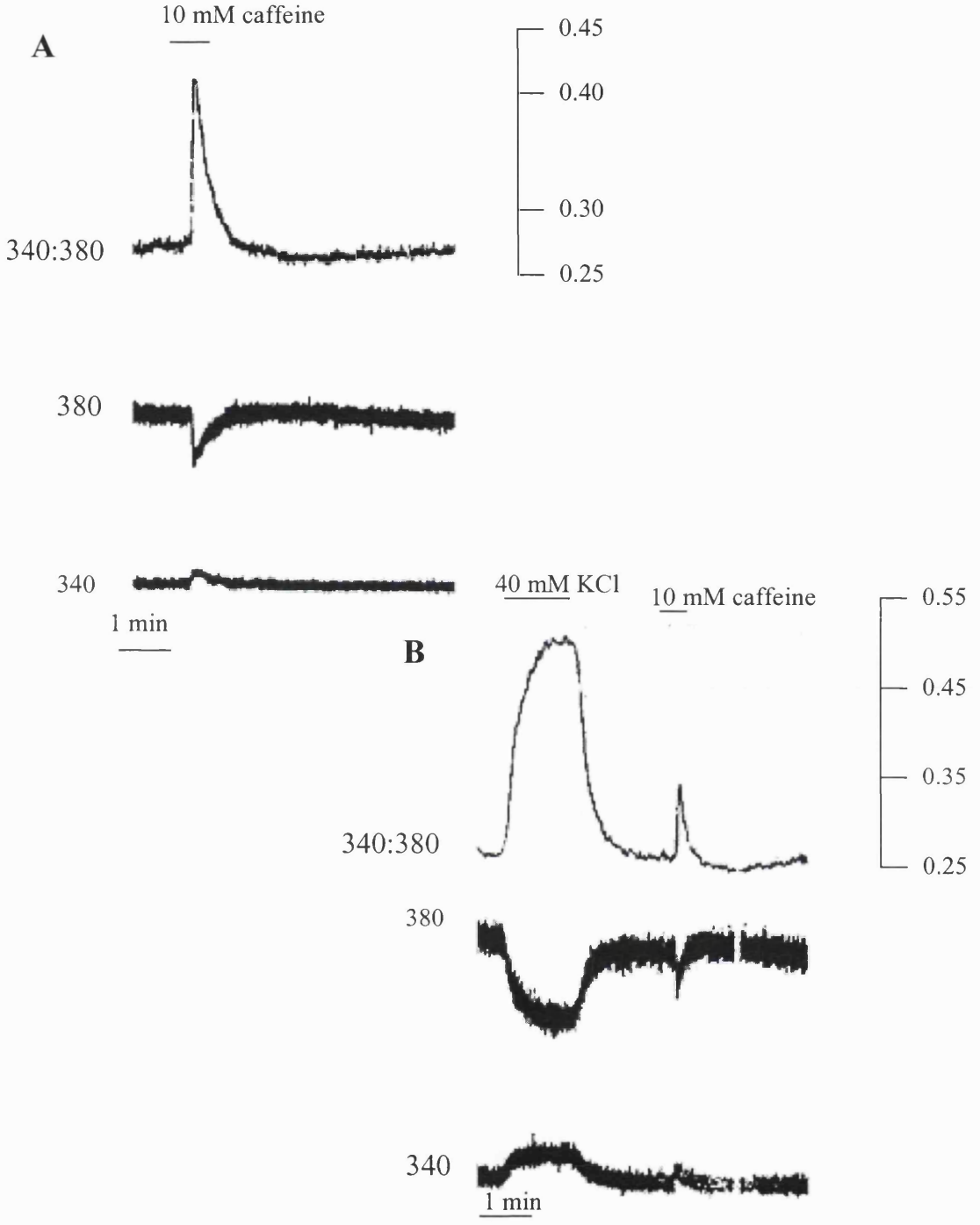

Plate 3. In A the increase in $[Ca^{2+}]_i$ in response to 10 mM caffeine in a myocyte from a sham-operated heart is illustrated as the ratio values. Resting $[Ca^{2+}]_i$ was 309 nM, increasing to 684 nM on application of caffeine. On removal of caffeine $[Ca^{2+}]_i$ fell rapidly to a nadir of 278 nM before returning to baseline. In B the increase in $[Ca^{2+}]_i$ in response to 40mM KCl is illustrated followed by a caffeine response in another cell from a sham-operated heart. Resting $[Ca^{2+}]_i$ was 332 nM, increasing to 1007 nM after KCl and 507 nM after caffeine. On removal of caffeine $[Ca^{2+}]_i$ fell to a nadir of 296 nM before returning to baseline.

$[Ca^{2+}]_i$ in response to 10mM caffeine and the heart-to-body weight ratio of the animal from which the cells were derived as shown in figure 3.34 ($r=-0.68$, $p<0.01$). The values for all the cells isolated from any particular hearts were grouped together and their mean value ± SD was determined and plotted as a function of the heart-to-body weight ratio of the animal from which they were derived.

Table 3.10. Change of $[Ca^{2+}]_i$ during exposure to 40 mM KCl in isolated myocytes measured using the fluorescent indicator, Fura-2. Values are shown mean ± SD. * denotes $p < 0.05$ compared to unoperated and combined control group.

	Baseline $[Ca^{2+}]_i$, nM	+ 40 mM KCl (nM)	Δ $[Ca^{2+}]_i$, nM
Unoperated (n=39)	220 ± 56	626 ± 72	407 ± 128
Sham-operated (n=22)	222 ± 63	559 ± 154	337 ± 120
Unoperated and Sham (n=61)	221 ± 58	602 ± 150	381 ± 129
Aortic-constricted (n=47)	247 ± 103	565 ± 216	317 ± 142*

Table 3.11. Change of $[Ca^{2+}]_i$ on application of 10 mM caffeine (after a brief exposure to 40 mM KCl) in isolated myocytes measured using the fluorescent indicator, Fura-2. Values are shown mean ± SD. * denotes $p<0.01$ compared to unoperated and sham-operated groups and combined control group.

	Baseline $[Ca^{2+}]_i$, nM	+ 10 mM Caffeine (nM)	Δ $[Ca^{2+}]_i$, nM
Unoperated (n=39)	234± 64	334 ±102	102 ± 64
Sham-operated (n=22)	249 ± 83	367 ± 134	117 ± 75
Unoperated and Sham (n=61)	244 ± 80	351 ± 122	107 ± 68
Aortic-constricted (n=46)	262 ± 109	322 ± 147	69 ± 51*

A second application of 10 mM caffeine, after a 2 minute quiescent period produced a significantly smaller rise in $[Ca^{2+}]_i$ in all groups (45 ± 395 nM, mean ± SD, n=24, $p<0.001$ in control group vs 37 ± 29 nM, mean ± SD, n=17, $p<0.001$ in aortic-constricted group). There was no difference in the magnitude of this response between myocytes from control and aortic-constricted hearts ($p>0.05$).

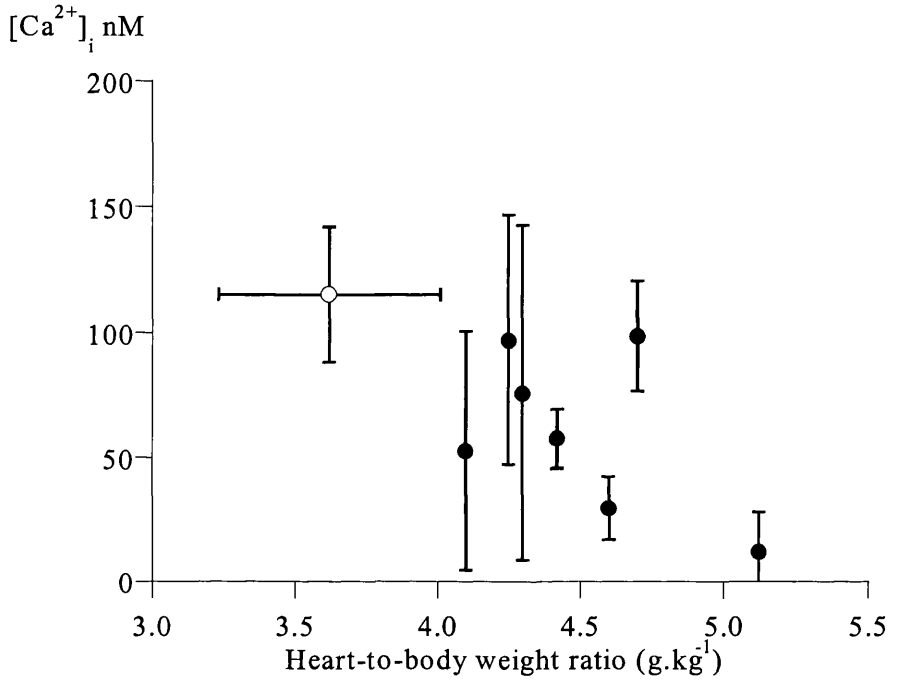

Figure 3.34. Relationship between SR calcium content, measured in isolated myocytes as the increase in $[Ca^{2+}]_i$ produced on application of 10 mM caffeine, and heart-to-body weight ratio. Data from 106 myocytes from 18 hearts. The values for all the cells isolated from any particular heart were grouped together and the mean ± SD plotted as a function of the heart-to-body weight ratio. Values for control hearts shown as open circles and values for aortic-constricted hearts as filled circles. Between 3 and 13 cells were used for the determination of each data point. Data fitted to a linear relationship, $r=-0.68$, $p<0.01$.

3.14.4. Effect of reduced external Na on SR Ca^{2+} content

Substitution of 147 mM NaCl Tyrode's with 29 mM NaCl Tyrode's (Chapter 2, section 2.3.2, table 2.2) caused an increase of $[Ca^{2+}]_i$ which returned towards baseline on reperfusion with 147 mM NaCl Tyrode's. These changes of $[Ca^{2+}]_i$ are presumably due

to activation of the Na^+-Ca^{2+}-exchanger. The increase of $[Ca^{2+}]_i$ was variable with some cells showing a rapid and marked increase as shown in figure 3.35 and plate 4 and other cells showing a smaller increase. The increase was not significantly different between cells from control and aortic-constricted hearts (p=0.64, table 3.12). Figure 3.36 shows the effect of different external concentrations of Na on $[Ca^{2+}]_i$.

Table 3.12. Change of $[Ca^{2+}]_i$ during superfusion with reduced external Na solution (29 mM NaCl Tyrode's) in isolated myocytes measured using the fluorescent indicator, Fura-2. Values are shown mean ± SD. No significant differences between aortic-constricted and any control group observed.

	Baseline $[Ca^{2+}]_i$, nM	+ 29 mM NaCl (nM)	Δ $[Ca^{2+}]_i$, nM
Unoperated (n=51)	258 ± 74	848 ± 644	591 ± 624
Sham-operated (n=13)	264 ± 82	600 ± 399	336 ± 389
Unoperated and Sham (n=64)	259 ± 75	798 ±608	540 ± 591
Aortic-constricted (n=39)	237 ± 75	842 ± 722	604 ±716

Subsequent application of 10 mM caffeine resulted in an increase of $[Ca^{2+}]_i$ which was significantly lower in myocytes from aortic-constricted hearts (table 3.13). A second application of 10 mM caffeine after a 2 minute quiescent period produced a smaller rise in $[Ca^{2+}]_i$ (61 ± 58, mean ± SD, n=25, $p<0.001$ in control group vs 38 ± 44, mean ± SD, n=13 in aortic-constricted group, $p>0.05$). There was no significant difference in the magnitude of this response between the myocytes isolated from control and aortic-constricted hearts ($p>0.05$).

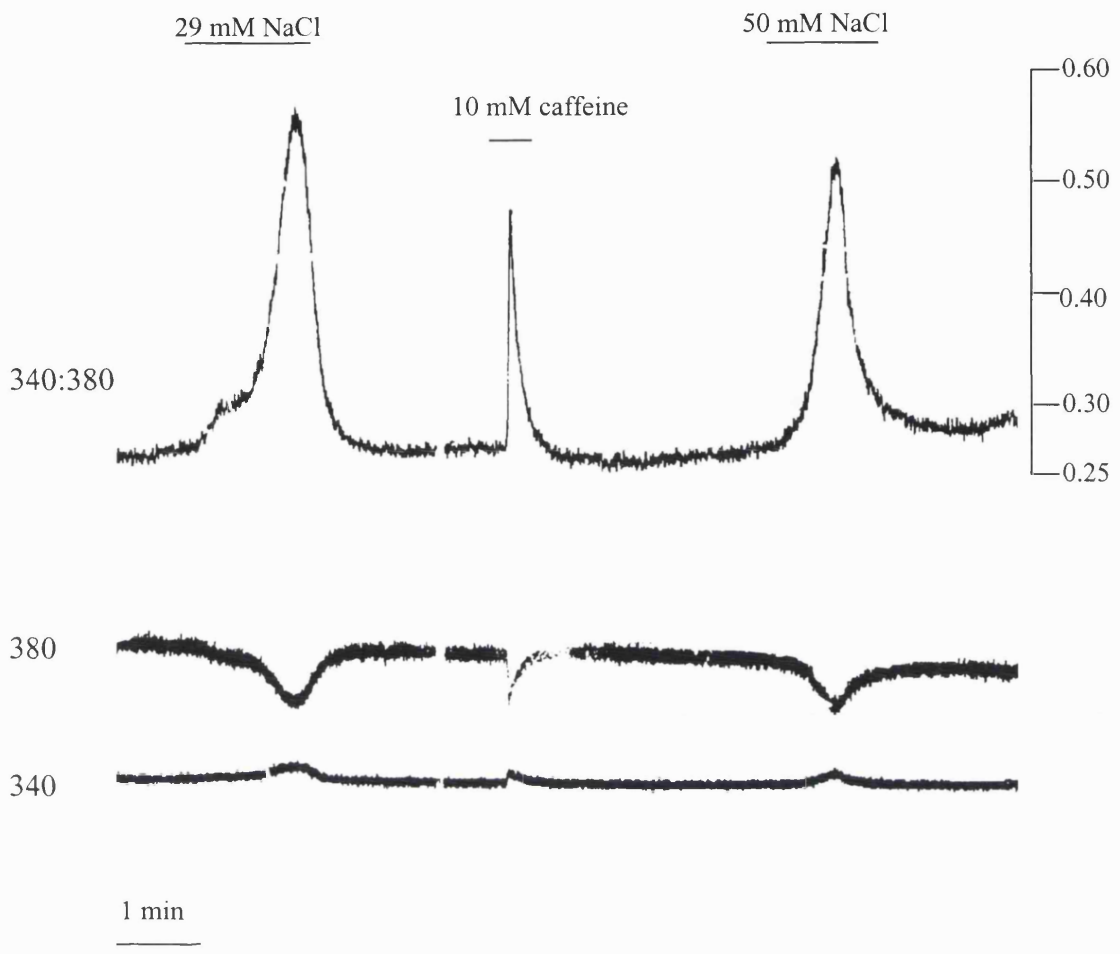

Plate 4. Change in $[Ca^{2+}]_i$ in response to superfusion with reduced external Na solution and 10 mM caffeine in a myocyte from a control heart illustrated as ratio signals. Resting $[Ca^{2+}]_i$ was 310 nM and increased to 1327 nM following 29mM external Na, 624 following 10 mM caffeine and 793 nM following 50 mM external Na.

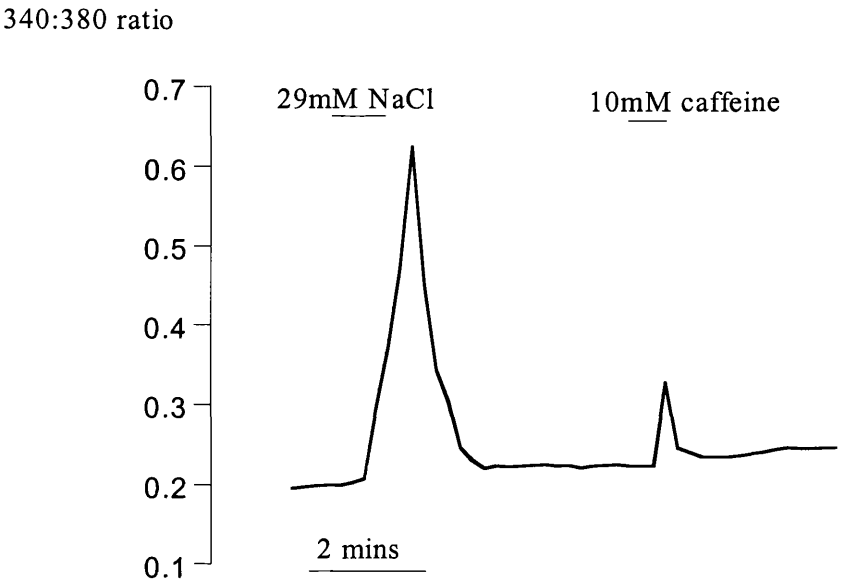

Figure 3.35. Derived plot showing the effect of reduced external Na concentration (29 mM) on $[Ca^{2+}]_i$ measured using the fluorescent indicator, Fura-2 and plotted as the ratio of fluorescence emitted at 340:380 nm in a myocyte from an aortic-constricted heart.

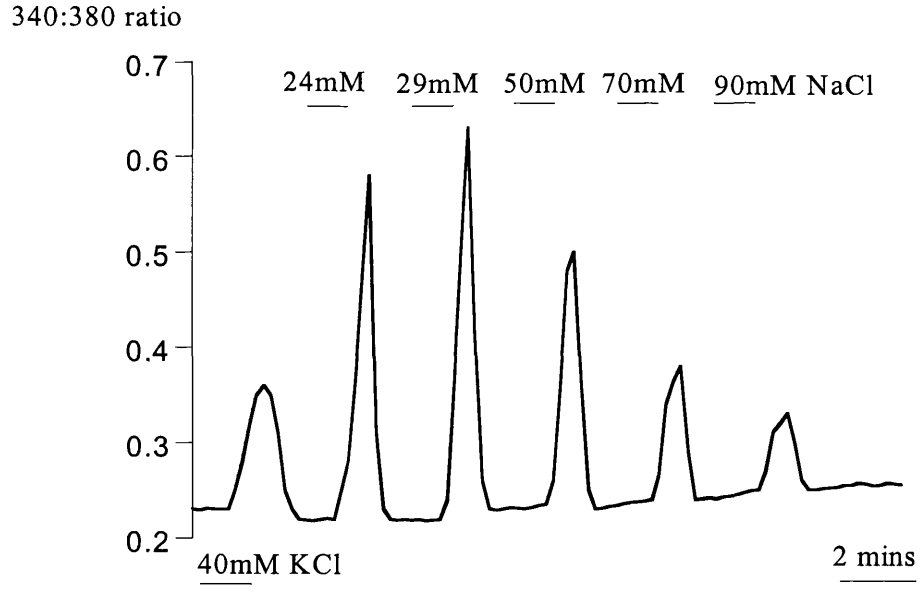

Figure 3.36. Derived plot showing the effect of altering external Na concentration on $[Ca^{2+}]_i$ measured using the fluorescent indicator, Fura-2 and plotted as the ratio of the fluorescence output at 340/380 nm in a myocyte isolated from a sham-operated heart.

Table 3.13. Change of $[Ca^{2+}]_i$ on application of 10 mM caffeine (after superfusion with reduced external Na solution (29 mM NaCl Tyrode's)) in isolated myocytes measured using the fluorescent indicator, Fura-2. Values are shown mean ± SD. * denotes p <0.001 compared to control groups.

	Baseline $[Ca^{2+}]_i$, nM	+ 10 mM Caffeine (nM)	Δ $[Ca^{2+}]_i$, nM
Unoperated (n=46)	292 ± 89	424 ± 141	129 ± 84
Sham operated (n=9)	257 ± 84	363 ± 100	106 ± 32
Unoperated and Sham (n=55)	286 ± 88	414 ± 137	126 ± 79
Aortic-constricted (n=38)	253 ± 82	325 ± 113	72 ± 70*

3.14.5. Estimation of the rate of Ca^{2+} efflux

The Ca^{2+} released from the SR by caffeine is pumped out of the cell mainly via an electrogenic Na^+-Ca^{2+} exchange (Bers *et al.*, 1989; Negretti *et al.*, 1995). The rate of this Ca^{2+} efflux was determined by measuring the time constant of the decay of the caffeine response. The change in $[Ca^{2+}]_i$ was plotted against time and a single exponential curve fitted to calculate the time constant of the recovery phase. Curve fitting was performed using the Scientific Analysis application; KaleidaGraph ™, for Windows, version 3.5, (Synergy Software (PCS Inc)).

Figure 3.37 shows typical curves from a control (A) and an aortic-constricted heart (B). In quiescent myocytes from control hearts $[Ca^{2+}]_i$ fell from a peak of 421 ± 91 nM to a nadir of 243 ± 70 nM (mean ± SD, n=34) with a recovery time constant, τ_1, of 10.6 ± 4.7 s. Corresponding values in 6 cells from aortic-constricted hearts were a peak of 444 ± 85 nM falling to a nadir of 279 ± 51 nM with a time constant of 11.7 ± 4.9 s (mean ± SD) ($p>0.05$ vs control).

However, as discussed above this response was very variable with a significant proportion of cells in the resting state showing no response to caffeine. Following KCl-

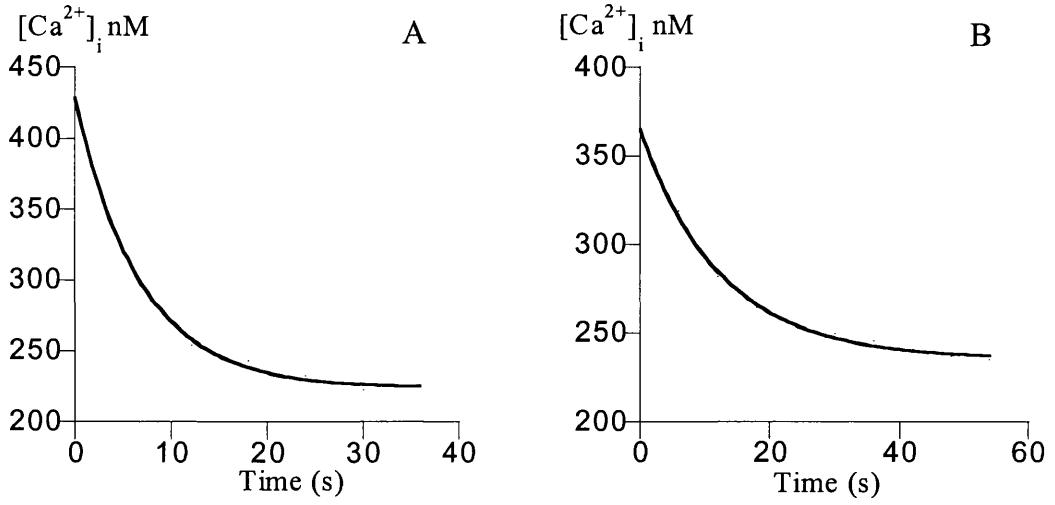

Figure 3.37. Time constant of the decay of the caffeine transient (τ_1) in a myocyte from a control heart (A) and a myocyte from an aortic-constricted heart (B). In A the $[Ca^{2+}]_i$ declined from 428 nM to 222 nM with a time constant of 6.7 s and in B the $[Ca^{2+}]_i$ declined from 364 nM to 227 nM with a time constant of 12.5 s.

induced depolarisation, most cells showed a transient increase in $[Ca^{2+}]_i$ when caffeine was subsequently applied and this intervention was therefore used in all subsequent experiments. The data are summarised in table 3.14. In 28 myocytes from unoperated control hearts $[Ca^{2+}]_i$ fell from a peak of 358 ± 128 nM to a nadir of 215 ± 66 (mean ± SD) with a recovery time constant of 10.5 ± 3.8 s (mean ± SD). Corresponding values in 18 myocytes from sham-operated hearts were a peak of 406 ± 186 nM to a nadir of 233 ± 84 (mean ± SD) with a recovery time constant of 8.6 ± 3.8 s (mean ± SD). These results were not significantly different from each other. In 40 myocytes from aortic-constricted hearts $[Ca^{2+}]_i$ fell from a peak of 344 ± 126 nM falling to a nadir of 233 ± 68 nM (mean ± SD) with a time constant of 15.0 ± 5.5 s (mean ± SD). This was significantly slower than that in either the unoperated or sham-operated control group ($p<0.001$). A significant relationship was observed between the time constant of the decay of the caffeine transient and heart-to-body weight ratio as shown in figure 3.38 ($r=0.57$, $p<0.01$).

Table 3.14. Peak and nadir of $[Ca^{2+}]_i$ and the time constant of the decay of the caffeine response (after a brief exposure to 40 mM KCl) in isolated myocytes. $[Ca^{2+}]_i$ measured using the fluorescent indicator, Fura-2. Values are shown mean ± SD. * denotes $p<0.001$ compared to control groups.

	Peak $[Ca^{2+}]_i$ nM	Nadir $[Ca^{2+}]_i$ nM	Time constant (s)
Unoperated (n=28)	358 ± 128	215 ± 66	10.5 ± 3.8
Sham-operated (n=18)	406 ± 186	233 ± 84	8.6 ± 3.8
Unoperated+sham (n=46)	374 ± 155	222 ± 75	9.74 ± 3.87
Aortic-constricted (n=40)	344 ± 126	233 ± 68	15.0 ± 5.5 *

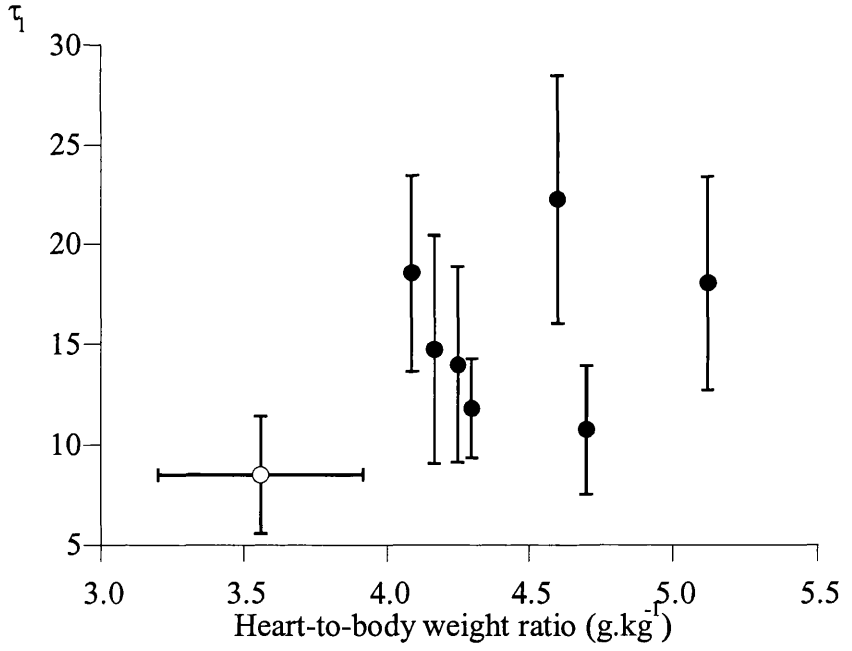

Figure 3.38. Relationship between the time constant of the recovery phase of the caffeine transient (τ_1) and heart-to-body weight ratio. Data from 86 cells from 17 hearts. The values for all the cells isolated from any particular heart were grouped together and the mean ± SD plotted as a function of the heart-to-body weight ratio. Values for control hearts shown as open circles and values for aortic-constricted hearts as filled circles. Between 3 and 13 cells were used for the determination of each data point.

3.14.6. Effect of reduced external [Na] on the rate of Ca^{2+} efflux

The rate of Ca^{2+} efflux was also calculated in myocytes from control and aortic-constricted hearts using the caffeine transients produced after exposure to reduced external Na as illustrated in plate 5. During caffeine-induced Ca^{2+} transients in reduced sodium solutions, the $[Ca^{2+}]_i$ decline is much more dependent on transport of Ca^{2+} by the mitochondrial Ca uniporter and the sarcolemmal Ca-ATPase (Bassani *et al.*, 1992). As described above 10 mM caffeine was applied after a brief exposure to Tyrode's solution containing 29 mM NaCl (Chapter 2, section 2.3.2, table 2.2). As shown in figure 3.39 the time constants in myocytes from control and aortic-constricted hearts were prolonged compared to those after KCl-induced depolarisation in normal Tyrode's (10.0 ± 3.9 vs 17.3 ± 10.3 s, mean ± SD, n=27, $p<0.001$ for control and 15.1 ± 5.7 vs 19.4 ± 9.6 s, mean ± SD, n=17, $p = 0.019$ for aortic-constricted group, paired Student's t-tests).

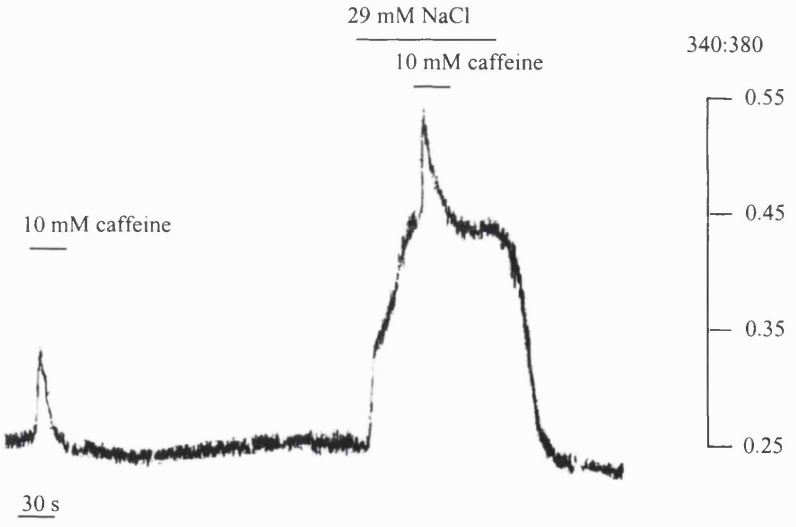

Plate 5. Change in $[Ca^{2+}]_i$ in response to 10 mM caffeine before and during superfusion with reduced external [Na] solution plotted as 340:380 fluorescence ratio. Resting $[Ca^{2+}]_i$ was 264nM and increased to 454 nM on caffeine exposure with a recovery time constant of 11.4s. $[Ca^{2+}]_i$ increased to 818 nM on superfusion with 29 mM NaCl and the recovery time constant of the second caffeine transient was 16.9s.

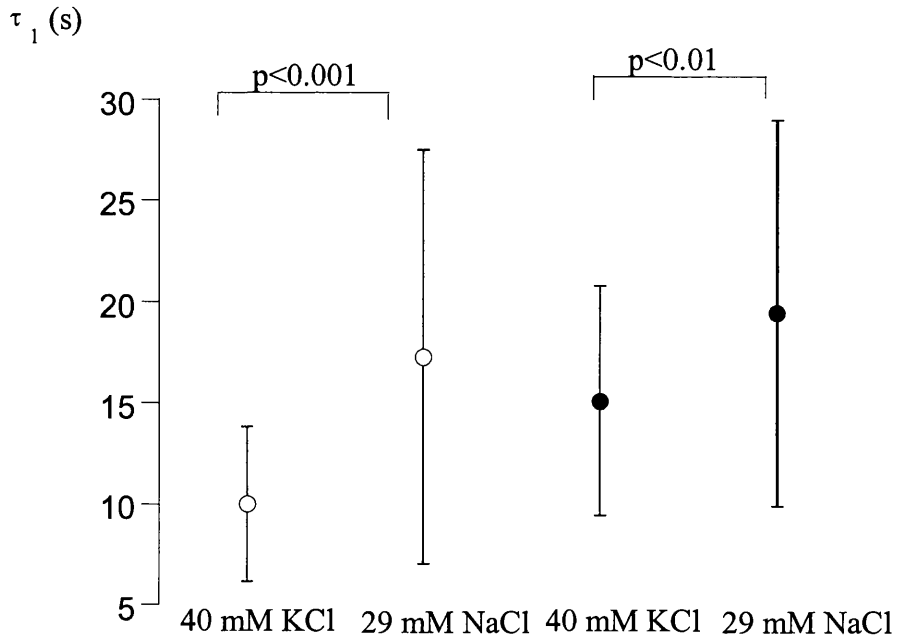

Figure 3.39. Time constant (τ_1) of the recovery phase of the caffeine transient after KCl-induced-depolarisation and reducing external [Na] in myocytes from control (open circles) and aortic-constricted (closed circles) hearts. Values are mean ± SD. Paired Student's t-test.

3.14.7. Refilling of the SR

In some myocytes after removal of caffeine a transient undershoot of $[Ca^{2+}]_i$ was observed which then recovered to baseline levels. It has been suggested that the undershoot results from the depleted SR offering a transient greater uptake gradient which gradually equilibrates with the pre-intervention $[Ca^{2+}]_i$ as the store refills (Baro *et al.*, 1993). The change in $[Ca^{2+}]_i$ was plotted against time and a single exponential curve fitted to calculate the time constant of the recovery phase of the undershoot. Curve fitting was performed using the Scientific Analysis application; KaleidaGraph ™, for Windows, version 3.5, (Synergy Software (PCS Inc)).

In 16 myocytes from control hearts $[Ca^{2+}]_i$ increased from a nadir of 197 ± 66 nM to baseline of 225 ± 76 nM (mean ± SD) with a time constant of 51.8 ± 16.3 s (mean ± SD). Corresponding values in 24 myocytes from aortic-constricted hearts were a nadir of 247 ± 67 nM to baseline of 277 ± 76 nM (mean ± SD) with a significantly slower time constant of 71.2 ± 33.9 s (mean ± SD) ($p<0.05$). A significant relationship was observed

between the time constant of the recovery of the undershoot and heart-to-body weight ratio as shown in figure 3.40 ($r=0.73$, $p<0.01$).

The time constant of the recovery of the undershoot was significantly slower than the time constant of the decay of the caffeine response. The ratio of the time constant of the recovery of the undershoot to the time constant of the decay of the caffeine transient was similar in the myocytes from control and aortic-constricted hearts (5.9 ± 3.7 vs 6.0 ± 3.4, mean $\pm$ SD, $p>0.05$).

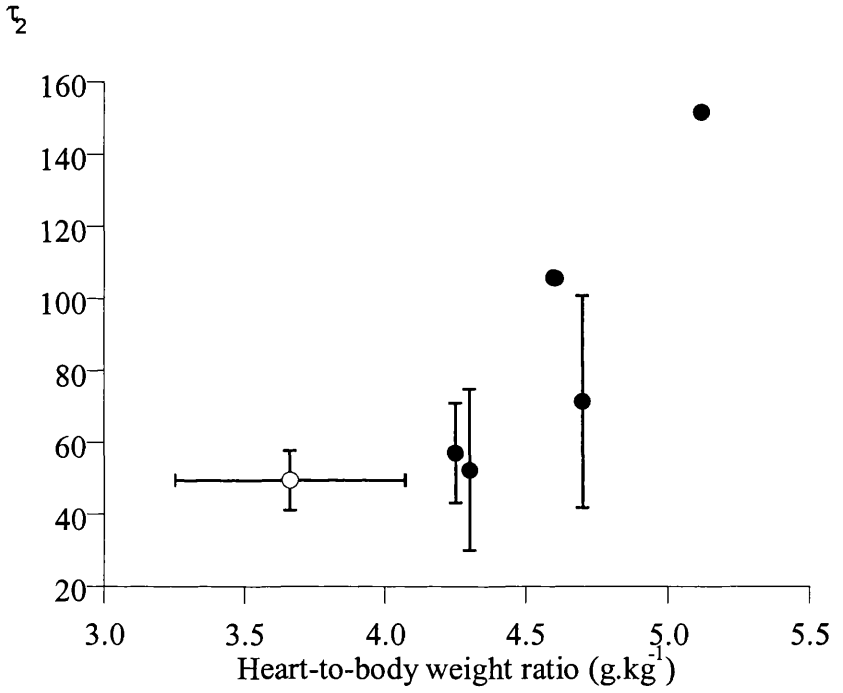

Figure 3.40. Relationship between the time constant of the recovery phase of the undershoot of the caffeine transient (τ_2) and heart-to-body weight ratio. Data from 40 cells from 12 hearts. The values for all the cells isolated from any particular heart were grouped together and the mean $\pm$ SD plotted as a function of the heart-to-body weight ratio. Values for control hearts shown as open circles and values for aortic-constricted hearts as filled circles. Between 1 and 9 cells were used for the determination of each data point.

Summary

1. Resting $[Ca^{2+}]_i$ was not significantly different between myocytes isolated from control and aortic-constricted hearts.
2. The Ca^{2+} released from the SR by caffeine was significantly reduced in myocytes from aortic-constricted hearts and there was a significant correlation between the change of $[Ca^{2+}]_i$ and heart-to-body weight ratio.
3. The time constant (τ_1) of the decay phase of the caffeine transient was prolonged in myocytes from aortic-constricted hearts and correlated with heart-to-body weight ratio.
4. The time constant of the recovery phase (τ_2) of the undershoot was also prolonged in myocytes from aortic-constricted hearts and correlated with heart-to-body weight ratio.
5. Reduction of external sodium caused an increase in $[Ca^{2+}]_i$ which was not significantly different between myocytes from control and aortic-constricted hearts.

These findings suggest that the SR Ca^{2+} content is reduced and / or the ability of the SR to release and re-accumulate Ca^{2+} is impaired in this model of left ventricular hypertrophy.

3.15. Na^+-K^+-ATPase pump isoforms

3.15.1. Quantitative immunoblotting

Western blotting or immunoblotting was used to determine the relative quantities of the isoforms of the α subunit of the Na^+-K^+-ATPase pump in samples from right and left ventricular samples from sham-operated, aortic constricted and debanded guinea-pigs.

3.15.2. Calsequestrin in hypertrophy

The infiltration of new cell types and collagen deposition in hypertrophied hearts could have a diluting effect on the protein of interest. Furthermore as myocyte size increases, the membrane does not increase relatively as much as the intracellular volume so the cytosol has a diluting effect as well. Equal volumes of sample (10% weight / volume of the homogenate) were loaded from sham-operated and aortic constricted hearts and to correct for any differences in the amount of protein added the samples were also analysed for calsequestrin which is not altered by the process of hypertrophy (Arai *et al.,* 1996; Tsutsui *et al.,* 1997; Schotten *et al.*, 1999; Shorofsky *et al.,* 1999; Somura *et al.,* 2001). Figure 3.41 shows calsequestrin levels in the different groups. The sample that gave the greatest signal was defined as 100% and the other values are expressed as a percentage of this sample. No significant difference was observed between calsequestrin levels in sham-operated, aortic-constricted and debanded hearts. Calsequestrin levels were lower in right ventricular samples from all three groups but the difference was only significant in the sham-operated group ($p<0.05$).

3.15.3. α-isoform expression in hypertrophy

Rat brain was used as a positive control for the α_3 isoform. Each α isoform was detected as a specific band at M_r ~100 kD. Figure 3.42 is an immunoblot showing the proteins detected using antiserum specific for the α_1-isoform. No difference in α_1-isoform levels was observed between sham-operated and aortic-constricted hearts. Figure 3.43 shows α_1-isoform levels expressed as the ratio of α_1-isoform:calsequestrin in the different groups.

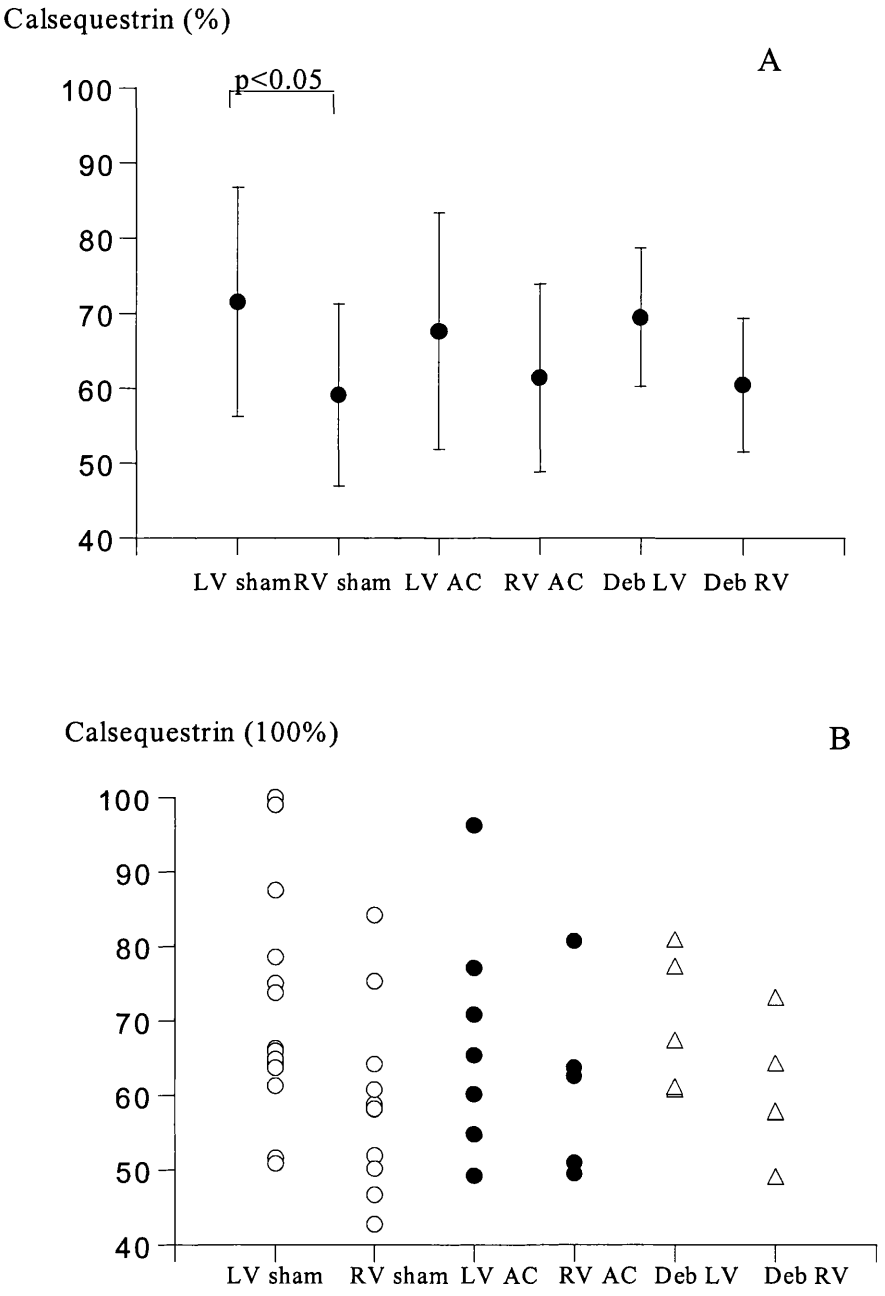

Figure 3.41. Densitometric quantification of western blot analysis of calsequestrin in right (RV) and left ventricular (LV) samples from sham-operated, aortic-constricted (AC) and debanded (deb) guinea-pig hearts. The maximum calsequestrin signal recorded was taken as 100% and the other values expressed as a percentage of this sample. (n=14 for sham, n=7 for AC and n=5 for deb). The mean ± SD values are shown in A and the individual data points are shown in B.

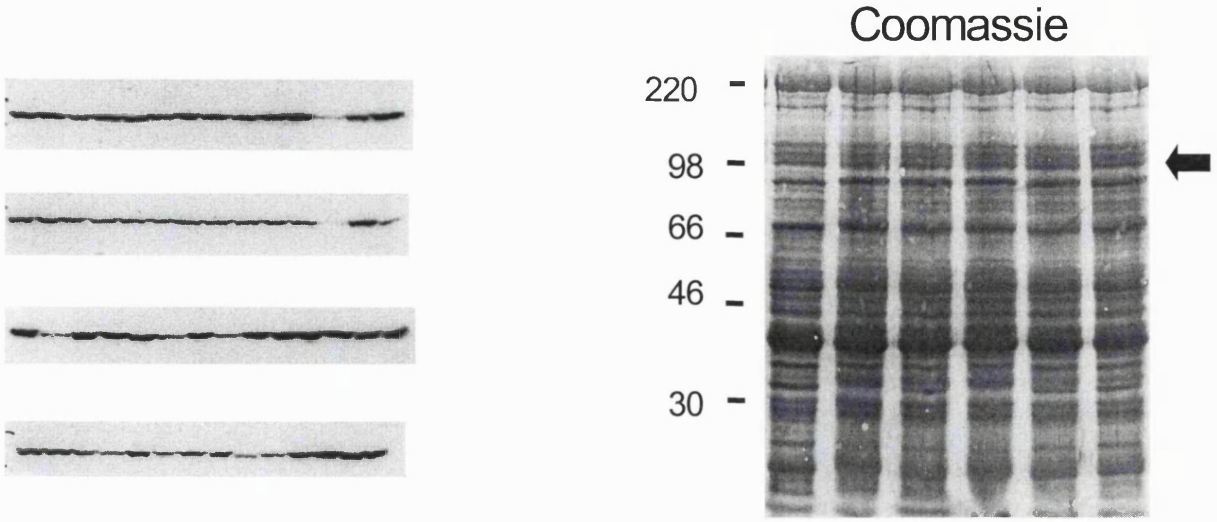

A B

Figure 3.42. A. Immunological detection of the α_1-isoform of the Na^+-K^+-ATPase pump. Western blots of right and left ventricular samples from sham-operated, aortic-constricted and debanded hearts loaded randomly. The α_1-isoform was detected with a monoclonal antibody specific for α_1. (The blank lanes are samples of lung tissue). B shows distribution of molecular weight markers. The α_1-isoform runs exactly with the 98 marker (arrowed)

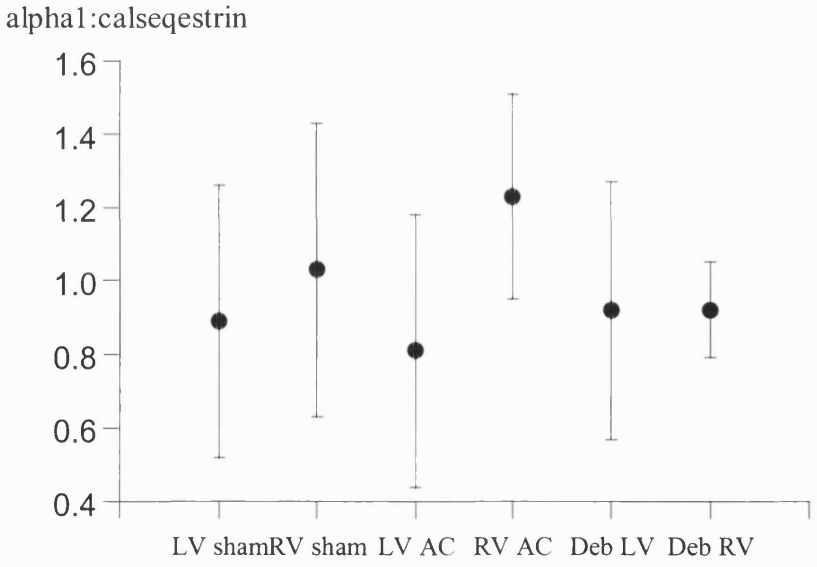

Figure 3.43. Densitometric quantification of western blot analysis of the α_1-isoform of the Na^+-K^+-ATPase pump in right (RV) and left ventricular (LV) samples from sham-operated, aortic-constricted (AC) and debanded (deb) guinea-pig hearts. Values are mean ± SD and expressed as the ratio of the α_1-isoform to calsequestrin. (n=14 for sham, n=7 for AC and n=5 for deb)

The α_2 isoform was undetectable in both right and left ventricular samples from sham-operated and aortic constricted hearts using either the commercially available antibody (rabbit polyclonal from Upstate Biotechnology, USA) or the McB2 mouse monoclonal from Dr KJ Sweadner, Massachusetts General Hospital, Boston MA, USA (Urayama *et al.*, 1989). The ratio of α_3-isoform:calsequestrin levels is shown in figure 3.44 and was not significantly different between the groups. The ratio of the α_3-isoform:α_1-isoform was also not different between the various groups (data not shown).

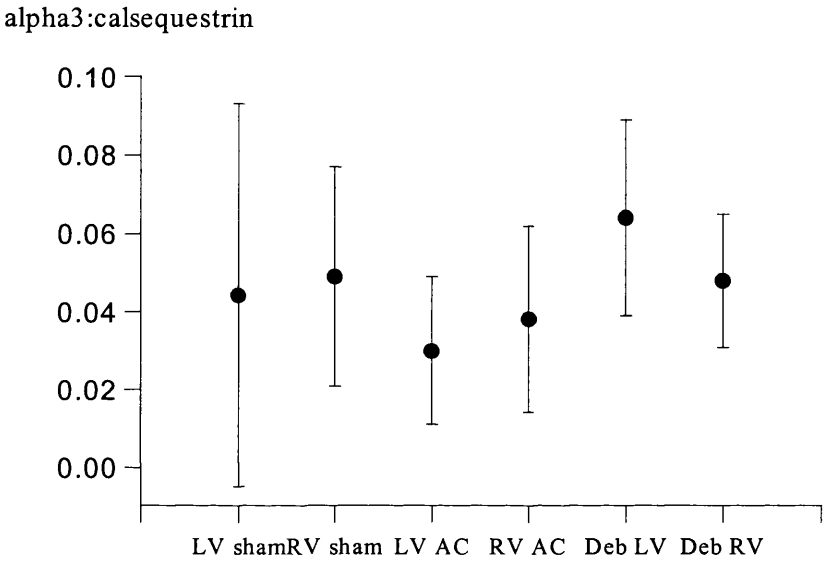

Figure 3.44. Densitometric quantification of western blot analysis of the α_3-isoform of the Na^+-K^+-ATPase pump in right (RV) and left ventricular (LV) samples from sham-operated, aortic-constricted (AC) and debanded (deb) guinea-pig hearts. Values are mean ± SD and expressed as the ratio of the α_3-isoform to calsequestrin. (n=14 for sham, n=7 for AC and n=5 for deb)

3.16. The sarcoplasmic reticulum Ca^{2+}-ATPase pump (SERCA2)

No change in the SERCA2 levels were observed between sham-operated, aortic-constricted and debanded hearts (figure 3.35).

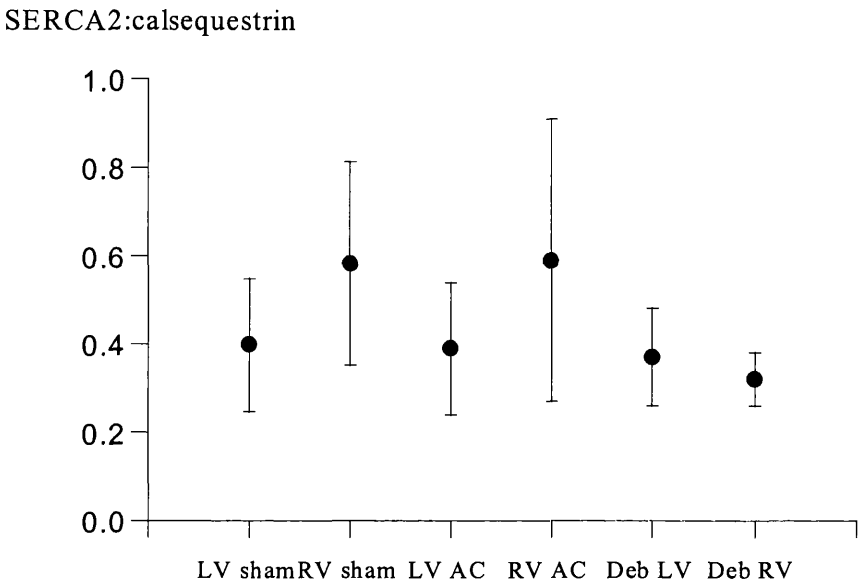

Figure 3.35. Densitometric quantification of western blot analysis of SERCA2 pump in right (RV) and left ventricular (LV) samples from sham-operated, aortic-constricted (AC) and debanded (deb) guinea-pig hearts. Values are mean ± SD and expressed as the ratio of the SERCA2 to calsequestrin. (n=14 for sham, n=7 for AC and n=5 for deb)

3.17. Summary

As expected calsequestrin expression was unaffected by the hypertrophy process. Both the α_1 and the α_3 isoforms of the Na^+-K^+-ATPase pump were expressed in the guinea - pig but the α_2-isoform was not detected by the antibodies used in this study. No change in the SERCA2A expression was observed in hypertrophy. These findings may be due to the small numbers of samples studied and are discussed further in Chapter 4, Section 4.2.4.1).

Chapter 4: Discussion

4.1 Methods

4.1.1. The model of hypertrophy

While the use of human tissue is ideal in attempting to investigate the properties of myocardial hypertrophy, many problems exist with respect to availability and suitability of the biopsies provided. Advantages of animal models of hypertrophy include the ability to perform control experiments and allowing different stages of the disease process to be studied. The method of ascending thoracic aortic constriction in the guinea-pig used in this thesis resulted in significant cardiac and myocardial hypertrophy as assessed by heart-to-body weight ratio and histological measurements (Cooklin *et al.*, 1998) with a mortality of less than 10%. The contractile response of normal guinea-pig myocardium resembles that of the human with a positive force-frequency response and absence of post-rest potentiation. From an electrophysiological viewpoint, guinea-pig action potential morphology resembles that of the human quite closely, with the absence of a phase 1 notch unlike the dog (Boyden *et al.*, 1988) but a maintained plateau phase unlike the rat (Aronson, 1980).

Qualitative anatomical and physiological comparisons can be made between the hypertrophy induced using this model and the pathological process as it occurs in humans. Induction of LVH by ascending thoracic aorta constriction most closely approximates the morphological changes seen in aortic stenosis in humans (Weber *et al.*, 1987). Electrophysiological studies of whole hearts (Winterton *et al.*, 1994) and isolated preparations (Cooklin *et al.*, 1998; Carey *et al.*, 2001) of this model have demonstrated impaired conduction velocity, a change that is similar to that in isolated human myocardium (McIntyre & Fry, 1997) and also parallels the delayed ventricular activation and propensity to ventricular arrhythmias seen in LVH in the human heart. Impaired coronary flow reserve and elevated coronary resistance have also been demonstrated in this model (O'Gorman *et al.*, 1992) which is similar to the changes in coronary haemodynamics seen in patients with LVH (Marcus *et al.*, 1982; Opherk *et al.*, 1984).

In clinical studies regression of LVH has been well documented such as after aortic valve replacement for aortic stenosis (Ikonomidis *et al.*, 2000) or treatment with angiotensin

converting enzyme inhibitors (Sleight *et al.*, 2001). In this model removal of the previously placed constriction resulted in regression of established LVH. However, after 43 days, heart-to-body weight ratios did not completely reverse to control values. After 100 day regression seemed to be complete and indeed in this model cellular hypertrophy has been shown to reverse to control values at this stage (Botchway, 2001). Several studies have shown that there is collagen deposition during the process of hypertrophy (Weber *et al.*, 1987, Brilla *et al.,* 1991) which may persist in regression. Some studies have shown no reversal (Dussaillant *et al.*, 1996; Dixon *et al.*, 1997; Yang *et al.*, 1997) while others have shown some reversal of collagen deposition (Brilla *et al.,* 1996) associated with regression of left ventricular mass. The residual hypertrophy seen in this study is probably due to some degree of residual collagen deposition that developed during the hypertrophic process and may persist even after the removal of the aortic constriction.

Banding of the ascending aorta has been successfully employed to produce LVH in other species including the dog (Bache *et al.*, 1990), the pig (Breisch *et al.*, 1986a), the cat (Cameron *et al.*, 1983), the ferret (Bentivegna *et al.*, 1991; Wang *et al.,* 1994), the rabbit (Milnes & MacLeod, 2001) and the rat (van der Laarse *et al.*, 1989).

Other methods of inducing LVH include renal artery stenosis (Brilla *et al.*, 1990), infra-renal aortic banding (Ryder *et al.,* 1993), cathecholamine administration (Laylock *et al.*, 1996; Wong et al., 1998), thyroxine administration (Arai *et al.*, 1991; Tomanek *et al.,* 1993) growth hormone secreting tumours (Xu & Best, 1991) and physical training (Breisch *et al.*, 1986b; Belichard *et al.*, 1992). Rat models of hypertension also result in LVH. The SHR is a polygenic model of long-term pressure-overload induced hypertrophy. In the Dahl-salt sensitive rat, administration of salt (1% NaCl) and deoxycorticosterone acetate results in hypertension and LVH in uninephrectomised guinea-pigs (Tiritilli & Ruff, 1994). LVH has also been demonstrated in transgenic rats [TG(mREN2)27] overexpressing the mouse renin gene (Flesch *et al.*, 1997).

Many animal models of hypertension, in particular those produced by supra-renal aortic constriction are associated with an increase in both angiotensin II (AII) and aldosterone (AL) (Liard & Spadone., 1985; Crandall *et al.*, 1991). However, no change in AII levels has been demonstrated in the guinea-pig model of ascending aortic-constriction used in

these studies (Kingsbury *et al.*, 1999). It has been postulated that it is the ventricular loading provided by the increased afterload that is largely responsible for myocyte hypertrophy, whilst circulating factors such as AII and AL are responsible for the accumulation of collagen. Thus, the hypertrophy seen with infra-renal aortic-constriction, where AII and AL are normal is not associated with significant fibrosis despite significant hypertension (Brilla *et al.*, 1990) and the degree of fibrosis in the SHR rat is reduced with low doses of angiotensin-converting enzyme inhibitors which have no significant anti-hypertensive effect (Brilla *et al.*, 1991). Ascending aortic constriction may be expected to result in increased activity of the renin-angiotensin-aldosterone axis. However, evidence for this is lacking in our model (Kingsbury *et al.*, 1999) and in another study in dogs there was no increase in plasma renin activity with ascending aortic-constriction (Andersen *et al.,* 1994). In the latter study it was hypothesised that elevated left atrial pressure inhibited renin secretion by reflex mechanisms and elevated plasma atrial natriuretic peptide (ANP). However, even if our model is not one of "pure" myocyte hypertrophy, the presence of fibrosis is generally regarded as an important determinant of function in pathological hypertrophy (Weber *et al.*, 1987) and is responsible for abnormal myocardial stiffness which accompanies the development of LVH (Doering *et al.*, 1988). Furthermore, models of LVH produced by infra-renal aortic banding tend to be associated with very mild degrees of hypertrophy (Ryder *et al.*, 1993).

4.1.2. Measurement of intracellular [Na^+] using ion-selective microelectrodes

The use of Na^+-sensitive microelectrodes allows direct and continuous monitoring of free $[Na^+]_i$, and relatively direct calibration. The electrodes are sensitive enough to detect small changes in ion concentration. One of the limitations is that the cell has to be impaled with the Na^+-sensitive microelectrode and membrane potential must be measured separately and simultaneously usually with a second intracellular microelectrode. In this study different cells were penetrated with Na^+-sensitive microelectrodes and conventional KCl microelectrodes but it is assumed that the membrane potential of all cells is similar due to electrotonic coupling. The equivalence of the membrane potential recorded by the two electrodes after cell impalement was tested as described in the results and only when identical depolarisations (within 1 mV) were recorded by raising the extracellular [KCl] were the results analysed. Another potential problem is that following impalement, the bath solution or electrode contents

might leak into the sarcoplasm and thus alter the ionic composition. The values of $[Na^+]_i$ obtained in quiescent muscle in this study are similar to those obtained by others using Na^+-sensitive electrodes, the fluorescent indicator SBFI and / or ^{23}Na NMR measurements (table 4.1).

A number of these studies report estimated Na^+ activity (a^i_{Na}) values as this is what the Na^+-selective electrode measures, rather than concentration i.e. measured Na^+ concentration is converted into activity by multiplying by an activity coefficient of 0.76. This activity coefficient assumes that the ionisation of Na in the cytoplasm is the same as that in the external medium. In order to allow comparison between the different studies a^i_{Na} values have been converted back to $[Na^+]_i$ values.

There is considerable variation in the values obtained in these different studies. Some of this variation may be explained by species differences, the temperature at which the $[Na^+]_i$ was measured, and the method of measurement. In table 4.2 the results are grouped according to temperature and the method of measurement. Values measured using SBFI are generally lower than those measured with ISE's. Experiments performed at <35 °C when the Na^+-K^+-ATPase pump would be partially inactive generally report higher $[Na^+]_i$ values. This can be seen clearly for ISE measurements but SBFI measurements were not obviously different. This may reflect the fact that most of the measurements performed at ≥ 35 °C were performed in rat myocardium and $[Na^+]_i$ values in rat (Shattock & Bers, 1989; Borzak *et al.,* 1992; Donoso *et al.*, 1992; Harrison *et al.*, 1992b; Baartscheer *et al.,* 1997; Park *et al.,* 1999; Despa *et al.*, 2002) and ferret myocardium (Chapman *et al.*, 1983; Guarnieri, 1988; Baudet *et al.*, 1991; Blatter & McGuigan., 1991) are generally higher than in other species.

Table 4.1. Summary of published values for $[Na^+]_i$ in muscle strips, isolated myocytes and intact heart. SBFI = sodium-binding benzofuran isopthalate, ISE = ion selective microelectrode, NMR = nuclear magnetic resonance spectroscopy. Values are mean ± SD or SEM for $[Na^+]_i$. (Values of $[Na^+]_i$ in parentheses are quoted a^i_{Na} by authors).

Method	Species	Preparation	$[Na^+]_i$	Temp °C	Reference
SBFI	Rabbit	Isolated myocytes	4.5±0.4mM	Room	Despa *et al.*, 2002
SBFI	Rabbit	Isolated myocytes	3.8±0.23mM (2.9±0.17)		Levi *et al.*, 1994a
SBFI	Guinea-pig	Isolated myocytes	6.4±0.5mM	Room	Hayashi *et al.*, 1994
SBFI	Guinea-pig	Isolated myocytes	6.7±0.4mM (5.1±0.3)	26 °C	Harrison *et al.*, 1992b
SBFI	Guinea-pig	Isolated myocytes	6.6±0.6mM	Room	Satoh *et al.*, 1994
SBFI	Guinea-pig	Isolated myocytes	7.1±0.9mM	37 °C	Gray *et al.*, 2001
SBFI	Rat	Isolated myocytes	11.1±0.7mM	Room	Despa *et al.*, 2002
SBFI	Rat	Isolated myocytes	10.7±1.2mM	27 °C	Donoso *et al.*, 1992
SBFI	Rat	Isolated myocytes	10.3±0.4mM (7.8±0.3)	26 °C	Harrison *et al.*, 1992b
SBFI	Rat	Isolated myocytes	14.0±2.0mM	37 °C	Borzak *et al.*, 1992
SBFI	Rat	Isolated myocytes	7.6±1.5mM	35±1 °C	Ruß *et al.*, 1996
SBFI	Rat	Isolated myocytes	9.6±0.4mM	37 °C	Baartscheer *et al.*, 1997
SBFI	Rat	Isolated myocytes	10.9±0.7mM (8.3±0.5)		Levi *et al.*, 1994a
SBFI	Rat	Isolated perfused heart	10.2±0.7mM	35 °C	Park *et al.*, 1999
SBFI	Rat	Isolated perfused heart	3.0±0.15mM	37 °C	Maier *et al.*, 1997

ISE	Guinea-pig	Whole heart	11.6±3.7mM (8.8±2.8)	31-33 °C	Kléber, 1983
ISE	Guinea-pig	Papillary muscle	5.3±1.3mM (4.0±1.0)	36-37 °C	Wang *et al.*, 1988
ISE	Guinea-pig	Papillary muscle	7.6±4.5mM (5.8±3.4)	36 °C	Cohen *et al.*, 1982
ISE	Guinea-pig	Papillary muscles (RV)	6.2±0.4mM (4.7±0.3)	35 °C	Wang *et al.*, 1993
ISE	Rabbit	Isolated myocytes	11.1±2.0mM (8.4±1.5)	37 °C	Desilets & Baumgarten, 1986
ISE	Rabbit	Papillary muscle	7.5±3.5mM (5.7±2.7)	25 °C	Lee & Fozzard, 1975
ISE	Rabbit	Papillary muscle	9.5±0.7mM (7.2±0.5)	30 °C	Shattock & Bers, 1989
ISE	Rabbit	Papillary muscles	10.8±0.5mM (8.2±0.4)	35 °C	Hool *et al.*, 1995
ISE	Ferret	Papillary muscles	14.4±1.3mM (10.9±1.0)	22 °C	Chapman *et al.*, 1983
ISE	Ferret	Papillary muscles	10.3±1.4	19-22 °C	Baudet *et al.*, 1991
ISE	Ferret	Papillary muscles	11.8±1.2mM (9.0±0.9)	36-37 °C	Guarnieri, 1988
ISE	Ferret	Ventricular trabeculae	8.5±0.5 mM	36±0.5°C	Fry *et al.*, 1987
ISE	Ferret	Papillary muscles	13.4±1.2mM	25 °C	Blatter & McGuigan, 1991
ISE	Sheep	Purkinje fibres	9.6±2.7mM (7.2±2.0)	35 °C	Ellis, 1977
ISE	Sheep	Purkinje fibres	9.1±1.8mM (6.9±1.4)	35 °C	Ellis, 1985
ISE	Sheep	Purkinje fibres	9.9±2.9mM (7.5±2.2)	35±1 °C	Ellis & MacLeod, 1985
ISE	Sheep	Purkinje fibres	11.7±0.4mM (8.9±0.3)	35±0.5 °C	Gretler, 1985
ISE	Sheep	Purkinje fibres	7.3±3.8mM (5.5±2.9)	35 °C	Bright & Ellis, 1992

ISE	Sheep	Ventricular trabeculae	8.4±1.6mM (6.4±1.2)	34±1 ° C	Sheu & Fozzard, 1982
ISE	Rat	Papillary muscle	14.9±0.3mM (11.3±0.4)	36±1 ° C	Lagadic-Gossmann & Feuvray, 1991
ISE	Rat	Papillary muscle	16.7±0.9mM (12.7±0.6)	30 °C	Shattock & Bers, 1989
^{23}Na NMR	Rat	Myocyte suspensions	8.8±1.2 mM	30 °C	Wittenberg & Gupta, 1985
^{23}Na NMR	Rat	Isolated perfused heart	8.4±2.3 mM	35 °C	Jelicks & Gupta, 1994
^{23}Na NMR	Guinea-pig	Isolated perfused heart	6.4±0.7 mM	35 °C	Jelicks & Siri, 1995
ISE	Guinea-pig	Papillary muscle	7.4±1.4 mM	37 °C	This study

Table 4.2. Effect of temperature, species and the method of measurement of $[Na^+]_i$. SBFI = sodium-binding benzofuran isopthalate, ISE = ion selective microelectrode. Values are mean ± SEM for $[Na^+]_i$, * denotes $p<0.05$ compared to measurements with ISE's at <35 °C

Species	SBFI		ISE		
	<35 °C	≥35 °C		<35 °C	≥35 °C
All	8.0±1.5mM (n=7)	8.6±1.5mM (n=6)	All	11.9±1.2mM (n=7)	8.8±0.51 mM (n= 15)*
Rat	10.7±0.2mM (n=3)	8.9±1.8mM (n=5)	Rat	16.7±0.9mM (n=1)	14.9±0.3mM (n=1)
			Guinea-pig		6.8±0.4 mM (n=5)

The ISE measurements of $[Na^+]_i$ reported in most studies are the mean ± SD of the estimated ion concentration. However, Fry *et al* (1990) have shown that while the potential differences measured with intracellular Na-sensitive ISE's are normally distributed, the estimated Na^+ concentrations are positively skewed. Thus it is more appropriate to calculate the mean value and standard deviation of the potential difference or the pNa and afterwards perform the antilogarithmic transformation. As was seen in

this study (Chapter 3, table 3.8) this method of calculation reduces the mean $[Na^+]_i$ compared to the more usual approach of performing logarithmic transformation on the individual potential difference measurements. This may partly explain why values of $[Na^+]_i$ obtained with ISE's shown are often higher than values obtained with other methods.

4.1.3. Epifluorescence microscopy and determination of intracellular pH

The use of the pH-sensitive fluorescent dye BCECF in isolated cells allows relatively non-invasive quantitative measurement of pH_i and has been successfully used in isolated cardiac myocytes. Compared to other methods such as the distribution of weak acids and bases and NMR spectroscopy it has a reasonably fast time resolution and is therefore suitable for measuring the relatively rapid changes in pH_i occurring in these studies. Cells were exposed to the acetoxymethylester of the parent compound that is lipid soluble and diffuses freely across the cell membrane. Once the BCECF was within the sarcoplasm it was hydrolysed to the active form of the fluorochrome that is polar and lipid insoluble and was trapped inside the cell. The viability of the myocytes was unaffected by this process.

As described in the literature, compartmentalisation of the dye can occur with the cell. In this cell type the fraction of the dye incorporated into intracellular organelles varies from 8 to 40% (Borzak *et al.*, 1990; Bond *et al.*, 1993; Wang *et al.*, 1994; Peréz *et al.*, 1995; Schäfer *et al.*, 2000). As the majority of the indicator is cytoplasmic, changes of the BCECF ratio signal are likely to mainly reflect a change of cytoplasmic pH (Wang *et al.*, 1994). Therefore the potential error in pH_i measurements due to compartmentalisation should be relatively small and in this study correction of the data for compartmentalisation was not performed.

The ratiometric method used in this study for measurement of pH_i by BCECF and $[Ca^{2+}]_i$ by Fura-2 has considerable advantage when an epifluorescence technique is used. By comparing the fluorescent output of the dye at two different wavelengths, generally one at which the fluorescence intensity varies with the concentration of the ion and one at which it less affected, a ratio of two values rather than absolute fluorescence intensities can be used as an index of H^+ or Ca^{2+} concentration. This form of analysis removes

errors attributable to variability of dye loading in individual cells, loss of dye from the cell and / or bleaching by the light source (Eisner *et al.*, 1989).

4.1.4. Limitations of epifluorescence microscopy for determination of pH_i and H^+ buffering capacity

Problems with this technique mainly centre on calibration. Calibration was achieved by exposing the cell to solutions of known external pH, each containing the H^+ selective ionophore, nigericin. This cationophore is incorporated into the cell membrane and mediates cation-H exchange, thus equilibrating the H^+, Na^+ and K^+ gradients and clamps the intracellular concentration to the extracellular values. This permits variation of the intracellular pH through titration of the extracellular medium. The extracellular solutions were designed to mimic the sarcoplasm and allow cell integrity to be maintained during the calibration process. Errors in calibration could have arisen if the sarcoplasm had not completely equilibrated with the calibrating solution and this blunting could have produced systematic errors in the quantitative assessment of pH_i. To minimise this care was taken to ensure that the signal changes had stabilised before measurements were taken. Calibration errors could also have occurred as a result of increased signal noise, reflecting the intolerance of cells to high pH as it was sometimes noted that calibration failed at pH 9.0.

The use of HEPES as a buffer in the calibrating solution could lead to errors in calibration of the pH_i signal. The pK_a of HEPES is 7.5, hence buffering of the pH 7.0 calibration solution should have been effective but errors could have arisen at pH 4.0 and 9.0. However, it is unlikely that this was the case in this study as the pH of the calibrating solution was checked immediately prior to use with a pH meter that was calibrated at regular intervals. A better alternative would have been to buffer the pH 4.0 calibrating solution with high concentration s of 2-[N-morpholino] ethane-sulphonic acid (MES, pK_a 6.1) and the pH 9.0 calibrating solution with 3-[cyclohexylamino]-2-hydroxyl-1-propanesulphonic acid (CAPSO, pK_a 9.6).

The values of pH_i obtained in this study in normal myocytes are similar to those obtained by others either measured in muscle strips using pH-sensitive microelectodes, single cells using fluorescent indicators, BCECF and SNARF-1

(carboxyseminaphthorhodafluor), and / or in whole heart using NMR (tables 4.3 and 4.7). This would suggest that any potential errors from the above factors were small. Unlike $[Na^+]_i$, the temperature of the experiment did not appear to effect the pH_i in quiescent cells in keeping with the findings of Ellis & Thomas in the rat (1976).

Table 4.3. Summary of values for pH_i in muscle strips, isolated myocytes and intact heart. BCECF = 2',7'-bis(carboxyethyl)-5(6)-carboxyfluorescein, SNARF-1 = carboxyseminaphthorhodafluor, ISE = ion-selective microelectrode, NMR = nuclear magnetic resonance spectroscopy. Values are mean ± SD or SEM for pH_i.

Method	Species	Preparation	pH_i	Temp °C	Extracellular buffer	Reference
BCECF	Rat	Cultured myocyte	7.3±0.02	37 °C	HEPES	Weissberg *et al.*,1989
BCECF	Rat	Isolated myocyte	7.17±0.6	35±1 °C	HEPES	Ruß *et al.*, 1996
BCECF	Rat	Isolated myocyte	7.08±0.07	37 °C	HCO_3^-/CO_2	Hayashi *et al.*, 1992
BCECF	Rat	Isolated myocyte	7.06±0.03	37 °C	HCO_3^-/CO_2	Noda *et al.*, 1992
BCECF	Rat	Isolated myocyte	7.08±0.08	28 °C	HEPES	Kanaya *et al.*, 1998
BCECF	Rat	Isolated Myocyte	7.16±0.05	30 °C	HEPES	Eisner *et al.*, 1989
BCECF	Rat	Isolated Myocyte	7.13±0.03	37 °C	HEPES	Schäfer *et al.*, 2000
BCECF	Rabbit	Isolated Myocyte	7.01±0.04	27 °C	HCO_3^-/CO_2	Nakanishi *et al.*, 1990
		Whole heart	7.1±0.09			
BCECF	Rabbit	Isolated perfused heart	7.03±0.06	30±1°C	HCO_3^-/CO_2	Mohabir *et al.*, 1991
BCECF	Rabbit	Isolated perfused heart	7.13±0.03	37 °C	HCO_3^-/CO_2	Ataka *et al.*, 1992

BCECF	Guinea-pig	Isolated myocyte	7.06±0.18	37 °C	HCO_3^-/CO_2	Wallis *et al.*, 1997
BCECF	Cat	Papillary muscle	7.15±0.04 7.23±0.02	30 °C	HEPES HCO_3^-/CO_2	Camilión de Hurtado *et al.*, 1995
BCECF	Cat	Papillary muscle	7.10±0.02 7.13±0.03	30 °C	HEPES HCO_3^-/CO_2	Camilión de Hurtado *et al.*, 1996
SNARF-1	Guinea-pig	Isolated myocyte	7.14±0.02	37 °C	HEPES	Lagadic-Gossmann *et al.*, 1992
SNARF-1	Guinea-pig	Isolated myocyte	7.07±0.01	37 °C	HEPES	Leem *et al.*, 1999
SNARF-1	Rat	Isolated perfused heart	7.38±0.03	35 °C	HEPES	Park *et al.*, 1999
ISE	Rabbit	Purkinje fibre	7.24	37 °C	HEPES	Bielen *et al.*, 1990
ISE	Guinea-pig	Isolated myocyte	6.99±0.01	36 °C	HEPES	Bountra *et al.*, 1990
ISE	Guinea-pig	Papillary muscle	7.16±0.03 7.13±0.08	33±1 °C	HEPES HCO_3^-/CO_2	Shida *et al*, 1994
ISE	Ferret	Ventricular trabeculae	6.99±0.01	36±0.5 °C	HCO_3^-/CO_2	Fry *et al.*, 1987
ISE	Ferret	Papillary muscle	7.26±0.16	25±0.5 °C	HEPES	Blatter & McGuigan, 1991
ISE	Sheep	Purkinje fibres	7.10±0.21	35 °C	HEPES	Bright & Ellis, 1992
ISE	Sheep	Purkinje fibres	7.26±0.12	35 °C	HEPES	Deitmer & Ellis, 1980
ISE	Sheep	Purkinje fibre	7.2±0.05	35 °C	HEPES	Ellis & Thomas,
	Rat	Ventricular trabeculae	7.2±0.03 7.17±0.06	35 °C 20 °C	HEPES	1976
^{31}P NMR	Ferret	Isolated perfused heart	6.98	30 °C	HCO_3^-/CO_2	Allen *et al.*, 1985b

^{31}P NMR	Rats	Isolated perfused heart	7.04±0.01	37 °C	HCO_3^-	Jeffrey *et al.*, 1987
^{31}P NMR	Rats	Isolated perfused heart	7.19±0.04	37 °C	HEPES	Pike *et al.*, 1993
BCECF	Guinea-pig	Isolated myocyte	7.22±0.12 7.22±0.01	37 °C	HEPES HCO_3^-/CO_2	This study

An additional problem exists for the calculation of intracellular buffering capacity. BCECF acts an intracellular H^+ buffer itself and thus will tend to oppose the changes in H^+ being determined and may lead to overestimation of the buffering capacity of the cell. The pK_a of BCECF measured in these experiments was 6.96 ± 0.11, which are in good agreement with others and is within the physiological range (Eisner *et al.*, 1989). However, the mean value for β_i obtained here in control myocytes was 31.1 ± 15.2 mequiv.l^{-1}.pH $unit^{-1}$ which is similar to values of between 18-50 mequiv.l^{-1}.pH $unit^{-1}$ measured in isolated cells using pH sensitive microelectrodes (Bielen *et al.*, 1990; Bountra *et al.*, 1990; Vaughan-Jones & Wu, 1990; Blatter & McGuigan, 1991; Do *et al.*, 1996). Studies in multicellular preparations tend to overestimate β_i as diffusion into multicellular tissue mass occurs relatively slowly and may be incomplete (Bountra *et al.*, 1990). Use of the isolated myocyte preparation removes this problem.

4.1.5. Use of Fura-2 to measure $[Ca^{2+}]_i$.

There are limitations to the use of Fura-2 to measure $[Ca^{2+}]_i$. The Ca^{2+} sensitivity of Fura-2 *in-vivo* may be different from that of the free acid *in-vitro* (Scanlon *et al.*, 1987) which was used to calibrate the Fura-2 in this study. The recorded signal may also contain some components such as cell autofluorescence from pyridine nucleotides that are not related to $[Ca^{2+}]_i$, but this effect has been shown to contribute <10% to cell fluorescence (Frampton *et al.*, 1991a) and in this study background autofluorescence was subtracted from each signal before the ratio was obtained. Like BCECF, Fura-2 may be compartmentalised within the cell so that the recorded fluorescence signals contain components from non-cytoplasmic sources especially the mitochondria and would not be an accurate estimate of cytoplasmic $[Ca^{2+}]_i$. However this effect is likely to be small and the fluorescent signal from intracellular stores has been shown to be less than 10%

(Eisner *et al.*, 1989; Frampton *et al.*, 1991a; Nakaniski *et al.*, 1990; Schäfer *et al.*, 2000). Another potential problem is that Fura-2 may act as a Ca^{2+} buffer (Noble & Powell, 1990; Siri *et al.*, 1991) and will decrease the $[Ca^{2+}]_i$ and slow the rate of decline of the calcium transient. This effect is also likely to be small as in rat cardiac myocytes Frampton *et al* (1991b) showed that while the time course of contraction was slowed by ~14%, that of relaxation was unchanged in Fura-2 loaded cells and the size of the Ca^{2+} transient was reduced by ~ 30%. All of these effects are likely to affect cells from control and hypertrophied hearts and therefore unlikely to influence our comparative data.

The inherent inaccuracies in the calibration process especially *in-vitro* calibration may explain why the values of resting $[Ca^{2+}]_i$ measured in this study are higher than those reported by others using Fura-2 (table 4.4). It is unlikely that the higher values reflect poor cell viability as care was taken to only select elongated, striated cells for study. It should be emphasised that calibrated signals for Fura-2 are at best an approximation and the absolute levels of resting and peak $[Ca^{2+}]_i$ are still debated. The advantage of calibration as opposed to reporting the ratio values is that it allows some semi-quantitative evaluation of interventions

4.1.6. Use of isolated myocytes

Of concern is the validity of results derived from isolated cells when considering the function of whole tissue. It is possible that the process of isolation disturbs cell function sufficiently to distort ion concentration gradients across the sarcolemma and such a disturbance may be more marked in pathological states such as hypertrophy. However, studies using ISE's and fluorescent indicators give similar values and more recently application of techniques such as magnetic resonance spectroscopy applied to whole tissue has helped to assess the validity of these results as similar values (Tables 4.1 and 4.3) are reported for pH_i and $[Na^+]_i$ as in isolated preparations.

Table 4.4. Summary of values for resting $[Ca^{2+}]_i$ in muscle strips, isolated myocytes and intact heart. NMR = nuclear magnetic resonance spectroscopy, Values are mean ± SD or SEM for $[Ca^{2+}]_i$.

Method	Species	Preparation	$[Ca^{2+}]_i$	Temp	Buffer	Calibration	Reference
Fura-2	Rabbit	Isolated myocytes	169±22 nM	27 °C	HCO_3^- /CO_2	*In-vitro*	Nakanishi *et al.*, 1990
Fura-2	Rabbit	Isolated perfused heart	188±19 nM	37 °C	HCO_3^- /CO_2	*In-vivo*	Ataka *et al.*, 1992
Fura-2	Rat	Isolated myocytes	76±8 nM	37 °C	HCO_3^- /CO_2	*In-vivo*	Hayashi *et al.*, 1992
Fura-2	Rat	Isolated myocytes	75±5 nM	37 °C	HCO_3^- /CO_2	*In-vivo*	Noda *et al.*, 1992
Fura-2	Rat	Isolated myocytes	131±47 nM	37 °C	HEPES	*In-vivo*	Borzak *et al.*, 1990
Fura-2	Mouse	Ventricular trabeculae	50-110 nM	21±1°C	HCO_3^- /CO_2	*In-vivo*	Gao *et al.*, 1998
Fura-2	Human	Isolated myocytes	95±47 nM	35 °C	HEPES	*In-vitro*	Beucklemann *et al.*, 1992
Indo-1	Rabbit	Isolated perfused heart	315±25 nM	30±1°C	HCO_3^- /CO_2	*In-vivo*	Mohabir *et al.*, 1991
Indo-1	Mice	Isolated myocytes	127±11 nM	22 °C	HEPES	*In-vitro*	Terracciano *et al.*, 1998
Fluo-3	Dog	Isolated myocytes	108±20 nM	Not given	HEPES	*In-vitro*	Sipido *et al.*, 2000
Aequorin	Human	Ventricular trabeculae	230±50 nM	30 °C	HCO_3^- /CO_2	*In-vivo*	Gwathmey *et al.*, 1990
ISE	Sheep	Ventricular trabeculae	272±62nM	34±1 °C	HCO_3^- /CO_2	*In-vitro*	Sheu & Fozzard, 1982
ISE	Ferret	Ventricular trabeculae	270±60mM	36±0.5 °C	HCO_3^- /CO_2	*In-vitro*	Fry *et al.*, 1987
^{19}F NMR	Ferret	Isolated heart	202±22nM	30 °C	HEPES	*In-vivo*	Marban *et al.*, 1988
Fura-2	Guinea-pig	Isolated myocytes	247±68 nM	37 °C	HCO_3^- /CO_2	*In-vitro*	This study

4.1.7. SDS-PAGE Western blots and the Na^+-K^+-pump isoforms

In this study Western blotting was used to determine whether changes occurred in the α-subunit isoforms in hypertrophy that might explain the increase of intracellular [Na^+]. However, this method has limitations in that it is only semi-quantitative and there may be uncertainties regarding the affinities of the antibodies used in different species. Other methods of Na^+-K^+-ATPase quantification such as ouabain-binding and estimation of Na^+-K^+-ATPase activity are available but also have limitations. The major problem regarding Na^+-K^+-ATPase quantification in myocardium is the presence of large quantities of nonspecific ATPases. This necessitates membrane purification procedures prior to Na^+-K^+-ATPase activity measurements and membrane material is invariably lost. Thus the recovered fraction of Na^+-K^+-ATPase may not be representative of the *in-vivo* situation and as outlined in the introduction there is still a lot of controversy over the changes in pump activity found in hypertrophy using these methods. Another approach is to measure Na^+-K^+ pump current using the whole cell voltage clamp technique in isolated myocytes (Shattock & Matsuura, 1993). This method allows measurement of sodium pump function in situ in intact cells, thus largely overcoming the possibility that isolation of the enzyme for ATPase measurements may artefactually alter enzyme activity. This method has not been studied in hypertrophied myocardial tissue.

4.2. Results

4.2.1. Mechanical function in hypertrophy

Normal guinea-pig myocardium demonstrated a positive force-frequency relationship whereas in hypertrophied myocardium from aortic constricted guinea-pigs a depression of the force-frequency relationship was observed which correlated with the degree of hypertrophy as assessed by heart-to-body weight ratio. These findings suggest that there is a progressive decline in left ventricular contractile function as hypertrophy progresses. It is likely that the decline in the force-frequency relationship is a consequence of hypertrophy as in two right ventricular papillary muscles obtained from hearts with LVH but normal right ventricles, the force frequency response was positive. These results are in keeping with previous findings in human myocardial preparations from patients with varying degrees of hypertrophy due to aortic and mitral valve disease (Gray *et al.*, 2001).

In addition, biphasic force-frequency responses have been demonstrated in patients with severe hypertenisve LVH (Inagaki *et al.*, 1999) and in patients with hypertrophic cardiomyopathy and severe LVH even in the absence of left ventricular dysfunction (Somura *et al.*, 2001). Both these *in-vivo* studies showed that the maximum first derivative of left ventricular pressure (LV dP/dt_{max}) initially increased with increasing heart rate induced by pacing but then declined as heart rate was further increased to a maximum of 130 beats per minute. It is important to remember that this index of contractile function is dependent on loading conditions.

4.2.2. The rise of $[Na^+]_i$ and the force-frequency relationship in hypertrophy

$[Na^+]_i$, measured using ion-selective microelectrodes, was increased in hypertrophied guinea-pig myocardial preparations. The results support the hypothesis that a negative force-frequency relationship in hypertrophied guinea-pig is due to the raised $[Na^+]_i$. A negative relationship has also been described in normal myocardium from several species, including rat and ferret; a feature of these tissues is the relatively high $[Na^+]_i$ compared to myocardium from species with a positive relationship (Shattock & Bers, 1989). The finding that the force-frequency relationship could be converted from a positive to a negative one in normal guinea-pig myocardium by artificially raising the $[Na^+]_i$ with strophanthidin lends support to this hypothesis as did the finding of post-rest potentiation in the hypertrophied hearts and also observed in normal rat myocardium (Shattock & Bers, 1989). Further support for the role of $[Na^+]_i$ in determining the force-frequency response comes from the study of Mubagwa *et al* (1997) which showed that the monensin-induced reversal of the positive force-frequency response in rabbit and guinea-pig myocardium was associated with an increase of $[Na^+]_i$ caused by the ionophore.

Figure 4.1 shows that the increase of $[Na^+]_i$ and reduction of the $T_{1.6/0.8}$ ratio was already established with moderate hypertrophy and did not change further with continued growth of the left ventricle, whereas intracellular pH continued to fall in moderate and severe LVH. Furthermore, other cellular changes such as increased gap junction resistance (and consequently reduced conduction) are only seen in more severe hypertrophy (Cooklin *et al.*, 1997). The temporal dissociation of changes to these variables raises the important

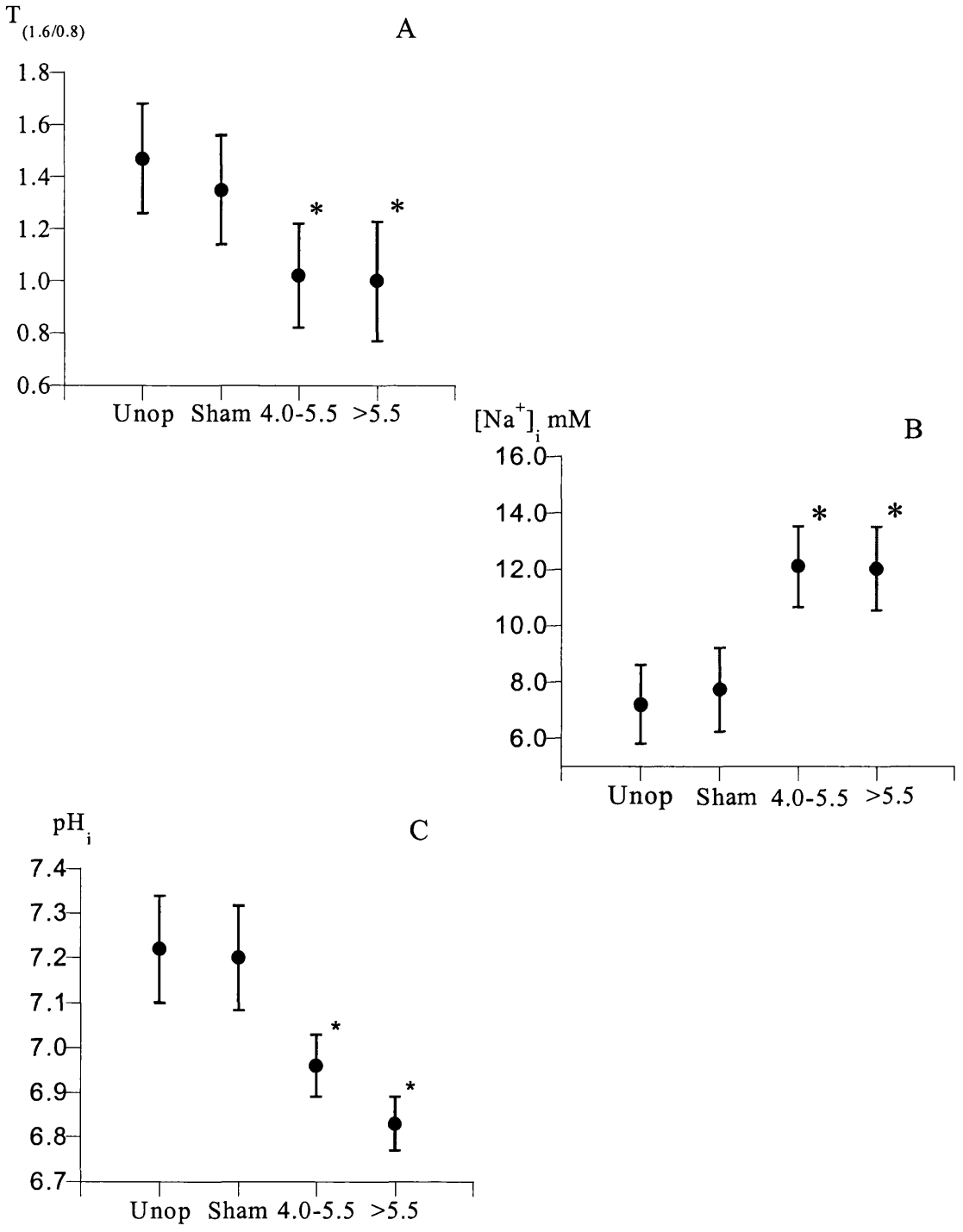

Figure 4.1. Changes to the force-frequency relationship (A), myocardial $[Na^+]_i$ (B) and pH_i (C) in normal LV myocardium from unoperated (unop) and sham-operated hearts (sham), moderate LVH (HBR 4.0-5.5 $g.kg^{-1}$) and severe LVH (HBR >5.5 $g.kg^{-1}$). * denotes $p<0.001$ compared to unoperated or sham-operated groups.

point that an increase of $[Na^+]_i$ may represent an initial change in LVH and may be causal in other cellular changes.

The increase of $[Na^+]_i$ cannot be attributed to the age of the animal. The sham-operated and the constricted animals were left for similar times post-operation; 60-100 days to produce moderate hypertrophy and about 250 days to generate severe hypertrophy. Furthermore, the similarity of $[Na^+]_i$ values in the sham-operated and unoperated control groups suggest that the operative procedures required to place the constricting ring around the aorta do not *per se* raise the $[Na^+]_i$.

To reduce the risk of hypoxia which could impair contractile function and elevate $[Na^+]_i$ in the isolated preparations, the preparation diameter was less than 1mm, a rapid flow of well-oxygenated Tyrode's solution was ensured and a relatively low stimulation rate was used as the physiological rate in the guinea-pig is ≈200 beats per minute (>3Hz). Preparations of similar size were used from control and hypertrophied animals. Furthermore care was taken to impale superficial cells of the preparation microelectrodes in where hypoxia is unlikely.

A rise of the intracellular $[Na^+]$ in hypertrophied guinea-pig myocardium is consistent with other reports (table 4.5). An NMR study showed that $[Na^+]_i$ increased in compensated hypertrophy in aortic-constricted guinea-pigs (Jelicks & Siri, 1995), but declined again in the failing hypertrophied heart. Another NMR study found that $[Na^+]_i$ was significantly greater in spontaneously hypertensive rat hearts (Jelicks & Gupta, 1994), and Clarke *et al* (1990) showed that ischaemia generated a larger rise of $[Na^+]_i$ in hypertrophied rat hearts compared to controls. However, in a ferret model of right ventricular hypertrophy no increase of $[Na^+]_i$ was observed (Baudet *et al.*, 1991), although these experiments were carried out at 20°C when the Na-pump would be partially inactive and the $[Na^+]_i$ consequently already raised.

The decline of the force-frequency relationship when $[Na^+]_i$ is raised is probably due to excessive Ca^{2+} influx through Na^+-Ca^{2+} exchange and overload of intracellular stores. In support of this is the finding that high concentrations of cardiac glycosides have been shown to reduce twitch force and the force-frequency relationship and the intracellular $[Ca^{2+}]$ as the SR is unable to retain Ca^{2+} when the resting SR concentration rises above normal levels (Allen *et al.*, 1985a).

Table 4.5. Studies of $[Na^+]_i$ in myocardial hypertrophy. NMR = nuclear magnetic resonance spectroscopy, ISE = ion selective microelectrodes. Values are mean ± SD * denotes $p<0.01$, ** denotes $p<0.05$ and *** $p<0.001$.

Species	Model	Method	$[Na^+]_I$ mmol.l^{-1}			Reference
			Normal	Hypertrophy	Failure	
Guinea-pig	Thoracic aortic constriction	NMR Spectroscopy	6.4±0.7	12.8±1.2*	8.7±1.9	Jelicks & Siri, 1995
Rat	Spontaneous hypertension	NMR Spectroscopy	8.4±2.3	17.3±3.6**		Jelicks & Gupta, 1994
Ferret	Pulmonary artery banding	ISE	10.3±1.4	10.7±1.6		Baudet *et al.*, 1991
Guinea-pig	Thoracic aortic-constriction	ISE	7.4±1.4	12.1±1.3***		This study

Using the $[Na^+]_i$ and $[Ca^{2+}]_i$ measured in this study the reversal potential for a simple 3:1 Na^+-Ca^{2+} exchanger can be calculated, assuming the system is in equilibrium, *i.e.* there are no other removal systems from the sarcoplasm. The electrochemical gradients for Ca^{2+} and Na^+ are thus:

$$-RT \ln ([Ca^{2+}]_o/[Ca^{2+}]_i) + 2FE = 3 (-RT \ln ([Na^+]_o/[Na^+]_i) + FE)$$

$$i.e.\ [Ca^{2+}]_o/[Ca^{2+}]_i = ([Na^+]_o/[Na^+]_i)^3 \exp (-FE/RT)$$

but the equilibrium potential for Ca^{2+}, $E_{Ca} = (RT/2F) \ln ([Ca^{2+}]_o/[Ca^{2+}]_i)$

and the equilibrium potential for Na^+, $E_{Na} = (RT/F) \ln ([Na^+]_o/[Na^+]_i)$

The value of E at which the gradients are in balance, the reversal potential, $E_{Na\text{-}Ca}$ is

$$E_{Na\text{-}Ca} = 3E_{Na}\text{-}2E_{Ca}$$

In normal myocardium for $[Na^+]_o$ = 147 mM; $[Na^+]_i$ = 7.4 mM and $[Ca^{2+}]_o$ = 1.8 mM; $[Ca^{2+}]_i$ = 247 nM, E_{Na} = 79.8 mV and E_{Ca} = 118.8 mV. Therefore $E_{Na.Ca}$ = 1.8 mV.

In hypertrophied myocardium for $[Na^+]_o$ = 147 mM; $[Na^+]_i$ = 12.1 mM and $[Ca^{2+}]_o$ = 1.8 mM; $[Ca^{2+}]_i$ = 235 nM, E_{Na} = 66.7 mV and E_{Ca} = 119.4 mV. Therefore $E_{Na.Ca}$ = -38.7 mV.

During diastole, when $E_{Na.Ca}$ is positive to E_m, Ca^{2+} extrusion via Na^+-Ca^{2+} extrusion is thermodynamically favoured and when E_m is positive to $E_{Na.Ca}$ Ca^{2+} entry is thermodynamically favoured. Two situations illustrate conditions where the latter is the case; firstly as shown in the left hand panel (A) of figure 4.2. during depolarisation the rise in E_m during the action potential exceeds the rise of $E_{Na.Ca}$ secondary to sarcolemmal Ca^{2+} influx and the exchange reverses and secondly, when $[Na^+]_i$ is elevated in which case $E_{Na.Ca}$ becomes more negative. This is illustrated in figure 4.2, panel B. A rise of $[Na^+]_{i+}$ from 7 to 10 mM will increase $E_{Na.Ca}$ by ~30 mV, thus reducing the driving force for Ca^{2+} extrusion thereby elevating Ca^{2+} and consequently tension.

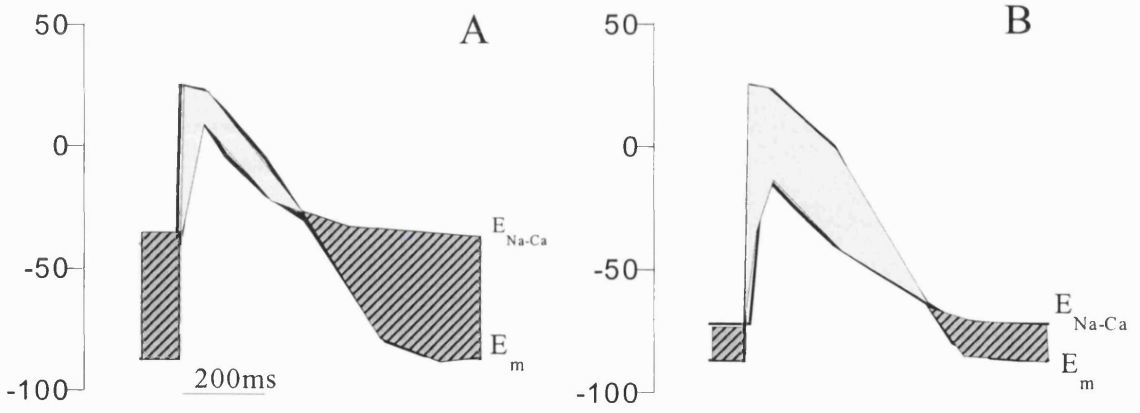

Figure 4.2. Membrane potential (E_m) and equilibrium potential for Na^+-Ca^{2+}-exchange ($E_{Na.Ca}$). $[Na^+]_i$ =7.0 mM in panel A and 10.0 mM in panel B. The dark shading represents circumstances during which Ca^{2+} extrusion is favoured *i.e.* $E_{Na.Ca} > E_m$. The light shading represents the time during which Ca^{2+} entry is favoured i.e. $E_{Na.Ca} < E_m$ and the exchange reverses. In panel B it can be seen that from electrochemical considerations Ca^{2+} entry will predominate.

In normal guinea-pig myocardium, Ca^{2+} extrusion will be favoured at the resting potential and Ca^{2+} entry during the action potential, whereas in hypertrophied hearts, when the $[Na^+]_i$ is increased, Ca^{2+} entry at resting potential and Ca^{2+} loss during repetitive activity will be favoured (Shattock & Bers, 1989).

The observation that hypertrophied hearts demonstrated post-rest potentiation can also be explained by the higher $[Na^+]_i$ measured in the hypertrophied hearts. The $[Na^+]_i$ measured in these hearts was similar to that measured in rat ventricle (Shattock & Bers, 1989). Using Ca-selective microelectrodes Shattock & Bers (1989) demonstrated a net loss of cellular Ca^{2+} at rest and a net gain during stimulation in the rabbit, whereas in the rat there was a net gain of Ca^{2+} during rest and a loss during stimulation. The higher $[Na^+]_i$ in the hypertrophied guinea-pig hearts would favour Ca^{2+} entry via the Na^+-Ca^{2+}-exchanger at resting membrane potential leading to rest-potentiation, whereas the lower $[Na^+]_i$ in the normal hearts would favour Ca^{2+} extrusion at rest leading to rest decay as seen in this study.

4.2.3. Effects of reduced $[Na]_o$ on the force-frequency relationship

Further support for the role of the Na^+-Ca^{2+}-exchanger in determining the inotropic response of the myocardium to increased stimulation frequency comes from the experiments where external Na was reduced. Reducing external Na from 147 mM to 50 mM produced an increase of twitch tension. However, when external Na was progressively reduced, twitch tension failed to increase in response to increasing frequency of stimulation. In isolated guinea-pig myocytes, Mêmе *et al* (2001) showed that with reduction of external [Na] there was a net systolic loss of $[Ca^{2+}]$ as a result of decreased Ca^{2+} entry via the L-type Ca^{2+} current and increased Ca^{2+} efflux via Na^+-Ca^{2+}-exchange while SR Ca^{2+} content increased as a result of diastolic Ca^{2+} influx via Na^+-Ca^{2+}-exchange. Of note, these experiments were performed at a holding potential of -40 mV and at physiological diastolic potentials of ~ -80 mV the driving force for Ca^{2+} entry would be less. Reducing external [Na] from 147 to 29 mM will reduce the Na^+ reversal potential (E_{Na}) and will also reduce the $[Na^+]_i$. Fry *et al* (1987) showed that when external Na was reduced to 29.4 mM, $[Na^+]_i$ falls to 2.9mM. Thus $E_{Na} = 62.1$ mV and if intracellular Ca^{2+} rises to 500 nM, $E_{Ca} = 95$ mV. Thus $E_{Na.Ca} = -3.7$. Thus the driving force for Ca^{2+} extrusion will be reduced thereby elevating Ca^{2+} and consequently tension

whereas during repetitive activity, Ca^{2+} loss will be favoured resulting in a decline in tension at higher frequencies.

It was observed that in a number of preparations the tension generated in 29 mM Na was less than that in 50 mM Na. One possible explanation for this finding is that in low external [Na] solutions, up to 30% of the calcium accumulated by the cell is sequestered in other sites like the mitochondria (Fry *et al.*, 1987).

To verify, or otherwise, that the degradation of the force-frequency relationship in LVH is mirrored in the magnitude of Ca^{2+} release on stimulation, further experiments to measure the Ca^{2+} transients during a change of stimulation rate would be desirable but could not be performed within the time constraints of this study.

4.2.4. Mechanisms underlying the rise of $[Na^+]_i$ in hypertrophy

There are several possible explanations for the rise of $[Na^+]_i$ in hypertrophy. Intracellular pH also declines in hypertrophy and this could increase $[Na^+]_i$ via the Na^+/H^+-exchanger. However the finding that the rise of $[Na^+]_i$ occurs early in hypertrophy, whilst pH_i continues to fall throughout (figure 4.3), would suggest that this is not the primary cause in this model. Furthermore as discussed below there was no evidence in this study to support increased activity of the Na^+/H^+-exchanger in this model of hypertrophy.

4.2.4.1. Role of the Na^+-K^+-ATPase pump in the rise of $[Na^+]_i$ in hypertrophy

Alteration to the kinetics and activity of the Na^+-K^+-ATPase pump is an alternative possibility to explain the raised $[Na^+]_i$. Reduced pump activity has been described in a number of models of hypertrophy including SHR rats (Nakanishi *et al.*, 1989), cats with pulmonary artery banding (Silver & Houser, 1985; Nirasawa & Akera, 1987), pigs with thoracic aortic banding (Khatter & Hoeschen, 1984), one-kidney, one-clip hypertensive rats (Whitmer *et al,* 1986) and humans with LVH (Ellingsen *et al.*, 1994), and would be consistent with the slowed recovery from a raised $[Na^+]_i$ recorded in these experiments.

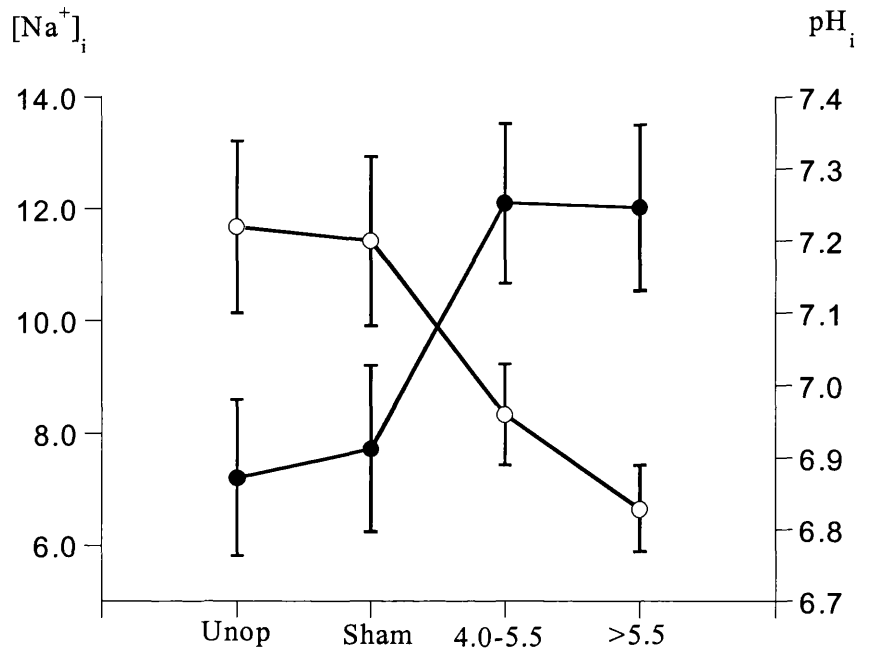

Figure 4.3. Values of $[Na^+]_i$ (filled circles) and pH_i (open circles) in unoperated (unop) and sham operated hearts (sham) , moderate LVH (HBR 4.0-5.5 $g.kg^{-1}$) and severe LVH (HBR >5.5 $g.kg^{-1}$)

The time constant of recovery, τ, of $[Na^+]_i$ and pH_i is larger in multicellular preparations than in isolated myocytes (Bountra *et al.*, 1990) due to diffusion constraints in the former preparation and also the artificial damping of the signals due to the high impedance of the ion-selective electrodes. The frequency response of the ISE-headstage system was checked by imposing sinusoidal voltage changes from an external source. The response was flat at frequencies $\leq$ 0.01 Hz yielding a time constant for the recording system of ~16 seconds which is faster than the time course of recovery of $[Na^+]_i$. Therefore the ISE-head-stage system will not have imposed significant damping of the biological system. Furthermore, because preparation sizes were similar in control and hypertrophied hearts comparison of τ values is still possible using the same methodology.

The raised $[Na^+]_i$ in this model of hypertrophied myocardium could result from a reduced number of Na^+-K^+-ATPase pump sites or altered expression of the α-subtype isoform as outlined in the introduction (Chapter 1, section 1.8.1). The interest in changes of α-isoform expression is that the α-isoforms exhibit different sensitivities to the $[Na^+]_i$, with

the α_1-subtype having a K_m of ~ 12 mM and the α_2 and α_3 subtypes having high K_m values ~ 22-33 mM (Zahler *et al.*, 1997b). Thus, if isoform expression changed from an exclusively α_1-subtype to a more mixed pattern, a rise of $[Na^+]_i$ would occur. This was investigated by quantitative immunoblotting to determine the relative quantities of the α_1, α_2 and α_3 isoforms of the Na-pump. In keeping with previous findings (McDonough & Schmitt, 1985; Sweadner *et al.*, 1994; McDonough *et al.*, 1996), the predominant isoform expressed in both control and hypertrophied guinea-pig hearts was α_1. Small quantities of the α_3-isoform were also detected but we were unable to detect the α_2-isoform. No differences in protein levels between sham-operated, aortic constricted and debanded hearts were observed. This may be due to the small numbers of samples studied and the wide variation in protein levels in normal myocardium.

There is controversy in the literature as to whether the α_2-isoform is present in the guinea-pig (table 4.6) and others have also only detected the α_1-isoform (McDonough & Schmitt, 1985; Sweadner *et al.*, 1994; McDonough *et al.*, 1996). Failure to detect the α_2-isoform in this study may have been lack of sensitivity of the antibodies used. However, the monoclonal rat antibody obtained from KJ Swaedner (Massachusetts General Hospital, Boston MA, USA, Urayama *et al.*, 1989) used has broad species cross-reactivity and others have detected the α_2-isoform in guinea-pig using this antibody (Ramírez-Gil *et al.*, 1998; Trouve *et al.*, 2000) and shown an increase in hypertrophy. Some of these differences in α_2 detection may be related to the preparation (crude myocardial preparation vs sarcolemmal membranes) or the small amount of protein used in Western blot assays.

The failure to detect the α_2-isoform in this study could also be due to varying degrees of protein degradation by endogenous proteases in the samples. The samples used were obtained from the hearts after papillary muscles were removed for electrophysiological experiments. Inevitably there was a time delay while this preparation was secured before the specimens were frozen in liquid N_2. Care was taken however to ensure oxygenation of the preparation in Tyrode's solution at 37 °C during this delay.

The wide standard deviations of the data suggest considerable variability in α-isoform protein levels in normal myocardium. This could be due to stability of the protein or

Table 4.6. Summary of studies of the α-isoforms of the Na^+-K^+-ATPase pump. * not detected

Species	Model	Preparation	Isoform	Amount of protein	Antibody	Source	Results	Reference
Guinea-pig	Aldosterone-salt induced hypertension	Crude particulate preparation	α_1	60 μg	Rat polyclonal	R Mercer	α_1 mRNA and protein ↔	Ramírez-Gil *et al.*, 1998
			α_2	120 μg	Rat (McB2) monoclonal	KJ Sweadner	α_2 mRNA and protein ↑	
			α_3	120 μg	Rat polyclonal	R Mercer	α_3 mRNA ↑ α_3 protein undetectable	
Guinea-pig	Abdominal aortic constriction	Crude particulate preparation	α_1	60 μg	Rat polyclonal	R Mercer	α_1 mRNA and protein ↔	Trouve *et al.*, 2000
			α_2	60 μg	Rat (McB2) monoclonal	KJ Sweadner	α_2 mRNA and protein ↑	
			α_3	100 μg	Rat polyclonal	R Mercer	α_3 mRNA ↑ α_3 protein undetectable	
Guinea-pig		Crude particulate preparation	α_1	100 μg	Rat (McK1) monoclonal	KJ Sweadner		Sweadner *et al.*, 1994
			α_2 *	100 μg	Rat (McB2) monoclonal	KJ Sweadner		
			α_3 *	100 μg	Rat polyclonal	R Mercer		
Guinea-pig		Isolated myocytes	α_1		Mouse (McK1) monoclonal	KJ Sweadner		McDonough *et al.*, 1996
			α_2 *		Rat (McB2) Monoclonal	KJ Sweadner		
			α_3 *		Rat polyclonal	T Pressley		
Guinea-pig		Microsomal preparations	α_1	40 μg	Specific antibodies (details not supplied)			Berrebi-Bertrand *et al.*, 1991
			α_2	40 μg				
Guinea-pig		Sarcolemmal fraction	α_1	70 & 280 μg	Guinea-pig kidney			McDonough & Schmitt 1985
			α_2 *					

regional differences. Zahler *et al* (1993) reported reduced α-isoform mRNA expression in endocardium compared to epicardium in human autopsy specimens. The samples used in this study were transmural and therefore included both endocardium and epicardium.

It has been suggested that changes in α-isoform expression are related to the increased intravascular pressure rather than hypertrophy. This is supported by the study of Herrera *et al* (1988) where the down-regulation of α_2 and α_3 mRNA was seen in the left ventricle of hypertensive rats even in the absence of hypertrophy. Most models showing altered isoform expression in hypertrophy are associated with systemic hypertension (Chapter 1, section 1.8.1.1, table 1.2). The model of ascending aortic constriction used here is substantially different and systemic hypertension does not occur. Therefore, it is possible that the release of neurohormonal agents, growth factors or proto-oncogenes from non-cardiac tissues due to systemic hypertension may affect isoform expression, rather than hypertrophy per se. This suggests that altered α-isoform expression is not the cause of the elevated $[Na^+]_i$ seen in this study and other cause need to be considered.

Downregulation of Na^+-K^+-ATPase pump function may be mediated either by a genomic effect with a reduction in the rate of synthesis of new pump units or by an increase in the rate of internalisation of pumps pre-existing in the cell membrane. Thus, even if protein levels of the α-isoforms and pump activity are unaltered by the process of hypertrophy in this model, it is possible that pump function could be reduced by other mechanisms. Furthermore, oxidative stress such as might arise on reperfusion after ischaemia, causes inhibition of the Na^+-K^+-ATPase pump, leading to a rise in intracellular Na^+ and an enhanced cellular calcium uptake via Na^+-Ca^{2+} exchange (Shattock & Matsuura, 1993).

The use of other methods to quantify Na^+-K^+-ATPase activity, such as measurement of Na-pump current in voltage-clamped myocytes or using K-dependent 3-0-methylfluorescein phosphatase (3-OMFPase) or K-dependent paranitrophenyl phosphatase activity (pNPPase) determinations in crude homogenates, might have provided additional information on pump function in this model of hypertrophy but were not possible in the time constraints for this study.

4.2.5. pH_i in hypertrophy

The data in this thesis showed that the intracellular pH of cells isolated from hypertrophied hearts were acidotic compared to those isolated from sham-operated and unoperated animals. Furthermore, there was a significant correlation between the decrease of pH_i and the degree of hypertrophy as determined by measurement of heart-to-body weight ratio. Comparison with published data of values of pH_i in hypertrophy is shown in table 4.7.

As can be seen the evidence available is conflicting. Using ^{31}P NMR, a fall in pH_i has been demonstrated in patients with LVH but the numbers were small (de Roos *et al.*, 1992). In isolated perfused hearts from rats with abdominal aortic constriction, a fall in pH_i was also demonstrated using ^{31}P NMR and the pH difference was accentuated by a reduction in perfusion pressure (Aufferman *et al.*, 1990). Wallis *et al* (1997) demonstrated a fall in pH_i that correlated with the degree of hypertrophy using isolated myocytes from the same guinea-pig model as in this study. Other studies in SHR rats (Astaire *et al.*, 1992; Pérez *et al.*, 1995) and rats with abdominal aortic constriction (Saborowski *et al.*, 1973; Oldershaw *et al.*, 1988) have shown an increase of pH_i in hypertrophy, while others have shown no effect of hypertrophy on pH_i (Lortet *et al.*, 1993; Wu *et al,* 1994; Do *et* al., 1996; Ito *et al.*, 1997b; Wisløff *et al.*, 2001).

In light of the conflicting evidence, caution must be exercised in interpretation of the results obtained here. The cell isolation procedure might contribute to the measured acidosis, as it is possible that cells isolated from hypertrophied myocardium might be more susceptible to damage from enzymatic digestion protocols. Consequently they might be metabolically compromised and acidotic. However, the isolation procedure typically yielded a similar proportion (between ~50 and 80 %) of viable striated cells from both hypertrophied and control hearts making this proposition less likely. This hypothesis could be tested by using alternative methods to determine pH_i that are not dependent on cell isolation such as ion-selective microelectrodes in muscle strips or ^{31}P-NMR in whole hearts. Furthermore, no attempt was made to distinguish between endocardial and epicardial cells in the isolation procedure and the latter population of cells may undergo more significant hypertrophy *in vivo* (Weber *et al.*, 1988).

Table 4.7. Summary of values of pH_i in hypertrophied myocardium. SHR= spontaneously hypertensive rat, DMO = distribution of the weak acid 5,5-dimethyl-2,4-oxazolidinedione, BCECF = 2',7',-bis(carboxyethyl)-5(6)-carboxyfluorescein, SNARF = Carboxy-seminaphthothodafluor-1, NMR = nuclear magnetic resonance spectroscopy, ISM = ion-selective microelectrodes. Values are mean ± SEM. * $p< 0.05$, † $p<0.01$, ‡ $p<0.001$.

Species	Model	Method	pH_i control	pH_i, hypertrophy	Reference
Rat	Abdominal aortic banding	DMO	6.95	7.07 †	Saborowski *et al.*, 1973
Rat	Abdominal aortic banding	DMO	7.00±0.01	7.06±0.01‡	Oldershaw *et al.*, 1988
Rat	Abdominal aortic banding	^{31}P-NMR	7.1±0.03	6.86±0.15*	Auffermann *et al.*, 1990
Rat	SHR	BCECF	7.09±0.03	7.19±0.02†	Astarie *et al.*, 1992
Rat	SHR	BCECF	7.10±0.04	7.23±0.03*	Pérez *et al.*, 1995
Rat	SHR	BCECF	7.28±0.02	7.29±0.02	Wu *et al.*, 1994
Rat	Endurance training	BCECF	7.27±0.34	7.26±0.35	Wisløff *et al.*, 2001
Rat	SHR	^{31}P-NMR	7.25±0.09	7.12±0.5	Lortet *et al.*, 1993
Rat	Thoracic aortic banding	SNARF	7.10±0.01	7.07±0.02	Ito *et al.*, 1997b
Ferret	Banded pulmonary artery	ISM	7.03±0.01	7.04±0.02	Do *et al.*, 1996
Guinea-pig	Thoracic aortic banding	BCECF	7.08±0.03	6.86±0.04‡	Wallis *et al.*, 1997
Human	HOCM	^{31}P-NMR	7.15±0.03	7.07±0.07*	De Roos *et al.*, 1992
Guinea-pig	Thoracic aortic banding	BCECF	7.22±0.12	6.95±0.08‡	This study

4.2.6. Mechanisms underlying intracellular acidosis in hypertrophy

Intracellular acidosis can be produced by two mechanisms; either by a net reduction of extrusion of H^+ equivalents or by an increase of intracellular H^+ production. The increase of $[Na^+]_i$ observed in this model will reduce the Na^+ gradient across the cell membrane and hence the driving force available for the Na^+-H^+-exchanger to extrude H^+. Reduced H^+ extrusion could also occur as a result of a decrease in membrane density of the Na^+-H^+ exchanger or its efficiency.

The increase in $[Na^+]_i$ could reduce the activity of the Na^+-H^+-exchanger and thereby slow pH_i recovery from intracellular acidosis. Using HEPES as extracellular buffer, Na^+-H^+-exchange is the only mechanism regulating pH_i, therefore the steady state pH_i values can be directly correlated to Na^+-H^+-exchange activity. Although the time constant of recovery from an intracellular acid load was slower in hypertrophied myocytes from aortic constricted hearts, there was no difference in the acid extrusion rate over the range of pH_i studied. Acid extrusion rates increased at low values of pH_i in both groups. Do *et al* (1996) also reported no change in acid extrusion rate in ferrets with right ventricular hypertrophy. In this study the β_i at peak acidosis was used to calculate the rate of H^+ extrusion. Other studies have used the β_i at the mid-point of pH_i recovery. Recalculating the results using this value increases the H^+ extrusion rate in all the groups but the results are not significantly different (6.2 ± 4.3 for control vs 5.3 ± 2.3 mequiv.l^{-1}.min^{-1} for aortic-constricted, $p > 0.05$).

An alternative explanation for the acidosis seen in the hypertrophied hearts is an increase in production of metabolic acids, especially lactic acid. Experimental observations of stimulation-rate dependent changes of pH_i in Purkinje fibres have shown a decrease of extracellular pH by up to 0.15 pH units in unbuffered extracellular solutions following a 2 Hz train of contractions (Bountra *et al.*, 1988). In perfused ferret hearts, a rate-dependent fall of pH_i attributable to the generation of lactic acid was observed (Allen *et al.*, 1986). More recently, Wallis *et al* (2001) demonstrated that under conditions of maximal inotropic stimulation, hypertrophied myocytes showed action potential changes that were consistent with ATP depletion and also constructed a simple diffusion model for oxygen demonstrating that hypertrophied myocytes were likely to develop an hypoxic core.

These findings suggest that pH_i in cardiac muscle is greatly influenced by the metabolic state of the tissue and there is evidence that the metabolic status of the cell is altered in hypertrophied myocardium. Anaerobic metabolism as determined by total lactate production oxygen consumption ratio was found to be increased in hypertrophied hearts compared to sham-operated controls (McAinsh *et al.*, 1995). In rats with hypertrophy induced by abdominal aortic-constriction the contribution of glycolysis to ATP production was greater in hypertrophied hearts than in controls (Allard *et al.*, 1994). These changes would increase cellular lactate production predisposing the sarcoplasm to acidosis.

4.2.7. Functional implications of the fall in pH_i in hypertrophy

The intracellular acidosis could contribute to the contractile dysfunction observed in this model of hypertrophy. A fall of pH_i of as little as 0.2 pH units (similar to the change observed in these studies) can lead to a 50% reduction in contractile force (Fabiato & Fabiato, 1978; Vaughan-Jones *et al.*, 1987; Bountra & Vaughan-Jones, 1989). A fall of pH_i reduces the sensitivity of contractile proteins to Ca^{2+} (Orchard & Kentish, 1990), attenuates I_{Ca} (Kaibara & Kameyama, 1988) and also reduces the sequestration of Ca^{2+} ions by the SR (Orchard & Kentish, 1990). These effects could impair systolic and diastolic function. However, in this study the twitch tension at 1 Hz stimulation frequency was not significantly less in hypertrophied myocardium, whereas the force-frequency relationship was reduced. Acidosis has also been shown to inhibit the Na^+-Ca^{2+}-exchanger, regardless of the direction in which it is operating (Philipson *et al.*, 1982). Thus if the Na^+-Ca^{2+}-exchanger extrudes Ca^{2+} from the cell during diastole, inhibition will lead to an increase of $[Ca^{2+}]_i$, whereas if the exchanger reverses during the action potential, inhibition will lead to less Ca^{2+} entry during the action potential and as action potential shortens at higher frequencies of stimulation this could contribute to the depression of the force-frequency relationship in hypertrophy.

The fall in pH_i observed in hypertrophy could also contribute to the electrophysiological abnormalities reported in hypertrophy (Chapter 1, section 1.1). Conduction velocity is reduced by up to 22% both in this model of hypertrophy and in human LVH caused by aortic stenosis (McIntyre *et al.*, 1997; Cooklin *et al.*, 1998). Equivalent intracellular

acidosis in human and dog myocardium reduces conduction velocity by between 9 and 18% (McIntyre *et al.,* 1997; Vorperian *et al.*, 1994) and thus may account for a significant porportion of the decline in conduction velocity seen in this model of hypertrophy. A fall in pH_i has been shown to reduce conductance of connexin 43 channels (Firek & Weingart, 1995; Hermans *et al.,* 1995). Decrease of pH_i also prolongs action potential duration (Fry & Poole-Wilson, 1981; Nattel *et al.*, 1981), and thus may contribute to the prolongation of the action potential seen in many models of hypertrophy.

4.2.8. Intracellular buffering capacity in hypertrophy

The intrinsic or non-bicarbonate buffering capacity of the sarcoplasm, β_i, was determined by manipulation of pH_i by the application and subsequent removal of NH_4Cl, from bicarbonate-free external solution in isolated myocytes. Under conditions of acid-loading, a considerable proportion of accumulated H^+ is rapidly transported out of the cell (Blatter & McGuigan, 1991) leading to an overestimation of β_i. To reduce this error the experiments were performed in the presence of 1 mM amiloride. However, a slow recovery of pH_i was observed in the presence of amiloride in these experiments suggesting that it does not achieve a 100% block of proton extrusion.

β_i was increased in hypertrophied hearts and is in keeping with previous findings in rat myocardium (Saborowski *et al.*, 1973; Oldershaw & Cameron., 1989). The mechanism of the increase of β_i with hypertrophy remains unclear, although it has been suggested that the increased protein synthesis in hypertrophy improves intracellular H^+ buffering capacity, thus improving the ability of the myocardium to withstand acute acid-base changes (Oldershaw & Cameron, 1988). The finding that β_i was inversely related to pH_i, irrespective of the tissue of origin is in keeping with similar findings in normal (Lagadic-Gossmann *et al.*, 1992; Leem *et al.*, 1999) and hypertrophied guinea-pig hearts (Wallis *et al.*, 1997) and in ferrets with right ventricular hypertrophy, although no change in pH_i was observed in the latter model (Do *et al.,* 1996) and suggests an alternative mechanism for the increase in β_i seen in hypertrophy. This finding suggests that the 'effective pK_a' of H^+ buffering by the sarcoplasm is lower than the normal pH_i of the cell. This would enhance pH stability within the normal cell and any tendency for the pH_i to fall, produced for example by a sudden metabolic load or ischaemia, would tend to be

resisted. As the acidosis became more severe the buffering system resisting the change would become more effective.

4.2.9. Characterisation of recovery from acid-load in normal guinea-pig myocytes

In paired experiments it was observed that pH_i recovery from acid-loading was faster in CO_2/HCO_3^-- buffered. Acid extrusion was also greater than that estimated in HEPES-buffer. These findings showed that recovery from intracellular acidosis in the absence of HCO_3^- was almost wholly due to Na^+-H^+-exchanger activity, although 1 mM amiloride did not completely block recovery. In the more physiological situation with HCO_3^- present, recovery was enhanced, presumably due to Na^+-HCO_3^--cotransport. Other studies have demonstrated that this additional H^+ efflux is due to Na^+-HCO_3^--cotransport and can be inhibited by DIDS (4,4'-di-isothiocyanatostilbene-2-2'-disulphonic acid); (Lagadic-Gossmann *et al.*, 1992; Ng *et al.*, 1993; Leem *et al.*, 1999).

A slow recovery of pH_i was observed in the presence of amiloride in HEPES-buffered solutions suggesting that it does not achieve a 100% block of proton extrusion via the Na^+-H^+-exchanger. The reduction of external Na^+ inhibits acid extrusion on both the Na^+-H^+-exchanger and the Na^+-HCO_3^--exchanger. In HEPES-buffered solution with zero extracellular Na, acid extrusion was effectively blocked. In CO_2/HCO_3^--buffered solution, the inward driving force for Na was reduced but not abolished due to the presence of 24 mM Na (as $NaHCO_3$) in the external solution and therefore acid extrusion was reduced below that with 1 mM amiloride but not completely abolished.

4.2.10. $[Ca^{2+}]_i$ in hypertrophy

Diastolic $[Ca^{2+}]_i$ was unchanged in this model of hypertrophy, in keeping with findings in other models of right (Gwathmey & Morgan, 1985; Gwathmey *et al.*, 1995) and left ventricular hypertrophy (Brandes *et al.*, 1998; McCall *et al.*, 1998; Maier *et al.*, 1998) (table 4.7).

In the resting state a significant proportion of cells in this study did not respond to caffeine. Superfusion with high-[K] solutions should load the cell and has been shown to

Table 4.7. Summary of values of $[Ca^{2+}]_i$ in hypertrophied myocardium. * results expressed as log of the fractional luminescence, (L/L_{max})

Species	Model	Method	$[Ca^{2+}]_I$ Control	$[Ca^{2+}]_I$ Hypertrophy	Reference
Rat	Suprarenal aortic constriction	Indo-1	163±19 nM	157±13 nM	McCall *et al.*, 1998
Rat	Suprarenal aortic constriction	Indo-1	293±39 nM	271±31 nM	Maier *et al.*, 1998
Rat	Suprarenal aortic constriction	Indo-1	~150 nM	~150 nM	Brandes *et al.*, 1998
Ferret	Pulmonary artery banding	Aequorin	-4.7±0.2 *	-4.6±0.2 *	Gwathmey & Morgan., 1985
Ferret	Pulmonary artery banding	Aequorin	-3.11±0.1*	-3.11±0.3*	Gwathmey *et al.*, 1995
Guinea-pig	Thoracic aortic constriction	Fura-2	247±68 nM	235±75 nM	This study

increase cellular Ca^{2+} uptake in cardiac muscle (Wendt & Langer,1977; Fry *et al.*, 1981). Depolarisation with elevated $[K^+]$ has been shown to reduce $[Na^+]_i$, and increase $[Ca^{2+}]_i$ via Na^+-Ca^{2+} exchange (Sheu & Fozzard, 1982). In this study, perfusing the cells with a depolarising solution in which the KCl concentration was increased from 4 mM to 40 mM, would be expected to change the membrane potential by ~60 mV and as expected resulted in an increase of $[Ca^{2+}]_i$. The magnitude of this increase was not different in the sham-operated and aortic constricted hearts.

4.2.11. Caffeine and SR calcium content

The data in this thesis showed that the SR Ca^{2+} content assessed by measuring the magnitude of the caffeine-induced Ca^{2+} transient was reduced in aortic-constricted

compared to control guinea-pigs and there was a significant correlation between the $\Delta[Ca^{2+}]_i$ and the degree of hypertrophy as determined by measurement of heart-to-body weight ratio. The decay phase of the caffeine transient and the recovery phase of the undershoot were slower in aortic constricted myocytes and also correlated with heart-to-body weight ratio. However, no changes in calsequestrin or SERCA2 protein levels were found using quantitative immunoblotting.

The absolute change of $[Ca^{2+}]$ on application of caffeine was smaller than that reported by some other studies. This may be for several reasons: Ca^{2+} release in this model may be less; the calculation of $[Ca^{2+}]_i$ is dependent on the Fura-2 calibration and may differ from other studies; the rate of caffeine delivery to the cell may be slower and attenuate the response. The latter is considered not to be a significant factor, however, as the upstroke of the Ca^{2+}-transient is comparable to other studies (C. Wu, personal communication). However, experiments with cells from control and hypertrophied hearts were carried out under identical conditions so that the conclusions reached in the study can be considered to be justified.

Caffeine activates SR Ca^{2+} release channels, thereby promoting SR Ca^{2+} release and preventing Ca^{2+} re-accumulation by the SR and was therefore used as an estimate of SR Ca^{2+} content in this study. However, Ca^{2+} efflux via Na^{+}-Ca^{2+} exchange may limit the peak of the caffeine-induced Ca^{2+} transient. This has been shown to occur in the rabbit (Bassani *et al.,* 1992) but not in rat (Bassani *et al.,* 1994a) or ferret myocardium (Bassani *et al.,* 1994b). It is unclear as to whether caffeine releases all of the Ca^{2+} stored within the SR or releases Ca^{2+} from the same SR pool as that released by a physiological stimulus and studies to date provide conflicting results. Studies in isolated rabbit myocytes suggest that caffeine empties the releasable Ca^{2+} pool in the SR (Bassani *et al.,* 1993b) whereas during a twitch only half of the SR Ca^{2+} content is released (Bassani *et al.,* 1993a). Other studies, however, showed good correlation between the size of the Ca^{2+} transient released by electrical stimulation and that released by caffeine (Smith *et al.,* 1988; Frampton *et al.,* 1991a).

Calsequestrin is the predominant Ca^{2+} storage protein and has a high capacity and low affinity for Ca^{2+}. Its primary function is to sequester large amounts of Ca^{2+} in the lumen of the SR, thereby reducing the luminal concentration of free Ca^{2+} and facilitating further

uptake of Ca^{2+} by the SR. There was no significant change in mRNA levels of calsequestrin in this study suggesting that the calcium storage capacity of the SR is unaltered in this model of hypertrophy. This suggests that the reduced caffeine-induced Ca transients observed in aortic constricted hearts are due to reduced fractional release of Ca^{2+} rather than reduced SR Ca^{2+} loading. However, we did not measure calreticulin levels in this study. Calreticulin is another Ca^{2+} binding protein that differs from calsequestrin in having a high affinity and low capacity for Ca^{2+}. Its expression is downregulated during cardiac muscle differentiation but there is evidence that it may be reexpressed in hypertrophied myocardium (Tsutsui *et al.,* 1997) and contribute to alterations in Ca^{2+} storage capacity.

Continuous application of caffeine prevents net SR calcium reuptake and the rate of decline of $[Ca^{2+}]_i$ during caffeine exposure provides information about Ca^{2+} extrusion primarily by Na^+-Ca^{2+}- exchange in normal Tyrode's or the combined action of the mitochondrial Ca uniporter and the sarcolemmal Ca-ATPase in reduced extracellular Na solution. These transport systems remove Ca^{2+} from the cytoplasm simultaneously and are interdependent because of their common influence and dependence on $[Ca^{2+}]_i$. The slow decline in $[Ca^{2+}]_i$ during caffeine-induced Ca^{2+} transients after exposure to low-Na solutions is presumably due to slow transport of Ca^{2+} by the mitochondrial uniporter and the sarcolemmal Ca^{2+}-ATPase and from the time constant we can infer that aortic constriction did not affect Ca^{2+} removal by these combined processes. The decline in $[Ca^{2+}]_i$ in normal Tyrode's solution is due primarily to Ca^{2+} extrusion via Na^+-Ca^{2+}-exchange (Bassini *et al.*, 1992) and was slower in myocytes from aortic constricted hearts suggesting that Na^+-Ca^{2+}-exchange activity may be reduced in this model of hypertrophy and would be consistent with the raised $[Na^+]_i$. This is contrary to the finding of McCall *et al* (1998) in rats with abdominal aortic constriction where Na^+-Ca^{2+}-exchange activity was reported to be unchanged by abdominal aortic banding but the experiments in that study were carried out at 23°C, when $[Na^+]_i$ might be raised in control animals, and low work levels which could have masked differences between the groups.

4.2.12. The SR Ca^{2+}-ATPase (SERCA2) pump in hypertrophy

The prolongation of the relaxation phase of the twitch seen in a number of models of hypertrophy (Gwathmey & Morgan, 1985; Davey *et al.*, 2001; Yoneda *et al.*, 2001) could be explained by reduced Ca^{2+} uptake into the SR which is largely dependent on the SR Ca^{2+}-ATPase pump. In this study there was no difference in SERCA2 protein levels in this model of hypertrophy compared to controls but we did not measure pump function as SR re-uptake was measured in the presence of caffeine. As discussed in the introduction this is in keeping with some but not all studies in hypertrophied myocardium (Chapter 1, section 1.8.2). However, it is important to remember that *in vivo* function of SERCA2 may not be directly related to its abundance measured in a Western blot and there is evidence that activity of SERCA2 can be altered by changes in its regulation. Phospholamban (PLB) is a SR protein that associates with SERCA2 and inhibits its Ca^{2+} transport rate. Phosphorylation of PLB by either protein kinase or calmodulin-dependent protein kinase causes it to dissociate from SERCA2, resulting in enhanced Ca^{2+} transport. Therefore alterations in PLB phosphorylation or PLB/SERCA2 ratios could contribute to altered Ca^{2+} in hypertrophy. Reduced PLB/SERCA2 protein ratio was observed in mice with decompensated but not compensated LVH (Ito *et al.*, 2000) and in rats a decreased ratio was observed with progression from compensated to decompensated hypertrophy (Okayama *et al.*, 1997).

The presence of a Ca^{2+}-ATPase with a different kinetic cycle could alter Ca^{2+} transport activity. Five different isoforms of the Ca^{2+}-ATPase have been described but only SERCA2A has been found in the normal heart and studies to date have shown no evidence of isoform shifts in hypertrophied muscle (de la Bastie *et al.*, 1990).

Further assessment of the role of the SR in regulating intracellular Ca^{2+} as myocyte hypertrophy occurs could have been provided by combining fluorescent measurements of intracellular Ca^{2+} with voltage-clamp studies. In this way which flux through the L-type Ca^{2+} channel or Na^{+}-Ca^{2+} exchanger can be estimated by integration of the current traces when other routes have been eliminated as described by Varro *et al* (1993).

Conclusions

These experiments support the hypothesis that changes to the cell physiology of the myocardium occur during the compensated phase of LVH which may eventually lead to the decompensated phase of contractile and electrophysiological dysfunction.

LVH in a guinea-pig model of supra-aortic stenosis was accompanied by a decline in the force-frequency relationship which was related to the degree of hypertrophy. This is similar to findings in hypertrophied human myocardial preparations.

The decline in contractile function is accompanied by changes to intracellular ion regulation. $[Na^+]_i$ increases, pH_i declines, and the ability of the SR to regulate Ca^{2+} release declines as hypertrophy progresses. The rise of $[Na^+]_i$ occurred in moderate LVH with little further increase in severe hypertrophy, whereas intracellular pH continued to decline in severe hypertrophy. This suggested that the rise of $[Na^+]_i$ is an early change in LVH and may be causal in bringing about the other changes to pH_i and SR Ca^{2+} transport.

The increase of $[Na^+]_i$ could contribute not only to the contractile dysfunction in hypertrophy but also to the electrophysiological abnormalities such as reduced conduction velocity and increased gap-junction resistance observed in other studies.

The mechanism of the rise of $[Na^+]_i$ remains unclear. There was no evidence for increased activity of the Na^+-H^+ exchanger, while Na^+-Ca^{2+}-exchanger activity was reduced in this model of hypertrophy. Furthermore, no changes in Na^+-K^+-ATPase pump isoforms at protein level were observed but this does not exclude an alteration in pump activity as a cause. Further experiments are required to address the cause of the increase of $[Na^+]_i$ in hypertrophy.

References:

Aggarwal R, Shorofsky SR, Goldman L, and Balke CW (1997). Tetrodotoxin blockable calcium currents in rat ventricular myocytes. A third type of cardiac cell sodium current. *Journal of Physiology*, **505**: 353-369.

Ahmmed GU, Hong Dong P, Song G, Ball NA, Xu Y, Walsh RA, and Chiamvimonvat N (2000). Changes in Ca^{2+} cycling proteins underlie cardiac action potential prolongation in a pressure-overloaded guinea-pig model with cardiac hypertrophy and failure. *Circulation Research,* **86**: 558-578

Allard MF, Schonekess BO, Henning SL, English DR, and Lopaschuk GD (1994). Contribution of oxidative metabolism and glycolysis to ATP production in hypertrophied hearts. *American Journal of Physiology*, **267:** H742-H750

Allen DG, and Blinks JR (1978). Calcium transients in aequorin-injected frog cardiac muscle. *Nature*, **273**: 509-513

Allen DG, Eisner DA, Pirolo JS, and Smith GL (1985a). The relationship between intracellular calcium and contraction in calcium-overloaded ferret papillary muscles. *Journal of Physiology*, **364**: 169-182

Allen DG, Elliot AC, and Smith GL (1986). Intracellular acidosis on increasing the frequency of stimulation in isolated ferret hearts is partly attributable to increased lactic acid production. *Journal of Physiology*, **377:** 113P

Allen DG, Morris PG, Orchard CH and Pirolo JS (1985b). A nuclear magnetic resonance study of metabolism in the ferret heart during hypoxia and inhibition of glycolysis. *Journal of Physiology*, **361**: 185-204

Andersen JL, Andersen LJ, Thrasher TN, Keil LC and Ramsay DJ (1994). Left heart and arterial baroreceptors interact in control of plasma vasopressin, renin, and cortisol in awake dogs. *American Journal of Physiology,* **266:** R879-R888

Anderson PAW, Manring A, and Johnson EA (1973). Force-frequency relationship: a basis for a new index of cardiac contractility. *Circulation Research*, **33**: 665-671

Anderson PAW, Manring A, Arentzen CE, Scott Rankin J, and Johnson EA (1977). Pressure-induced hypertrophy of cat right ventricle: an evaluation with the force-interval relationship. *Circulation Research,* **41**: 582-588

Arai M, Otsu K, MacLennan DH, Alpert NR, and Periasamy M (1991). Effect of thyroid hormone on the expression of mRNA encoding sarcoplasmic reticulum proteins. *Circulation Research,* **69**: 266-276

Arai M, Suzuki T, and Nagai R (1996). Sarcoplasmic reticulum genes are upregulated in mild cardiac hypertrophy but down regulated in severe cardiac hypertrophy induced by pressure overload. *Journal of Molecular and Cellular Cardiology*, **28**: 1583-1590

Aronow WS, Epstein S, Koenigsberg M, and Schwartz KS (1988). Usefulness of echocardiographic left ventricular hypertrophy, ventricular tachycardia and complex ventricular arrhythmias in predicting ventricular fibrillation or sudden cardiac death in elderly patients. *American Journal of Cardiology,* **62:** 1124-1125

Aronson RS (1980). Characteristics of action potentials of hypertrophied myocardium from rats with renal hypertension. *Circulation Research*, **47:** 443-454

Astaire C, David DM, Millanvoye VBE, Fretss BM, and Devynck MA (1992). Cytosolic pH in cultured cardiac myocytes and fibroblasts from newborn spontaneously hypertensive rats. *American Journal of Hypertension,* **5:** 281-287

Ataka K, Chen D, Levitsky S, Jimenez E, and Feinberg H (1992). Effect of ageing on intracellular Ca^{2+}, pH_i and contractility during ischaemia and reperfusion. *Circulation,* **86**[suppl II]: II371-II376

Aufferman W, Wu ST, Derugin N, Parmley W, Higgins C, Kapelko V, and Wikman-Coffelt J (1990). 31P magnetic resonance spectroscopy of pressure overload

hypertrophy in rats: effect of reduced perfusion pressure. *Cardiovascular Research*, **24**: 57-64

Baartscheer A, Schumacher CA, and Fiolet JWT (1997). Small changes of cytosolic sodium in rat ventricular myocytes measured with SBFI in emission ratio mode. *Journal of Molecular and Cellular Cardiology*, **29**: 3375-3383

Bache RJ, Dai XZ, and Baran KW (1990). Effect of pinacidil on myocardial blood flow in the chronically pressure overloaded hypertrophied left ventricle. *Journal of Cardiovascular Pharmacology,* **16**: 890-895

Bailey BA, and Houser SA (1992). Calcium transients in feline left ventricular myocytes with hypertrophy induced by slow progressive pressure overload. *Journal of Molecular and Cellular Cardiology*, **24**: 365-373

Baro I, Eisner DA. Raimbach SJ, and Wray S (1989). Intracellular pH regulation and buffering power in single, isolated vascular and intestinal smooth muscle cells. *Journal of Physiology,* **417**: 161P

Baro I, O'Neill SC, and Eisner DA (1993). Changes of intracellular [Ca^{2+}] during refilling of sarcoplasmic reticulum in rat ventricle and vascular smooth muscle. *Journal of Physiology*, **465:** 21-41

Bassani JWM, Bassani RA, and Bers DM (1993a). Twitch-dependent SR Ca accumulation and release in rabbit ventricular myocytes. *American Journal of Physiology*, **265:** C533-C540

Bassani JWM, Bassani RA, and Bers DM (1993b). Ca^{2+} cycling between sarcoplasmic reticulum and mitochondria in rabbit cardiac myocytes. *Journal of Physiology*, **460**: 603-621

Bassani JWM, Bassani RA, and Bers DM (1994a). Relaxation in rabbit and rat cardiac cells: species-dependent differences in cellular mechanisms. *Journal of Physiology*, **476:** 279-293

Bassani JWM, Yuan W and Bers DM (1995). Fractional SR Ca^{2+} release is regulated by trigger Ca^{2+} and SR Ca^{2+} content in cardiac myocytes. *American Journal of Physiology*, **268**: C1313-C1319

Bassani RA, Bassani JWM and Bers DM (1992). Mitochondrial and sarcolemmal Ca^{2+} transport reduce $[Ca^{2+}]_i$ during caffeine contractures in rabbit cardiac myocytes. *Journal of Physiology*, **453**: 591-608

Bassani RA, Bassani JW, and Bers DM (1994b). Relaxation in ferret ventricular myocytes: unusual interplay among cardiac transport systems. *Journal of Physiology*, **476**: 295-308

Baudet S, Noireaud, J, and Léoty C (1991). Intracellular Na activity measurements in the control and hypertrophied heart of the ferret: an ion sensitive microelectrode study. *Pflügers Archives*, **418**: 313-318

Belichard P, Pruneau D, Salzmann JL, and Rouet R (1992). Decreased susceptibility to arrhythmias in hypertrophied hearts of physically trained rats. *Basic Research in Cardiology*, **87**: 344-355

Ben-David J, Zipes DP, Ayres GM and Pride HP (1992). Canine left ventricular hypertrophy predisposes to ventricular tachycardia induction by early phase 2 afterdepolarisations after administration of BAY K 8644. *Journal of American College of Cardiology*, **20**: 1576-1584

Bénitah J-P, Bailly P, D'Agrosa M-C, Da Ponte J-P, Delgado C, and Lorente P (1992). Slow inward current in single cells isolated from adult human ventricles. *Pflügers Archives*, **421**: 176-187

Bentivegna LA, Ablin LAW, Kihara Y, and Morgan JP (1991). Altered calcium handling in left ventricular pressure-overload hypertrophy as detected with aequorin in the isolated, perfused ferret heart. *Circulation Research,* **69:** 1538-1545

Berrebi-Bertrand I, Maixent JM, Guede FG, Gerbi A, Charlemagne D and Lelièvre LG (1991). Two functional Na^+/K^+-ATPase isoforms in the left ventricle of the guinea-pig heart. *European Journal of Biochemistry,* **196**: 129-133

Berrebi-Bertrand I, and Maixent JM (1994). Immunodetection and enzymatic characterisation of the alpha-3 isoform of the Na,K-ATPase in dog heart. *FEBS Letters*, **348:** 55-60

Bers DM, Bassani JWM, and Bassani RA (1996). Na-Ca exchange and Ca fluxes during contraction and relaxation in mammalian ventricular muscle. *Annals New York Academy of Science,* **779**: 430-442

Bers DM, Bassani RA, Bassani JWM, Baudet S and Hryshko LV (1993). Paradoxical twitch potentiation after rest in cardiac muscle: increased fractional release in SR calcium. *Journal of Molecular and Cellular Cardiology*, **25**: 1047-1057

Bers DM, Bridge JHB, and Spitzer KW (1989). Intracellular Ca^{2+} transients during rapid cooling contractures in guinea-pig ventricular myocytes. *Journal of Physiology*, **417**: 537-553

Bers DM, and Christensen DM (1990). Functional interconversion of rest decay and ryanodine effects in rabbit and rat ventricle depends on Na/Ca exchange. *Journal of Molecular and Cellular Cardiology*, **22**: 715-723

Bers DM, Christensen DM, and Nguyen TX (1988). Can Ca^{2+} entry via Na^+-Ca^{2+} exchange directly activate cardiac muscle contraction? *Journal of Molecular and Cellular Cardiology*, **20**: 405-414

Beuckelmann DJ, Näbauer M, and Erdmann E (1991). Characteristics of calcium-current in isolated human ventricular myocytes from patients with terminal heart failure. *Journal of Molecular and Cellular Cardiology,* **23:** 929-937

Beuckelmann DJ, Näbauer M, and Erdmann E (1992). Intracellular calcium handling in isolated ventricular myocytes from patients with terminal heart failure. *Circulation,* **85**: 1046-1055

Bielen FV, Bosteels S, and Verdonck F (1990). Consequences of CO_2 acidosis for transmembrane Na^+ transport and membrane current in rabbit cardiac Purkinje fibres. *Journal of Physiology*, **427**: 325-345

Bikkina M, Larson MG, and Levy D (1993). Asymptomatic ventricular arrhythmias and mortality risk in subjects with left ventricular hypertrophy. *Journal American College Cardiology,* **22**: 1111-1116

Blatter LA, and McGuigan JAS (1991). Intracellular pH regulation in ferret ventricular muscle; the role of Na-H exchange and the influence of metabolic substrates. *Circulation Research*, **68:** 150-161

Boateng SY, Naqui RU, Koban MU, Yacoub MH, MacLeod KT, and Boheler KR (2001). Low-dose ramipril treatment improves relaxation and calcium cycling after established cardiac hypertrophy. *American Journal of Physiology*, **280:** H1029-H1038

Boateng SY, Seymour AM, Bhutta NS, Dunn MJ, Yacoub MH, and Boheler KR (1998). Sub-antihypertensive doses of ramipril normalise sarcoplasmic reticulum calcium ATPase expression and function following cardiac hypertrophy in rats. *Journal of Molecular and Cellular Cardiology,* **30**: 2683-2694

Bond JM, Chacon E, Herman B, and Lemasters JJ (1993). Intracellular pH and Ca^{2+} homeostasis in the pH paradox of reperfusion injury to neonatal rat cardiac myocytes. *American Journal of Physiology*, **265**: C129-C137

Book CBS, Moore RL, Semanchik A, and Ng YC (1994a). Cardiac hypertrophy alters expression of Na^+-K^+-ATPase subunit isoform expression at mRNA level and protein levels in rat myocardium. *Journal of Molecular and Cellular Cardiology*, **26:** 591-600

Book CBS, Wilson RP, and Ng YC (1994b). Cardiac hypertrophy in the ferret increases expression of the Na^+-K^+-ATPase α_1- but not the α_3-isoform. *American Journal of Physiology,* **266:** H1221-H1227

Borzak S, Kelly RA, Kramer BK, Matoba Y, Marsh JD and Reers M (1990). In situ calibration of fura-2 and BCECF fluorescence in adult rat ventricular myocytes. *American Journal of Physiology*, **259:** H973-H981

Borzak S, Reers M, Arruda J, Sharma VK, Sheu SS, Smith TW, and Marsh JD (1992). Na^+ efflux mechanisms in ventricular myocytes: measurement of $[Na^+]_i$ with Na^+-binding benzofuran isophthalate. *American Journal of Physiology*, **263:** H866-H874

Botchway A (2001). Regression of left ventricular hypertrophy: investigation of electrophysiological changes during regression of left ventricular mass. PhD, University of London.

Bouchard RA, Clarke RB, and Giles WR (1993). Role of sodium-calcium exchange in activation of contraction in rat ventricle. *Journal of Physiology,* **472**: 390-413

Bountra C, Kaila K, and Vaughan-Jones RD (1988). Effect of repetitive activity upon intracellular pH, sodium and contraction in sheep cardiac Purkinje fibres. *Journal of Physiology*, **398**: 341-360

Bountra C, Powell T, and Vaughan-Jones RD (1990). Comparison of intracellular pH transients in single ventricular myocytes and isolated ventricular muscle of guinea-pig. *Journal of Physiology*, **424**: 343-365

Bountra C and Vaughan-Jones RD (1989). Effect of intracellular and extracellular pH on contraction in isolated, mammalian cardiac myocytes. *Journal of Physiology*, **418:** 163-187

Bouron A, Potreau D and Raymond G (1992). The L type calcium current in single hypertrophied cardiomyocytes from the right ventricle of ferret heart. *Cardiovascular Research,* **26**: 662-370

Boyden PA, Gardner PI, and Wit AL (1988). Action potentials of cardiac muscle in healing infarcts: response to norepinephrine and caffeine. *Journal of Molecular and Cellular Cardiology*, **20**: 523-537

Boyett MR, Hart G, Levi AJ, and Roberts A (1987). Effects of repetitive activity on developed force and intracellular sodium in isolated sheep and dog Purkinje fibres. *Journal of Physiology*, **388:** 295-322

Brandes R, Maier LS, and Bers DM (1998). Regulation of mitochondrial [NADH] by cytosolic [Ca^{2+}] and work in trabeculae from hypertrophic and normal rat hearts. *Circulation Research*, **82**: 1189-1198

Breisch EA, White FC, Nimmo LE, and Bloor CM (1986a). Cardiac vasculature and flow during pressure-overload hypertrophy. *American Journal of Physiology*, *251*: H1031-H1037

Breisch EA, White FC, Nimmo LE, McKirnan MD, and Bloor CM (1986b). Exercise-induced cardiac hypertrophy: a correlation of blood flow and microvasculature. *Journal of Applied Physiology*, **60**: 1259-1267

Bright CM, and Ellis D (1992). Intracellular pH changes induced by hypoxia and anoxia in isolated sheep heart Purkinje fibres. *Experimental Physiology*, **77:** 165-177

Bril A, Forest MC, and Gout B (1991). Ischaemia and reperfusion induced arrhythmias in rabbits with chronic heart failure. *American Journal of Physiology*, **261**: H301-H307

Brilla CG, Janicki JS, and Weber KT (1991). Impaired diastolic function and coronary reserve in genetic hypertension. Role of instertitial fibrosis and medial thickening of intramyocardial coronary arteries. *Circulation Research*, **60**: 107

Brilla CG, Matsubara L, and Weber KT (1996). Advanced hypertensive heart disease in spontaneously hypertensive rats. Lisinopril mediated regression of myocardial fibrosis. *Hypertension*, **28:** 269-275

Brilla CG, Pick R, Tan LB, Janicki JS, and Weber KT (1990). Remodeling of the rat right and left ventricles in experimental hypertension. *Circulation Research*, **67**: 1355-1364

Brooks WW, Bing OHL, Litwin SE, Conrad CH and Morgan JP (1994). Effect of treppe and calcium on intracellular calcium and function in the failing heart from the spontaneously hypertensive rat. *Hypertension*, **24**: 347-356

Brooks WW, Bing OHL, Boluyt MO, Malhotra A, Morgan JP, Satoh N, Colucci WS and Conrad CH (2000). Altered inotropic responsiveness and gene expression of hypertrophied myocardium with captopril. *Hypertension*, **35**: 1203-1312

Brooksby P, Levy AJ and Jones JV (1993). Investigation of the mechanisms underlying the increased contraction of hypertrophied myocytes isolated from the spontaneously hypertensive rat. *Cardiovascular Research,* **27**: 1268-1277

Bryant SM, Shipsey SJ and Hart G (1997). Regional differences in electrical and mechanical properties of myocytes from guinea-pig hearts with mild left ventricular hypertrophy. *Cardiovascular Research,* **35**: 315-323

Buckler KJ, Denyer JC, Vaughan-Jones RD and Brown HF (1990). Intracellular pH regulation in rabbit isolated sino-atrial node cells. *Journal of Physiology,* **426**: 22P

Calderone A, Takahashi N, Izzo NJ, Thaik CM, and Colucci WS (1995). Pressure- and volume-induced left ventricular hypertrophies are associated with distinct myocyte phenotypes and differential induction of peptide growth factor mRNA's. *Circulation,* **92**: 2385-2485

Camilión de Hurtado MC, Alvarez BV, Peréz NG, and Cingolani HE (1996). Role of an electrogenic Na^+-HCO_3^- cotransport in determining myocardial pH_i after an increase in heart rate. *Circulation Research*, **79**: 698-713

Camilión de Hurtado MC, Peréz NG, and Cingolani HE (1995). An electrogenic sodium-bicarbonate cotransport in the regulation of myocardial intracellular pH. *Journal of Molecular and Cellular Cardiology*, **27**: 231-242

Cameron JS, Myerburg RJ, Wong SS, Gaide MS, Epstein K, Alvarez TR, Gelband H, Guse PA, and Bassett AL (1983). Electrophysiologic consequences of chronic experimentally induced left ventricular pressure overload. *Journal of American College of Cardiology*, **2**: 481-487

Capasso JM, Palackal T, Olivetti G, and Anversa P (1990). Left ventricular failure induced by long term hypertension in rats. *Circulation Research*, **66**: 1400-1412

Capasso JM, Strobeck JE, Malhotra A, Scheuer J, and Sonnenblick EH (1982). Contractile behaviour of rat myocardium after reversal of hypertensive hypertrophy. *American Journal of Physiology*, **242**: H882-H889

Carey PA, Turner M, Fry CH, and Sheridan DS (2001). Reduced anisotropy of action potential conduction in left ventricular hypertrophy. *Journal of Cardiovascular Electrophysiology*, **12**: 830-835

Carey RA, Bove AA, Coulson RL, and Spann JF (1978). Recovery of myosin-ATPase after relief of pressure-overload hypertrophy of cat myocardium. *American Journal of Physiology*, **234**: H711-H717

Carl SL, Felix K, Caswell AH, Brandt NR, Ball WJ Jr, Vaghy PL, Meissner G and Ferguson DG (1995). Immunocolocalisation of sarcolemmal dihydropyridine receptor and sarcoplasmic reticular triadin and ryanodine receptor in rabbit ventricle and atrium. *Journal of Cell Biology,* **129**: 673-682

Chapman RA, Coray A and McGuigan JAS (1983). Sodium/calcium exchange in mammalian ventricular muscle: a study with sodium-sensitive microelectrodes. *Journal of Physiology*, **343:** 253-276

Charlemagne D, Mayoux E, Poyard M, Oliviero P and Geering K (1987). Identification of two isoforms of the catalytic sub-unit of Na,K,-ATPase in myocytes from adult rat heart. *Journal Biological Chemistry*, **262**: 8941-43

Charlemagne D, Orlowski J, Oliviero P, Rannou F, Saint Beuve C, Swynghedauw B, and Lane LK (1994). Alteration of Na,K-ATPase subunit mRNA and protein level in hypertrophied rat ventricle. *Journal of Biological Chemistry*, **269**: 1541-1547

Cheng H, Lederer WJ, and Cannell MB (1993). Calcium sparks: elementary events underlying excitation-contraction coupling in heart muscle. *Science,* **262**: 740-744

Chiappe de Cingolani G, Morgan P, Mundina-Weilenmann C, Casey J, Fujinaga J, Camilión de Hurtado M, and Cingolani H (2001). Hyperactivity and altered mRNA isoform expression of the Cl^-/HCO_3^- anion-exchanger in the hypertrophied myocardium. *Cardiovascular Research,* **51**: 71-79

Clarke K, Kohler S, and Ingwall SJ (1990). Intracellular sodium in the hypertrophied rat heart during ischaemia and reperfusion. *Circulation*, **70**: 496A

Cleemann L, Wang W, and Morad M (1998). Two-dimensional confocal images of organisation density and gating of focal Ca^{2+} release sites in rat cardiac myocytes. *Proceedings of the National Academy of Science, USA*, **95:** 10984-10989

Cohen CJ, Fozzard HA, and Sheu SS (1982). Increase in intracellular sodium ion activity during stimulation in mammalian cardiac muscle. *Circulation Research,* **50**: 651-662

Cooklin M, Wallis WRJ, Sheridan DJ, and Fry CH (1997). Changes in cell-to-cell coupling associated with left ventricular hypertrophy. *Circulation Research*, **80**: 765-771

Cooklin M, Wallis WRJ, Sheridan DJ, and Fry CH (1998). Conduction velocity and gap junction resistance in hypertrophied, hypoxic guinea-pig left ventricular hypertrophy. *Experimental Physiology,* **83**: 763-770

Cooper GI (1987). Cardiocyte adaptation to chronically altered load. *Annual Reviews in Physiology,* **49:** 501-518

Cooper IC, and Fry CH (1990). Mechanical restitution in isolated mammalian myocardium: species differences and underlying mechanisms. *Journal of Molecular and Cellular Cardiology*, **22**: 439-452

Cooper IC, Fry CH, and Webb-Peploe MM (1992). Mechanical restitution of isolated human ventricular myocardium subjected to an in-vivo pressure and volume overload. *Cardiovascular Research*, **26:** 978-982

Coste P, Clementy J, Besse P, and Bricaud H (1988). Left ventricular hypertrophy and ventricular dysrhythmic risk in hypertensive patients: evaluation of programmed electrical stimulation. *Journal of Hypertension*, **6** (suppl 4): 116-118

Crandall DL, Goldstein BM, Ferraro GD, and Cervoni P (1991). Relationship of cardiac haemodynamic and biochemical adaptations to mortality during long-term aortic constriction. *Proceedings of the Society of Experimental and Biological Medicine*, **198**: 747-753

Cuocolo A, Sax FL, Brush JE, Maron BJ, Bacharach SL, and Bonow RO (1990). Left ventricular hypertrophy and impaired diastolic filling in essential hypertension. Diastolic mechanisms for systolic dysfunction during exercise. *Circulation,* **81**: 978-986

Dart C and Vaughan-Jones RD (1992). Na^+-HCO_3^-cotransport in the sheep cardiac Purkinje fibre. *Journal of Physiology,* **451**, 365-385

Davey PP, Bryant SM, and Hart G (2001). Rate-dependent electrical, contractile and restitution properties of isolated left ventricular myocytes in guinea-pig hypertrophy. *Acta Physiologica Scandinavica*, **171:** 17-28

Davies CH, Davia K, Bennett JG, Pepper JR, Poole-Wilson PA, and Harding SE (1995). Reduced contraction and altered frequency response of isolated ventricular myocytes from patients with heart failure. *Circulation*, **92:** 2540-2549

Deitmer JW, and Ellis D (1980). Interactions between the regulation of the intracellular pH and sodium activity of sheep cardiac Purkinje fibres. *Journal of Physiology*, **304**: 471-488

de la Bastie, Levitsky D, Rappaport L, Mercadier J-J, Marotte F, Wisnewsky C, Brovkovich V, Schwartz K, and Lompré A-M (1990). Function of the sarcoplasmic reticulum and expression of its Ca^{2+}-ATPase gene in pressure overload-induced cardiac hypertrophy in the rat. *Circulation Research*, **66:** 554-564

Delbridge LM, Connell PJ, Morgan TO, and Harris PJ (1996). Contractile function of cardiomyocytes from the spontaneously hypertensive rat. *Journal of Molecular and Cellular Cardiology*, **28**: 723-733

Delbridge LM, Satoh H, Yuan W, Bassani JW, Qi M, Ginsburg KS, Samarel AM, and Bers DM (1997). Cardiac myocyte volume, Ca^{2+} fluxes and sarcoplasmic reticulum loading in pressure overload hypertrophy. *American Journal of Physiology,* **272:** H2425-H2435

de Roos A, Doornbos J, Luyten PR, Oosterwaal LJ, Van DWE, and Den HJ (1992). Cardiac metabolism in patients with dilated and hypertrophic cardiomyopathy: assessment with proton-decoupled P-31 MR spectroscopy. *Journal of Magnetic Resonance Imaging*, **2**: 711-719

Desilets M, and Baumgarten CM (1986). K^+, Na^+ and Cl^- activities in ventricular myocytes isolated from rabbit heart. *American Journal of Physiology*, **251**: C197-C208

Despa S, Islam MA, Pogwizd SM, and Bers DM (2002). Intracellular $[Na^+]$ and Na^+ pump rate in rat and rabbit ventricular myocytes. *Journal of Physiology,* **539**: 133-143

Dixon IM, Yu H, Reid NL, Scammell-La FT, Werner JP, and Jasmin G (1997). Cardiac collagen remodelling in the cardiomyopathic Syrian hamster and the effect of lorsartan. *Journal of Molecular and Cellular Cardiology*, **29:** 1837-1850

Do E, Ellis D, and Noireaud J (1996). Intracellular pH and intrinsic H^+ buffering capacity in normal and hypertrophied right ventricle of ferret heart. *Cardiovascular Research,* **31**: 729-738

Doering CW, Jalil JE, Janicki JS, Pick R, Aghili S, Abrahams C, and Weber KT (1988). Collagen network remodelling and diastolic stiffness of the rat left ventricle with pressure overload hypertrophy. *Cardiovascular Research*, **22**: 686-695

Donoso P, Mill JG, O'Neill SC, and Eisner DA (1992). Fluorescence measurements of cytoplasmic and mitochondrial sodium concentration in rat ventricular myocytes. *Journal of Physiology*, **448:** 493-509.

Dussaillant GR, Gonzalez H, Cespedes C, and Jalil JE (1996). Regression of left ventricular hypertrophy in experimental renovascular hypertension: diastolic dysfunction depends more on myocardial collagen than it does on myocardial mass. *Journal of Hypertension*, **14**: 1117-1123

Eisner DA, Lederer WJ, and Vaughan-Jones RD (1981). The dependence of sodium pumping and tension on intracellular sodium activity in voltage-clamped sheep Purkinje fibres. *Journal of Physiology*, **273**: 211-240

Eisner DA, Lederer WJ, and Vaughan-Jones RD (1984). The quantitative relationship between twitch tension and intracellular sodium activity in sheep cardiac Purkinje fibres. *Journal of Physiology*, **355:** 251-266

Eisner DA, Nichols CG, O'Neill SC, Smith GL, and Valdeolmillos M (1989). The effects of metabolic inhibition on intracellular calcium and pH in isolated rat ventricular cells. *Journal of Physiology*, **411**: 393-418

Ellingsen Ø, Holthe MR, Svindland A, Aksnes G, Sejersted OM, and Ilebekk A (1994). Na, K-pump concentration in hypertrophied human hearts. *European Heart Journal*, **15:** 1184-1190

Ellis D (1977). The effects of external cations and ouabain on the intracellular sodium activity of sheep heart Purkinje fibres. *Journal of Physiology*, **273**: 211-240

Ellis D (1985). Effects of stimulation and diphenylhydantoin on the intracellular sodium activity in Purkinje fibres of sheep heart. *Journal of Physiology,* **362**: 331-348

Ellis D, and MacLeod (1985). Sodium-dependent control of intracellular pH in Purkinje fibres of sheep heart. *Journal of Physiology,* **359**: 81-105

Ellis D and Thomas RC (1976). Direct measurement of the intracellular pH of mammalian cardiac muscle. *Journal of Physiology*. **262**: 755-771

Emdad L, Uzzaman M, Takagishi Y, Honjo H, Uchida T, Severs NJ, Kodama I, and Murata Y (2001). Gap junction remodelling in hypertrophied left ventricles of aortic-banded rats: prevention by angiotensin II type-1 receptor blockade. *Journal of Molecular Cellular Cardiology*, **33:** 219-231

Ennis IL, Alvarez BV, Camilión de Hurtado MC, and Cingolani HE (1998). Enalpril induces regression of cardiac hypertrophy and normalisation of pH_i regulatory mechanisms. *Hypertension*, **31**: 961-967

Fabiato A, and Fabiato F (1978). Effects of pH on the myofilaments and the sarcoplasmic reticulum of skinned cells from cardiac and skeletal muscles. *Journal of Physiology*, **276:** 233-255

Fabiato A, and Fabiato F (1979). Calcium-induced release of calcium from the sarcoplasmic reticulum of skinned cells from adult human, dog, cat, rabbit, rat, and frog hearts and from fetal and new-born rat ventricles. *Annals of New York Academy of Science*, **307**: 491-522

Feldman AM, Weinberg EO, Ray PE, and Lorell BH (1993). Selective changes in cardiac gene expression during compensated hypertrophy and the transition to cardiac decompensation in rats with chronic aortic banding. *Circulation Research*, **73**: 184-192

Firek L, and Weingart R, (1995). Modification of gap junction conductance by divalent cations and protons in neonatal rat heart cells. *Journal of Molecular and Cellular Cardiology*, **27:** 1633-1643

Fisone G, Cheng SXJ, Nairn AC, Czernik AJ, Hemmings HC, Jr, Hoog JO, Bertorello AM, Kaiser R, Bergman T, Jornvall H, Aperia A, and Greengard P (1994). Identification of the phosphorylation site for cAMP-dependent protein kinase on Na^+, K^+-ATPase and effects of site-directed mutagenesis. ***Journal of Biological Chemistry,*** **269**: 9368-9373

Flesch M, Schiffer F, Zolk O, Pinto Y, Rosenkranz S, Hirth-Dietrich C, Arnold G, Paul M, and Bohm M (1997). Contractile systolic and diastolic dysfunction in renin-induced hypertensive cardiomyopathy. *Hypertension,* **30**: 383-391

Frampton JE, Harrison SM, Boyett MR and Orchard CH (1991a). Ca^{2+} and Na^+ in rat myocytes showing different force-frequency relationships. *American Journal of Physiology*, **261**: C739- C750

Frampton JE, Orchard CH, and Boyett MR (1991b). Diastolic, systolic and sarcoplasmic reticulum [Ca^{2+}] during inotropic interventions in isolated rat myocytes. *Journal of Physiology*, **437**: 351-375

Fry CH, Gray RP, and Sheridan DS (2001). Discontinuous action potential propagation in hypertrophied left ventricular myocardium. *Journal of Physiology,* **536P:** 79P

Fry CH, Hall SK, Blatter LA, and McGuigan (1990). Analysis and presentation of intracellular measurements obtained with ion-selective microelectrodes. *Experimental Physiology,* **75**: 187-198

Fry CH, Harding DP, and Mounsey JP (1987). The effects of cyanide on intracellular ion exchange in ferret and rat ventricular myocardium. *Proceedings of the Royal Society*, **230:** 53-75

Fry CH and Langley SEM (2001). *Ion-selective electrodes for biological systems.* Harwood Academic Publishers, Amsterdam.

Fry CH, and Poole-Wilson PA (1981). Effects of acid-base changes on excitation-contraction coupling in guinea-pig and rabbit cardiac ventricular muscle. *Journal of Physiology*, **313**: 141-160

Fry CH, Powell T and Twist VW (1981). Net calcium fluxes in isolated rat ventricular muscle cells. *Journal of Physiology*, **315**: 17P

Fry CH, Powell T, Twist VW and Wood VPT (1984). Net calcium fluxes in isolated rat ventricular myocytes: an assessment of mitochondrial calcium accumulating capacity. *Proceedings Royal Society Medicine*, **223**: 223-238.

Gao WD, Perez NG, and Marban E (1998). Calcium cycling and contractile activation in intact mouse cardiac muscle. *Journal of Physiology*, **507:** 175-184

Gillis AM, Mathison HJ, Kulisz E, and Lester WM (1998). Dispersion of ventricular repolarisation in left ventricular hypertrophy: influence of afterload and dofetilide. *Journal of Cardiovascular Electrophysiology*, **9**: 988-997

Gómez AM, Benitah JP, Henzel D, Vinet A, Lorente P, and Delgado C (1997a). Modulation of electrical heterogeneity by compensated hypertrophy in rat left ventricle. *American Journal of Physiology*, **272:** H1078-H1086

Gómez AM, Valdivia HH, Cheng H, Lederer MR, Santana LF, Cannell MB, McCune SA, Altschuld RA and Lederer WJ (1997b). Defective excitation-contraction coupling in experimental cardiac hypertrophy and heart failure. *Science*, **276**: 810-806

Gray RP, McIntyre H, Sheridan DJ, and Fry CH (2001). Intracellular sodium and contractile function in hypertrophied human and guinea-pig myocardium. *Pflügers Archives,* **442**: 117-123

Gretler DD (1985). Strophanthidin and potassium on intracellular sodium activity in sheep heart. *Journal of Molecular and Cellular Cardiology*, **17:** 1105-1113

Grynkiewicz G, Poenie M, and Tsien RY (1985). A new generation of Ca^{2+} indicators with greatly improved flourescent properties. ***Journal of Biological Chemistry,*** **260**: 3440-3450

Guarnieri T (1988). Decrease in the transmembrane sodium activity gradient in ferret papillary muscle as a prerequisite to the calcium paradox. *Journal of Clinical Investigation,* **81**: 1938-1944

Gulch RW, Baumann R, and Jacob R (1979). Analysis of myocardial action potential in left ventricular hypertrophy. *Basic Research in Cardiology*, **74**: 69-82

Gwathmey JK, Liao R, and Ingwall JS (1995). Comparison of twitch force and calcium handling in papillary muscles from right ventricular pressure overload hypertrophy in weanling and juvenile ferrets. *Cardiovascular Research*, **29**: 475-481

Gwathmey JK, and Morgan JP (1985). Altered calcium handling in experimental pressure-overload hypertrophy in the ferret. *Circulation Research*, **57**: 836-843

Gwathmey JK, Slawsky MT, Hajjer RJ, Briggs GM, and Morgan JP (1990). Role of intracellular calcium handling in force-interval relationships in human ventricular myocardium. *Journal of Clinical Investigation*, **85**: 1599-1613

Haefliger JA, Castillo E, Waeber G, Bergonzelli GE, Aubert JF, Sutter E, Nicod P, Waeber B, and Meda P (1997). Hypertension increases connexin43 in a tissue-specific manner. *Circulation Research*, **95**: 1007-1014

Haider AW, Larson MG, Benjamin EJ, and Levy D (1998). Increased left ventricular mass and hypertrophy are associated with increased risk for sudden death. *Journal American College Cardiology,* **32:** 1454-1459

Hall SK, and Fry CH (1992). Magnesium affects excitation, conduction and contraction of isolated cardiac muscle. *American Journal of Physiology*, **263**: H622-H633

Hanf R, Drubaix I, Marotte F and Lelièvre LG (1988). Rat cardiac hypertrophy: altered sodium-calcium exchange in sarcolemmal vesicles. *FEBS Letters*, **236**: 145-9

Harrison SM, Frampton JE, McCall E, Boyett MR and Orchard CH (1992a). Contraction and intracellular Ca^{2+}, Na^{+} and H^{+} during acidosis in rat ventricular myocytes. *American Journal of Physiology*, **31**: C347-C357

Harrison SM, McCall E, and Boyett MR (1992b). The relationship between contraction and intracellular sodium in rat and guinea-pig ventricular myocytes. *Journal of Physiology*, **449**: 517-550

Hayashi H, Miyata H, Noda N, Kobayashi A, Hirano M, Kawai T, and Yamazaki N (1992). Intracellular Ca^{2+} concentration and pH_i during metabolic inhibition. *American Journal of Physiology*, **262**: C628-C634

Hayashi H, Satoh H, Noda N, Terada H, Hirano M, Yamashita Y, Kobayashi A, and Yamazaki N (1994). Simultaneous measurement of intracellular Na^{+} and Ca^{2+} during K^{+}-free perfusion in isolated myocytes. *American Journal of Physiology*, **266**: C416-C422

Heilmann C, Lindl T, Müller W and Pette D (1980). Characterisation of cardiac microsomes from spontaneously hypertensive rats. *Basic Research in Cardiology,* **75**: 92-96

Hermans MMP, Kortekaas P, Jongsma HJ, and Rook MB (1995). pH sensitivity of the cardiac gap junction proteins, connexin 45 and 43. *Pflügers Archives*, **431**: 138-140

Herrera VLM, Chobanian AV, and Ruiz-Opazo N (1988). Isoform-specific modulation of Na^+-K^+-ATPase alpha-subunit gene expression in hypertension. *Science*, **241:** 221-223

Hicks MN, McIntosh MA, Kane KA, Rankin AC, and Cobbe SM (1995). The electrophysiology of rabbit hearts with left ventricular hypertrophy under normal and ischaemic conditions. *Cardiovascular Research,* **30**: 181-186

Hool LC, Whalley DW, Doohan MM, and Rasmussen HH (1995). Angiotensin-converting enzyme inhibition, intracellular Na^+, and Na^+-K^+ pumping in cardiac muscle. *American Journal of Physiology*, **268**: C366-C375

Hori M, Nakatsubo N, Kagiya T, Imai K, Sato H, Iwakura K, Kitabatake H and Kamada T (1990). The role of norepinehedrine-induced protein synthesis in neonatal cultured cardiomyocytes. *Japanese Circulation Journal,* **54**: 535-539

Houghton JL, Frank MJ, Carr AA, von Dohlen TW, and Prisant LM (1990). Relations among impaired coronary flow reserve, left ventricular hypertrophy and thallium perfusion defects in hypertensive patients without obstructive coronary artery disease. *Journal American College Cardiology*, **15**: 43-51

Ikonomidis I, Tsoukas A, Parthenakis F, Gournizakis A, Kassimatis A, Rallidis L, and Nihoyannopoulos P (2001). Four year follow-up of aortic valve replacement for isolated aortic stenosis: a link between reduction in pressure, regression of left ventricular hypertrophy, and diastolic function. *Heart*, **86:** 309-316

Inagaki M, Yokota M, Izawa H, Ishiki R, Nagata K, Iwase M, Yamada Y, Koide M, and Sobue T (1999). Impaired force-frequency relations in patients with hypertensive left ventricular hypertrophy. *Circulation,* **99**: 1822-1830

Ito K, Yan Xinhua, Tajima M, Su Z, Barry WH, and Lorell BH (2000). Contractile reserve and intracellular calcium regulation in mouse myocytes from normal and hypertrophied failing hearts. *Circulation Research*, **87**: 588-595

Ito N, Bartunek J, Spitzer KW, and Lorell BH (1997b). Effects of the nitric oxide donor sodium nitroprusside on intracellular pH and contraction in hypertrophied myocytes. *Circulation,* **95:** 2303-2311

Ito N, Kagaya Y, Weinberg EO, Barry WH, and Lorell BH (1997a). Endothelin and angiotensin II stimulation of Na^+-H^+ exchange is impaired in cardiac hypertrophy. *Journal of Clinical Investigation,* **99:** 125-135

Ito Y, Suko J, and Chidsey CA (1974). Intracellular calcium and myocardial contractility: calcium uptake of the sarcoplasmic reticulum fractions in hypertrophied and failing rabbit hearts. *Journal of Molecular and Cellular Cardiology,* **6**: 237-247

Jager H, Wozniah G, Akinturk IH, Hehriein FW, and Scheiner-Bobis G (2001). Expression of sodium pump isoforms and other sodium or calcium ion transporters in the heart of hypertensive patients. *Biochimica et Biophysica Acta*, **1513**: 149-159

James PF, Grupp IL, Grupp G, Woo AL, Askew GR, Croyle ML, Walsh RA, and Lingrel JB (1999). Identification of a specific role for Na,K-ATPase α_2 isoform as a regulator of calcium in the heart. *Molecular Cell*, **3**: 555-563

Jeffrey FMH, Malloy CR, and Radda GK (1987). Influence of intracellular acidosis on contractile function in the working heart. *American Journal of Physiology*, **253**: H1499-H1505

Jelicks LA, and Gupta RK (1994). Nuclear magnetic resonance measurement of intracellular sodium in the perfused normotensive and spontaneously hypertensive rat heart. *American Journal of Hypertension*, **7**: 429-435

Jelicks LA, and Siri FM (1995). Effects of hypertrophy and heart failure on $[Na^+]_i$ in pressure-overloaded guinea-pig heart. *American Journal of Hypertension*, **8**: 934-943

Jewell EA, and Lingrel JB (1991). Comparison of the substrate dependence properties of the rat Na,K-ATPase alpha 1, alpha2, and alpha3 isoforms expressed in HeLa cells. *Journal of Biological Chemistry*, **266**: 16925-16930

Kaibara M, and Kameyama M (1988). Inhibition of the calcium channel by intracellular protons in single ventricular myocytes of the guinea-pig. *Journal of Physiology*, **403**: 621-640

Kaila K and Vaughan-Jones RD (1987). Influence of sodium-hydrogen exchange on intracellular pH, sodium and tension in sheep cardiac Purkinje fibres. *Journal of Physiology*, **390**: 93-118

Kanaya N, Zakhary DR, Murray PA, and Damron DS (1998). Thiopental alters contraction, intracellular Ca^{2+} and pH in rat ventricular myocytes. *Anaesthesiology*, **89**: 202-214

Kannel WB, Doyle JT, McNamara PM, Quickenton P, and Gordon T (1975). Precursors of sudden coronary death: factors related to the incidence of sudden death. *Circulation*, **51**: 606-613

Kannel WB, and Sorlie P (1981). Left ventricular hypertrophy in hypertension: prognostic and pathological implications (the Framingham Study). In: Staurer BE, ed. *The heart in hypertension* (Boehringer-Mannheim Symposium Series). Berlin: Springer-Verlag, 223-242

Kannel W (1992). Left ventricular hypertrophy as a risk factor in arterial hypertension. *European Heart Journal*, **13** (suppl): 82-88

Kaufmann RL, Hamburger H and Wirth H (1971). Disorder of excitation-contraction coupling of cardiac muscle from cats with experimentally produced right ventricular hypertrophy. *Circulation Research*, **28**: 346-357

Keung EC (1989). Calcium current is increased in isolated myocytes from hypertrophied rat myocardium. *Circulation Research*, **64**: 753-763

Khatter JC, and Hoeschen RJ (1984). Reduced number of digitalis receptor sites in the hypertrophied pig myocardium. *Basic Research in Cardiology*, **79**: 396-401

Kingsbury MP, Huang W, Giuliatti S, Turner M, Hunter R, Parker K, and Sheridan DS (1999). Investigation of distal aortic compliance and vasodilator responsiveness in heart failure due to proximal aortic stenosis in the guinea-pig. *Clinical Science*, **96**: 241-251

Kléber AG (1983). Resting membrane potential, extracellular potassium and intracellular sodium activity during acute global ischaemia in isolated perfused guinea-pig hearts. *Circulation Research*, **52:** 442-450

Kleiman RB, and Houser SR (1988). Calcium currents in normal and hypertrophied isolated feline ventricular myocytes. *American Journal of Physiology*, **255:** H1434-1442

Koch-Weser J, and Blinks JR (1963). The influence of the interval between beats on myocardial contractility. *Pharmacology Reviews*, **15**: 601-652

Kohya T, Yokoshiki H, Tohse N, Kanno M, Nakaya H, Saito H, and Kitabatake A (1995). Regression of left ventricular hypertrophy prevents ischaemia-induced lethal arrhythmias. *Circulation Research*, **76**: 892-899

Kohmoto O, Levy AJ, and Bridge JHB (1994). Relation between reverse sodium-calcium exchange and sarcoplasmic reticulum calcium release in guinea-pig ventricular cells. *Circulation Research*, **74**: 550-554

Kowey P, Friechling TD, Sewter J, Wu Y, Sokil A, Paul J, and Norcella J (1991). Electrophysiological effects of left ventricular hypertrophy, effect of calcium and potassium channel blockade. *Circulation*, **83:** 2067-2075

Laylock SK, Kane KA, McMurray J, and Parratt JR (1996). Captopril and norepinephrine-induced hypertrophy and haemodynamics in rats. *Journal of Cardiovascular Pharmacology*, **27**: 667-672

Laemmli UK, (1970). Cleavage of structural proteins during assembly of the head of bacteriophage T4. ***Nature,*** **227**: 680-685

Lagadic-Gossmann D, Buckler KJ, and Vaughan-Jones RD (1992). Role of bicarbonate in pH recovery from intracellular acidosis in the guinea-pig ventricular myocyte. *Journal of Physiology*, **458,** 361-384

Lagadic-Gossmann D, and Feuvray D (1991). Intracellular sodium activity in papillary muscle from diabetic rat hearts. *Experimental Physiology*, **76**: 147-149

LeBlanc N, Cartier D, Martin M and Cole WC (1996). Ca^{2+} permeation through Na^{+} channels in guinea-pig ventricular myocytes. *Biophysical Journal,* **70**: A279

LeBlanc N, and Hume JR (1990). Sodium current induced release of calcium from cardiac sarcoplasmic reticulum. *Science,* **248**: 372-376

Lecarpentier Y, Waldenström A, Clergue M, Chemla D, Oliviero P, Martin JL, and Swynghedauw B (1987). Major alterations in relaxation during cardiac hypertrophy induced by aortic stenosis in guinea-pig. *Circulation Research*, **61**: 107-116

Lee CO, and Fozzard HA (1975). Activities of potassium and sodium in rabbit heart muscle. *Journal of General Physiology*, **65**: 694-708

Leem CH, Lagadic-Gossmann D, and Vaughan-Jones RD (1999). Characterisation of intracellular pH regulation in the guinea-pig ventricular myocyte. *Journal of Physiology*, **517:** 159-180

Lemaire S, Piot C, Seguin J, Nargeot J and Richard S (1995). Tetrotodotoxin-sensitive Ca^{2+} and Ba^{2+} currents in human atrial cells. *Receptors and Channels*, **3:** 71-81

Levi AJ, Lee CO, and Brooksby P (1994a). Properties of the fluorescent sodium indicator "SBFI" in rat and rabbit cardiac myocytes. *Journal of Cardiovascular Electrophysiology*, **5**: 241-257

Levi AJ, Spitzer KW, Kohmoto O and Bridge JHB (1994b). Depolarisation-induced Ca entry via Na-Ca exchange triggers SR release in guinea-pig cardiac myocytes. *American Journal of Physiology*, **266**: H1422-H1433

Levitsky DO, Benevolensky DS, Levchenko TS, Smirov VN, and Chazov EI (1981). Calcium-binding rate and capacity of the cardiac sarcoplasmic reticulum. *Journal of Molecular and Cellular Cardiology,* **13**: 785-796

Levy D, Anderson KM, Savage DD, Balkus SA, Kannel WB, and Castelli WP (1987). Risk of ventricular arrhythmias in left ventricular hypertrophy: the Framingham Heart study. *American Journal Cardiology,* **60**: 560-563

Levy D, Anderson KM, Savage DD, Kannel WB, Christiansen JC, and Castelli WP (1988). Echocardiographically detected left ventricular hypertrophy: prevalence and risk factors: the Framingham Heart Study. *Annals Internal Medicine*, **180**: 7-13

Levy D, Garrison RJ, Savage DD, Kannel WB, and Castelli WP (1990). Prognostic implications of echocardiographically determined left ventricular mass in the Framingham study. *New England Journal of Medicine,* **332**: 1561-1566

Liard JF and Spadone JC (1985). Regional circulations in experimental coarctation of the aorta in conscious dogs. *Journal of Hypertension*, **3**: 281-291

Limas CJ, Spier SS, and Kahlon J (1980). Enhanced calcium transport by sarcoplasmic reticulum in mild cardiac hypertrophy. *Journal of Molecular and Cellular Cardiology*, **12:** 1103-1116

Ling, ET and DeBold AJ (1976). An improved method for the production of congestive heart failure in the guinea-pig. *Laboratory Animals* **10**, 285-289

Litwin SE, and Bridge JHB (1997). Enhanced Na^{+}-Ca^{2+} exchange in the infarcted heart: implications for excitation-contraction coupling. *Circulation Research,* **81**: 1083-1093

Lloyd Jones DM (2001). The risk of congestive heart failure: sobering lessons from the Framingham Heart Study. *Current Cardiological Reports*, **3:** 184-90

Lompre AM. Anger M and Levitsky D (1994). Sarco(endo)plasmic reticulum calcium pumps in the cardiovascular system: function and gene expression. *Journal of Molecular and Cellular Cardiology*, **26**: 1109-1121

López-López JR, Shacklock PS, Balke CW, and Wier WG (1995). Local calcium transients triggered by single L-type calcium channel currents in cardiac cells. *Science*, **268:** 1042-1045

Lortet S, Heckmann M, Aussedat J, Ray A, Vincent M, Sassard J, Zimmer HG, and Rossi A (1993). Alteration of cardiac energy state during development of hypertension in rats of the Lyon strain: a 31P-NMR study on the isolated heart. *Acta Physiologica Scandinavica,* **149**: 311-321

Lowry OH, Rosebrough NJ, Farr A, and Randall RJ (1951). Protein measurement with the Folin phenol reagent. *Journal of Biological Chemistry*, **193**: 265-275

McAinsh AM, Turner MA, O'Hare D, D, Nithythyananthan R, Johnson D, O'Gorman DJ, and Sheridan DJ (1995). Cardiac hypertrophy impairs recovery from ischaemia because there is a reduced reactive hyperaemic response. *Cardiovascular Research*, **30**: 113-121

McCall E, Ginsburg KS, Bassani RA, Shannon TR, Qi M, Samarel AM and Bers DM (1998). Ca flux, contractility and excitation-contraction coupling in hypertrophic rat ventricular myocytes. *American Journal of Physiology*, **274**: H1348-H1372

McDonald TF, Pelzer S, Trautwein W and Pelzer D (1994). Regulation and modulation of calcium channels in cardiac, skeletal, and smooth muscle cells. *Physiological Reviews*, **74:** 365-507

McDonough AA and Schmitt CA (1985). Comparison of subunits of cardiac, brain and kidney Na^+-K^+-ATPase. *American Journal of Physiology*, **248:** C247-C251

McDonough AA, Zhang Y, Shin V, and Frank JS (1996). Subcellular distribution of sodium pump isoforms in mammalian cardiac myocytes. *American Journal of Physiology,* **270:** C1221-C1227

McIntyre H, and Fry CH (1997). Abnormal action potential conduction in isolated human hypertrophied left ventricular myocardium. *Journal of Cardiovascular Electrophysiology*, **8**: 887-894

McIvor ME, Orchard CH and Lakatta EG (1988). Dissociation of changes in apparent myofibrillar Ca^{2+} sensitivity and twitch relaxation induced by adrenergic and cholinergic stimulation in isolated ferret cardiac muscle. *Journal of General Physiology*, **92**: 509-529

McLenachan JM, Henderson E, Morris KI, and Dargie HJ (1987). Ventricular arrhythmias in patients with hypertensive left ventricular hypertrophy. *New England Journal of Medicine*, **317:** 787-792

Maier LS, Brandes R, Pieske B, and Bers DM (1998). Effects of left ventricular hypertrophy on force and Ca^{2+} handling in isolated rat myocardium. *American Journal of Physiology*, **274**: H1361-1370

Maier LS, Pieske B, and Allen DG (1997). Influence of stimulation frequency on $[Na^{+}]_i$ and contractile function in Langendorff-perfused heart. *American Journal of Physiology*, **273**: H1246-H1254

Maixent JM, Charlemange D, De la Chapelle B, and Lelière LG (1987). Two Na,K-ATPase isoenzymes in canine cardiac myocytes. Molecular basis of inotropic and toxic effects of digitalis. *Journal of Biological Chemistry,* **262**: 6842-6848

Mann DL, Urable Y, Kent RL, Vinciguerra S, and Cooper G (1991). Cellular versus myocardial basis for the contractile dysfunction of hypertrophied myocardium. *Circulation Research*, **68:** 402-415

Marban E, Kitakaze M, Chacko VP, and Pike MM (1988). Ca^{2+} transients in perfused hearts revealed by gated ^{19}F NMR spectroscopy. *Circulation Research*, **63**: 673-678

Marcus ML, Doty DB, Hiratzka LF, Wright CB, and Eastham CL (1982). Decreased coronary reserve: a mechanism for angina pectoris in patients with aortic stenosis and normal coronary arteries. *New England Journal of Medicine,* **307:** 1362-1366

Martinez ML, Heredia MP, and Delgado C (1999). Expression of T-type Ca^{2+} channels in ventricular cells from hypertrophied rat hearts. *Journal of Molecular and Cellular Cardiology*, **31**: 1617-1625

Martins JB, Kim W, and Marcus ML (1989). Chronic hypertension and left ventricular hypertrophy facilitate induction of sustained ventricular tachycardia in dogs 3 hours after left circumflex coronary artery occlusion. *Journal of American College of Cardiology,* **14**: 1365-1373

Marx SO, Reiken S, Hisamatsu Y, Jayaraman T, Burkhoff D, Rosemblit N, and Marks AR (2000). PKA phosphorylation dissociates FKBP12.6 from the calcium release channel (ryanodine receptor): defective regulation in failing hearts. *Cell,* **101**: 365-376

Matsui H, MacLennan DH, Alpert NR, and Periasamy M (1995). Sarcoplasmic reticulum gene expression in pressure-overload-induced hypertrophy in rabbit. *American Journal of Physiology*, **268**: C252-C258

Maughan D, Low E, Littin R, Brayden J, and Alpert N (1979). Calcium-activated muscle from hypertrophied rabbit hearts. Mechanical and correlated biochemical changes. *Circulation Research*, **44:** 279-287

Maurer P, and Weingart R (1987). Cell pairs isolated from adult guinea-pig and rat hearts: effects of $[Ca^{2+}]_i$ on nexal membrane resistance. *Pflügers Archives*, **409**: 394-402

Même W, O'Neill S, and Eisner D (2001). Low sodium inotropy is accompanied by diastolic Ca^{2+} gain and systolic loss in isolated guinea-pig ventricular myocytes. *Journal of Physiology*, **530***:* 487-495

Mercadier JJ, Bouveret P, Gorza L, Schiaffino S, Clarke WA, Zak R, Swynghedauw B, and Schwartz K (1983). Myosin isoenzymes in normal and hypertrophied human ventricular myocardium. *Circulation Research*, **53:** 52-62

Messerli FH, Nunez BD, Nunez MM, Garavagalia GE, Schmieder RE and Ventura HO (1989). Hypertension and sudden death. Disparate effects of calcium entry blocker and diuretic therapy on cardiac dysrhythmias. *Archives of Internal Medicine*, **149:** 1263-1267

Meyer M, Schillinger W, Pieske B, Holubarsch C, Heilmann C, Posival H, Kuwajima G, Mikoshiba K, Just H, and Hasenfuss G (1995). Alterations of sarcoplasmic reticulum proteins in failing dilated cardiomyopathy. *Circulation*, **92:** 778-784

Mill JG, Novaes MA, Galon M, Nogueira JB and Vassallo DV (1998). Comparison of the contractile performance of the hypertrophied myocardium from spontaneously hypertensive and normotensive infarcted rats. *Canadian Journal of Physiology and Pharmacology*, **76:** 387-394

Milnes JT, and MacLeod (2001). Reduced ryanodine receptor to dihydropyridine receptor ratio may underlie slowed contraction in a rabbit model of left ventricular cardiac hypertrophy. *Journal of Molecular and Cellular Cardiology*, **33**: 473-485

Mirsky I, Pfeffer JM, Pfeffer MA, and Braunwald E (1983). The contractile state as the major determinant in the evolution of left ventricular dysfunction in the spontaneously hypertensive rat. *Circulation Research*, **53**: 767-778

Miyamoto MI, del Monte F, Schmidt U, DiSalvo TS, Bin Kang Z, Matsui T, Guerrero JL, Gwathmey JK, Rosenzweig A, and Hajjar RJ (2000). Adenoviral gene transfer of SERCA2a improves left-ventricular function in aortic-banded rats in transition to heart failure. *Proceedings National Academy of Science, USA,* **97**: 793-798

Mohabir R, Lee H-C, Kurz RW, and Clusin WT (1991). Effects of ischaemia and hypercapnic acidosis on myocyte calcium transients, contraction and pH_i in perfused rabbit hearts. *Circulation Research,* **69**: 1525-1537

Momtaz A, Coulombe A, Richer P, Mercadier JJ, and Coraboeuf E (1996). Action potential and plateau ionic currents in moderately and severely DOCA-salt hypertrophied rat hearts. *Journal of Molecular and Cellular Cardiology,* **28**: 2511-2522

Moore RL, Yelamarty RV, Misawa H, Scaduto RC, Pawlush DG, Elensky M and Cheung JY (1991). Altered Ca^{2+} dynamics in single cardiac myocytes from renovascular hypertensive rats. *American Journal of Physiology*, **260:** C327-C337

Moreno AP, Sàez JC, Fishman GI, and Spray DC (1994). Human connexin 43 gap junction channels. Regulation of unitary conductances by phosphorylation. *Circulation Research*, **74**: 1050-1057

Mubagwa K, Flameng W, and Carmeliet E (1994). Resting and action potentials of nonischaemic and ischaemic human ventricular muscle. *Journal of Cardiovascular Electrophysiology,* **5**: 659-671

Mubagwa K, Lin W, Sipido KR, Bosteels S, and Flameng W (1997). Monensin-induced reversal of positive force-frequency relationship in cardiac muscle: role of intracellular sodium in rest-dependent potentiation of contraction. *Journal of Molecular and Cellular Cardiology*, **29**:977-989

Mulieri LA, Hasenfuss G, Leavitt B, Allen PD, and Alpert NR (1992). Altered myocardial force-frequency relation in human heart failure. *Circulation*, **85:** 1743-1750

Nagai R, Zarain-Herzberg A, Brandl CJ, Fujii J, Tada M, MacLennan DH, Alpert NR and Periasamy M (1989). Regulation of myocardial Ca^{2+}-ATPase and phospholamban mRNA expression in response to pressure overload and thyroid hormone. *Proceedings of National Academy of Science, USA,* **86**: 2966-2970

Nakanishi H, Makin N, Matsui H, Yano K, and Yanaga T (1989). Sarcolemmal Ca transport activities in cardiac hypertrophy caused by pressure overload. *American Journal of Physiology*, **257**: H349-H356

Nakanishi T, Seguchi M, Tsuchiya T, Yasukouchi S and Takao A (1990). Effect of acidosis on intracellular pH and calcium concentration in the newborn and adult rabbit myocardium. *Circulation Research,* **67:** 111-123

Naqvi RU, and MacLeod KT (1994). Effect of hypertrophy on mechanisms of relaxation in isolated cardiac myocytes from guinea-pig. *American Journal of Physiology*, **267**: H1851-H1861

Naqvi RU, Tweedie D, and MacLeod KT (2001). Evidence for the action potential mediating changes to contraction observed in cardiac hypertrophy in the rabbit. *International Journal of Cardiology,* **77:** 189-206

Nattel S, Elharrar V, Zipes DP, and Bailey JC (1981). pH-dependent electrophysiological effects of quinidine and lidocaine on canine cardiac Purkinje fibres. *Circulation Research*, **48**: 55-61

Negretti N, Varro A, and Eisner DA (1995). Estimate of net calcium fluxes and sarcoplasmic reticulum calcium content during systole in rat ventricular myocytes. *Journal of Physiology*, **486**: 581-591

Ng LL, Davies JE and Quinn P (1993). Intracellular pH regulation in isolated myocytes from adult rat heart in HCO_3^- containing and HCO_3^--free media. *Clinical Science*, **84:** 133-139

Ng YC, and Akera T (1987). Two classes of ouabain binding sites in ferret heart and two forms of Na^+-K^+-ATPase. *American journal of Physiology*, **252**: H1016-H1022

Ng YC, and Book CB (1992). Expression of Na^+-K^+-ATPase α1 and α3-isoforms in adult and neonatal ferret hearts. *American Journal of Physiology,* **263**; H1430-H1436

Nirasawa Y, and Akera T (1987). Pressure-induced cardiac hypertrophy: changes in Na^+-K^+-ATPase and glycoside action in cats. *European Journal of Pharmacology*, **137:** 77-83

Noble D, and Powell T (1990). The attenuation and slowing of calcium signals in cardiac muscle by fluorescent indicators. *Journal of Physiology*, **425**, 54P.

Noda N, Hayashi H, Miyata H, Suzuki S, Kobayashi A, and Yamazaki N (1992). Cytosolic Ca^{2+} concentration and pH of diabetic rat myocytes during metabolic inhibition. *Journal of Molecular and Cellular Cardiology,* **24:** 435-446

Nordin C, Siri F, and Aronson RS (1989). Electrophysiological characteristics of single myocytes isolated from hypertrophied guinea-pig hearts. *Journal of Molecular Cellular Cardiology,* **21**: 729-739

Nuss HB and Houser SR (1991). Voltage dependence of contraction and calcium current in severely hypertrophied feline ventricular myocytes. *Journal of Molecular and Cellular Cardiology,* **23**: 717-726

Nuss HB, and Houser SR (1992). Sodium-calcium exchange mediated contractions in feline ventricular myocytes. *American Journal of Physiology,* **263:** H1161-H1169

Nuss HB, and Houser SR (1993). T-type Ca^{2+} current is expressed in hypertrophied adult feline left ventricular myocytes. *Circulation Research*, **73:** 777-782

O'Farrell PH (1975). High resolution two-dimensional electrophoresis of proteins. *Journal of Biological Chemistry*, **250**: 4007-4021

O'Gorman DJ, Thomas P, Turner MA, and Sheridan DJ (1992). Investigation of impaired coronary vasodilator reserve in guinea-pig hearts with pressure-induced hypertrophy. *European Heart Journal,* **13**: 697-703

Ohkusa T, Hisamatsu Y, Yano M, Kobayashi S, Tatsuno H, Saiki Y, Kohno M, and Matsuzaki M (1997). Altered cardiac mechanism and sarcoplasmic reticulum function in

pressure-overload-induced cardiac hypertrophy in rats. *Journal of Molecular and Cellular Cardiology*, **29:** 45-54

Ohta K, Kim S, Hamaguchi A, Miura K, Yukimura T, and Iwao H (1995). Expression of sarcoplasmic reticulum Ca^{2+}-ATPase mRNA in the hypertrophied heart of young spontaneously hypertensive rats. *Clinical Experiments in Pharmacology and Physiology*, **1** (suppl): S228-S229

Okayama H, Hamada M, Kawakami H, Ikeda S, Hashida H, Shigematsu Y, and Hiwada K (1997). Alterations in expression of sarcoplasmic reticulum gene in Dahl rats during the transition from compensatory myocardial hypertrophy to heart failure. *Journal of Hypertension*, **15:** 1767-1774.

Oldershaw PJ, and Cameron IR (1988). The effects of long-standing hypertensive left ventricular hypertrophy on intracellular pH and intracellular electrolytes in rats. *International Journal of Cardiology,* **18:** 143-149

Oldershaw PJ, and Cameron IR (1989). In vitro buffering capacity of cardiac and skeletal muscle tissue in normotensive and hypertensive rats. Assessment using pCO_2 equilibration of homogenates. *International Journal of Cardiology*, **23:** 27-32

Opherk D, Mall G, Zebe H, Schwarz F, Weihe E, Manthey J, and Kubler W (1984). Reduction of coronary reserve: a mechanism for angina pectoris in patients with arterial hypertension and normal coronary arteries. *Circulation*, **69:** 1-7

Orchard CH, Hamilton DL, Astles P, McCall E, and Jewell BR (1991). The effect of acidosis on the relationship between calcium and force in isolated ferret cardiac muscle. *Journal of Physiology*, **436**: 559-578

Orchard CH and Kentish JC (1990). Effects of changes of pH on the contractile function of cardiac muscle. *American Journal of Physiology*, **258**: C967-C981

Orchard CH, and Lakatta E (1985). Intracellular calcium transients and developed tension in rat heart muscle; a mechanism for the negative interval relationship. *Journal of General Physiology*, **86**: 637-651

Orlowski J, and Lingrel JB (1988). Tissue-specific and developmental regulation of Na,K-ATPase catalytic isoform and beta subunit mRNA's. *Journal of Biological Chemistry*, **263**: 10436-10442

Park C-O, Xiao X-H, and Allen DG (1999). Changes in intracellular Na^+ and pH in rat heart during ischaemia: role of Na^+/H^+ exchanger. *American Journal of Physiology*, **276:** H1581-H1590

Peréz NG, Alvarez BV, Camilión de Hurtado MC, and Cingolani HE (1995). pH_i regulation in the myocardium of the spontaneously hypertensive rat. Compensated enhanced activity of the Na^+-H^+-exchanger. *Circulation Research,* **77**: 1192-1200

Peters NS, Coromilas J, Severs NJ, and Wit AL (1997). Disturbed connexin 43 gap junction distribution correlates with the location of reentrant circuits in the epicardial border zone of healing canine infarcts that cause ventricular tachycardia. *Circulation*, **95**: 988-996

Peters NS, del Monte F, MacLeod KT, Green CR, Poole-Wilson PA, and Severs NJ (1993a). Increased cardiac myocyte gap-junction membrane early in renovascular hypertension. *American Journal of Cardiology,* **21**: 59A

Peters NS, Green CR, Poole-Wilson PA, and Severs NJ (1993b). Reduced content of connexin 43 gap junctions in ventricular myocardium from hypertrophied and ischaemic human hearts. *Circulation,* **88:** 864-875

Petrecca K, Atanasiu R, Grinstein S, Orlowski J, and Shrier A (1999). Subcellular localisation of the Na^+-H^+-exchanger NHE1 in rat myocardium. *American Journal of Physiology*, **276**: H709-H717

Philipson KD, Bersohn MM, and Nishimoto AY (1982). Effects of pH on Na^+-Ca^{2+} exchange in canine cardiac sarcolemmal vesicles. *Circulation Research*, **50**: 287-293

Pieske B, Maier LS, Bers DM, and Hasenfuss G (1999). Ca^{2+} handling and sarcoplasmic reticulum Ca^{2+} content in isolated failing and non-failing human myocardium. *Circulation Research*, **85:** 38-46

Pike MM, Su Luo C, Clark MD, Kirk KA, Kitakaze M, Madden MC, Cragoe EJ Jr, and Pohost GM (1993). NMR measurements of Na^+ and cellular energy in ischaemic rat heart: role of Na^+-H^+-exchange. *American Journal of Physiology*, **34**: H2017-H2026

Price EM, and Lingrel JB (1988). Structure-function relationships in the Na,K,-ATPase subunit: site-directed mutagenesis of glutamine-111 to arginine and asparagine-122 to aspartic acid generates a ouabain-resistant enzyme. *Biochemistry*, **27**: 8400-8408

Pye MP, and Cobbe SM (1992). Mechanisms of ventricular arrhythmias in cardiac failure and hypertrophy. *Cardiovascular Research*, **26**: 740-750

Quan WL, and Rudy Y (1990). Unidirectional block and re-entry of cardiac excitation: a model study. *Circulation Research*, **66**: 367-382

Ramírez-Gil JF, Trouvé P, Mougenot N, Carayon A, Lechat P, and Charlemagne D (1998). Modifications of myocardial Na^+,K^+-ATPase isoforms and Na^+/Ca^{2+} exchanger in aldosterone/salt induced hypertension in guinea-pigs. *Cardiovascular Research*, **38:** 451-462

Rink TJ, Tsien RY, and Pozzan T (1982). Cytoplasmic pH and free Mg^{2+} in lymphocytes. *Journal of Cell Biology*, **95**: 189-196

Rodrigo GC, and Chapman RA (1991). The calcium paradox in isolated guinea-pig ventricular myocytes: effects of membrane potential and intracellular sodium. *Journal of Physiology*, **434**: 627-645

Roos A and boron WF (1981). Intracellular pH. *Physiological Reviews*, **61:** 296-434

Ruß U, Balser C, Scholz W, Albus U, Lang HJ, Weichert A, Schölkens BA, and Gögelein H (1996). Effects of the Na^+/K^+ exchange inhibitor HOE 642 on intracellular pH, calcium and sodium in isolated rat ventricular myocytes. *Pflügers Archives*, **433**: 26-43

Ryder KO, Bryant SJ, Winterton SJ, Turner MA, Flores NA, Sheridan DJ, and Hart G (1991). Electrical and mechanical characteristics of isolated ventricular myocytes from guinea-pigs with left ventricular hypertrophy and congestive heart failure. *Journal of Physiology,* **438**: 181P

Ryder KO, Bryant SM, and Hart G (1993). Membrane current changes in left ventricular myocytes isolated from guinea-pigs after abdominal aortic coarctation. *Cardiovascular Research,* **27:** 1278-1287

Saborowski F, Scholand C, Lang D and Albers C (1973). Intracellular pH and CO_2 combining curve of hypertrophic cardiac muscle in rats. *Respiratory Physiology*, **18:** 171-177

Santana LF, Cheng H, Gómez AM, Cannell MB, and Lederer WJ (1996). Relation between the sarcolemma Ca^{2+} current and Ca^{2+} sparks and local control theories for cardiac excitation-contraction coupling. *Circulation Research,* **78**: 166-171

Satoh H, Hayashi H, Noda N, Terada H, Kbayashi A, Hirano M, Yamashita Y, and Yamazaki N (1994). Regulation of $[Na^+]_i$ and $[Ca^{2+}]_i$ in guinea pig myocytes: dual loading of fluorescent indicators SBFI and fluo 3. *American Journal of Physiology,* **266**: H568-H576

Saupe KW, Lim CC, Ingwall JS, Apstein CS, Eberli FR (2000). Comparison of hearts with 2 types of pressure-overload left ventricular hypertrophy. *Hypertension*, **35**: 1167-1176

Scamps F, Mayoux E, Charlemagne D, and Vassort G (1990). Calcium current in single cells isolated from and hypertrophied rat heart: effects of β-adrenergic stimulation. *Circulation Research*, **67:** 199-208

Scanlon M, Williams DA and Fay FS (1987). A Ca^{2+} insensitive form of Fura-2 associated with polymorphonuclear leukocytes. *Journal of Biological Chemistry*, **262**: 6308-6312

Schäfer Y, Ladilov V, Schäfer M, and Piper HM (2000). Inhibition of NHE protects reoxygenated cardiomyocytes independently of anoxic Ca^{2+} overload and acidosis. *American Journal of Physiology,* **279**: H2143-H2150

Schotten U, Koenigs B, Rueppel M, Schoendube F, Boknik P, Schmitz W, and Hanrath P (1999). Reduced myocardial sarcoplasmic reticulum Ca^{2+}-ATPase protein expression in compensated primary and secondary human cardiac hypertrophy. *Journal of Molecular and Cellular Cardiology,* **31**: 1483-1494

Schouten VJA (1990). Interval dependence of force and twitch duration in rat heart explained by Ca^{2+} pump inactivation in sarcoplasmic reticulum. *Journal of Physiology*: **431:** 427-444

Schussheim AE, and Radda GK (1995). Altered Na^{+}-H^{+}-exchange activity in the spontaneously hypertensive perfused rat heart. *Journal of Molecular and Cellular Cardiology*, **27**: 1475-1481

Seed WA, and Walker JM (1988). Relation between beat interval and force of the heartbeat and its clinical implications. *Cardiovascular Research*, **22**: 303-314

Sen L, and Smith TW (1994). T-type Ca^{2+} channels are abnormal in genetically determined cardiomyopathic hamster hearts. *Circulation Research*, **75:** 149-155

Shacklock LF, Wier WG, and Balke CW (1995). Local Ca^{2+} transients (Ca^{2+} sparks) originate at transverse tubules in rat heart cells. *Journal of Physiology*, **487**: 601-608

Shamraj OI, Grupp IL, Grupp G, Melvin D, Gradoux N, Kremers W, Lingrel JB, and De Pover A (1993). Characterisation of Na/K-ATPase. its isoforms, and the inotropic response to ouabain in isolated failing human hearts. *Cardiovascular Research*, **27**: 2229-2237

Shamraj OI, and Lingrel JB (1994). A putative fourth Na^+-K^+-ATPase alpha-subunit gene is expressed in testes. *Proceedings National Academy of Science, USA,* **91:** 12952-12956

Shattock MJ (1984). Studies on the isolated papillary muscle preparation with particular emphasis on the effects of hypothermia. PhD, University of London.

Shattock MJ, and Bers DM (1989). Rat vs rabbit ventricle: Ca flux and intracellular Na assessed by ion-selective microelectrodes. *American Journal of Physiology,* **256**: C813-C822

Shattock MJ, and Matsuura H (1993). Measurement of Na^+-K^+ pump current in isolated rabbit ventricular myocytes using the whole-cell voltage-clamp technique. *Circulation Research,* **72**: 91-101

Sheu S-S, and Fozzard HA (1982). Transmembrane Na^+ and Ca^{2+} electrochemical gradients in cardiac muscle and their relationship to force development. *Journal of General Physiology*, **80**: 325-351

Shida S, Nakaya H, Matsumoto S and Kanno M (1994). β_1 adrenoreceptor mediated decrease in pH_i in quiescent ventricular myocardium. *Cardiovascular Research,* **28**: 112-118

Shorofsky SR, Aggarwal R, Corretti M, Baffa JM, Strum JM, Al-Seikhan BA, Kobayashi YM, Jones LR, Wier WG, and Balke CW (1999). Cellular mechanisms of altered contractility in the hypertrophied heart: big hearts, big sparks. *Circulation Research*, **84:** 424-434

Shull GE, Greeb J and Lingrel JB (1986). Molecular cloning of three distinct forms of the Na^+,K^+-ATPase α-subunit from rat brain. *Biochemistry*, **25:** 8125-8132

Silver LH, and Houser SR (1985). Decreased sodium-potassium pump activity in isolated hypertrophied feline ventricular myocytes. *Life Sciences*, **37**: 607-615

Sipido KR, Volders PGA, de Groot M, Verdonck F, Van de Werf F, Wellens HJJ, and Vos MA (2000). Enhanced Ca^{2+} release and Na/Ca exchange activity in hypertrophied canine ventricular myocytes. *Circulation*, **102**: 2137-2150

Siri FM, Krueger J, Nordin C, Ming Z, and Aronson RS (1991). Depressed intracellular calcium transients and contraction in myocytes from hypertrophied and failing guinea-pig hearts. *American Journal of Physiology*, **261:** H514-H530

Siri FM, Nordin C, Factor SM, Sonnenblick E and Aronsin R (1989). Compensatory hypertrophy and failure in gradual pressure-overload guinea-pig heart. *American Journal of Physiology,* **257**: H1016-H1024

Sleight MJ, Sleight P, Lonn E, Johnson D, Pogue J, Yi Q, Bosch J, Sussex B, Probstfield J, and Yusuf S: Heart Outcomes Prevention Evaluation (HOPE) Investigators (2001). Reduction of cardiovascular risk by regression of electrocardiographic markers of left ventricular hypertrophy by the angiotensin-converting enzyme inhibitor ramipril. *Circulation*, **104:** 1582-1584

Smith GL, Valdeomillos M, Eisner DA, and Allen DG (1988). Effects of rapid application of caffeine on intracellular calcium concentration in ferret papillary muscles. *Journal General Physiology*, **92**: 351-358

Somura F, Izawa H, Iwase M, Takeichi Y, Ishiki R, Nishizawa T, Noda A, Nagata K, Yamada Y, and Yokota M (2001). Reduced myocardial sarcoplasmic reticulum Ca^{2+}-ATPase mRNA expression and biphasic force-frequency relations in patients with hypertrophic cardiomyopathy. *Circulation,* **104**: 658-63

Spach MS, and Heidlage JF (1995). The stochastic nature of cardiac propagation at a microscopic level: electrical description of myocardial architecture and its application to conduction. *Circulation Research*, **76**: 366-380

Spach MS, Miller WT, Geselowitz DB, Barr RC, Kootsey JM, and Johnson EA (1981). The discontinuous nature of propogation in normal canine cardiac muscle: evidence for recurrent discontinuities of intracellular resistance that affect the membrane currents. *Circulation Research*, **48**; 39-54

Stein B, Bartel S, Kirchhefer U, Kokott S, Krause EG, Neumann J, Schmitz W, and Scholz H (1996). Relation between contractile function and regulatory cardiac proteins in hypertrophied hearts. *American Journal of Physiology*, **270**: H2021-H2028

Stilli D, Sgoifo A, Macchi E, Zaniboni M, De Iasio S, Cerbai E, Mugelli A, Lagrasta C, Olivetti G, and Musso E (2001). Myocardial remodelling and arrhythmogenesis in moderate cardiac hypertrophy in rats. *American Journal of Physiology,* **280**: H142-H150

Sun B, Leem C, and Vaughan-Jones RD (1996). Novel chloride-dependent acid loader in the guinea-pig ventricular myocyte: part of a dual acid-loading mechanism. *Journal of Physiology,* **495**: 65-82

Sun X-H, Protasi F, Takahashi H, Ferguson DG, and Franzini-Armstrong C (1995). Molecular architecture of membrane involved in excitation-contraction coupling of cardiac muscle. *Journal of Cell Biology*, **129**: 659-671

Sweadner KJ (1989). Isoenzymes of the Na^+/K^+-ATPase. *Biochimica et Biophysica Acta*, **988:** 185-220

Sweadner KJ, Herrera VLM, Amato A, Moellmann A, Gibbsons DK, and Repke KRH (1994). Immunological identification of Na^+-K^+-ATPase isoforms in myocardium. *Circulation Research,* **74**: 669-678

Szlachcic J, Tubau JF, O'Kelly B, Ammon S, Daiss K, and Massie BM (1992). What is the role of silent coronary artery disease and left ventricular hypertrophy in the genesis

of ventricular arrhythmias in men with essential hypertension. *Journal of the American College of Cardiology*, **19**: 803-808

Takewaki S, Kuro-o M, Hiroi Y, Yamazaki T, Noguchi T, Miyagishi A, Nakahara K, Masanori A, Manabe I, Yazaki Y and Nagai R (1995). Activation of Na^+-H^+ antiporter (NHE-1) gene expression during growth, hypertrophy and proliferation of the rabbit cardiovascular system. *Journal of Molecular and Cellular Cardiology*, **27**: 729-742

Tanaka H, Sekine T, Kawanishi T, Nakamura R, and Shigenobo K (1998). Intrasarcomere [Ca^{2+}] gradients and their spatio-temporal relation to Ca^{2+} sparks in rat cardiomyocytes. *Journal of Physiology*, **508:** 145-152

Terracciano CMN, De Souza AI, Philipson KD, and MacLeod KT (1998). Na^+-Ca^{2+} exchange and sarcoplasmic reticulum Ca^{2+} regulation in ventricular myocytes from transgenic mice overexpressing the Na^+-Ca^{2+} exchanger. *Journal of Physiology*, **512:** 651-667

Thollon C, Kreher P, Charlton V, and Rossi A (1989). Hypertrophy induced alteration of action potential and effects of the inhibition of angiotensin converting enzyme by perindropril in infarcted rat hearts. *Cardiovascular Research,* **23**: 224-230

Thomas AP, and Delaville F (1991). The use of fluorescent indicators for the measurement of cytosolic free calcium in cell populations and single cells. In McCormack & Cobbold eds: *Cellular Calcium, a Practical Approach.* In I.R.L. Press, Oxford University Press, New York

Thomas G, Balke CW, and Shorofsky SR (1995). Calcium entry through sodium channels causes release of calcium from the sarcoplasmic reticulum in rat ventricular cells. *Biophysics Journal*, **68**: A179

Tiritilli A, and Ruff F (1994). Induction of hypertension and cardiac hypertrophy in guinea-pig by DOCA salt. *Methods Find Experimental Clinical Pharmacology*, **16**, 391-396

Tomanek RJ, Butters CA and Zimmermann MB (1993). Initiation of cardiac hypertrophy in response to thyroxine is not limited by age. *American Journal of Physiology*, **264**: H1041-H1047

Topol EJ, Traill TA, and Fortuin NJ (1985). Hypertensive hypertrophic cardiomyopathy of the elderly. *New England Journal of Medicine*, **312**: 277-83

Towbin H, Staehelin T, and Gordon J (1979). Electrophoretic transfer of proteins from polyacrylamide gels to nitrocellulose sheets: procedure and some applications. *Proceedings of the Royal Academy of Sciences of the USA,* **76**: 4350-4354

Trouve P, Carre P, Belikova I, Leclercq C, Dakhli T, Soufir L, Coquard I, Ramirez-Gil J, and Charlemange D (2000). Na^+-K^+-ATPase α_2-isoform expression in guinea-pig hearts during transition from compensation to decompensation. *American Journal of Physiology*, **279:** H1972-H1981

Tsutsui H, Ishibashi Y, Imanaka-Yoshida K, Yamamoto S, Yoshida T, Sugimachi M, Urabe Y, and Takeshita A (1997). Alterations in sarcoplasmic reticulum calcium-storing proteins in pressure-overload cardiac hypertrophy. *American Journal of Physiology*, **41:** H168-H175

Turner, M.A, Thomas P, and Sheridan DJ (1992). An improved method for direct laryngeal intubation in the guinea-pig. *Laboratory animals*, **26:** 25-28

Urayama O, Shutt H, and Sweadner KJ (1989). Identification of three isoenzyme proteins of the catalytic subunit of the Na,K-ATPase in rat brain. *Journal of Biological Chemistry*, **264:** 8271-8280

Uzzaman M, Honjo H, Takagishi Y, Emdad LM, Magee AI, Severs NJ, and Kodama I (2000). Remodelling of gap junction coupling in hypertrophied right ventricles of rats with monocrotaline-induced pulmonary hypertension. *Circulation Research*, **86:** 871-878

van der Laarse A, Vliegen HW, van der Nat KH, Hollaar L, Egas JM, Swier GP, and van der Broek AJ (1989). Comparison of myocardial changes between pressure induced hypertrophy and normal growth in the rat heart. *Cardiovascular Research,* **23**: 308-314

Vanheel B, de Hemptinne A, and Leusen I (1985). Intracellular pH and contraction of isolated rabbit and cat papillary muscle: effect of superfusate buffering. *Journal of Molecular and Cellular Cardiology*, **17**: 23-29

Varro A, Negretti N, Hester SB, and Eisner DA (1993). An estimate of the calcium content of the sarcoplasmic reticulum in rat ventricular myocytes. *Pflügers Archives*, **423**: 158-160

Vaughan-Jones RD (1982). Chloride activity and its control in skeletal and cardiac muscle. *Philosophical Transactions of the Royal Society of London Series B, Biological Sciences,* **299**: 537-548

Vaughan-Jones RD, Eisner DA, and Lederer WJ (1987). Effects of changes of intracellular pH on contraction in sheep cardiac Purkinje fibres. *Journal of General Physiology*, **89:** 1015-1032

Vaughan-Jones RD, Lederer WJ, and Eisner DA (1983). Ca^{2+} ions can affect intracellular pH in mammalian cardiac muscle. *Nature*, **301**: 522-524

Vaughan-Jones RD, and Wu M-L (1990). pH dependence of intrinsic H^{+} buffering power in the sheep cardiac Purkinje fibre. *Journal of Physiology*, **425**: 429-448

Vaughan-Jones RD, Wu M-L, and Bountra C (1989). Sodium-hydrogen exchange and its role in controlling contractility during acidosis in cardiac muscle. *Molecular and Cellular Biochemistry*, **89**: 157-162

Vorperian VR, Wisialowski TA, Deegan R, and Roden DM (1994). Effect of hypercapnic acidemia on anisotropic propogation in the canine ventricle. *Circulation*, **90**: 456-461

Waldenström A, Lecarpentier Y, Clergue M, Oliviero P, Schwartz K, Van Thiem N, and Swynghedauw B (1985). Dissociation of myofibrillar ATPase activity and contractile function in hypertrophied guinea-pig hearts. *Circulation,* **72** (suppl III): 336

Wallis W, Cooklin M, Sheridan DJ, and Fry CH (2001). The action of isoprenaline on the electrophysiological properties of hypertrophied left ventricular myocytes. *Archives Physiological Biochemistry*, **109**: 117-126

Wallis WRJ, Wu C, Cooklin M, Sheridan DJ, and Fry CH (1997). Intracellular pH and H^+ buffering capacity in guinea-pigs with left ventricular hypertrophy induced by constriction of the thoracic aorta. *Experimental Physiology*, **82**: 227-230

Wang DY, Chae SW, Gong QY, and Lee CO (1988). Role of a^i_{Na} in positive force-frequency staircase in guinea pig papillary muscle. *American Journal of Physiology*, **255**: C798-C807

Wang GX, Schmied R, Ebner F, and Korth M (1993). Intracellular sodium activity and its regulation in guinea-pig atrial myocardium. *Journal of Physiology*, **465**: 73-88

Wang J, Flemal K, Qui Z, Ablin L, Grossman W, and Morgan JP (1994). Ca^{2+} handling and myofibrillar Ca^{2+} sensitivity in ferret cardiac myocytes with pressure-overload hypertrophy. *American Journal of Physiology*, **267**: H918-H924

Wang J, Schwinger RHG, Frank K, Müller-Ehmsen J, Martin-Vasallo P, Pressley TA, Xiang A, Erdmann E, and McDonagh AA (1996). Regional expression of sodium pump alpha subunit isoforms and Na^+-Ca^{2+} exchanger in human heart. *Journal of Clinical Investigation,* **98**: 1650-1658

Wang X, Levi AJ, and Halestrap AP (1994). Kinetics of the sarcolemmal lactate carrier in single heart cells using BCECF to measure pH_i. *American Journal of Physiology,* **267:** H1759-H1769

Weber KT, Clark WA, Janicki JS, and Shroff SG (1987). Physiologic versus pathological hypertrophy and the pressure-overloaded myocardium. *Journal of Cardiovascular Pharmacology,* **10**: 537-549

Weber KT, Janick JS, Shroff SG, Pick R, Chen RM, and Bashey RI (1988). Collagen remodelling of the pressure-overloaded, hypertrophied nonhuman primate myocardium. *Circulation Research,* **62:** 757-765

Weissberg Pl. Little PJ, Cragoe EJ, and Bobik A (1989). The pH of spontaneously beating cultured rat heart cells is regulated by an ATP-calmodulin-dependent Na^+/H^+ antiport. *Circulation Research,* **64**: 676-685

Wendt IR, and Langer GA (1977). The sodium-calcium relationship in mammalian myocardium; the effect of Na deficient perfusion on calcium fluxes. *Journal of Molecular and Cellular Cardiology*, **9:** 551-564

Whitmer KR, Lee JH, Martin AF, Lane LK, Lee SW, Schwartz A, Overbeck HW, and Wallick ET (1986). Myocardial Na,K-ATPase in one-kidney, one-clip hypertensive rats. *Journal of Molecular and Cellular Cardiology*, **18**: 1085-1095

Wier WG, and Balke CW (1999). Ca^{2+} release mechanisms, Ca^{2+} sparks and local control of excitation-contraction coupling in normal heart muscle. *Circulation Research*, **85**: 770-776

Wier WG, and Yue DT (1986). Intracellular calcium transients underlying the short-term force-interval relationship in ferret ventricular myocardium. *Journal of Physiology*, **376:** 507-530

Winterton SJ, Turner MA, O'Gorman DJ, Flores NA, and Sheridan DJ (1994). Hypertrophy causes delayed conduction in human and guinea-pig myocardium: accentuation during ischaemic reperfusion. *Cardiovascular Research*, **28**: 47-53

Wise RG, Huang CL, Gresham GA, Al-Shafei AI, Carpenter TA, and Hall LD (1998). Magnetic resonance imaging analysis of left ventricular function in normal and spontaneously hypertensive rats. *Journal of Physiology*, **513**: 873-887

Wisenbaugh T, Allen P, Cooper G, Holzgrefe H, Beller G and Carabello B (1983). Contractile function, myosin ATPase activity isoenzymes in the hypertrophied pig left ventricle after a chronic progressive pressure overload. *Circulation Research*, **53**: 332-341

Wisløff U, Loennechen JP, Falck G, Beisvag V, Currie S, Smith G and Ellingsen Ø (2001). Increased contractility and calcium sensitivity in cardiac myocytes isolated from endurance trained rats. *Cardiovascular Research,* **50**: 495-508

Wittenberg BA, and Gupta RK (1985). NMR studies of intracellular sodium ions in mammalian cardiac myocytes. *Journal of Biological Chemistry*, **260**: 2031-2034

Wolk R, Sneddon KP, Dempster J, Kane KA, Cobbe SM, and Hicks MN (2000). Regional electrophysiological effects of left ventricular hypertrophy in isolated rabbit hearts under normal and ischaemic conditions. *Cardiovascular Research*, **48**: 120-128

Wong K, Boheler KR, Bishop J, Petrou M, and Yacoub MH (1998). Clenbuterol induces cardiac hypertrophy with normal functional, morphological and molecular features. *Cardiovascular Research*, **37**: 115-122

Wu M-L, Tsai M-L, and Tseng Y-Z (1994). DIDS-sensitive pH_i regulation in single rat cardiac myocytes in nominally HCO_3^--free conditions. *Circulation Research*, **75**: 123-132

Wu M-L, and Vaughan-Jones RD (1997). Interaction between Na^+ and H^+ ions on Na-H exchange in sheep cardiac Purkinje fibres. *Journal of Molecular and Cellular Cardiology*, **29:** 1131-1140

Xiao Y-F, and McArdle JJ (1994). Elevated density and altered pharmacological properties of myocardial calcium current of the spontaneously hypertensive rat. *Journal of Hypertension,* **12**: 783-790

Xu XP, and Best PM (1991). Decreased transient outward K^+ current in ventricular myocytes from acromegalic rats. *American Journal of Physiology*, **260:** H935-H942

Yang CM, Kandaswamy V, Young D, and Sen S (1997). Changes in collagen phenotypes during progression and regression of cardiac hypertrophy. *Cardiovascular Research*, **36**: 236-245

Yarmazaki T, Komuro I, Kudoh S, Zou Y, Nagai R, and Aikawa R (1998). Role of ion channels and exchanger in mechanical stretch-induced cardiomyocyte hypertrophy. *Circulation Research,* **82:** 430-437

Yoneda T, Kihara Y, Ohkusa T, Iwanaga Y, Inagaki K, Takeuchi Y, Hayashida W, Ueyama T, Hisamatsu Y, Fujita M, Hatac S, Matsuzaki M and Sasayama S (2001). Calcium handling and sarcoplasmic-reticular protein functions during heart failure transitions in ventricular myocardium from rats with hypertension. *Life Sciences,* **70**: 143-157

Zahler R, Gilmore-Herbert M, Baldwin JC, Franco K, and Benz Jr EJ, (1993). Expression of alpha isoforms of Na-K-ATPase in human heart. *Biochimica et Biophysica Acta,* **1149**: 189-194

Zahler R, Gilmore-Herbert M, Sun W, and Benz EJ (1997a). Na,K-ATPase isoform gene expression in normal and hypertrophied dog heart. *Basic Research in Cardiology*, **91**: 256-266

Zahler R, Sun W, Ardito T, and Kashgarian M (1996). Na-K-ATPase α-isoform expresion in heart and vascular endothelia: cellular and developmental regulation. *Americal Journal of Physiology,* **270**: C361-C371

Zahler R, Zhang ZT, Manor M, and Boron WF (1997b). Sodium kinetics of Na,K-ATPase α-isoforms in intact transfected HeLa cells. *Journal of General Physiology*, **110**: 201-213

6.0. Publications from thesis

Papers

Gray RP, McIntyre H, Sheridan DJ, and Fry CH (2001). Intracellular sodium and contractile function in hypertrophied human and guinea-pig myocardium. *Pfügers Archives,* **442**: 117-123

Abstracts

Gray RP, McIntyre H, and Fry CH (1996). Variation of the force-frequency relationship in hypertrophied myocardium. *Journal of Physiology*, **495,P**: 169P.

Gray RP, Carey P, Sheridan DJ, and Fry CH (1997). The relationship between intracellular $[Na^+]_i$ and the force-frequency response in hypertrophied guinea-pig myocardium. *Journal of Physiology*, **504,P**: 72P.

Variation of the force-frequency relationship in hypertrophied myocardium

R Gray, *H McInytre, CH Fry.

Institute of Urology and Nephrology, University College London, London W1P 7PN and *The Conquest Hospital, St. Leonards-on-Sea, East Sussex, TN37 7RD.

Normal myocardium from most species shows a positive force-frequency relationship whereas in failing myocardium a negative relationship is found (Mulieri *et al.* 1992). In species like the rat where the force-frequency relationship is negative the intracellular [Na^+], ([Na^+]$_i$) is raised (Shattock & Bers, 1989). We wished to test the hypothesis that in hypertrophy the force-frequency response is impaired and that this might be related to a rise in [Na^+]$_i$.

Human myocardial specimens were obtained from patients undergoing cardiac surgery for correction of aortic or mitral valve lesions. Local Ethics committee approval was obtained and the patients gave informed consent. Left ventricular hypertrophy was induced in guinea-pigs by ascending aortic constriction under halothane(2%), N_2O(49%) and O_2(49%) anaesthesia (Winterton *et al.* 1994). Preparations were superfused with Tyrode's at 35°C and isometric tension was measured. The response to increasing stimulation frequency is expressed as the ratio of tension generated at 1.6 and 0.8Hz, ($T_{(1.6/0.8)}$). Ratios >1.0 and <1.0 equate with positive and negative force-frequency relationships, respectively. [Na^+]$_i$ was measured in normal guinea-pig ventricular myocytes, loaded with the [Na^+] sensitive fluorescent indicator SBFI, in increasing concentrations of strophanthidin.

In isolated human preparations there was a progressive decline from a positive to a negative force-frequency relationship which correlated with cell diameter ($r=-0.58, n=31, p=0.002$). Compared to normal guinea-pig myocardium, hypertrophied guinea-pig hearts (heart:body weight ratios $3.3\pm0.4*10^{-3}$gm and $5.7\pm1.3*10^{-3}$gm respectively [mean$\pm$SD]) showed a negative force-frequency relationship ($T_{(1.6/0.8)}=1.72\pm0.32, n=25$ and 0.97 ± 0.20 $n=10$, respectively: $p=0.029$). On exposure to strophanthidin, (10nM to 3μM) a progressive inotropic effect was observed in normal guinea-pig myocardium, however the force-frequency relationship changed from positive to negative (*e.g.* $T_{(1.6/0.8)}=1.64\pm0.18$ at 0μM, 1.2 ± 0.15 at 0.3μM and 0.67 ± 0.19 at 3μM, $n=13$) and this was associated with an increase in [Na^+]$_i$ (*e.g.* 5.9 ± 0.4mM at 0μM and 10.1 ± 0.7mM at 0.3μM).

The decline in force-frequency relationship in normal guinea-pig myocardium exposed to strophanthidin is associated with a progressive rise in [Na^+]$_i$. A decline in the force-frequency relationship is observed in hypertrophied myocardium from humans and guinea-pigs and in humans the decline is related to the degree of hypertrophy. Thus hypertrophy may be associated with a progressive rise in [Na^+]$_i$ which we plan to test subsequently.

REFERENCES

Mulieri, L.A., Hasenfuss, G., Leavitt, B., Allen, P.D. & Alpert, N.R. (1992) *Circulation* **85**, 1743-1750

Shattock, M.J., Bers, D.M. (1989). *Am J Physiol* **256**, C813-C821.

Winterton, S.J., Turner, M.A., O'Gorman, D.J., Flores, N.A. & Sheridan, D.J. (1994). *Cardiovasc. Res.* **28**, 47-53

Relationship between intracellular sodium and the force-frequency response in control and hypertrophied guinea-pig myocardium

R.P. Gray [1], P Carey [1,2], D.J. Sheridan [2], C.H. Fry [1]. Institute of Urology & Nephrology, University College London, UK[1] and Academic Department of Cardiology, St Mary's Hospital, London, UK[2].

Left ventricular hypertrophy (LVH) following increased mechanical load is associated with increased cardiovascular mortality due to heart failure and arrhythmias. LVH is also associated with a reduced force-frequency relationship(Gray *et al* 1996). We wished to test the hypothesis that the reduced force-frequency relationship was related to an increase of intracellular sodium, $[Na^+]_i$, in hypertrophied guinea-pig myocardium.

LVH was induced in guinea-pigs by ascending aortic constriction under Halothane(2%), N_2O(49%) and O_2 anaesthesia (Winterton *et al* 1994). Sham operated guinea-pigs served as controls. Papillary muscles were stimulated to contract electrically *in-vitro* and isometric tension was measured. The response to increasing stimulation frequency is expressed as the ratio of the tension generated at 1.6 and 0.8Hz, ($T_{(1.6/0.8)}$). Ratios >1.0 and <1.0 equate with positive and negative force-frequency relationships respectively. $[Na^+]_i$ was measured in the same papillary muscles using ion selective microelectrodes(Fry *et al* 1987).

Constricted guinea-pigs showed significant cardiac hypertrophy compared to control animals (heart:body weight ratio ($5.7\pm1.1x10^{-3}$gm, n=12 vs $3.6\pm0.3x10^{-3}$gm, n=21, $p<0.001$). In right ventricular papillary muscles from normal and hypertrophied guinea-pigs a positive force-frequency relationship was observed ($T_{(1.6/0.8)}=1.7\pm0.14$ [mean±SD], n=6 and 1.44±0.04, n=2, respectively) and $[Na^+]_i$ was 6.5±0.5 mmol.l^{-1}, n=6 and 7.05±0.8 mmol.l^{-1}, n=2, respectively. Compared to control myocardium, left ventricular papillary muscles from hypertrophied guinea-pigs showed a depressed force-frequency relationship ($T_{(1.6/0.8)}$= 1.39±0.21,n=21 and 1.02±0.18, n=12:$p<0.001$) which correlated negatively with heart:body weight ratio ($r=-0.51$,$p<0.01$). $[Na^+]_i$ was significantly higher in left ventricular papillary muscles from hypertrophied myocardium compared to control (13.6±2.7 mmol.l^{-1}, n=12, compared to 7.6±2.3 mmol.l^{-1}, n=21:$p<0.001$). There were significant relationships between $[Na^+]_i$ and heart:body weight ratio, ($r=0.57$:$p<0.001$ and between $[Na^+]_i$ and the force-frequency relationship, ($r=-0.69$:$p<0.001$).

There is a significant relationship between the development of left ventricular hypertrophy and an increase in $[Na^+]_i$. These results suggest that the decline in the force-frequency relationship in hypertrophied myocardium is related to this increase in $[Na^+]_i$.

REFERENCES

Gray R., McIntyre H. & Fry C.H. (1996). *J Physiol*, **495.P**: 169 P
Winterton, S.J., Turner M.A., O'Gorman D.J., Flores N.A. & Sheridan D.J. (1994). *Cardiovasc Res*, **28:** 47-53.
Fry C.H., Harding D.P. & Mounsey J.P. (1987). *Proc R Soc Lond*, **230**: 53-75.

Pflügers Arch - Eur J Physiol (2001) 442:117–123
DOI 10.1007/s004240000512

ORIGINAL ARTICLE

R.P. Gray · H. McIntyre · D.S. Sheridan · C.H. Fry

Intracellular sodium and contractile function in hypertrophied human and guinea-pig myocardium

Received: 30 October 2000 / Received after revision: 28 November 2000 / Accepted: 29 November 2000 / Published online: 15 February 2001

Abstract We tested the hypothesis that in left ventricular myocardial hypertrophy (LVH) the positive staircase effect is impaired and is related to a raised intracellular [Na^+] ([Na^+]$_i$). Human myocardial specimens were obtained from patients undergoing mitral and aortic valve surgery, the latter group had LVH. LVH was induced in guinea-pigs by ascending aortic constriction. The extent of hypertrophy was quantified by measuring myocyte cross-section area, echocardiographic mass (in humans) and heart-to-body weight ratio (in guinea-pigs). The response to increasing stimulation frequency was expressed as the ratio of tension generated at 1.6 and 0.8 Hz ($T_{1.6/0.8}$); ratios greater and less than 1.0 equate with positive and negative force/frequency relationships respectively. [Na^+]$_i$ was measured using ion-selective microelectrodes. In human and guinea-pig myocardium $T_{1.6/0.8}$ values decreased and [Na^+]$_i$ increased with hypertrophy. For guinea-pig myocardium $T_{1.6/0.8}$ decreased from 1.39±0.05 to 1.02±0.05 and [Na^+]$_i$ increased from 7.3±1.4 to 12.1±1.3 mM in LVH. There was a close relationship between the reduction of $T_{1.6/0.8}$ and increase of [Na^+]$_i$ which was also observed when the [Na^+]$_i$ was increased with strophanthidin in normal myocardium. The recovery of a raised [Na^+]$_i$ after an acute acidosis was slowed in hypertrophied myocardium and stabilised at a higher level, suggesting that the membrane mechanisms that regulate [Na^+]$_i$ are reset.

Keywords Intracellular [Na^+] · Force-frequency relationship · Hypertrophied myocardium

R.P. Gray · C.H. Fry (✉)
The Institute of Urology and Nephrology,
University College London, 48 Riding House Street,
London W1W 7EY, UK
e-mail: c.fry@ucl.ac.uk
Tel.: +44-20-76799376, Fax: +44-20-76799584

H. McIntyre
The Conquest Hospital, The Ridge, St Leonards-on-Sea,
E. Sussex, TN37 7RD, UK

D.S. Sheridan
Academic Cardiology Unit, Imperial College School of Medicine,
St Mary's Hospital Medical School, London W2 1NY, UK

Introduction

Left ventricular hypertrophy (LVH) is an adaptive process that enables the heart to compensate for an increased mechanical load, but, left untreated, LVH is associated with the eventual development of heart failure [14] and arrhythmias [13]. The mechanisms whereby a well-compensated hypertrophied heart eventually decompensates are not yet understood. In vitro abnormalities of contractile function have been demonstrated when hypertrophy is severe or heart failure has developed [25], whilst in less-severe hypertrophy peak tension is normal although the twitch may be prolonged due to a relaxation delay [8]. It would be valuable to measure functional myocardial changes earlier in the development of hypertrophy in order to investigate the cellular defects that result in electro-mechanical disorders. Much current understanding of myocardial physiology in hypertrophy is derived from artificial animal models. Given the species differences and the various models of experimental hypertrophy used, a comparison of data from animal models with that from human myocardium would be valuable to allow animal data to be applied to the human condition.

Normal myocardium from humans and most animal species demonstrates a positive force/frequency relationship i.e. increasing stimulus frequency increases contractility, whereas in failing myocardium a negative relationship is found [18]. Negative force/frequency relationships are also seen in rat and ferret myocardium [12] as well as in atrial myocardium [24] and a common feature of myocardium exhibiting such force/frequency relationships is a relatively high intracellular [Na^+] ([Na^+]$_i$), [22, 24].

The aim of this study was to test the hypothesis that, in a guinea-pig model of hypertrophy, the force/frequency relationship is impaired and is accompanied by a rise in [Na^+]$_i$. Both variables were measured in the same preparation to facilitate comparison of data. In addition, the results were compared with similar measurements from hypertrophied human myocardium.

Materials and methods

Myocardial tissue

Human myocardium was obtained from patients undergoing elective aortic or mitral valve replacements. Ethical committee approval was obtained and the patients gave informed consent. Clinical and investigative details were obtained when possible from the patients' notes, including cardiac catheter and echocardiographic data. A wedge of myocardium from the upper septum was taken prior to aortic valve replacement and a segment of papillary muscle was excised during removal of the diseased mitral valve. Samples were transported to the laboratory in polypropylene vials filled with pre-gassed Tyrode's solution. Transit time was 3–25 min; no deterioration of muscle function has been reported for up to 30 min [9] and there was no correlation between any experimental variable and transport time for the samples used in this study. No patient had a clinical history of heart failure.

LVH was induced in male Dunkin-Hartley guinea-pigs (600–800 g) by constricting the ascending thoracic aorta with a high-density plastic disc (internal diameter 2.0 mm) under anaesthesia (0.22 ml kg^{-1} pentobarbitone sodium, followed by inhalation of a 49%/49%/2% N_2O:O_2:halothane mixture). Animals recovered after wound closure with post-operative analgesia with buprenorphine (50 μg kg^{-1} s.c.) [26]. Controls were either unoperated animals or sham-operated animals that underwent the same operation, but without clip placement. At 50–250 days post-operation the animals were weighed immediately prior to study and then killed by cervical dislocation. The hearts were removed immediately, weighed and placed in gassed Tyrode's solution at 37 °C. No animals showed evidence of heart failure and all procedures were performed according to the Guidance on the Operation of the Animals (Scientific Procedures) Act 1986, Her Majesty's Stationery Office, London, England.

Isolated preparations

Left ventricular papillary muscles were removed from control (sham-operated) and aortic-constricted guinea-pig hearts. For human myocardial preparations the fibre orientation of the biopsy sample was identified under ×20 magnification and a "v"-shaped section removed with a razor. The muscle dimensions were measured using a binocular microscope with a calibrated eyepiece graticule, with 100-μm markers and ×40 or ×80 magnification. Preparations were generally 0.7 mm or less in diameter (and never greater than 1 mm) and 3–5 mm long – see Discussion about prevention of hypoxia in the muscle core.

Tension recordings

Isolated preparations were mounted horizontally in a superfusion trough, tied at one end to a fixed hook and at the other end to an isometric force transducer using 100-μm silk thread. Preparations were superfused with Tyrode's solution containing in mM: NaCl 118, KCl 4.0, $NaHCO_3$ 24, NaH_2PO_4 0.4, $MgCl_2$ 1.0, $CaCl_2$ 1.8, glucose 6.1, Na pyruvate 5.0. The solution was gassed with a mixture containing 95%O_2/5% CO_2, pH 7.35±0.03. All experiments were performed at 36±0.5 °C. Preparations were stimulated electrically and peak isometric twitch tension in response to increasing frequency of stimulation (0.5–2.0 Hz) measured.

$[Na^+]_i$ measurement

$[Na^+]_i$ was measured with ion-selective microelectrodes (ISEs) in 39 guinea-pig papillary muscles used for tension recordings. Successful recordings were also made in six human preparations. Membrane potential (E_m) was recorded with 3 M KCl-filled microelectrodes made from thick-walled borosilicate glass. Na^+-ISEs were made from the same glass; they were exposed to dimethyldichlorosilane vapour for 3 min and heated at 200 °C for 40 min. A small sample of Na^+-selective material, *N,N',N''*-triheptyl-*N,N',N''*-trimethyl-4,4',4''-propylidyne-tris(3-oxabutyramide) with Na tetraphenylborate (ETH227; Fluka, Poole, Dorset, UK), was introduced into the tip of the microelectrode from the rear and the remainder filled with a solution containing 10 mM NaCl and 140 mM KCl. The Na^+-ISEs record both E_m and the change in $[Na^+]$ when penetrating a cell. The equivalence of E_m values (within 0.5 mV) recorded by the two microelectrodes after cell impalement was tested by superfusing the preparation with Tyrode's solution containing 40 mM KCl. The Na^+-ISEs were calibrated in mixed NaCl and KCl solutions, containing also (mM) $MgCl_2$ 3.0, ethyleneglycol-bis(β-aminoethylether)-*N,N,N',N'*-tetraacetic acid (EGTA) 2.0 and 4-(2-hydroxyethyl)-1-piperazineethanesulphonic acid (HEPES) 5.0; pH 7.1. $[Na^+]$ was varied between 0 and 147 mM, with $[Na^+]+[K^+]=147$ mM. All measurements were made with reference to a 3 M KCl junction. The method has been previously described in detail [10].

Histology

Samples of the human myocardial biopsies were placed in 10% formol saline. Sections (3–5 μm) were cut from paraffin-embedded blocks and stained using a standard haematoxylin and eosin procedure. Cell circumference was measured at the plane across the nucleus at ×400 magnification with a calibrated eyepiece graticule and a transverse cross-sectional area calculated [2]. In each preparation at least 50 cells were measured from each of two sections 20–30 μm apart. The SD of the measurement from an individual section was 10% or less of the mean, the two mean values were averaged and results accepted if there was less than 5% discrepancy. Assessment of the degree of fibrosis was performed on a slide stained for connective tissue using a trichrome MSB stain. Percentage fibrosis was estimated with a 12×12 eyepiece graticule by counting the proportion of intersections laying over extracellular space.

Statistical analysis

Results are expressed as mean±SD or ±SEM if several measurements were made on one preparation. Groups were compared using paired or unpaired Student's *t*-tests. The null hypothesis was rejected when $P \leq 0.05$.

Results

Assessment of hypertrophy and base-line properties

Human myocardial preparations were divided into two groups: from patients undergoing mitral valve replacement (unloaded ventricles; age 60±15 years, $n=16$) or aortic valve replacement (pressure-overloaded ventricles; age 65±11 years, $n=15$). The mean echocardiographic left ventricular mass (in grams) and cell cross-section area (square micrometre) in samples from the two groups were: 211±99 vs. 442±96 g respectively ($P<0.001$, $n=10$, 9) and 281±8 vs. 412±9 μm^2 ($P<0.001$, $n=16$, 15) respectively. The pressure gradient across the aortic valve in the pressure-overloaded group was 88±24 mmHg and is henceforth referred to as hypertrophied group; data are compared with the control unloaded group.

For the guinea-pig model the heart:body weight ratio (HBR) was used as an index of hypertrophy. The sham-operated and unoperated animals were combined to a single control group with an HBR of 3.55±0.30 g kg^{-1}

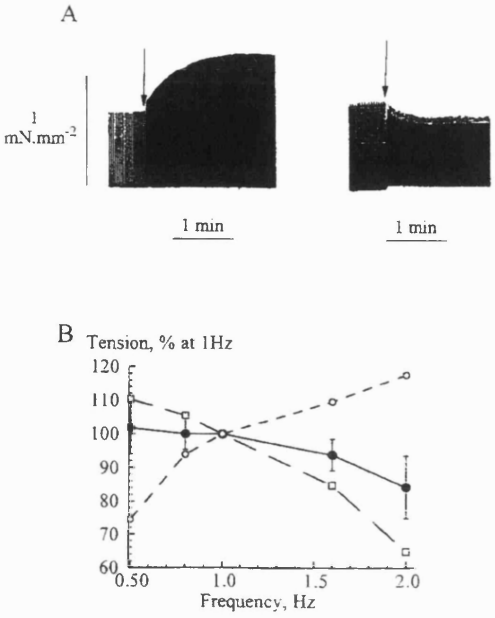

Fig. 1A, B Force/frequency relationships in normal and hypertrophied human myocardium. **A** Traces from samples taken from patients with mitral stenosis (*left*) and aortic stenosis (*right*) when the stimulation rate was doubled from 30 to 60 min^{-1} at the *arrows*. The *right-hand* trace shows *pulsus alternans* at the higher rate. **B** Mean force/frequency relationship for human myocardium (*closed symbols*) and the most extreme positive (*open circles*) and negative (*open squares*) relationships

(n=22). The HBR of the aortic-constricted group was significantly greater (5.73±1.10 g kg^{-1}, n=12, P<0.001). Peak isometric forces generated by the human preparations were 0.83±0.12 and 0.56±0.21 mN mm^{-2} for the control and hypertrophied groups respectively (P>0.05). For the guinea-pig preparations the values were 1.29±0.42 and 1.00±0.65 mN mm^{-2} for the two groups (P>0.05).

Force/frequency relationships

Figure 1A shows examples of isometric contractions from two human myocardial preparations when the frequency of stimulation was increased from 0.5 to 1.0 Hz. The left-hand trace was from a control preparation and shows a positive staircase with increasing frequency; the right-hand trace shows a decrease of force, with the appearance in this example (and in one other preparation from a total of 15) of alternate large and small contractions (*pulsus alternans*). Figure 1B shows mean steady-state isometric tension as a function of stimulation frequency in isolated human myocardial preparations, expressed as the percentage of that generated at 1 Hz. The closed circles represent the mean responses from all preparations, where there was a reduction of isometric tension when stimulation frequency was increased. However, the force/frequency relationship showed considerable variability and Fig. 1B also shows the most positive

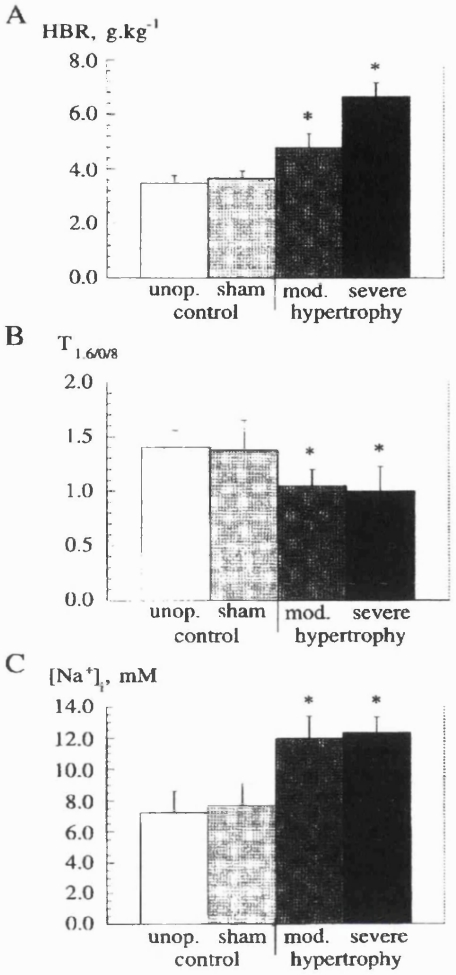

Fig. 2 **A** Heart-to-body weight ratios (*HBR*), **B** force/frequency relationship (expressed as the ratio of peak tensions developed at 1.6 and 0.8 Hz, $T_{1.6/0.8}$) and **C** intracellular [Na^+] ($[Na^+]_i$) in myocardium from unoperated, sham-operated, mildly hypertophied and severely hypertrophied hearts. Means±SD, *P<0.05 vs. sham-operated hearts

(open circles) and most negative (open squares) relationships obtained.

To compare quantitatively the range of responses between preparations the ratio of peak tension when the stimulation frequency was doubled from 0.8 to 1.6 Hz ($T_{1.6/0.8}$) was recorded; thus ratios above and below 1 equate with positive and negative force/frequency relationships respectively.

Force/frequency relationships and $[Na^+]_i$. Guinea-pig myocardium

Figure 2 shows values of HBR (Fig. 2A), $T_{1.6/0.8}$ (Fig. 2B) and $[Na^+]_i$ (Fig. 2C), obtained in preparations from aortic-constricted and sham-operated hearts as well as a further control set from unoperated animals. Data from aortic-constricted hearts were divided into two sets, one with

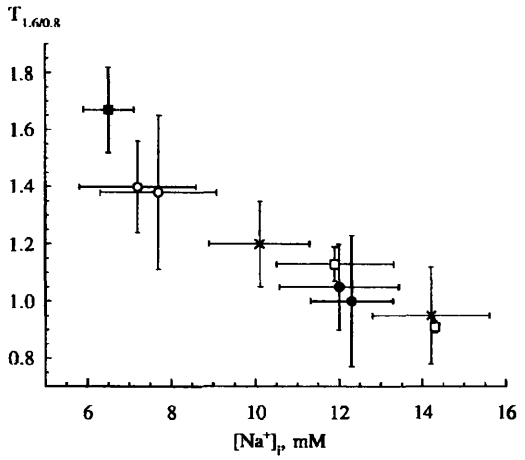

Fig. 3 The relationship between $T_{1.6/0.8}$ and $[Na^+]_i$ in guinea-pig and human myocardium. Data from guinea-pig right ventricle (*closed square*), left ventricle from sham-operated and unoperated hearts (*open circles*, see text for details) and moderately and severely hypertrophied left ventricle (*closed circles*). Shown also are data from strophanthidin-treated guinea-pig left ventricle (*crosses*) and human myocardium from patients with mitral valve and aortic valve disease (*open squares*). Means±SD

moderate hypertrophy (HBR 4.0–5.5 g kg^{-1}) and another with severe hypertrophy (HBR above 5.5 g kg^{-1}). As stated above, HBR was significantly larger in the aortic-constricted groups than in the sham-operated and unoperated groups. The $T_{1.6/0.8}$ ratio was reduced significantly in the aortic-constricted groups (moderate LVH 1.05±0.15, n=6; severe LVH 1.00±0.23, n=6) compared with the two control groups (sham-operated 1.38±0.27, n=10; unoperated 1.40±0.16, n=12). The decrease of the $T_{1.6/0.8}$ ratio was accompanied by increased $[Na^+]_i$ in the aortic-constricted groups (moderate LVH 12.0±1.4 mM, n=6; severe LVH 12.3±1.0 mM, n=6) compared with control (sham-operated 7.7±1.4 mM, n=10; unoperated 7.2±1.4 mM, n=12).

$[Na^+]_i$ was also measured in two right ventricular papillary muscles taken from hearts with LVH with values of 6.2 and 6.9 mM. These values compare with that of $[Na^+]_i$ of 6.5±0.6 mM (n=6) in similar muscles from unoperated hearts. Thus these limited data suggest that the increase of $[Na^+]_i$ in the aortic-constricted hearts was confined to the left ventricle.

The relationship between the $T_{1.6/0.8}$ ratio and $[Na^+]_i$ was further investigated by measuring both variables in the presence of strophanthidin. Superfusion with 0.3 and 1.0 μM strophanthidin increased $[Na^+]_i$ from a control of 7.1±0.9 mM (n=6) to 10.1±1.2 and 14.2±1.4 mM respectively and was accompanied by a reduction of the $T_{1.6/0.8}$ ratio from 1.38±0.14 to 1.20±0.15 and 0.95±0.17, respectively.

Force/frequency relationships and $[Na^+]_i$. Human myocardium

A similar trend in $T_{1.6/0.8}$ ratios was observed in human myocardial preparations. In control, unloaded hearts

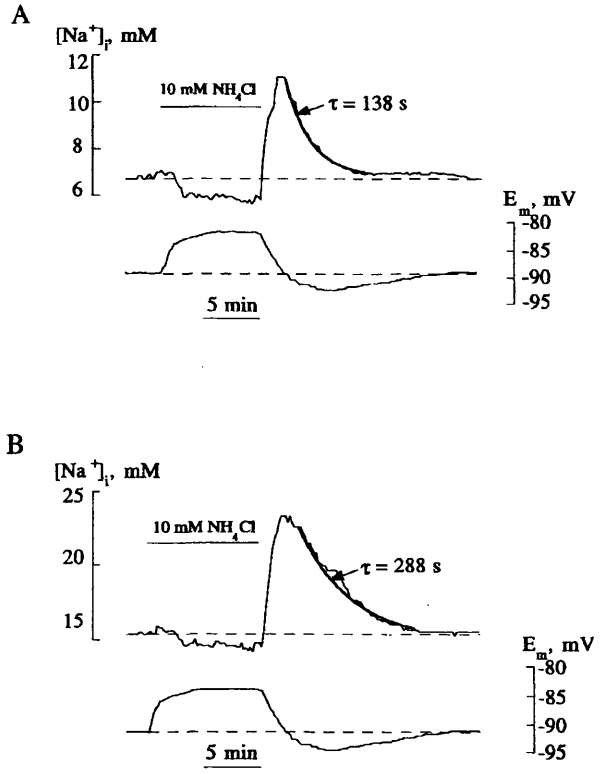

Fig. 4A, B Recordings of $[Na^+]_i$ and membrane potential (E_m) in guinea-pig myocardium. **A** Sham-operated animal. **B** Aortic-constricted animal. NH_4Cl (10 mM) was added to the superfusate as shown by the *horizontal bar*. The *dotted lines* show the pre-intervention control levels of $[Na^+]_i$ and E_m

(mitral valve disease) the value was 1.13±0.056 (n=16) and was significantly less (0.91±0.019, n=15, P<0.001) in preparations from hypertrophied hearts (aortic valve disease). Measurement of $[Na^+]_i$ was possible in six human preparations, although the success rate was less due to the higher proportion of connective tissue in the samples, the mean value was 12.7±1.6 mM. Two samples were from patients with aortic stenosis, with values of 14.0 and 14.3 mM, whilst the remainder were from patients with mitral valve disease (mean 11.8±1.4 mM); three of the latter patients had a history of taking digoxin several weeks prior to operation.

Figure 3 collects the above data from guinea-pig and human experiments and shows a strong negative relationship between the $T_{1.6/0.8}$ ratio and $[Na^+]_i$. These data are consistent with the hypothesis that the negative force/frequency relationship in hypertrophied guinea-pig and human heart is associated with a raised $[Na^+]_i$.

Recovery of $[Na^+]_i$ after intracellular acidosis

One cause of the raised $[Na^+]_i$ in hypertrophied tissue may be a reduced ability of the cell to extrude Na^+. This was tested by generating an intracellular acidosis after

termination of a brief exposure to 10 mM NH_4Cl. Figure 4 shows examples of recordings from preparations taken from a sham-operated animal (Fig. 4A) and a hypertrophied heart (Fig. 4B). Addition of NH_4Cl caused a small reduction of the $[Na^+]_i$ that was followed by a large increase upon its removal. With muscles from sham-operated hearts the $[Na^+]_i$ recovered from a peak of 11.4±0.8 to a mean of 6.2±0.4 mM with a time constant of 171±26 s (SEM, n=9). Corresponding experiments from aortic-constricted hearts showed a recovery of the $[Na^+]_i$ from 21.1±1.3 to 12.6±0.6 mM (n=6) with a time constant of 306±57 s. The recovery time constant and the final value of $[Na^+]_i$ were both significantly greater in the muscles from aortic-constricted hearts.

Discussion

The rise of $[Na^+]_i$ and force/frequency relationships in LVH

These experiments support the hypothesis that a negative force/frequency relationship in hypertrophied human and guinea-pig myocardium is due to a raised $[Na^+]_i$. The fact that the force/frequency relationship could be converted from positive to negative in normal guinea-pig myocardium by artificially raising the $[Na^+]_i$ with strophanthidin lent support to the hypothesis. A negative relationship has also been described in normal myocardium from several species, including rat and ferret; a feature of these tissues is the relatively high $[Na^+]_i$ compared with those with a positive relationship [22].

Data from aortic-constricted guinea-pig hearts were divided into two groups. Hearts were constricted for either 60–100 days or for about 250 days. The shorter period tended to generate a moderate hypertrophy (HBR 4.0–5.5; mean increase 32%) whilst the longer period produced a more severe growth (HBR above 5.5; mean increase 83%). However, the increase of $[Na^+]_i$ and reduction of the $T_{1.6/0.8}$ ratio was already established with moderate hypertrophy and did not change further with continued growth of the left ventricle. This pattern is in contrast to other cellular changes; intracellular acidosis develops progressively throughout myocardial growth [23], whilst increased gap junction resistance (and consequently reduced conduction) occurs only in more severe LVH [7]. The temporal dissociation of changes to these different variables raises the important point that an increase of $[Na^+]_i$ may represent an initial change during the development of LVH and may be causal in other cellular changes.

The increase of $[Na^+]_i$ cannot be attributed to the age of the animal. The sham-operated and the constricted animals were left for similar times post-operation; 60–100 days to produce moderate hypertrophy and about 250 days to generate severe hypertrophy. Furthermore, the similarity of $[Na^+]_i$ values in the sham-operated and unoperated control groups suggest that the operative procedures required to place the constricting ring around the aorta do not per se raise $[Na^+]_i$.

In human myocardial preparations the force/frequency relationship also declined with LVH. Tissue from patients with mitral valve disease was used as a control as there was no evidence of clinical or microscopic hypertrophy; both echocardiographic mass and cell cross-section area were within the normal ranges [17]. It is important to emphasise that the non-hypertrophied tissue was taken from papillary muscle and hypertrophied tissue from endocardial septum. However, it is unlikely that the different force/frequency relationships in the two groups were merely due to the site from which biopsy samples were taken. A previous study [20] has shown that endocardial trabeculae from normal ventricles show a positive force/frequency relationship of similar magnitude to those reported here for normal myocardium from papillary muscle.

It was possible to measure $[Na^+]_i$ in a small number of human samples, the mean was 12.7 mM; omitting the two samples from patients with aortic stenosis reduced this to 11.9 mM. The $T_{1.6/0.8}$ and $[Na^+]_i$ values fell within the range of the guinea-pig data (Fig. 3). The relatively high $[Na^+]_i$ and lower $T_{1.6/0.8}$ values for human myocardium, especially from the control group, compared with guinea-pig, could have several explanations: there is a real species difference and/or human preparations may have been affected by some of the patients having taking digoxin prior to operation. About 75% of the patients with mitral valve disease and 20% of those with aortic valve disease had been administered digoxin. If the effects of digoxin on the myocardium had persisted to the time at which biopsy samples were taken, this would have reduced more the control $T_{1.6/0.8}$ values and lessened the difference between the hypertrophied group. However, this factor would strengthen the conclusion that hypertrophy is associated with a significant reduction of the force/frequency relationship. We do not consider that biopsy samples suffered significant insult in transport from the operating theatre and laboratory; transit time was 3–25 min, with no correlation between this and in vitro characteristics [9]. To reduce the risk of hypoxia, which could impair contractile function and elevate $[Na^+]_i$ in both human and guinea-pig preparations, the preparation diameter was less than 1 mm, and usually 0.7 mm or less, and preparations were superfused rapidly with Tyrode's solution. The potential problems with interpreting data from human biopsy samples emphasises the need for well-validated animal models and their comparison with data from human samples.

Comparison with other studies

A rise of $[Na^+]_i$ in hypertrophied guinea-pig myocardium is consistent with other reports. A nuclear magnetic resonance (NMR) study has demonstrated an increase of

$[Na^+]_i$ with moderate left ventricular hypertrophic growth [11], whilst another has shown that ischaemia generates a larger rise of $[Na^+]_i$ in hypertrophied than in control hearts [6]. However, in a model of right ventricular hypertrophy no increase of $[Na^+]_i$ is observed [3], although these experiments were carried out at 20 °C, at which the Na-pump would be partially inactive and the $[Na^+]_i$ consequently already raised [21].

Causes of the rise of $[Na^+]_i$ and reduction of the force/frequency relationship

There are several possible explanations for the rise of $[Na^+]_i$ and decline of the $T_{1.6/0.8}$ ratio. The intracellular acidosis that accompanies hypertrophic growth [23] could increase $[Na^+]_i$ via the Na^+/H^+ exchanger. However, the rise of $[Na^+]_i$ occurs early in cardiac growth, whilst pH_i continues to fall throughout, suggesting that this is not the primary cause. Alteration to the kinetics and activity of the Na-pump is an alternative possibility to explain the raised $[Na^+]_i$. Reduced pump activity has been described in spontaneously hypertensive rats [19] and is consistent with the slowed recovery from a raised $[Na^+]_i$ recorded in these experiments. The time constant of recovery (τ) of $[Na^+]_i$ and pH_i is larger in multicellular tissue than in single cells [4] due to diffusion constraints in the former. However, because preparation sizes were similar in the control and hypertrophied samples comparison of τ values is still possible.

The Na-pump comprises an α-catalytic subunit and a smaller β-glycoprotein subunit. The α-subunit has the binding sites for Na^+, K^+, adenosine 5'-triphosphate (ATP) and ouabain. Several isoforms of the α-subunit have been identified. The α_1-subtype is expressed ubiquitously in myocardium and virtually exclusively in normal guinea-pig myocardium [16], with a Michaelis-Menten constant (K_m) for Na^+_i of about 12 mM. The α_2 and α_3 subtypes have a higher K_m (22–33 mM) [27] and are expressed during normal development and hypertrophy associated with hypertension [5, 15]. Thus it is possible that the raised $[Na^+]_i$ in obstructive hypertrophic myocardium described in the above experiments could result from a reduced number of pump sites or an altered expression of the α-subtype isoform. These possibilities are currently under examination.

Reduction of the force/frequency relation when $[Na^+]_i$ is raised is probably due to excessive Ca^{2+} influx through Na^+/Ca^{2+} exchange and overload of intracellular stores. High concentrations of cardiac glycosides reduce twitch force and the intracellular $[Ca^{2+}]$ as the sarcoplasmic reticulum is unable to retain Ca^{2+} as the resting sarcoplasmic concentration rises above normal levels [1].

Acknowledgements We thank the Wellcome Trust and the British Heart Foundation for financial assistance.

References

1. Allen DG, Eisner DA, Pirolo JS, Smith GL (1985) The relationship between intracellular calcium and contraction in calcium-overloaded ferret papillary muscles. J Physiol (Lond) 364:169–182
2. Baandrup U, Olsen EGJ (1981) Critical analysis of endomyocardial biopsies from patients suspected of having cardiomyopathy: morphological and morphometric aspects. Br Heart J 45:475–486
3. Baudet S, Noireaud J, Léoty C (1991) Intracellular Na activity measurements in the control and hypertrophied heart of the ferret: an ion sensitive microelectrode study. Pflügers Arch 418:313–318
4. Bountra C, Powell T, Vaughan-Jones RD (1990) Comparison of intracelluar pH transients in single ventricular myocytes and isolated ventricular muscle of guinea-pig. J Physiol (Lond) 424:343–365
5. Charlemange D, Orlowski J, Oliviero P, Rannou F, Beuve CS, Swynghedauw B, Lane LK (1994) Alteration of Na,K-ATPase subunit mRNA and protein levels in hypertrophied rat heart. J Biol Chem 269:1541–1547
6. Clarke K, Kohler S, Ingwall SJ (1990) Intracellular sodium in the hypertrophied rat heart during ischaemia and reperfusion (abstract). Circulation 70:496A
7. Cooklin M, Wallis WRJ, Sheridan DJ, Fry CH (1997) Changes in cell-to-cell coupling associated with left ventricular hypertrophy. Circ Res 80:765–771
8. Cooper GI (1987) Cardiocyte adaptation to chronically altered load. Annu Rev Physiol 49:501–518
9. Cooper IC, Fry CH (1990) Mechanical restitution in isolated mammalian myocardium: species differences and underlying mechanisms. J Mol Cell Cardiol 22:439–452
10. Fry CH, Harding DP, Mounsey JP (1987) The effects of cyanide on intracellular ionic exchange in ferret and rat ventricular myocardium. Proc R Soc Lond [Biol] 230:53–75
11. Jelicks LA, Siri FM (1995) Effects of hypertrophy and heart failure on $[Na^+]_i$ in pressure-overloaded guinea-pig heart. Am J Hypertens 8:934–943
12. Koch-Weser J, Blinks J R (1963) The influence of the interval between beats on myocardial contractility. Pharmacol Rev 15: 601–652
13. Levy D, Anderson KM, Savage DD, Balkus SA, Kannel WB, Castelli WP (1987) Risk of ventricular arrhythmias in left ventricular hypertrophy: the Framingham Heart study. Am J Cardiol 60:560–563
14. Levy D, Garrison RJ, Savage DD, Kannel WB, Castelli WP (1990) Prognostic implications of echocardiographically determined left ventricular mass in the Framingham study. New Engl J Med 332:1561–1566
15. Lucchesi PA, Sweadner KJ (1991) Postnatal changes in Na, K-ATPase isoform expression in rat cardiac ventricle. J Biol Chem 266:9327–9331
16. McDonagh A, Schmidt C (1985) Comparison of subunits of cardiac, brain and kidney Na^+-K^+-ATPase. Am J Physiol 248: C247–C251
17. McIntyre H, Fry CH (1997) Abnormal action potential conduction in isolated human hypertrophied left ventricular myocardium. J Cardiovasc Electrophysiol 8:887–894
18. Mulieri LA, Hasenfuss G, Leavitt B, Allen PD, Alpert NR (1992) Altered myocardial force-frequency relation in human heart failure. Circulation 85:1743–1750
19. Nakanishi H, Makino N, Hata T, Matsui H, Yano K, Yanaga T (1989) Sarcolemmal Ca^{2+} transport activities in cardiac hypertrophy caused by pressure overload. Am J Physiol 257: H349–H356
20. Schmidt U, Hajjar RJ, Helm PA, Kim CS, Doye AA, Gwathmey JK (1998) Contribution of abnormal sarcoplasmic reticulum ATPase activity to systolic and diastolic dysfunction in human heart failure. J Mol Cell Cardiol 30:1929–1937

21. Shattock MJ (1984) Studies on the isolated papillary muscle preparation with particular emphasis on the effects of hypothermia. PhD thesis, University of London
22. Shattock MJ, Bers DM (1989) Rat versus rabbit ventricle: Ca flux and intracellular sodium by ion-selective microelectrodes. Am J Physiol 256:C813–C821
23. Wallis WRJ, Wu C, Cooklin M, Sheridan DJ, Fry CH (1997) Intracellular pH and H^+ buffering capacity in guinea-pigs with left ventricular hypertrophy induced by constriction of the thoracic aorta. Exp Physiol 82:227–230
24. Wang GX, Schmied R, Ebner F, Korth M (1993) Intracellular sodium activity and its regulation in guinea-pig atrial myocardium. J Physiol (Lond) 465:73–88
25. Wilmhurst PT, Walker JM, Fry CH (1984) Inotropic and vasodilator effects of amrinone on isolated human tissue. Cardiovasc Res 18:302–309
26. Winterton SJ, Turner MA, O'Gorman DJ, Flores NA, Sheridan DJ (1994) Hypertrophy causes delayed conduction in human and guinea-pig myocardium: accentuation during ischaemic reperfusion. Cardiovasc Res 28:47–53
27. Zahler R, Zhang Z-T, Manor M, Boron WF (1997) Sodium kinetics of Na,K-ATPase a isoforms in intact transfected HeLa cells. J Gen Physiol 110:201–213